Department of Meteorology

University of Maryland
College Park, MD 20742

division of mathematical & physical sciences & engineering

LAND-SURFACE INFLUENCES ON WEATHER AND CLIMATE

Final Scientific Report
Under NASA Grant No. NAS5-26

Prof. Ferdinand Baer, Principal Investigator

Prof. Yale Mintz, Co-principal Investigator

Department of Meteorology, University of Maryland

College Park, MD 20742

June 1984

LAND-SURFACE INFLUENCES ON WEATHER AND CLIMATE

Final Scientific Report
Under NASA Grant No. NAS5-26

Prof. Ferdinand Baer, Principal Investigator

Prof. Yale Mintz, Co-principal Investigator

Department of Meteorology, University of Maryland

College Park, MD 20742

June 1984

Soon after the initiation of the grant, the national program for an ocean satellite system was canceled. In consultation with Dr. M. Halem, Head of the Global Modeling and Simulation Branch of the NASA/Goddard Laboratory for Atmospheric Sciences, the decision was therefore made that the work under the grant would be confined to the study of land surface influences on climate.

The accomplishments under the grant are contained in the following papers, which are attached:

I. "Influence of Land-Surface Evapotranspiration on the Earth's Climate", by J. Shukla and Y. Mintz. Science, 1982, v. 215, pp 1498-1501.

II. "The Sensitivity of Numerically Simulated Climates to Land-Surface Boundary Conditions", by Y. Mintz. Chapter 6 in The Global Climate, (J. T. Hughton, editor.) Cambridge University Press, Cambridge/London/New York, 1984, pp 79-105.

III. "Precipitation Measurement Requirements for General Circulation Model Development and Applications", by Y. Mintz. Report of the Workshop on Precipitation Measurements from Space, (D. Atlas and O. W. Theile, editors.) NASA Goddard Space Flight Center, Greenbelt MD, 1981, pp D.5-D.9.

IV. "A Brief Review of the Present Status of Global Precipitation Estimates", by Y. Mintz. Report of the Workshop on Precipitation Measurements from Space, (D. Atlas and O. W. Theile), editors. NASA Goddard Space Flight Center, Greenbelt MD, 1981, pp D.1-D.4.

V. "Global Fields of Monthly Normal Soil Moisture, as Derived from Observed Precipitation and an Estimated Potential Evapotranspiration", by Y. Mintz and Y. Serafini. (Will be submitted for journal publication.)

VI. "Climatology of the Terrestrial Seasonal Water Cycle", by C. J. Willmott, C. M. Rowe and Y. Mintz. (Will be submitted for journal publication.)

VII. "Influence of the Vegetation Structure on the Thermal Forcing of the Atmosphere", by Y. Mintz. Proceedings of the JSC Study Conference on the Physical Basis for Climate Prediction on the Seasonal, Annual and Decadal Time Scales, Leningrad, 13-17 September 1982, 11 pp.

VIII. "On the Design of an Interactive Biosphere for the GLAS General Circulation Model", by Y. Mintz, P. J. Sellers and C. J. Willmott. NASA/Goddard Space Flight Center, Technical Memorandum 84973, January 1983, 54 pp.

Reprint Series
19 March 1982, Volume 215, pp. 1498–1501

SCIENCE

Influence of Land-Surface Evapotranspiration on the Earth's Climate

J. Shukla and Y. Mintz

Influence of Land-Surface Evapotranspiration on the Earth's Climate

Abstract. *Calculations with a numerical model of the atmosphere show that the global fields of rainfall, temperature, and motion strongly depend on the land-surface evapotranspiration. This confirms the long-held idea that the surface vegetation, which produces the evapotransporation, is an important factor in the earth's climate.*

That vegetation influences climate—and, especially, that the clearing of forests reduces rainfall—is an old idea. For example, the biography of Christopher Columbus by his son Ferdinand (*1*) states that "on Tuesday, July 22d [1494], he departed for Jamaica. . . . The sky, air, and climate were just the same as in other places; every afternoon there was a rain squall that lasted for about an hour. The admiral writes that he attributes this to the great forests of that land; he knew from experience that formerly this also occurred in the Canary, Madeira, and Azore Islands, but since the removal of forests that once covered those islands they do not have so much mist and rain as before."

Averaged for the globe, and for the year, the measured river water drainage from the continents is about one-third as large as the measured precipitation, which means that the average land-surface evapotranspiration is about two-thirds as large as the precipitation (*2*). In some regions, during some months of the year, the land-surface evapotranspiration is larger than the precipitation. For example, averaged over the central and eastern United States, in July, the precipitation is about 90 mm per month and the evapotranspiration is about 120 mm per month (*3, 4*). This is possible because of the moisture that was stored in the plant root zone of the soil during the preceding months of the year.

But the fact that the land-surface evapotranspiration, acting through the vegetation, sometimes exceeds the precipitation does not necessarily mean that evapotranspiration will reduce or increase the precipitation. The connection between evapotranspiration and precipitation is difficult to ascertain because it depends on a large number of interacting thermodynamic and dynamical processes, which must be taken into account in a quantitative way.

Numerical models have been developed which quantitatively synthesize the many physical processes that produce the atmospheric general circulation and global climate, including the precipitation [for example, see (*5*)]. These models fairly successfully simulate the principal geographic and seasonal characteristics of the observed precipitation: the intertropical convergence rains over South America and Africa and their seasonal displacements; the summer monsoon rains over India and southeast Asia; the deserts in subtropical north and south Africa, North America, South America, Asia, and Australia; and, in the extratropics, the rainstorms and snowstorms of the wave cyclones in winter and the airmass convective rains of summer (*6*). By using one of these numerical models of the atmosphere and prescribing the land-surface evapotranspiration in a controlled sensitivity experiment, we can determine how this boundary condition influences the model-produced climate.

For the present experiment, the current version of the Goddard Laboratory for Atmospheric Sciences (GLAS) atmospheric general circulation model is used. Starting from a given initial state, the conservation equations for mass, momentum, moisture, and energy, expressed in finite-difference form for a spherical grid, are used to calculate the evolution of the pressure field at the earth's surface and of the fields of wind, temperature, and water vapor at nine levels between the surface and an elevation of 20 km. The fields of the convective clouds and precipitation and the large-scale upglide clouds and precipitation are also calculated, with a horizontal resolution of 4° of latitude and 5° of longitude over the globe and a nearly continuous variation in time. The prescribed surface boundary conditions are the ocean surface temperature, the large-scale topography and surface roughness, the surface albedo, and, in this experiment, the amount of moisture in the soil that is available for evapotranspiration. (In other applications the model soil moisture is a dependent variable, which varies with time according to the calculated precipitation and evapotranspiration.) Shukla *et al.* (*7*) have described the current GLAS model and evaluated its

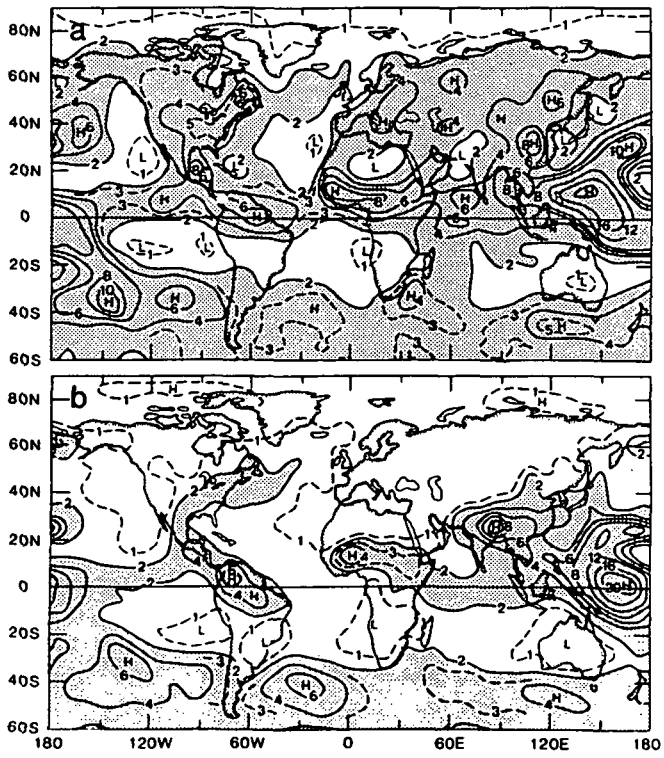

Fig. 1. Simulated July precipitation (millimeters per day) in (a) the wet-soil and (b) the dry-soil case.

0036-8075/82/0319-1498$01.00/0

ability to simulate the observed winter and summer season mean atmospheric fields and their intraseasonal variations.

We place two different constraints on the land-surface evapotranspiration: in one case the evapotranspiration is always set equal to the potential evapotranspiration calculated by the model (this is the evapotranspiration when the soil is moist and completely covered by vegetation); in the other case no evapotranspiration is allowed to take place. In principle, the first of these conditions would be physically realizable on an earth that is completely covered with vegetation and is irrigated where necessary, whereas the second would be approached on an earth that is completely and permanently devoid of vegetation. We refer to the calculations made with these two conditions as the wet-soil case and the dry-soil case.

Starting from an observed atmospheric state on 15 June, the integrations for the dry-soil and wet-soil cases were carried forward for 60 days. The results shown here are the time-averaged fields for July, the month when the Northern Hemisphere extratropics has the maximum potential evapotranspiration. An examination of the subsequent 15 days of integration, 1 to 15 August, showed that in both cases the July results had almost reached equilibrium with the prescribed boundary conditions.

Figure 1 shows the precipitation in the two cases. In the wet-soil case, the precipitation over Europe and over most of Asia is about 4 mm/day and does not differ much from the calculated potential evapotranspiration. But in the dry-soil case, Europe and most of Asia have almost no precipitation. Only over southeast Asia and India, in the dry-soil case, is there transport of water vapor from the ocean which produces heavy rain and in this case the precipitation in that region most closely resembles the observed summer rainfall.

Over most of North America the precipitation in the wet-soil case is between 3 and 6 mm/day, and for the most part it too is roughly equal to the local evapotranspiration. The exception is the southwest-northeast band of maximum rainfall across the eastern part of the continent, where there is a water vapor transport convergence of about 1 to 3 mm/day. But in the dry-soil case the precipitation over most of the continent is reduced to about 1 mm/day or less. Only the eastern part of the continent has a band of rainfall of about 2 mm/day, which consists of water transported from the ocean.

Over South America, the rainfall near the equator in the wet-soil case is about 6 mm/day, which is about 2 mm/day larger than the evapotranspiration. In the dry-soil case the rainfall is almost as large, all of it being water transported from the ocean.

Across Africa, at about 10°N, the precipitation in the wet-soil case is about 4 mm/day larger than the local evapotranspiration, but north and south of the rain band the precipitation is about 2 to 3 mm/day smaller than the evapotranspiration; this means that there are substantial convergences and divergences in the water vapor transports. In the dry-soil case, there is a band of rain of 3 to 4 mm/day centered at about 14°N, and this precipitation is about the same as the amount by which the precipitation exceeded the evapotranspiration in the wet-soil case; this means that the convergence of the water vapor transport by the atmospheric circulation is about the same in the two cases.

Figure 2 shows the calculated land-surface temperature. North of about 20°S, the land-surface temperature is about 15° to 25°C warmer in the dry-soil case. There are two reasons for this: (i) there is no evaporative cooling of the land surface (which, in the wet-soil case, amounts to 125 W/m^2 when averaged between 20°S and 60°N) and (ii) there is a large increase in the heating of the ground by solar radiation (an increase from 172 to 258 W/m^2 when averaged between 20°S and 60°N). This is because the calculated cloudiness is less when there is no land-surface evapotranspiration.

In the dry-soil case the net radiational heating of the land surface is balanced entirely by the conductive-convective transfer of sensible heat to the atmospheric planetary boundary layer, the lowest 1 to 2 km of the atmosphere. (This heat transfer to the atmosphere is 169 W/m^2 in the dry-soil case, compared to only 21 W/m^2 in the wet-soil case, when averaged for the land surface between 20°S and 60°N.) As a result, strong "thermal lows" develop over the land in the dry-soil case. Figure 3b shows these strong lows in the surface pressure reduced to sea level. The difference in the surface pressure, without reduction to sea level, is shown in Fig. 3c, and here we see the change in the geostrophic wind field at the earth's surface.

The decrease in surface pressure over the continents, about 5 to 15 mbar, is compensated by higher pressure over the oceans. But the pressure rise is not uniformly spread over the oceans. There is almost no change over the North Atlantic Ocean, and there is a large pressure rise over the mid-latitude North Pacific Ocean. The changes over the Northern Hemisphere continents and North Pacific Ocean greatly exceed the natural variability of the monthly mean July surface pressures that are produced by this general circulation model (the variability when the surface boundary conditions are held constant). In the extratropical South Atlantic and South Pacific, the

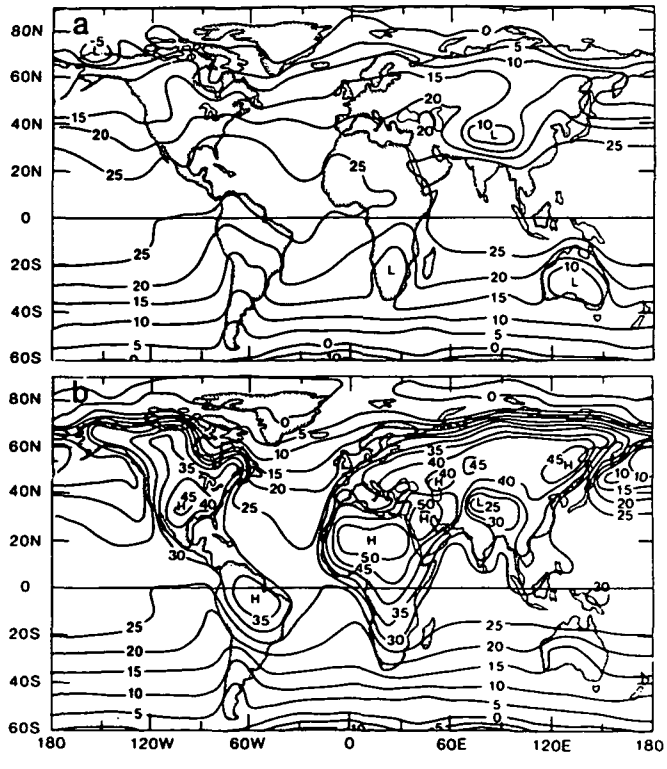

Fig. 2. Simulated July surface temperature (degrees Celsius) in (a) the wet-soil and (b) the dry-soil case.

differences in pressure between the two cases are just within the range of the natural variability of the monthly mean surface pressures produced by the model in those regions.

Examination of the vertical motion fields shows that in the dry-soil case there is an increased relative upward motion over the continents and sinking motion over the oceans. The accompanying low-level horizontal velocity convergence over the continents and divergence over the oceans generate and maintain the increased cyclonic vorticity over the continents and increased anticyclonic vorticity over the oceans. At the same time, the increased sinking motion over the oceans reduces the oceanic rainfall. But the increased rising motion over the continents does not increase the continental rainfall, because the land-surface evapotranspiration has been cut off.

There are three requirements for land-surface evapotranspiration: moisture in the soil; vegetation, to transfer the moisture from the soil to the interface with the atmosphere; and energy, to convert that moisture (water) to water vapor. Most of the energy comes from radiational heating of the surface and therefore depends on surface albedo. In nature the albedo depends on the vegetation, which in turn depends on the soil moisture. But in numerical calculations we can make these factors independent of one another. Thus, in the present experiment, we let the soil moisture change but keep the albedo constant. Charney *et al.* (*8*) (in their cases 2a, 3a, and 4) keep the soil moisture constant but let the albedo change, and that too changes the evapotranspiration, precipitation, and circulation.

Vegetation and clouds play complementary roles: the clouds convert atmospheric water vapor into liquid water, which is transferred to the soil; the vegetation converts soil water into water vapor, which is transferred to the atmosphere. In the extratropics, with its large seasonal changes, the soil plays a role analogous to that of the ocean. The ocean stores some of the radiational energy it receives in summer and uses it to heat the atmosphere over the ocean in winter. The soil stores some of the precipitation it receives in winter and uses it to humidify the atmosphere in summer.

If our calculations are indeed applicable to nature, the implication for forecasting extratropical summer rainfall is clear. In about the month of May the continental rainfall changes from the large-scale upglide condensation type to the cumulus convection type. If, after this change takes place, there is a large amount of moisture stored in the soil, the summer months that follow can have a large or small amount of rainfall, depending on the circulation conditions. But if the soil is dry, so that there is little or no evapotranspiration to keep the atmospheric planetary boundary layer moist, the remaining summer months will have little rainfall. Surface evapotranspiration, which requires moisture in the soil, is a necessary (though not sufficient) condition for extratropical summer precipitation. Observations of the soil moisture are therefore necessary for the precipitation predictions.

Finally, on the questions of whether the earth's vegetation cover and its modification by man have a significant influence on climate, and whether deforestation and afforestation, soil destruction and soil reclamation, or crop irrigation appreciably affect rainfall; the answer given by this study is that they do, if they are of large magnitude and large horizontal extent. But the exact response will vary from region to region, depending on how the large-scale circulation is modified.

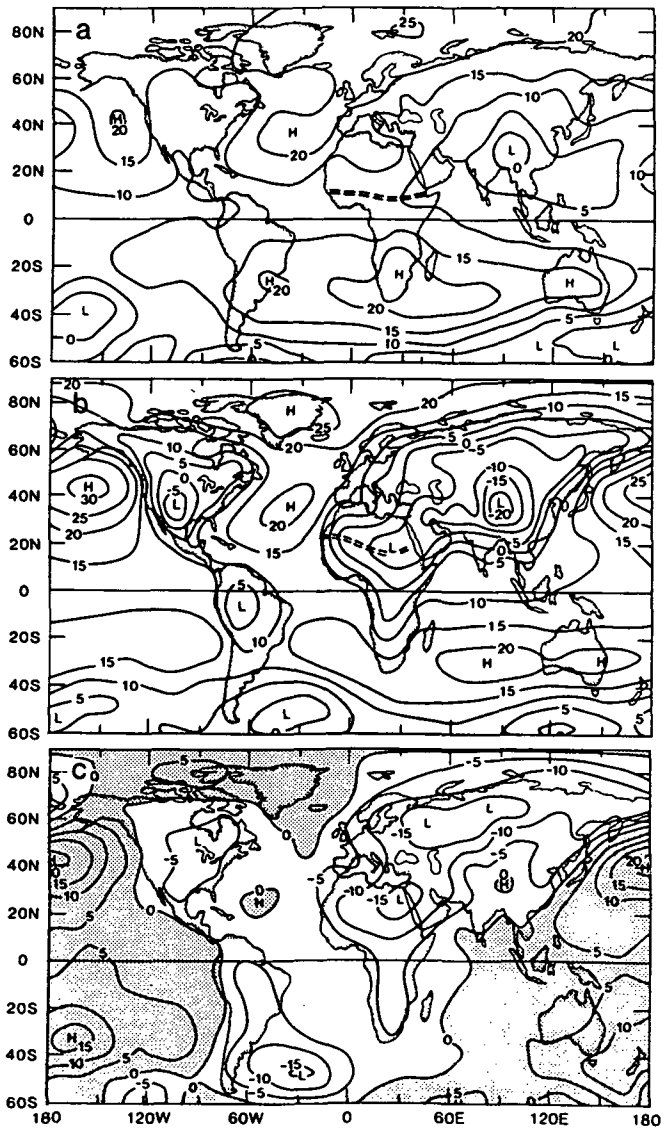

Fig. 3. Simulated July surface pressure reduced to sea level (millibars minus 1000) in (a) the wet-soil case and (b) the dry-soil case. (c) Difference between the surface pressure in the two cases.

J. SHUKLA
Laboratory for Atmospheric Sciences, NASA/Goddard Space Flight Center, Greenbelt, Maryland 20771
Y. MINTZ
Laboratory for Atmospheric Sciences, NASA/Goddard Space Flight Center, and *Department of Meteorology, University of Maryland, College Park 20771*

References

1. F. Colon, *The Life of Christopher Columbus by His Son Ferdinand*, translated and annotated by B. Keen (Rutgers Univ. Press, New Brunswick, N.J., 1959), pp. 142–143.
2. H. Baumgartner and E. Reichel, *The World Water Balance: Mean Annual Global Continental and Maritime Precipitation, Evaporation and Runoff* (Elsevier, Amsterdam, 1975).
3. J. R. Mather, *Publ. Climatol.* **17**, 3 (1964).
4. E. M. Rasmusson, *Mon. Weather Rev.* **96**, 720 (1968).
5. J. Chang, Ed. *Methods in Computational Physics*, vol. 17, *General Circulation Models of the*

Atmosphere (Academic Press, New York, 1977).
6. WMO/ICSU, *Report of the Joint Organizing Committee Study Conference on Climate Models: Performance, Intercomparison and Sensitivity Studies* [GARP (Global Atmospheric Research Program) Publication Series 22, World Meteorological Organization, Geneva, 1979], vol. I.
7. J. Shukla, D. Randall, D. Straus, Y. Sud, L. Marx, *Winter and Summer Simulations with the GLAS Climate Model* (National Aeronautics and Space Administration/Goddard Space Flight Center, Greenbelt, Md., in press).
8. J. Charney, W. J. Quirk, S. H. Chow, J. Kornfield, *J. Atmos. Sci.* 34, 1366 (1977).

2 December 1981

The sensitivity of numerically simulated climates to land-surface boundary conditions†

Yale Mintz
Department of Meteorology, University of Maryland, College Park, MD 20742
and Laboratory for Atmospheric Sciences, NASA Goddard Space Flight Center, Greenbelt, MD 20771

Abstract

This review describes, interprets, and compares 11 sensitivity experiments that have been made with general circulation models to see how land-surface boundary conditions can influence the rainfall, temperature, and motion fields of the atmosphere. In one group of experiments, different soil moistures or albedos are prescribed as time-invariant boundary conditions. In a second group, different soil moistures or different albedos are initially prescribed, and the soil moisture (but not the albedo) is allowed to change with time according to the governing equations for soil moisture. In a third group, the results of constant versus time-dependent soil moistures are compared.

All of the experiments show that the atmosphere is sensitive to the land-surface evapotranspiration: so that changes in the available soil moisture or changes in the albedo (which affects the energy available for evapotranspiration) produce large changes in the numerically simulated climates.

6.1 Introduction

6.1.1 *Some observational and theoretical considerations*

Averaged for the globe and for the year, the measured river water drainage from the continents is about a third as large as the measured precipitation (Baumgartner & Reichel, 1975, Table 9; Korzun, 1978, Table 150). This means that on the average the land-surface evapotranspiration is about two-thirds as large as the precipitation.

In some continental regions, during part of the year, the evapotranspiration is larger than the precipitation. This cannot be known from measurements of river flow, but can be derived from measurements of the transport of water vapor by the atmosphere. An example of this for the central and eastern United States, in July, is shown in Fig. 6.1.

On the left in the diagram is the vertical distribution of the water vapor transport divergence, as given by twice daily rawinsonde measurements for two July months, and averaged for the region 80–100°W, 30–47.5°N, which is an area of about (2000 km)^2 (Rasmusson, 1968, Table 1 and Fig. 2). From the surface to the 930 mb level there is a water vapor transport convergence of 1.4 gm/cm^2 per month: or 14 mm/month equivalent water depth. Above the 930 mb level there is divergence of 36 mm/month. Integrated over the entire depth of the atmosphere there is a net divergence (a net removal of water from the region) of 22 mm/month.

From the beginning to the end of July the change in the water vapor content of the atmosphere is very small. Therefore, the 22 mm of water that are removed from the region must come from the water stored in the soil, which means that the evapotranspiration

† Review paper presented at the *JSC Study Conference on Land Surface Processes in Atmospheric General Circulation Models*, Greenbelt, USA, 5–10 January 1981

is 22 mm/month larger than the precipitation. Inasmuch as the measured average July precipitation in this region is about 94 mm/month, the average July evapotranspiration must be about 116 mm/month (3.7 mm/day). (A comparable analysis for the central and eastern United States by Benton *et al.* (1953, Figs. 24, 26) gave a July evapotranspiration of 121 mm/month (3.9 mm/day).) We can interpret this water budget as follows:

The net radiational heating of the ground in this region, in July, is about 140 watt/m² (Budyko, 1963, Plate 21), which if used entirely for evapotranspiration would put about 150 mm/month (4.8 mm/day) of water into the air. But if we accept the aerologically derived evapotranspiration of 3.7 mm/day (LE = 107 watt/m²), there will be a sensible heat transfer from the ground to the atmosphere, $H = (R_N - LE) = (140 - 107) = 33$ watt/m²; and a Bowen ratio, (H/LE), equal to 0.31. Here, L = latent heat of evapotranspiration, E = evapotranspiration rate.

The 116 mm/month of water vapor, forced into the atmospheric planetary boundary layer by the radiational heating of the surface, combines with the 14 mm/month brought into the region by the water vapor transport convergence in the boundary layer; and the total of 130 mm/month of water vapor are transferred from the boundary layer to the free atmosphere.

In July, the condensation and precipitation in this region is predominantly of the convective type, with relatively little large-scale upglide condensation and precipitation. Therefore, the transfer of water vapor upward from the surface is predominantly by small-scale turbulent mixing within the planetary boundary layer, with a handover to cumulus convection which carries the water vapor from the top of the boundary layer into the free atmosphere.

Of the 130 mm/month of moisture carried into the free atmosphere by the cumulus cloud towers, 36 mm/month (in the form of water vapor, liquid water droplets and ice crystals) are detrained from the clouds into the cloud environment (where the water droplets and ice crystals evaporate) and are removed from the region by the divergence of the water vapor transport in the free atmosphere. The remaining 94 mm/month return to the earth's surface as the convective precipitation. The excess of the evapotranspiration over the precipitation, 22 mm/month, is the moisture withdrawn from the soil.

According to this analysis, the convective precipitation draws all of its moisture from the water vapor in the planetary boundary layer; and the amount of water vapor supplied to the boundary layer by the surface evapotranspiration is an order of magnitude larger than the amount supplied by the water vapor transport convergence. This suggests that the surface evapotranspiration is the main determinant of the precipitation.

The winter season water budget over the central and eastern United States is very different from that shown in Fig. 6.1. In winter the water vapor transport convergence does not change sign with height, but is convergent at all levels and produces a net import of water vapor to the region (Rasmusson, 1968, Table 1 and Fig. 2). In winter, the condensation and precipitation is predominantly of the large-scale upglide condensation type (frontal cloud and precipitation) which draws from the water vapor at all levels in the troposphere. Moreover, in winter the net radiational heating of the ground is small (Budyko, 1963, Plate 15) and, consequently, over the unforested part of this region the evapotranspiration is small. In winter, therefore, the land-surface evapotranspiration cannot have much influence on the precipitation or other fields. It is only in the tropics and in the summer season extratropics, where evapotranspiration is large and where the precipitation is of the type that draws its water vapor from the planetary boundary layer, that the land-surface evapotranspiration can be of major importance.

With respect to the tropics and the summer season extratropics, two questions immediately come to mind:

(i) If the surface evapotranspiration, by some means, is greatly reduced, can the boundary layer water vapor transport

Fig. 6.1. Water budget (mm/month) for central and eastern United States, in July. Divergence of the water vapor transport is from Rasmusson (1968).

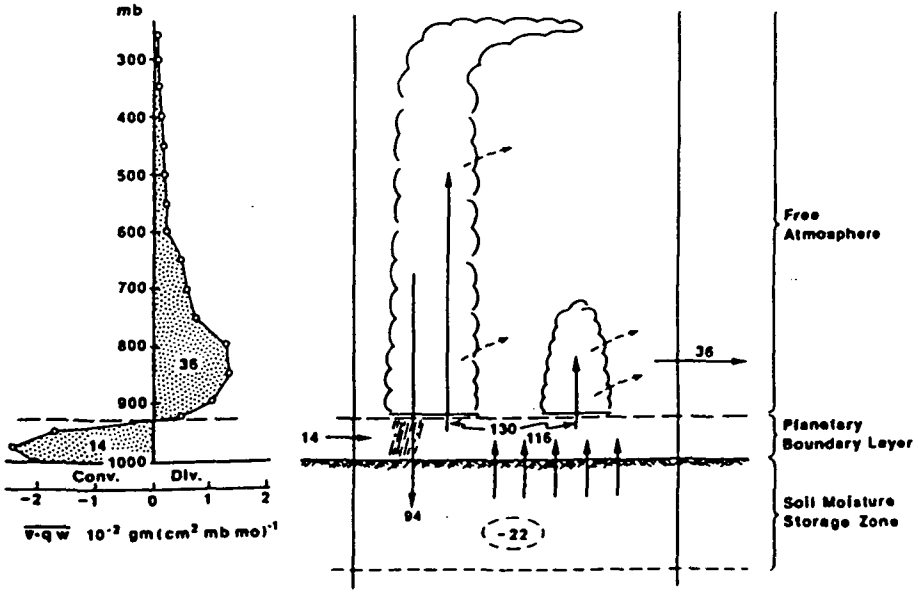

convergence increase by a corresponding amount and, in that way, maintain the precipitation?

(ii) If the surface evapotranspiration and the boundary layer water vapor transport convergence remain the same, can an increased detrainment and water vapor transport divergence in the free atmosphere stop the precipitation?

• To answer the first question, we write the water vapor transport convergence as $-\nabla\cdot q\mathbf{v} = -\mathbf{v}\cdot\nabla q - q\nabla\cdot\mathbf{v}$, where q is the water vapor mixing ratio and $\mathbf{v}$ is the horizontal velocity of the air.

The quantity $-\mathbf{v}\cdot\nabla q$ is positive when the air that leaves the region is drier than the air that enters. But if this drying is due to the removal of water vapor from the boundary layer by cumulus convection, then the convection will stop as soon as there is a small reduction in the boundary layer water vapor content. The observed rate of precipitation cannot be maintained by $-\mathbf{v}\cdot\nabla q$ over a distance which is greater than just a few cumulus convection cells, say a total distance of a few kilometers.

The other term, $-q\nabla\cdot\mathbf{v}$, can also maintain the observed rate of precipitation only over a restricted domain in the extratropics. The water vapor mixing ratio in the boundary layer of a maritime tropical air mass over the extratropical continents in summer, is of the order of ten parts per thousand. Therefore, a boundary layer that is 100 mb (1 km) deep must have a horizontal velocity convergence, $-\nabla\cdot\mathbf{v}$, of 0.37/day (0.43×10^{-5}/second) to produce a water vapor transport convergence of 3·7 mm/day. The characteristic velocity of the boundary layer air in the extratropics, in summer, is 2–3 m/second; and the angle between this vector velocity and the streamline of the non-divergent flow, integrated over the depth of the boundary layer, is about 10°. Thus, if we consider a circular region with radius r, we have $-\nabla\cdot\mathbf{v} = 0.43\times10^{-5}$ second = (3 m/second sin 10°) $2\pi r/\pi r^2$; or $r = 240$ km, and 480 km is the limiting diameter of the region where water vapor transport convergence in the boundary layer can produce the observed rate of precipitation.

In the extratropics, therefore, there is a size limit, of the order of a few hundred kilometers, beyond which boundary layer water vapor transport convergence cannot compensate for diminished evapotranspiration. It is only near the equator, where the divergent component of the velocity field is larger and the planetary boundary layer is deeper, that there can be appreciable water vapor transport convergence over a much larger sized area.

•• The answer to the second question: 'Can an increased detrainment and water vapor transport divergence in the free atmosphere stop the precipitation?', depends on whether the free atmosphere is supplied with dry air into which the cumulus cloud towers can detrain. That will happen only if, in addition to the boundary layer mass (and water vapor) convergence, there is also a mass convergence in the uppermost troposphere. Then, the cumulus cloud towers can detrain all of the water into the subsiding and diverging dry air of the middle troposphere, and not produce any precipitation at all. The best known example of extensive fields of non-precipitating cumulus clouds of this kind are the Trade Wind cumuli over the tropical oceans, where the subsiding air in the middle troposphere has its origin in the high-level outflow above the intertropical convergence zone. We also see such fair-weather cumulus clouds removing water vapor from the boundary layer, without producing precipitation, west of the trough lines and east of the ridge lines of the fast-transient and slow-transient waves in the extratropical westerlies, where both the longitudinal and the latitudinal scale can be as large as a few thousand kilometers. We can say, therefore, that on a scale larger than a few hundred kilometers, in the extratropics, land-surface evapotranspiration is a necessary (but not sufficient) condition for convective precipitation. The upper tropospheric circulation must also be favorable for precipitation.

Because so many interactive thermodynamical and hydrodynamical processes are involved, the best way to determine the overall influence of the land-surface boundary conditions on the rainfall, temperature and circulation is through experiments with atmospheric general circulation models. Existing general circulation models have been fairly successful in simulating the observed climate of the earth, including the principal geographical and seasonal characteristics of the precipitation (WMO, 1979). By making pairs of time-integrations, with all of the initial conditions and boundary conditions the same except for those which can affect the land-surface evapotranspiration, and comparing the two solutions, we can ascertain what the land-surface influence is.

In the existing general circulation models, the two boundary conditions that can affect the land-surface evapotranspiration are the soil moisture and the surface albedo. The soil moisture determines how large the evapotranspiration will be relative to the model calculated potential evapotranspiration (the evapotranspiration when soil moisture is fully available): the albedo is a major factor in determining the potential evapotranspiration itself.

The experiments that are being reviewed are grouped as follows:

(i) experiments with non-interactive soil moisture;
(ii) experiments with interactive soil moisture;
(iii) hybrid experiments.

In the first group, either different soil-moisture availabilities or different albedos are prescribed, and both of these parameters are kept constant with time. Such experiments reveal the sensitivity of the atmosphere to the boundary conditions. (These experiments are analogous to sensitivity experiments in which different non-interactive ocean-surface temperatures are prescribed: the so-called sea-surface temperature anomaly experiments).

In the second group, the soil moisture (but not the albedo) is interactive and changes with time according to the model's governing equations for soil moisture. When the albedos are the same in a pair of comparison runs, but the initial soil moistures are different, the integrations will either produce time-series that remain separate (intransitive) or converge to a common solution; and, if transitive, they will show how long it takes for the two initially different states to converge to a common state. When the albedos are different, this will be another kind of sensitivity experiment.

In the third group, the hybrid experiments, calculations with non-interactive and interactive soil moistures are compared. To the extent that the calculation with interactive soil moisture simulates the observed rainfall, temperature and circulation of the earth's atmosphere, the comparison will show how the earth's climate may be affected by such imposed changes in the land-surface evapotranspiration as might be brought about by large-scale

deforestation or afforestation, by soil erosion or reclamation, or by large-scale irrigation.

6.2

List of the experiments

(I) ***Experiments with non-interactive soil moisture***

(A) *Different soil moistures, with same albedo*

(1) Shukla & Mintz (1981)

(2) Suarez & Arakawa (personal communication)

(3) Miyakoda & Strickler (1981)

(B) *Different albedos, with same soil moisture*

(4) Charney, Quirk, Chow & Kornfield (1977)

(5) Carson & Sangster (1981)

(II) ***Experiments with interactive soil moisture***

(A) *Different initial soil moistures, with same albedo*

(6) Walker & Rowntree (1977)

(7) Rowntree & Bolton (1978)

(B) *Different albedos, with same initial soil moisture*

(8) Charney, Quirk, Chow & Kornfield (1977)

(9) Chervin (1979)

(III) ***Hybrid experiments***

Non-interactive v. interactive soil moistures

(10) Manabe (1975).

(11) Kurbatkin, Manabe & Hahn (1979)

6.3

(I) Experiments with non-interactive soil moisture

6.3.1

(A) *Different soil moistures, with same albedo*

6.3.1.1

Shukla and Mintz (1981)

The experiment of Shukla & Mintz (1981) used the general circulation model of the NASA Goddard Space Flight Center, Laboratory for Atmospheric Sciences. The properties of the GLAS model and its ability to simulate the regional and season characteristics of the observed climate of the earth have been described by Shukla *et al.* (1981). In the experiment, one climate simulation is made in which the land-surface evapotranspiration, E, is everywhere made equal to the model calculated potential evapotranspiration, E_p, which makes the evapotranspiration coefficient, $\beta = E/E_p = 1$. In the other case, no land-surface evapotranspiration is allowed to take place at all ($\beta \equiv 0$). The prescribed albedo is the same in both cases, and is a very slightly modified version of the one given by Posey & Clapp (1964). For convenience, the two calculations are called the 'wet-soil' case and the 'dry-soil' case. Both calculations were started from the same initial observed atmospheric state on 15 June. The results that are shown here are the averages for July.

In the wet-soil case, the calculated land-surface evapotranspiration is relatively constant (within about ± 1 mm/day) between latitudes 20°S and 60°N, with an average value of 4.3 mm/day, corresponding to an evaporative cooling of the surface of 125 watt/m², as shown in Fig. 6.2. Here, the sensible heat transfer to the atmosphere is 21 watt/m². In the dry-soil case, however, the land-surface evapotranspiration is zero and the sensible heat transfer is 169 watt/m².

The dry-soil case gives rise to much less cloudiness over the continents than the wet-soil case and, as a result, a larger amount of solar radiation reaches and is absorbed by the ground, 258 instead of 172 watt/m². The increased solar heating of the ground, as well as the elimination of the evaporative cooling, makes the ground warmer; and the higher ground temperature produces a greater long wave radiation emission from the ground, 550 instead of 419 watt/m². The atmosphere also becomes warmer in the dry-soil case, and there is an increase in the atmospheric long wave 'back radiation' to the ground; but because of the reduction in the cloudiness, the increase in the back radiation, from 393 to 461 watt/m², is only about half as large as the increase in the radiation emitted by the ground. The end result of all these large, but partially compensating, changes in the radiation transfers, is that there is only a relatively small change in the net (all-wavelength) radiational heating of the land surface: an increase of only 23 watt/m² from the wet-soil to the dry-soil case.

The top panel of Fig. 6.3 shows the global precipitation distribution in the wet-soil case. Over most of North America and most of Eurasia the precipitation is within about 1 mm/day of the local evapotranspiration. Only over southeast China does the precipitation exceed evapotranspiration by as much as 4 mm/day. Over South America there is heavy rain near the equator, which is about 2 mm/day greater than the land-surface evapotranspiration. Across Africa, at about 10°N, there is a band of rain which is about 4 mm/day greater than the local evapotranspiration. On the other hand, across Africa at about 25°N, and across Africa and South America at about 15°S, the precipitation is 2–3 mm/day smaller than the evapotranspiration. Thus, although in the wet-soil case there is a fairly uniform transfer of water vapor to the air by the land-surface evapotranspiration, within the tropics and subtropics there are convergences and divergences of the water vapor transports by the large-scale atmospheric circulation, which enhance or diminish the precipitation by substantial amounts.

The dry-soil case, shown in the bottom panel of Fig. 6.3,

Fig. 6.2. Surface energy transfers (watt/m²) averaged for the continents between 20°S and 60°N, in experiment of Shukla and Mintz (1981).

R_S solar raditional heating of the ground.

R_L long wave radiational cooling of the ground (difference between radiation emitted by ground and radiation absorbed by ground).

$R_N = (R_S - R_L)$ net (all-wavelength) radiational heating of the ground.

LE latent heat transfer from ground to atmosphere (evaporative cooling of the ground).

H conductive-convective heat transfer from ground to atmosphere.

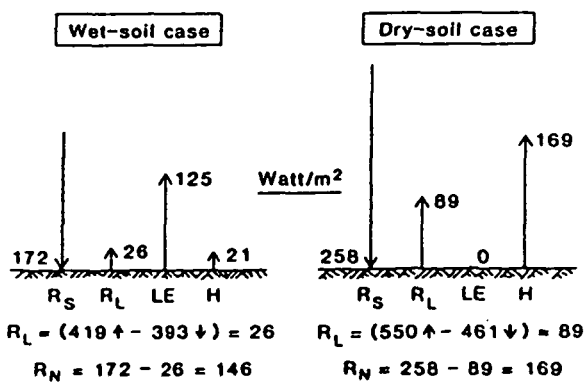

produces almost no precipitation at all over Europe and most of Asia; and over most of North America the precipitation is only about a quarter to a half of that of the wet-soil case. Over the equatorial part of South America, on the other hand, the rainfall in the dry-soil case is about the same as in the wet-soil case: i.e., about 6 mm/day; but, now, the water vapor which produces that precipitation comes only from the ocean.

Across north Africa, the rainband is about 400 km (one model grid interval) farther north in the dry-soil case than in the wet-soil case, and weaker by 3–4 mm/day. The precipitation in the dry-soil case is about the same as the amount by which the precipitation exceeded evapotranspiration in the wet-soil case: which is to say that the convergence of the water vapor transport by the atmospheric circulation is about the same in the two cases.

Perhaps the most surprising difference of all, when comparing the dry-soil case with the wet-soil case, is the southward and westward displacement of the region of maximum precipitation in southeast Asia. Over Bangladesh, the convergence in the water vapor transport from the ocean in the dry-soil case more than compensates for the absence of surface evapotranspiration. It is in the dry-soil case that the calculated precipitation most closely resembles the observed summer rainfall of southeast Asia.

Fig. 6.4 shows the ground-surface temperature. In the dry-soil case, in which there is no evaporative cooling of the ground and, because of the reduced cloudiness, more solar radiation is absorbed by the ground, the surface temperatures north of latitude 20°S are about 15°–30°C warmer than in the wet-soil case.

As shown in Fig. 6.2, the total non-radiational heat transfer to the atmosphere ($H+LE$) is not greatly different in the two cases (146 v. 169 watt/m^2); but in the dry-soil case all of this is sensible heat transfer, which is confined to the planetary boundary layer. In the wet-soil case, by contrast, the larger part of the transfer is in the form of latent heat which warms the free atmosphere and not the boundary layer, whether immediately and locally realized by convective condensation and precipitation or realized at some later time and distant place. Thus, there is a different vertical distribution, and sometimes a different horizontal distribution, of the diabatic heating. This can produce significant differences in the thermally forced atmospheric circulation and, by the geostrophic adjustment process, corresponding differences in the horizontal pressure distribution.

Fig. 6.5 shows the surface pressure fields. The top and center

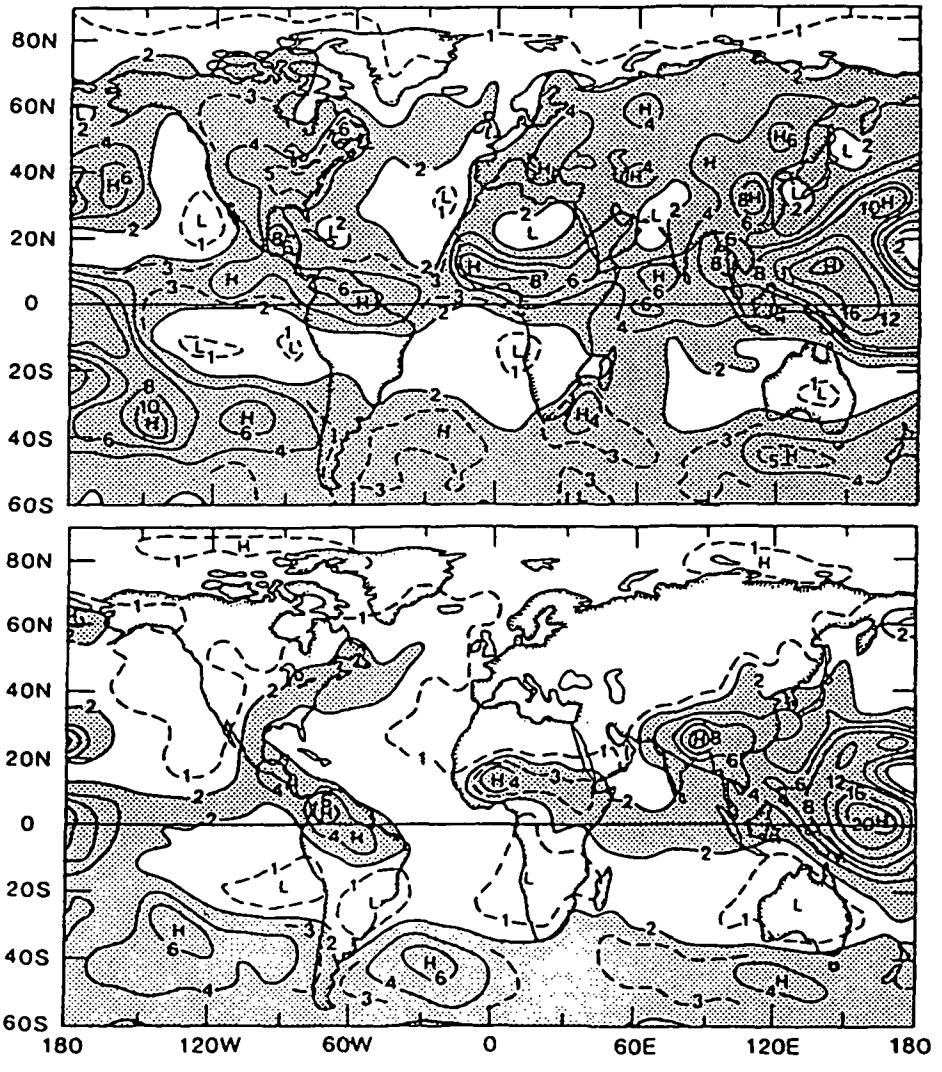

Fig. 6.3. Precipitation (mm/day) in wet-soil case (top) and dry-soil case (bottom), in experiment of Shukla & Mintz (1981). (Precipitation greater than 2 mm/day is shaded.)

panels show the surface pressures reduced to sea level, in the two cases. The bottom panel shows the difference between the two surface pressures, without reduction to sea level. It is here that we see the change in the surface geostrophic wind. Over most of the land the surface pressures are about 5–15 mb lower in the dry-soil case, which means enhanced cyclonic circulations over the continents.

In the wet-soil case the trough of low pressure across Africa coincides with the intertropical rainband, as may be seen by comparing the top panels of Figs. 6.3 and 6.5. This is the same relationship that we see over the tropical oceans. But in the dry-soil case the trough of low pressure is about 400–800 km north of the rainband; which is about the same relationship that is found over north Africa, in nature.

When the surface pressure is lower over the continents, it must be higher over the oceans. Most of the increase is in the mid-latitudes of the central and western North and South Pacific Oceans. Examination of the vertical motion field (not reproduced here) shows that in these ocean regions there is an increased subsiding motion in the dry-soil case. As Figs. 6.3 and 6.5 show, not only does the increased sinking motion suppress the oceanic precipitation, but the accompanying low-level horizontal velocity divergence, by generating anticyclonic vorticity, increases the anticyclonic circulation in these regions; and geostrophic adjustment produces the corresponding rise in surface pressure.

Over the Atlantic Ocean, the vertical motion field in the wet-soil case shows a band of rising motion and low-level velocity convergence, which coincides with the band of oceanic precipitation just north of the equator (top panel of Fig. 6.3). But in the dry-soil case there is sinking motion over all of the tropical Atlantic; and there is no oceanic rainband near the equator at all. Over the eastern half of the tropical Pacific, the same kind of change takes place, but it is not as pronounced. Thus, the change in the land-surface boundary condition also produces large changes in the circulation and rainfall over the oceans.

Fig. 6.4. Ground-surface temperature (°C) in wet-soil case (top) and dry-soil case (bottom), in experiment of Shukla & Mintz (1981).

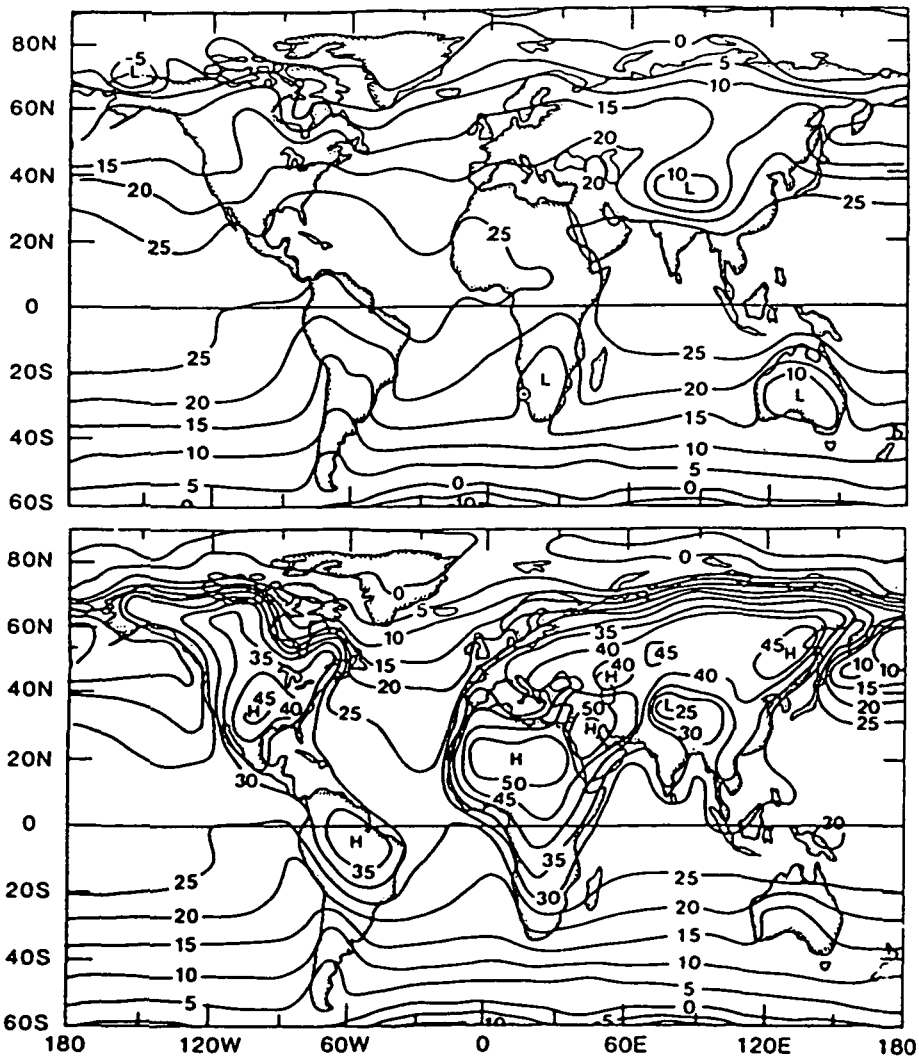

6.3.1.2

Suarez and Arakawa (personal communication)

At the reviewer's suggestion, the same wet-soil ($\beta = 1$) versus dry-soil ($\beta = 0$) sensitivity experiment was made with the University of California, Los Angeles (UCLA) general circulation model by M. Suarez & A. Arakawa (personal communication). (For a description of the model, see Arakawa & Lamb, 1977; Arakawa & Suarez, 1983; and Suarez *et al.* 1983.) There are substantial differences between the UCLA and the GLAS models, of which the most important, insofar as the present sensitivity experiment is concerned, may be the way in which the planetary boundary layer and cumulus convection are parameterized.

In the UCLA experiment the integrations for the two cases were started on the first day of July, with the initial state of the atmosphere taken from a previous general circulation simulation.

Fig. 6.5. Surface pressure reduced to sea level (mb minus 1000) in wet-soil case (top) and dry-soil case (center), in experiment of Shukla & Mintz (1981). Bottom map show the difference between the two surface pressures (mb).

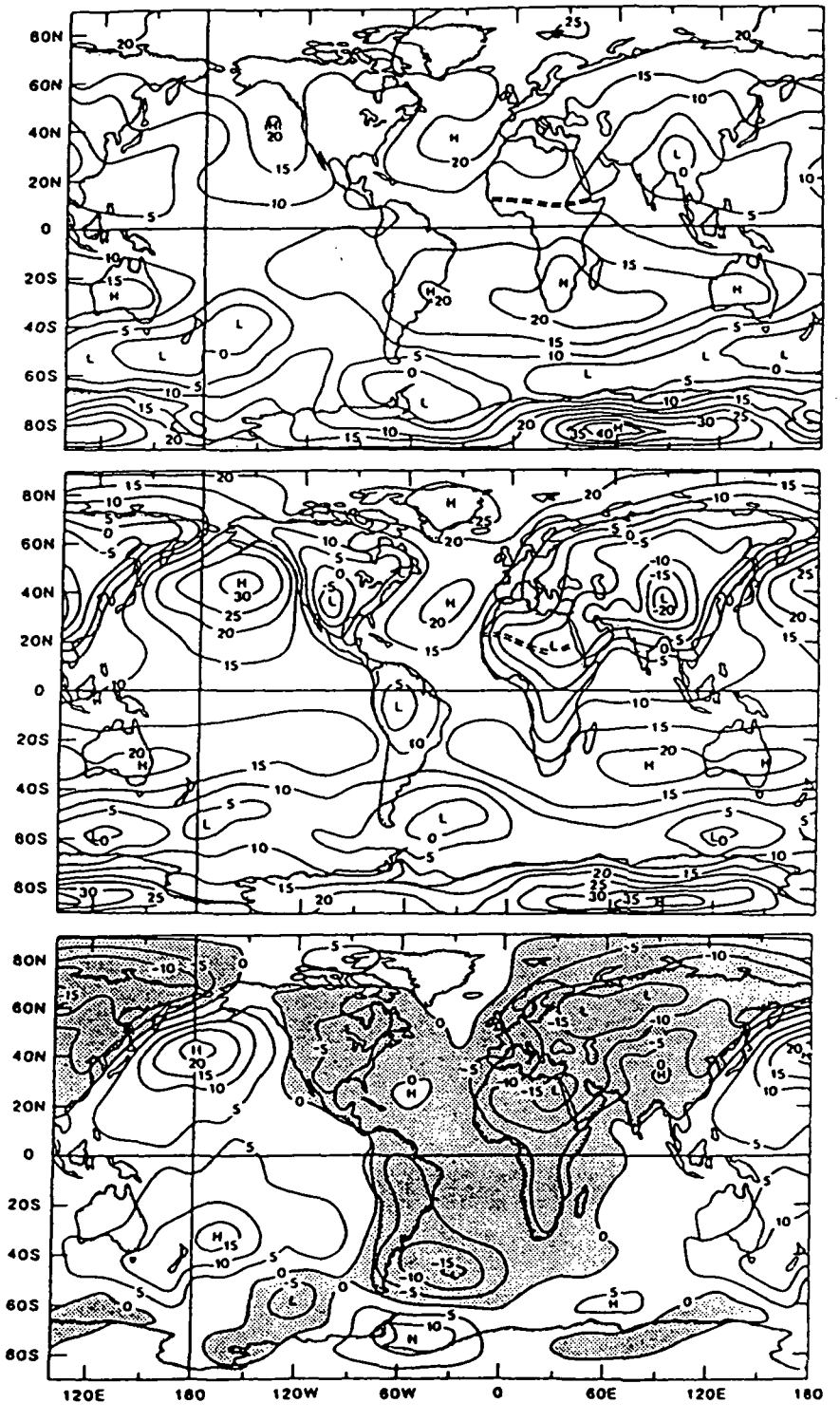

The results that are shown here are for the 31-day period starting on 16 July. Again, the prescribed surface albedo follows Posey & Clapp (1964).

In the wet-soil case, the calculated land-surface evapotranspiration was relatively constant (within about ± 1 mm/day) between 20°S and 60°N, with an average value of about 6 mm/day. This is about 1.7 mm/day larger than in the wet-soil case of the GLAS experiment, and is probably a consequence of the fact that the UCLA model produces less cloud cover than does the scheme used in the GLAS model and, thereby, a greater net radiational heating of the ground.

Fig. 6.6 shows that the precipitation in the wet-soil case is about 6 ± 1 mm/day over almost all of extratropical North America and Eurasia and, therefore, does not differ from the local evapotranspiration by more than about 1 mm/day. Within the tropics, however, the precipitation exceeds the local evapotranspiration by about 10 mm/day over the Indochina peninsula, by about 3–6 mm/day over a few small land areas that are close to the sea (Guatemala, southern India, southeast China, Columbia, Venezuela and northeast Brazil), and by a few mm/day over a large area adjacent to the Somali coast of north Africa. These are regions, therefore, of substantial water vapor transport convergences.

In the dry-soil case, shown in the bottom panel of Fig. 6.6, there is almost no continental precipitation at all. Only in an east–west band across north Africa is there a significant amount of precipitation, 2–5 mm/day, produced by a convergence of the water vapor transported from the oceans. The axis of this rainband, at 10°N, is about 1000 km south of the axis of the low-pressure trough which, in the dry-soil case, is at about 20°N.

The change in the precipitation over the oceans is very large near some of the tropical and subtropical coastlines, and especially where there are embayments. In the wet-soil case there are pronounced minima over the Gulf of Mexico and the Bay of Bengal

Fig. 6.6. Precipitation (mm/day) in wet-soil case (top) and dry-soil case (bottom), in the experiment of Suarez & Arakawa (personal communication). Contour interval is 2 mm/day. (Precipitation greater than 2 mm/day is shaded.)

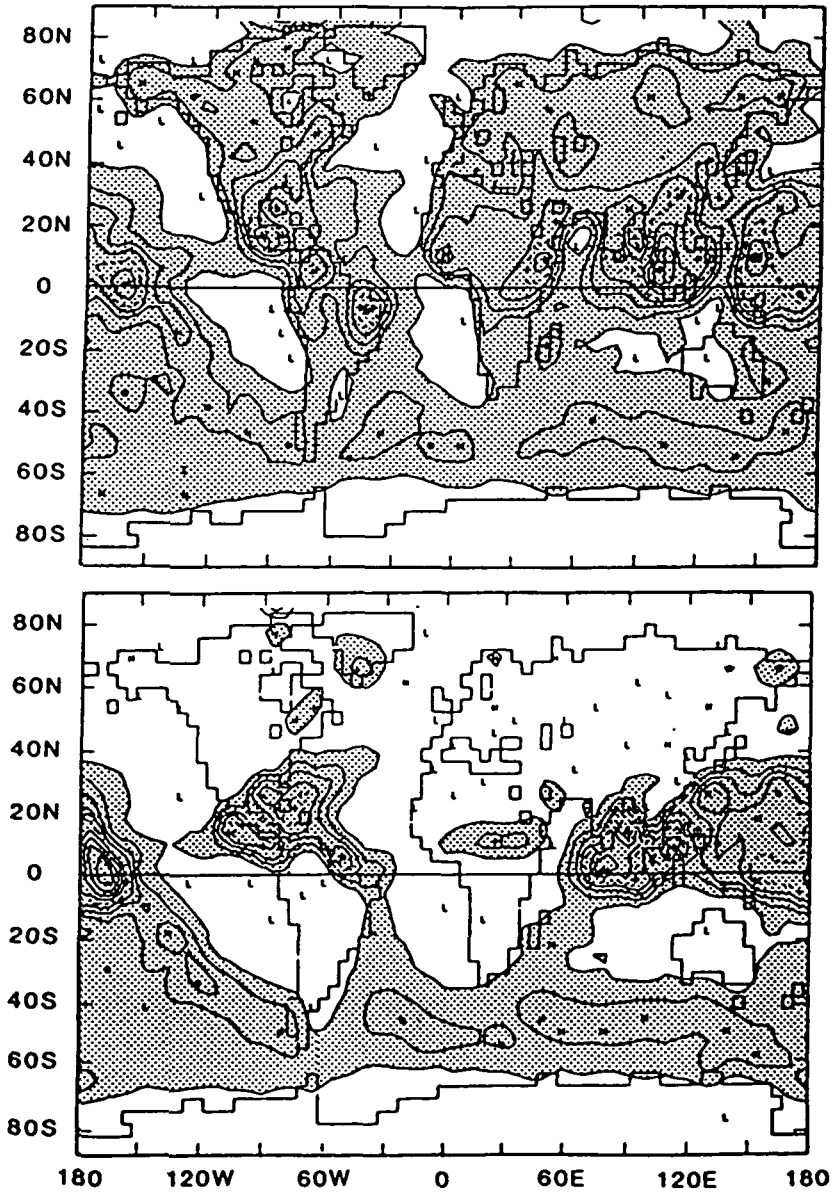

(accompanied by pronounced maxima over the adjacent land areas). But in the dry-soil case, the minima are replaced by maxima over the ocean embayments. Similarly, along the coasts of central America and northeast Brazil the land precipitation decreases and the nearshore ocean precipitation increases in going from the wet-soil to the dry-soil case.

The striking difference between the experiments with the UCLA model and those with the GLAS model is that, except for the Sahel region of Africa, the UCLA model produces almost no continental precipitation in the dry-soil case.

Examination of the water vapor transport field by the investigators showed that there are regions, such as northeast Brazil, where within the planetary boundary layer there is a large convergence of the water vapor transported from the ocean, in the dry-soil case, but no rain. The interpretation they made (Suarez & Arakawa, personal communication) is that with dry soil there is a very large diurnal variation of the ground-surface temperature, which produces a very large diurnal variation in the depth of the model's planetary boundary layer, growing in thickness during the day and collapsing at sunset; and that it is this diurnal oscillation which, without producing clouds, transfers the water vapor from the boundary layer to the free atmosphere, where the transport is divergent. This transfer of water vapor from the boundary layer to the free atmosphere by diurnal 'boundary layer–free atmosphere mixing' is not unlike the transfer by detrainment from fair-weather, non-precipitating cumulus clouds, described in the introduction. The same condition of upper troposphere velocity convergence and middle troposphere subsidence must be satisfied. Here it is the result of upper-level outflow from the region of intense convective precipitation over the adjacent ocean.

Fig. 6.7. Soil moisture availability, β, in July, as derived from antecedent 6 month precipitation. (From Miyakoda, *et al.*, 1979.)

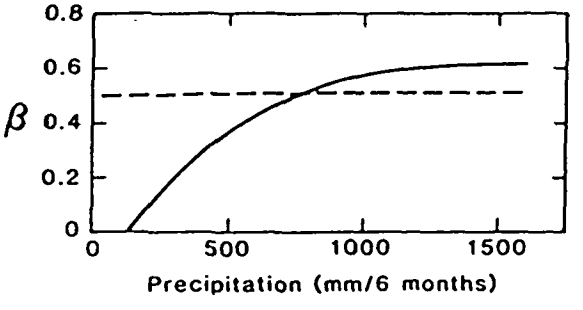

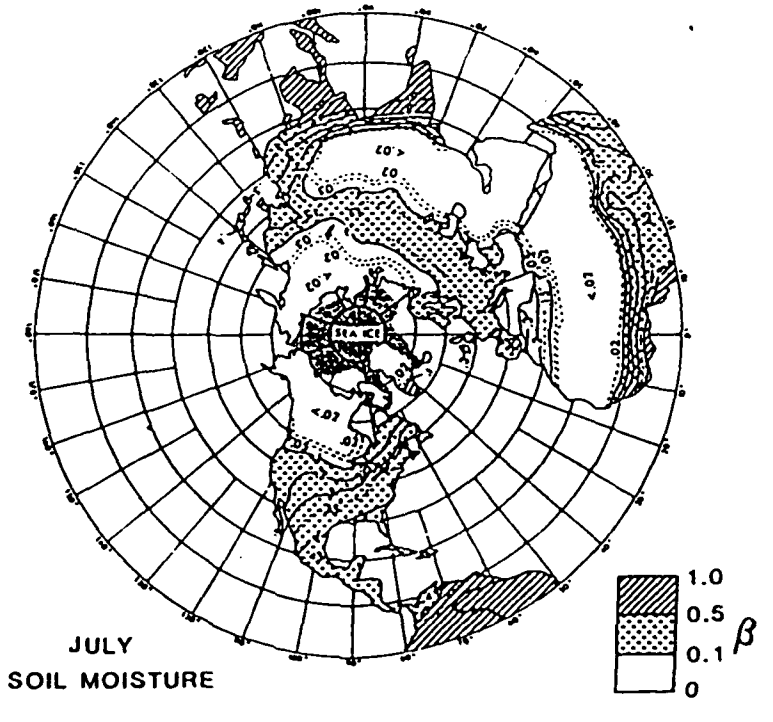

6.3.1.3

Miyakoda and Strickler (1981)

Miyakoda & Strickler (1981) used an early version of the general circulation model of the NOAA–Princeton Geophysical Fluid Dynamics Laboratory (Smagorinsky *et al.*, 1969) to make and compare two different sets of 14-day numerical weather predictions for the northern hemisphere, in July, when different distributions of the soil moisture availability, β, were prescribed.

The surface albedo was fixed and followed Posey & Clapp (1964). The clouds were climatologically prescribed as a function of latitude and height. The convective-adjustment scheme was used, in which the moist convective heating of the atmosphere and the convective precipitation depend only on the relative humidity and on the temperature difference between adjacent levels in the vertical. Thus there is no penetrative convection and, consequently,

Fig. 6.8. Evapotranspiration difference (top) and precipitation difference (bottom), when $\beta \equiv 0.5$ is replaced by $\beta(\lambda, \phi)$, in experiment of Miyakoda & Strickler (1981). (Contours for 0, ∓25, ∓100, ∓200, ∓500 mm/mo. Negative values are shaded.)

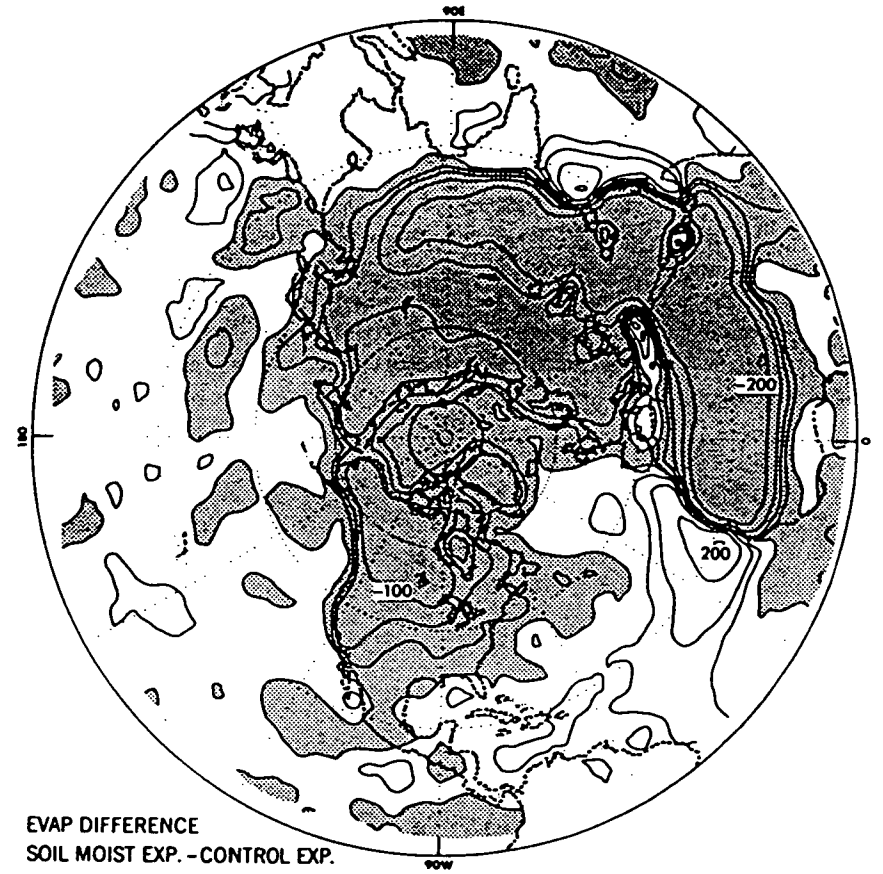

EVAP DIFFERENCE
SOIL MOIST EXP. - CONTROL EXP.

PRECIP DIFFERENCE
SOIL MOIST EXP. - CONTROL EXP.

Fig. 6.9. Surface temperature difference (top) (contour interval 2.5 °C) and difference in height of the 1000 mb surface (bottom) (contour interval 10 m; negative values shaded), in experiment of Miyakoda & Strickler (1981).

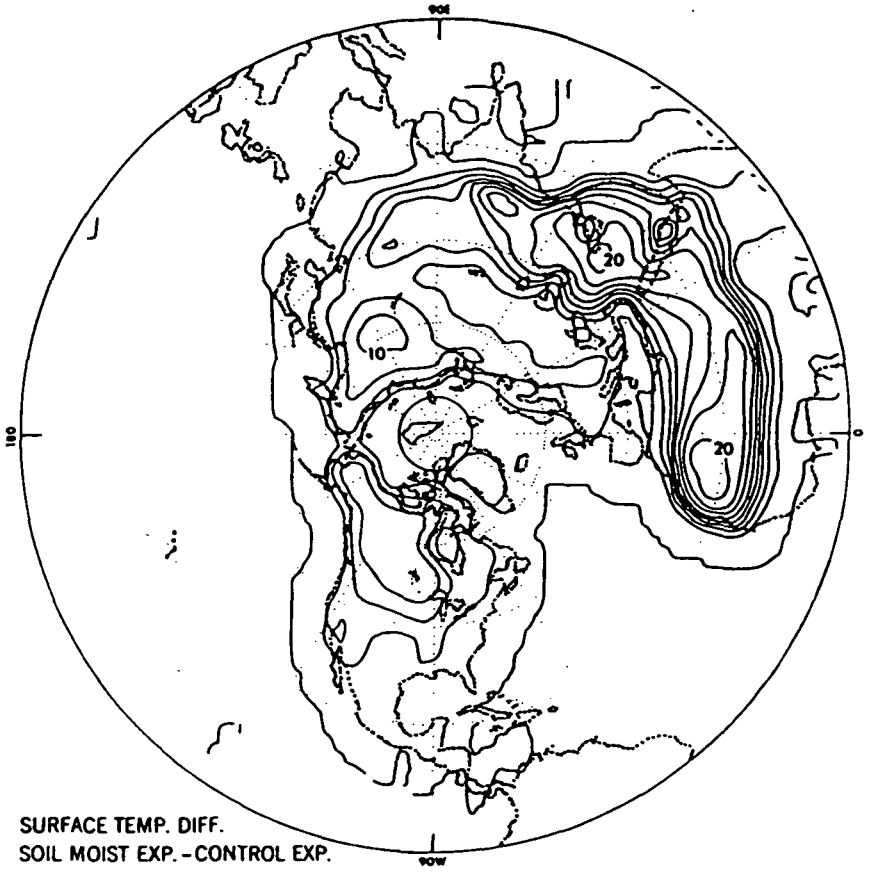

SURFACE TEMP. DIFF.
SOIL MOIST EXP. - CONTROL EXP.

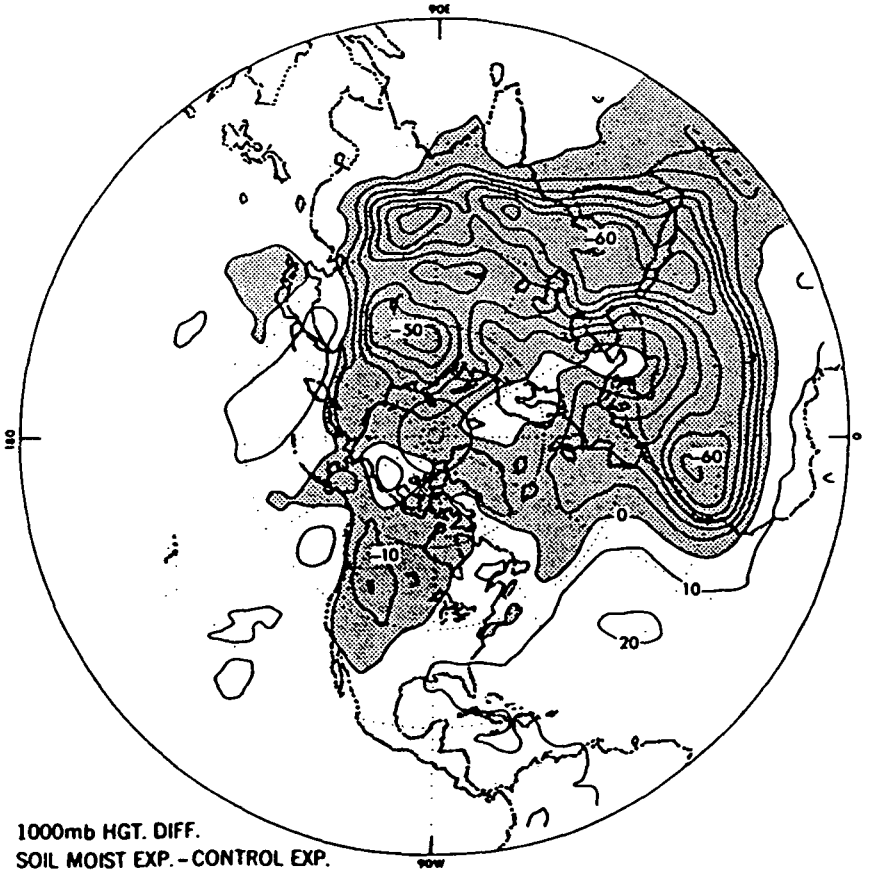

1000mb HGT. DIFF.
SOIL MOIST EXP. - CONTROL EXP.

the sensitivity of the convective heating and precipitation to the amount of water vapor in the model's planetary boundary layer is not as great as in the cumulus convection parameterization schemes of the GLAS and the UCLA models.

In one case, β was everywhere set equal to 0.5. For the other case, the authors sought a more realistic field of β; and for this they took the observed normal distribution of precipitation for the antecedent six-month period, February through July, and relabeled the isohyets as lines of constant β, according to the arbitrary function shown in the top panel of Fig. 6.7 (Miyakoda *et al.*, 1979). No account was taken of the antecedent evapotranspiration. Consequently, as the bottom panel of the figure shows, over the northern forests and the wet tundra regions of Canada and Siberia, β was made as low as in the subtropical deserts (although, in nature, it is near the maximum value of 1.0).

Figures 6.8 and 6.9 show the differences in the evapotranspiration, precipitation, surface temperature and height of the 1000 mb surface, for the case of $\beta = \beta(\lambda,\phi)$ minus the case of $\beta \equiv 0.5$, when the ensemble average is taken of the last 12 days of three sets of 14-day forecasts.

We see, in Fig. 6.8, that where β is reduced there is, in general, a reduction in evapotranspiration and precipitation. The largest reduction in evapotranspiration, of more than 7 mm/day, is over the central part of the north African and Asian deserts, with the axis of the maximum evapotranspiration reduction at about latitude 20°N across Africa. But the axis of the largest reduction in precipitation is at about 12°N across Africa (the Sahel), where the precipitation decreases by about 12 mm/day. As shown in Miyakoda & Strickler (1981, Fig. 7), the rainband of the intertropical convergence zone across north Africa does not change its position, but its magnitude goes down from 20 to 8 mm/day when the land-surface moisture source in the Sahara is eliminated. There is, obviously, a large change that takes place in the water vapor transport.

In the case where the average land-surface evapotranspiration became smaller, the average ocean evaporation became larger. In spite of that, the average ocean precipitation decreased, in agreement with the experiments made with the GLAS and UCLA models. Presumably it is, again, an enhancement of the sinking motion over the oceans that suppresses the ocean precipitation.

If we compare the top panel of Fig. 6.9 with the top panel of Fig. 6.8, we see that there is a negative correlation between the change in the land-surface temperature and the change in evapotranspiration.

When we compare the upper and lower panels of Fig. 6.9, we see that there is a negative correlation between the change in surface temperature and the change in the height of the 1000 mb surface. This is true even where the land-surface is not at a high elevation.

This experiment shows two important things: (1) that it does not require an extreme change in the soil moisture availability (β), such as a change from 1 to 0, in order to produce large changes in the precipitation, temperature and motion fields; and (2) that the influence of the land-surface evapotranspiration on the atmosphere operates very quickly. Miyakoda (personal communication) reports that sizeable differences in the surface temperature and precipitation appeared within a few days.

(In an earlier study of the role of the surface transfers of sensible and latent heat in numerical weather prediction, Gadd & Keers (1970, Figs. 4, 5, 6) showed that even in a very short range (18-hour) prediction for north-western Europe and the British Isles, in August, the inclusion of evaporation and sensible heat transfer from the land and the sea surfaces made a noticeable improvement in the predicted rainfall over the land.)

6.3.2

(B) ***Different albedos, with same soil moisture***

6.3.2.1

Charney, Quirk, Chow and Kornfield (1977)

This experiment was made by Charney *et al.* (1977) with the NASA Goddard Institute for Space Studies general circulation model, the properties and performance of which have been described by Somerville *et al.* (1974) and Stone *et al.* (1977).

The three runs that are shown here use the prescribed field of non-interactive soil moisture availability, β, from Stone *et al.* (1977), who assumed that $\beta = 2 \times (RH - 15)/85$, $\beta_{max} = 1$, where RH is the observed normal monthly mean relative humidity of the surface air. The observed relative humidities, for July, were taken from the tabulation by Schutz & Gates (1972). In the above formulation, $\beta = 1$ when the relative humidity is equal to or greater than 57.5%. Consequently, β was made equal to or close to 1, and the evapotranspiration therefore equal to or close to the potential evapotranspiration over most of the land surface of the earth. Only in a small region in the western United States and across the central Sahara was the prescribed July β smaller than 0.5.

In the run designated as case '2a', the ice-free and snow-free continents were assigned a surface albedo of 0.14; except that a higher albedo, 0.35, was assigned to the regions of the observed northern hemisphere deserts (see Fig. 6.19, below).

In a comparison run, '3a', the albedo was changed from 0.14 to 0.35 in three additional regions, the 'Sahel', 'Rajputana', and 'Western Great Plains', which are adjacent to deserts (Fig. 6.19). Otherwise everything was the same as in case 2a.

In a separate comparison run, case '4', everything was again the same as in case 2a, except that the change of albedo, from 0.14 to 0.35, was made in three regions that are within the observed rainy

Fig. 6.10. Evapotranspiration (top) and precipitation (bottom) (mm/day), in experiment with prescribed soil moisture availability (case 3a), of Charney *et al.* (1977).

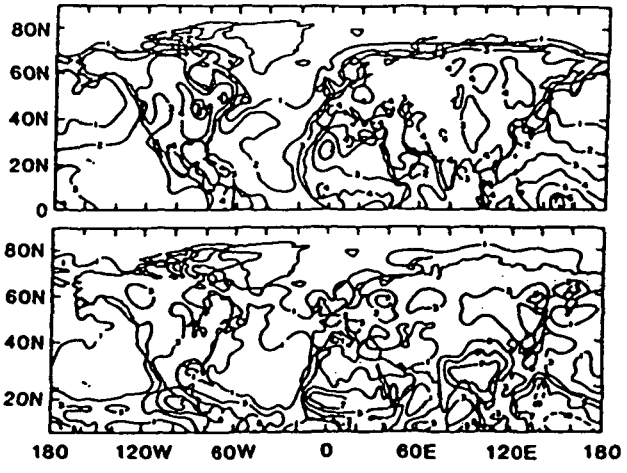

and vegetation covered areas of the earth. The locations of these regions, called 'Central Africa', 'Bangladesh', and 'Mississippi Valley' are given in the table.

The first numbered column of Table 6.1 shows the prescribed soil moisture availabilities for the six regions. In the Sahel region $\beta = 0.51$, and in the other regions β is 0.78 or more.

Fig. 6.10 shows the evapotranspiration and precipitation in the northern hemisphere, for case 3a. Over most of the continents the evapotranspiration and precipitation do not differ by more than about ± 1 mm/day. It is only over southeast China and Indochina, and where the intertropical rainband crosses Africa, that the precipitation exceeds the evapotranspiration by 3–4 mm/day. Near the Mediterranean coast of Africa and in the Middle East the precipitation is less than the evapotranspiration by about 2–4 mm/day.

Table 6.1 is a rearrangement of the data in Charney *et al.* (1977, Tables 4.1–4.4) and shows the components of the energy and water budgets at the earth's surface in the three desert-margin regions (case 2a v. 3a) and in the three humid regions (case 2a v. 4).

Table 6.1 *Components of the energy and water budgets, in experiment of Charney et al.* (1977)

						Energy balance					Water balance				
Region	Case No.	(1) β	(2) $(1-\alpha)$	(3) R_S	(4) R_L	(5) R_N	(6) LE	(7) H	(8) N	(9) T_A	(10) E	(11) $(-\overline{\nabla \cdot qv})$	(12) P	(13) $\frac{\Delta(-\overline{\nabla \cdot qv})}{\Delta E}$	(14) $\frac{\Delta P}{\Delta E}$
(1) Sahel (16–20°N, 17.5°W–37.5°E)	2a	0.51	0.86	169	58	111	107	4	0.70	26.0	3.7	3.7	7.4		
	3a	0.51	0.65	177	84	93	81	12	0.46	25.7	2.8	1.2	4.0		
			−24%	+5%	+49%	−18	−26	+8	−34%	−0.3	−0.9	−2.5	−3.4	2.8	3.8
(2) Rajputana (24–32°N, 67.5–77.5°E)	2a	0.92	0.86	180	48	132	119	13	0.77	24.9	4.1	0.8	4.9		
	3a	0.92	0.65	189	75	114	104	10	0.57	24.1	3.6	−1.3	2.3		
			−24%	+5%	+56%	−18	−15	−3	−26%	−0.8	−0.5	−2.1	−2.6	4.2	5.2
(3) Western Great Plains (32–48°N, 107.5–97.5°W)	2a	0.78	0.86	186	62	124	122	2	0.67	21.1	4.2	−0.5	3.7		
	3a	0.78	0.65	185	79	106	93	13	0.52	19.0	3.2	−1.0	2.2		
			−24%	+1%	+27%	−18	−29	+11	−22%	−2.1	−1.0	−0.5	−1.5	0.5	1.5
(4) Central Africa (8–12°N, 12.5°W–52.5°E)	2a	0.94	0.86	170	56	114	125	−11	0.72	22.2	4.3	0.7	5.0		
	4	0.94	0.65	171	69	102	104	−2	0.59	21.6	3.6	−1.7	1.9		
			−24%	+1%	+23%	−12	−21	+9	−18%	−0.6	−0.7	−2.4	−3.1	3.4	4.4
(5) Bangladesh (20–28°N, 77.5–87.5°E)	2a	1.00	0.86	149	38	111	113	−2	0.85	24.2	3.9	4.1	8.0		
	4	1.00	0.65	140	44	96	107	−11	0.78	23.6	3.7	4.3	8.0		
			−24%	−6%	+16%	−15	−6	−9	−8%	−0.6	−0.2	0.20	0	−1.0	0.0
(6) Mississippi Valley (32–48°N, 92.5–82.5°W)	2a	1.00	0.86	208	68	140	148	−8	0.57	22.1	5.1	−0.7	4.4		
	4		0.65	170	67	103	102	1	0.56	22.6	3.5	−0.2	3.3		
			−24%	−18%	−1%	−37	−4.6	+9	−2%	+0.5	−1.6	+0.5	−1.1	−0.3	0.7
Average for the six regions		0.86	0.86	177	55	122	122	0	0.71	23.4	4.2	1.4	5.6		
		0.86	0.65	172	70	102	98	4	0.58	22.8	3.4	0.2	3.6		
			−24%	−3%	+27%	−20	−24	+4	−18%	−0.6	−0.8	−1.2	−2.0	1.5	2.5

β average, for the region, of the prescribed soil moisture availability (ratio of evapotranspiration to potential evapotranspiration)
$(1-\alpha)$ fraction of the incident solar radiation that is absorbed by the ground (α = land-surface albedo)
R_S solar radiational heating of the ground (watt/m²)
R_L long wave (infrared) radiational cooling of the ground (difference between long wave radiation emitted by the ground and atmospheric 'back radiation' absorbed by the ground) (watt/m²)
$R_N = (R_S - R_L)$ net (all-wavelength) radiational heating of the ground (watt/m²)
LE latent heat transfer from ground to atmosphere (evaporative cooling of the ground)
H conductive–convective heat transfer from ground to atmosphere
N fraction of the sky covered by clouds of all types
T_A surface air temperature (°C)
E_T surface evapotranspiration (mm/day)
$(-\overline{\nabla \cdot qv})$ vertically integrated convergence of the water vapor transport (mm/day)
P precipitation (mm/day)
$\Delta P/\Delta E$ ratio of precipitation change to evapotranspiration change
For each region the third line shows either the absolute change between the two cases or the percentage change, where the % sign indicates the latter.

We see, in column (10), that in the Western Great Plains (where β was assigned the value of 0.78) and in the Mississippi Valley (where β was made 1.0), the evapotranspirations with albedo of 0.14, are, respectively, 4.2 mm/day (130 mm/month) and 5.1 mm/day (158 mm/month). These are in fair agreement with the aerologically derived evapotranspiration over the central and eastern United States in July, of 3.7 mm/day (116 mm/month), shown in Fig. 6.1. More important, however, as an indication of the reliability of the model, is the fact that the vertical integral of the water vapor flux convergence ($-\overline{\nabla \cdot qv}$), shown in column (11), is negative in the two regions, with values, respectively, of -0.5 mm/day (-16 mm/month) and -0.7 mm/day (-22 mm/month). This means that water vapor is being exported from these regions at about the same rate as the observed transport divergence, of 0.7 mm/day (22 mm/month), shown in Fig. 6.1.

In the other four regions, in the case with normal surface albedo, 2a, the vertical integrals of the water vapor transport convergence are positive, water vapor is being imported (so that precipitation is larger than evapotranspiration), which is what one would expect for these particular regions in the month of July.

Table 6.1 is replete with information about the performance of the model and its complex, non-linear response to the change in the surface albedo. But, for brevity, we will here examine only what happens in the Sahel, the region of greatest interest.

We see, in Table 6.1 (column 3), and in Fig. 6.11, that when the surface albedo is increased in the Sahel, from 0.14 to 0.35, the solar radiational heating of the surface does not become smaller: it becomes *larger*. This is because of the large decrease in the cloud cover, from 0.70 to 0.46 (column 8), which more than compensates for the increased albedo.

The cloud cover is less because (1) there is less evapotranspiration (a change from 3.7 to 2.8 mm/day); and (2) there is less convergence in the water vapor transport (a change from 3.7 to 1.2 mm/day).

The local evapotranspiration is reduced in the high-albedo case because there is more long wave radiational cooling of the ground (an increase from 58 to 84 watt/m²). Unfortunately, no record was kept of the ground-surface temperature, nor of the long wave emission by the ground; but it is most likely that it is the decrease in the downward long wave 'back radiation' from the atmosphere, $R_L\downarrow$, as a consequence of the decreased cloudiness, which increased the long wave cooling of the ground.

The sensible heat transfer from the ground to the atmosphere is small, in both cases.

By using arrows to indicate when a change in one parameter produces a change in another, we can describe what happens in the Sahel, in this experiment, as the coupling between a sequence of processes operating locally and a sequence that involves the large-scale atmospheric circulation. The local sequence is: albedo $\xrightarrow{\text{(changes)}}$ radiation $\xrightarrow{\text{(changes)}}$ evapotranspiration $\xrightarrow{\text{(changes)}}$ precipitation. The larger-scale sequence is: precipitation–condensation-heating $\xrightarrow{\text{(changes)}}$ large-scale circulation $\xrightarrow{\text{(changes)}}$ water vapor transport convergence $\xrightarrow{\text{(changes)}}$ precipitation.

The second of these two sequences is similar (but not identical) to the one in the Charney (1975) hypothesis on the dynamics of deserts. In that hypothesis the sequence is: albedo $\xrightarrow{\text{(changes)}}$ surface temperature $\xrightarrow{\text{(changes)}}$ large-scale circulation $\xrightarrow{\text{(changes)}}$ water vapor transport convergence $\xrightarrow{\text{(changes)}}$ precipitation. Here, the change in evapotranspiration plays no role. (A direct examination of the Charney hypothesis with a general circulation model would consist of a comparison of two runs, in both of which no evapotranspiration was allowed in the region of interest, but was allowed elsewhere, and the albedo in the region of interest was changed.) (See experiment in section 6.4.2.1.)

The relative importance of the two sequences of processes, when surface evapotranspiration does take place, may be seen in columns (13) and (14) of Table 6.1. We see, in column (13), that in the Sahel, Rajputana and Central Africa, the reduction in the water vapor flux convergence is between 2.8–4.2 times larger than the reduction in the evapotranspiration. But in the Western Great Plains, the reduction in the water vapor flux convergence is only half as large as the reduction in evapotranspiration. In Bangladesh and the Mississippi Valley, things go the other way: increasing the surface albedo again decreases the evapotranspiration; but it *increases* the water vapor flux convergence.

As indicated earlier, the response of the large-scale precipitation, temperature and motion fields to a change in the surface boundary conditions (whether soil moisture availability or albedo) will depend on many factors. Of particular importance is the horizontal scale and the latitude of the region in which the boundary condition is changed. Through the geostrophic adjustment process, the horizontal scale and the latitude determine whether the circulation change will be in the vertical plane (small-scale or low-latitude) or in the horizontal plane (large-scale and high-latitude). When the circulation change is in the vertical plane there is a positive feedback on the condensation heating, through water vapor transport convergence. But when the circulation change is in the horizontal plane there is a negative feedback on the condensation heating, because then the transport removes water

Fig. 6.11. The Sahel region energy budgets (watt/m²) (top) and water budgets (mm/day) (bottom), in experiment with prescribed soil moisture availability, of Charney *et al.* (1977). Case 2a is on the left, Case 3a is on the right. (For definitions of symbols, see notes to Table 6.1.)

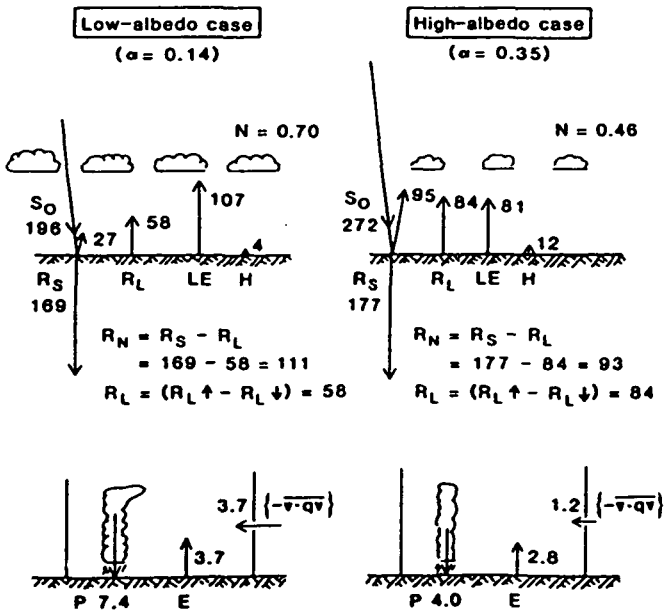

vapor, as well as sensible heat, from the region of the condensation heating.

6.3.2.2

Carson and Sangster (1981)

Another experiment in this category was made by Carson & Sangster (1981) with a low-resolution (N20) version of the British Meteorological Office five-layer general circulation model (Corby *et al.*, 1977). In both runs, evapotranspiration was made equal to the calculated potential evapotranspiration ($\beta \equiv 1$). In one case, the albedo of the snow-free land was everywhere set equal to 0.1. In the other case, it was everywhere set equal to 0.3. The remaining lower boundary conditions (sea-surface temperatures, sea ice, and

Fig. 6.12. Precipitation in the low-albedo case (top) and the high-albedo case (center), of experiment by Carson & Sangster (1981). The contours are for 1, 2, 5, 10 and 20 mm/day. (Light shading, precip. < 1 mm/day; heavy shading, precip. > 5 mm/day). The bottom panel is the difference in the precipitation: the low-albedo case minus the high albedo case (unshaded area is positive).

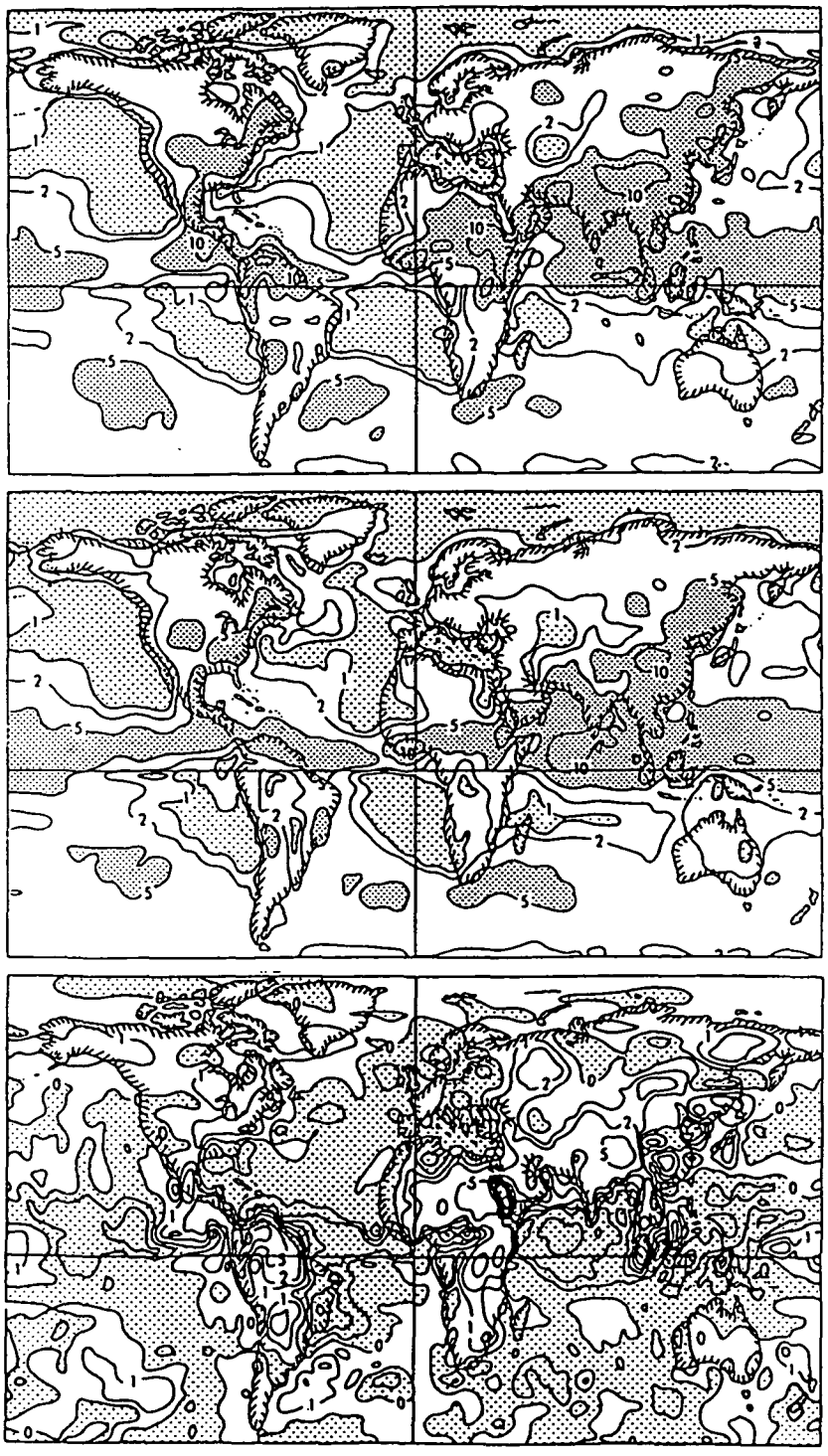

land snow cover), as well as the climatologically determined long wave radiational heating rates, were the observed July values.

Figure 6.12 shows the precipitation averaged over 90 days (days 21–110 of integration), where the top panel is the low-albedo case, the center panel is the high-albedo case, and the bottom panel is the difference between the two.

We see that the high-albedo case has less rainfall over most of the continental areas, but that over the oceans the rainfall is increased.

The averages of the land precipitation, and of other parameters, are shown in Table 6.2.

Like the experiment by Charney *et al.*, 6.3.2.1 above, this is an albedo change experiment with permanently wet soil. Here, too, the increase of albedo produces a decrease in evapotranspiration (−0.9 mm/day) and an even larger decrease in precipitation (−1.2 mm/day); but now the albedo is changed on the continental scale, whereas in 6.3.2.1 it was changed only over a few hundred kilometers in the widths of the various regions. It is not surprising, therefore, that in this experiment the contribution to the change in precipitation of the change in the water vapor transport convergence is only about a third as large as is the contribution by the change in the local evapotranspiration. Both experiments have about the same average water vapor transport convergence, 0.8 mm/day v. 0.85 mm/day. But in (4), where the albedo was changed from 0.14 to 0.35 over a number of small regions, the average change in the transport convergence in those regions was −1.2 mm/day. In (5), where the albedo is changed from 0.1 to 0.3 over all of the land, the change in the transport convergence is only −0.3 mm/day; showing, again, that the larger the horizontal scale the smaller is the role of the water vapor transport convergence in compensating for a decrease in the land-surface evapotranspiration.

6.4

(II) **Experiments with interactive soil moisture**

In all but one of the experiments that follow, the time-dependent soil moisture is governed by the equations:

$$\frac{\partial W}{\partial t} = P - E, \quad W_{\max} = W^*, \tag{6.1}$$

$$E = \beta E_p, \tag{6.2}$$

$$\beta = \frac{W}{kW^*}, \quad \beta_{\max} = 1, \tag{6.3}$$

where W is the available moisture stored in the soil, W^* is the available moisture storage capacity of the soil, P is the rate of precipitation, E is the rate of evapotranspiration, E_p is the rate of potential evapotranspiration, β is the soil moisture availability, and k is a prescribed coefficient (see Carson, 1981). In all of the models, E_p is evaporation calculated by an aerodynamic method, under the assumption that the vapor pressure at the surface is the saturation value for the calculated ground temperature.

6.4.1

(A) ***Different initial soil moistures, with same albedo***

6.4.1.1

Walker and Rowntree (1977)

Walker & Rowntree (1977) examined the interaction between time-dependent soil moisture and the calculated precipitation, temperature and circulation of the atmosphere, not in the global domain, but in a zonal channel between latitudes 16°S and 36°N, and extending over 32° of longitude with cyclic east–west boundary conditions. The land and sea distribution was made zonally symmetric, with land to the north and ocean to the south of 6°N latitude; this being an idealization of the western part of north Africa and the Gulf of Guinea.

The model was an 11-layer primitive equations model with 2° latitude–longitude resolution. The radiational part of the thermal forcing was taken as a constant radiational cooling of the atmosphere, of 1.2 K/day from the surface to the 200 mb level, with radiative equilibrium at higher levels (which means a constant radiational cooling of the atmosphere of 110 watt/m²); and with a constant net radiational heating of the land surface, R_N, of 150 watt/m². Thus, over the land, there was a prescribed horizontally uniform radiational heating (of 40 watt/m²) of the atmosphere– earth system; but over the ocean, the surface temperature, and not the surface radiation flux, was the prescribed boundary condition. The prescribed, zonally-symmetric ocean temperatures, from 16°S to 6°N, were the observed August normals at 0° longitude. The moist-convective adjustment scheme was used to obtain the convective precipitation and moist-convective heating of the air.

The available soil moisture and the land-surface evapotranspiration were calculated with the equations given at the beginning of this section; with W^* taken as 150 mm, and k taken as 0.333. Therefore, $\beta = 1$ when $W \geqslant 50$ mm.

Two integrations were made in which everything was the same, except that:

In case 1 (the initially dry-soil Sahara), W was initialized at zero in the latitude zone 14–32°N; and at 100 mm in the land zones 6–14°N and 32–36°N.

Table 6.2. *Albedo experiment of Carson & Sangster (1981) 90-day means (days 21–110), permanent July*

	Global Averages Over Land						
Surface albedo	(1) LE	(2) H	(3) E	(4) $(-\overline{\nabla \cdot qv})$	(5) P	(6) $\frac{\Delta(-\overline{\nabla \cdot qv})}{\Delta E}$	(7) $\frac{\Delta P}{\Delta E}$
0.1	104	35	3.6	1.0	4.6		
0.3	78	21	2.7	0.7	3.4		
Difference	−26	−14	−0.9	−0.3	−1.2	0.3	1.3

For definition of symbols, see Table 6.1.

Fig. 6.13. Variation with time of the zonally averaged precipitation (top) and soil moisture (bottom) in the case where, initially, the soil in the Sahara is completely dry. (Experiment of Walker & Rowntree, 1977.)

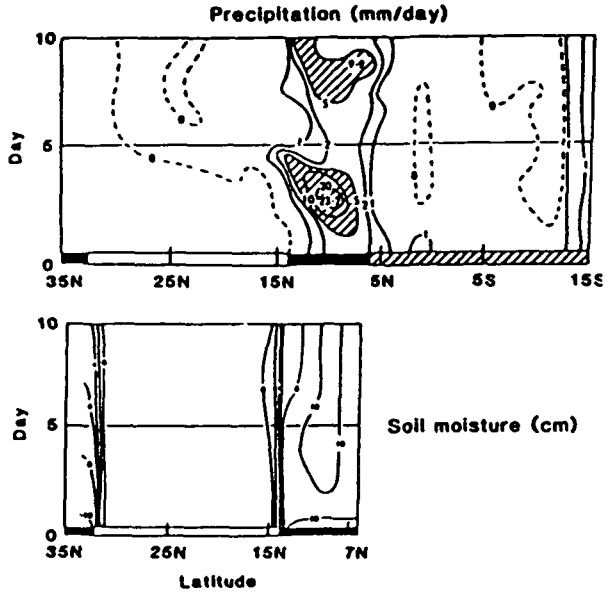

Fig. 6.14. Variation with time of the zonally averaged precipitation (top) and soil moisture (bottom) in the case where the initial soil moisture in the Sahara is 100 mm. (Experiment of Walker & Rowntree, 1977.)

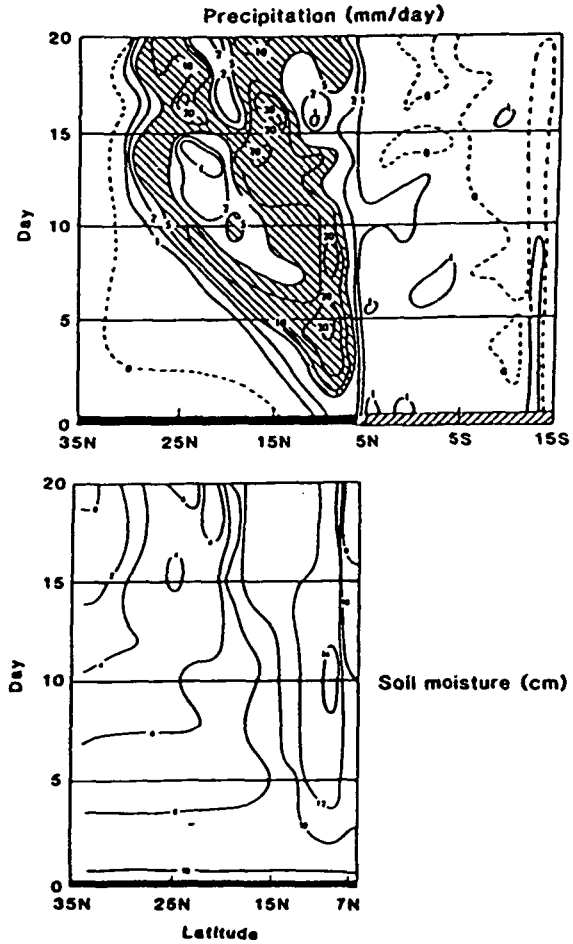

In case 2, (the initially moist-soil Sahara), W was initialized at 100 mm over all of the land region, 6–36°N.

Figures 6.13, 6.14 and 6.15 show the time-evolutions of the soil moisture and precipitation in the two cases.

In case 1 (Fig. 6.13), where the soil was initially dry between 14° and 32°N, it remains dry. There is almost no net water vapor transport into that region and, therefore, there is no precipitation and no water is added to the soil there. On the other hand, in the land region 6–14°N the initial soil moisture, of 100 mm, goes down to about 90 mm over the first seven days, showing an excess of evapotranspiration over precipitation which averages about 1.4 mm/day. The corresponding seven-day water vapor transport divergence, of about 1.4 mm/day, is the difference between a large northward transport of water vapor across the coastline by the mean meridional circulation (Walker & Rowntree, 1977, Fig. 4(*a*)) and an even larger equatorward eddy-transport of water vapor by the wave disturbance which developed and moved westward across the region. By the end of the integration period, this part of the system also appears to have reached a steady state, except for a short-period and small-amplitude variation produced by transient waves in the flow.

In case 2, the initially moist-soil Sahara, (Figs. 6.14 and 6.15), there is a rapid development of precipitation in the zone near the coast, which, after about two days, exceeds the evapotranspiration rate and the soil moisture starts to increase. The average precipitation in this coastal zone reaches 18 mm/day on day 5; with a maximum of 30 mm/day at 9°N. After that the precipitation rate

Fig. 6.15. Variation of the zonally averaged precipitation and soil moisture with time, in selected latitude zones across north Africa, in the case where the initial soil moisture in the Sahara is 100 mm. (Experiment of Walker & Rowntree, 1977.)

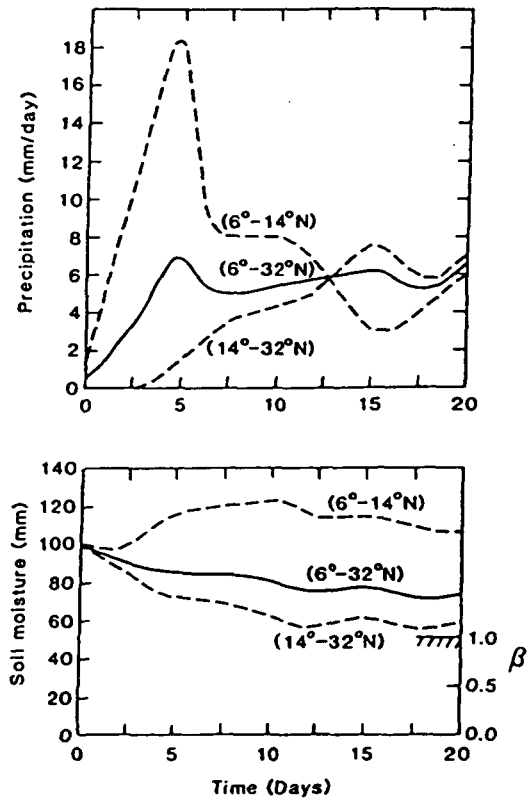

in this zone decreases rapidly and seems to be starting an oscillation about an average rate of around 6 mm/day. The prescribed $R_N = 150$ watt/m^2 would provide enough energy for $E = E_p = 5{\cdot}2$ mm/day; but the calculated evapotranspiration may be smaller or larger than this, depending on whether the sensible heat transfer at the surface is upward or downward.

Over the rest of the land region, 14–32°N, the evapotranspiration exceeds the precipitation until about day 12; and, thereafter, except for an oscillation produced by the transient wave disturbances, evapotranspiration equals precipitation and the soil moisture remains constant.

From what we see in these figures, it appears unlikely that the solutions for the initially dry-soil Sahara and the initially moist-soil Sahara will approach one another no matter how long the integrations were to continue. It seems safe to say that this highly simplified soil moisture–atmosphere system is intransitive.

6.4.1.2

Rowntree and Bolton (1978)

Rowntree & Bolton (1978) made an interactive soil moisture experiment with the five-layer, 500 km grid size, version of the British Meteorological Office general circulation model (described by Corby *et al.*, 1977).

For the calculation of the soil moisture and evapotranspiration, W^* was taken as 200 mm and k as 0.5; so that $\beta = 1$ when $W \geq 100$ mm.

Three 50-day integrations were made, all starting from the same initial atmospheric conditions on 27 May, but with different initial distributions of soil moisture.

In one run, designated C (for control), the initial soil moisture was set at 50 mm at all land points over the globe. Therefore, the initial soil moisture availability, β, was 0.5 everywhere.

In the run designated W (for wet-soil case) the initial soil moisture was set at 150 mm at all of the European land points that are within the region enclosed by the rectangle in Fig. 6.16; but with an initial value of 50 mm at all other land points over the globe. Thus, the initial β was 1 in the European region but, again, 0.5 at all other land points over the globe.

Fig. 6.16. Precipitation (mm/day) averaged for 15 June–15 July, in experiment of Rowntree & Bolton (1978). Center panel: control run, where the initial soil moisture, on 27 May, was 50 mm everywhere. Top panel: case where the European land points within the indicated rectangular region had an initial soil moisture of 150 mm. Bottom panel: case where the European land points within the indicated rectangular region had zero soil moisture initially

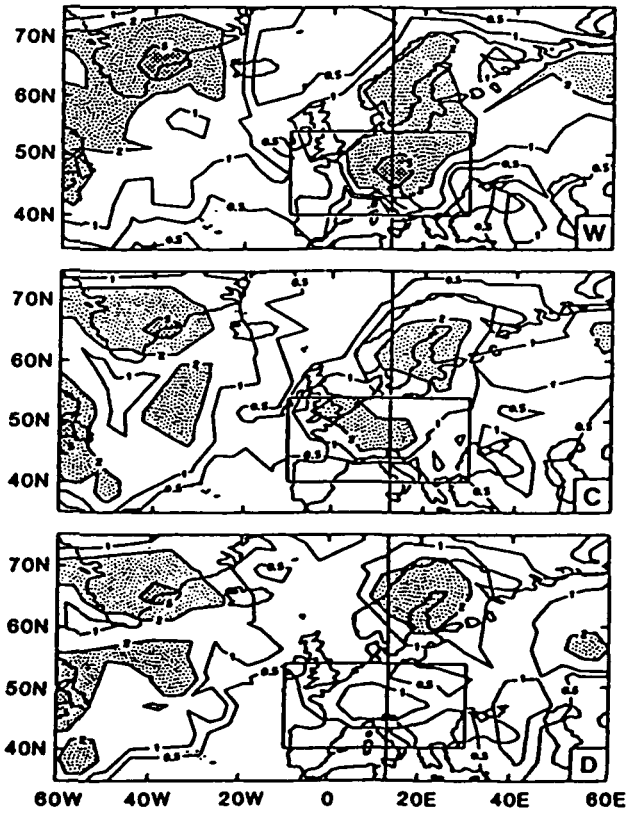

Fig. 6.17. Distribution of precipitation along the 13°E meridian, for the three fields shown in Fig. 6.16.

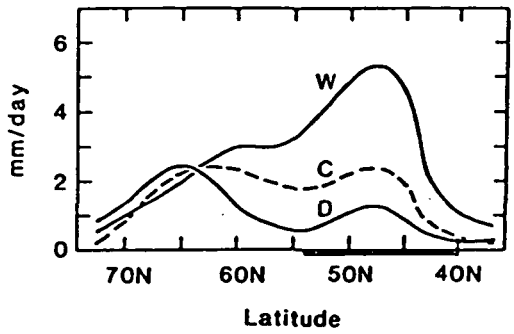

Fig. 6.18. Variation with time of ten-day averaged precipitation (top) and soil moisture (bottom), averaged for the European land points within the rectangular region shown in Fig. 6.16, for the three cases in the experiment of Rowntree & Bolton (1978).

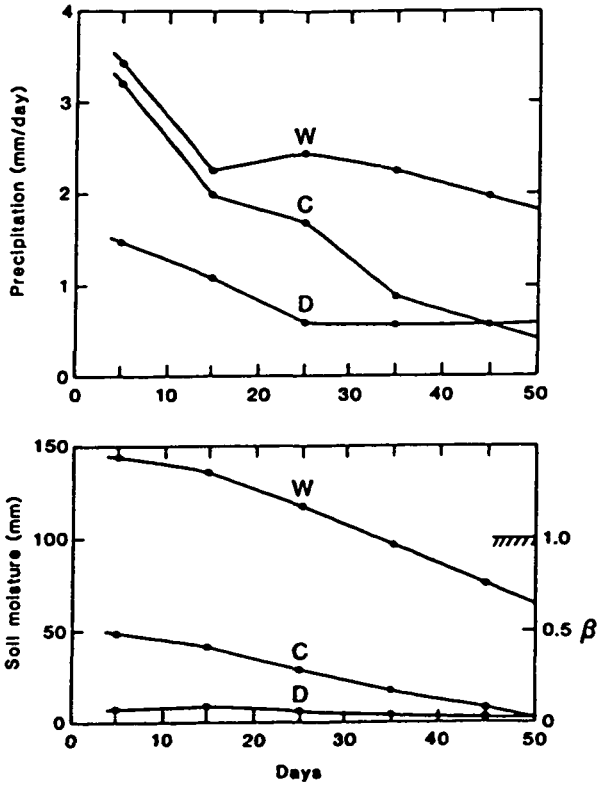

In the run D (the dry-soil case) the soil moisture in the European region was initialized at 0 mm (but, again, at 50 mm elsewhere). Now, the initial β, and hence the initial evapotranspiration, was zero in the European region.

Fig. 6.16 shows maps of the three rainfall distributions, averaged for the 30-day period, 15 June–15 July; and Fig. 6.17 shows meridional profiles of those time-averaged rainfalls along longitude 13°E, where the maximum rainfall occurs. In general the differences between the 30-day rainfalls are comparable to what are produced by the natural variability of a model atmosphere with fixed surface boundary conditions. But within the European region the time-averaged precipitation, for days 20–50 following initialization, was greatest in the case which initially had the most moisture in the soil, and smallest when the soil was initially devoid of moisture.

The changes in the precipitation and in the soil moisture with time are shown in Fig. 6.18, where the values are ten-day averages for the indicated European land region. We see that even after one-and-a-half months there are still large differences between the precipitation rates and between the soil moistures, when we compare the initially wet-soil case (W initially 100 mm) with the other two cases (W initially 50 mm and 0 mm). The slopes of the rainfall curve and soil moisture curve, for the initially wet-soil case, suggest that the system is transitive, but that the time required for convergence is several months.

6.4.2

(B) Different albedos, with same initial soil moisture.

6.4.2.1

Charney, Quirk, Chow and Kornfield (1977)

Charney *et al.* (1977) performed an experiment in which they compared two runs which had different albedo distributions, but the same initial soil moistures which could interact with the atmosphere.

The distribution of the land-surface albedo in the two cases is shown in the bottom panel of Fig. 6.19. In their run designated '2b', the albedos of 'permanent desert' (the regions with dotted shading) were assigned the value of 0.35; and everywhere else over the ice-free and snow-free land surface of the globe the albedo was taken as 0.14. In the comparison run, designated '3b', three regions adjacent to the permanent deserts, the 'Western Great Plains', 'Rajputana' and 'Sahel' (shown by the cross-ruled shading) were also assigned an albedo of 0.35. In both runs, the initial soil moisture was taken to be zero everywhere.

The change in the time-dependent soil moisture was calculated, in half-hourly time steps, from Eqs. (6.1) and (6.2) given at the beginning of this section, and with the function $\beta = \beta(W, W^*, E_p)$ (Charney *et al.*, 1977, p. 1368) which is shown in Fig. 6.20. (Diagram by personal communication from Y. Sud.) Over the range of E_p between 1.4 and 6.4 mm/day, this formulation for β was taken from Denmead & Shaw (1962), who obtained it from measurements of daily (24 hr) evapotranspiration and potential evapotranspiration, together with measured soil moisture.

In the experiment, this formula for β was inadvertently applied to the calculation of half-hourly values of evapotranspiration, and this made the calculated daily evapotranspiration an order of magnitude too small (because during the mid-day hours, when E_p is about π times as large as its 24-hour average, the β obtained in this way is extremely small for almost all values of

Fig. 6.19. Bottom panel: the assigned albedos in experiments of Charney *et al.* (1977). Unshaded land areas have an albedo of 0.14 in all cases, and dot-shaded areas have an albedo of 0.35 in all cases. In the cross-ruled areas the albedo was changed from 0.14 (in cases 2a and 2b) to 0.35 (in cases 3a and 3b). Top panel: precipitation (mm/day) in case 3b.

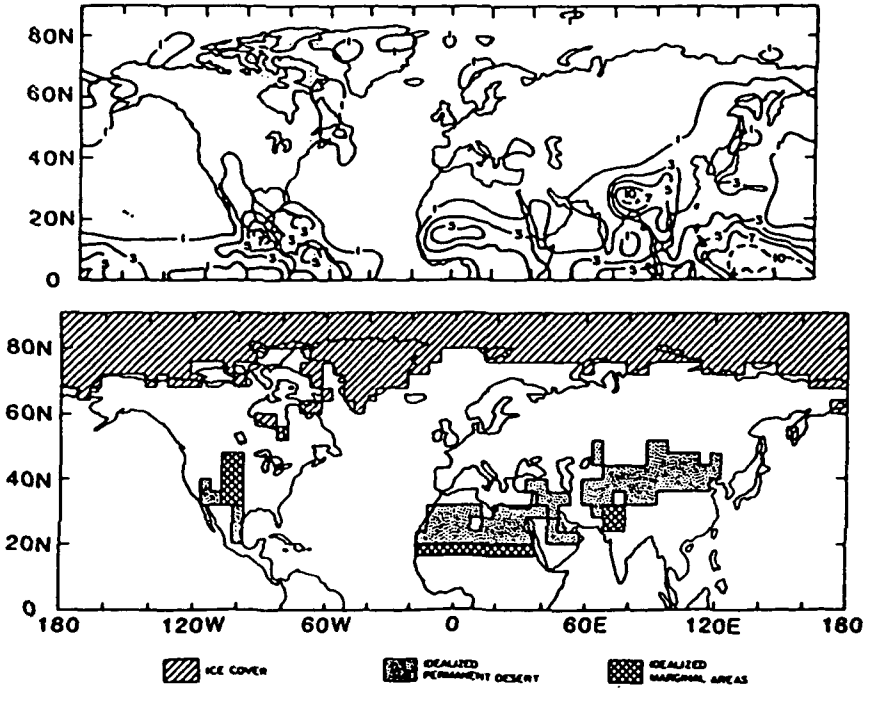

W/W^*; and during the night, when β can approach 1, E_p is negligible).

The top panel in Fig. 6.19 shows the calculated July precipitation in case 3b. At the beginning of the run, 18 June, almost all of the precipitation that falls on the land must be from water vapor transported from the ocean; and this situation must continue (because evapotranspiration is negligible) until the accumulation of the water in the soil brings W close to the soil storage capacity W^*, at which point β becomes equal to 1 for all values of E_p. For a precipitation of 5 mm/day, which is the mean July precipitation across north Africa in case 3b, it takes about 20 days, or until about 8 July, for the soil moisture, W, to approach or reach W^*, at which point β approaches or reaches 1. Elsewhere, β remains negligible, even until the end of July. It is therefore not surprising that in this experiment with interactive soil moisture, the precipitation, for days 14–44 following initialization with zero soil moisture, should resemble the persistently dry-soil case shown in the lower panel of Fig. 6.3.

Table 6.3 shows the energy and water balances of the three regions, in the two runs, for July (days 14–44 of the integration). We see, by comparing columns (11) and (12), that during this period (which, as indicated, is a transient stage for the soil moisture and evapotranspiration) the dominant term in the supply of water vapor for precipitation, in all cases, is the water vapor transport convergence. In the Sahel, the evapotranspirations for the month are 0.14 and 0.34 mm/day, which are only 4% and 12% of the monthly averaged precipitation rates. But almost all of this must be due to the evapotranspiration near the end of July, at which time, or shortly thereafter, the accumulated precipitation will make W approach, or equal, W^*.

With the small amounts of evapotranspiration, the cloud cover (column 8) is not very different in the low- and high-albedo cases. Consequently, unlike experiment 6.3.2.1 above, the change in the net radiational heating of the ground, R_N, is almost entirely due to the change in the solar radiational heating of the ground, R_S; and this produces the large change in the sensible heat transfer,

Fig. 6.20. The soil moisture availability function, $\beta = \beta$ (W, W*, E_p), used by Charney *et al.* (1977) in the albedo experiment with interactive soil moisture.

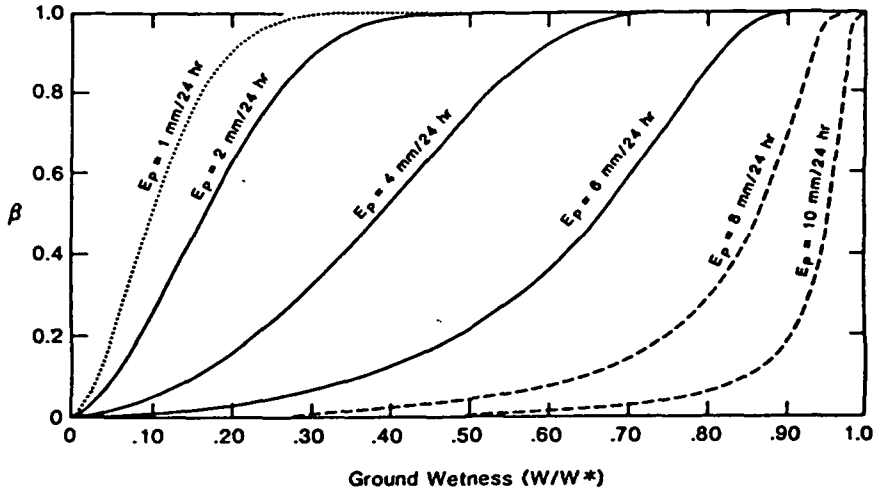

Table 6.3. *Components of the energy and water budgets, in experiment of Charney et al.* (1977)

					Energy balance					Water balance		
		(2)	(3)	(4)	(5)	(6)	(7)	(8)	(9)	(10)	(11)	(12)
Region	Case No.	$(1-\alpha)$	R_S	R_L	R_N	LE	H	N	T_A	E	$-\overline{\nabla \cdot qv}$	P
Sahel	2b	0.86	259	139	120	4	116	40	39.2	0.14	3.9	4.0
	3b	0.65	213	140	73	10	63	35	36.1	0.34	2.4	2.7
		−24%	−46	1	−47	6	−53	−12%	−3.1	0.20	−1.5	−1.3
Rajputana	2b	0.86	269	134	135	3	132	43	35.1	0.10	2.0	2.1
	3b	0.65	219	129	90	8	72	42	34.2	0.26	2.1	2.4
		−24%	−50	−5	−45	5	−60	−2%	−0.9	0.16	0.1	0.3
Western Great Plains	2b	0.86	302	172	130	0	130	21	37.5	0.00	0.8	0.8
	3b	0.65	245	161	84	3	81	20	31.4	0.10	0.3	0.4
		−24%	−57	11	−46	3	−49	−5%	−6.1	0.10	−0.5	−0.4

For definition of symbols, see Table 6.1

H. It is this change in the sensible heating of the planetary boundary layer which produces the change in the vertical velocity shown in the bottom panel of Fig. 6.21, the associated change in water vapor transport convergence, shown in column (11) of Table 6.3, and the change in precipitation shown in column (12) and in the top panel of Fig. 6.21. As the experiment stands, it does illustrate the mechanism of the Charney (1975*a*) 'dry-soil' desertification hypothesis: but not if the integrations were to continue; for then W will everywhere approach, or equal, W^* and the processes which depend on evapotranspiration will become important.

We note, furthermore, that this simple picture of the coupling of the water vapor transport convergence to the surface albedo does not hold for the Rajputana and Western Great Plains regions, even when the evapotranspiration is negligibly small. In both of these regions the changes in R_S, R_N, and H are about the same as the changes in the Sahel; but, unlike the Sahel, there is almost no change in the water vapor transport convergence. As already indicated, the response of the atmospheric circulation to a change in the boundary layer heating, H, will depend very much on the horizontal scale and latitude of the heating perturbation, as well as on the orientation of the region with respect to external moisture sources and the way in which the altered flow encounters the mountain barriers.

6.4.2.2

Chervin (1979)

Chervin (1979) used the NCAR general circulation model (described by Washington & Williamson, 1977) to examine the effect of a change in the land-surface albedo when the soil moisture is fully interactive. The change in soil moisture was calculated with the equations given at the beginning of this section, with $W^* = 150$ mm and $k = 0.75$.

The control was the average of a master run, which started from a state of rest and isothermalcy and was integrated for 120 days, plus four other runs, each of which started from day 30 of the master and ran until day 120. All of these were perpetual July integrations, in which the sun declination, the ocean-surface temperatures, and the snow-free land albedo (which followed Posey & Clapp, 1964) were held constant in time.

The run with a different albedo was also started from day 30 of the master and ran until day 120. The change in the albedo consisted of replacing the Posey & Clapp values by a constant albedo of 0.45 within two regions: (1) a large region over north Africa, extending from the Atlantic to the Red Sea and from latitude 7.5°N to the Mediterranean, and therefore covering the zone of the July intertropical convergence rain, as well as the Sahara Desert; and (2) a smaller region over the US High Plains (97.5–107.5°W, 27.5-52·5°N).

Over Africa, the control (Posey & Clapp) albedo varied from about 0.35 in the northern Sahara to about 0.08 near the southern boundary of the region where the albedo will be changed. Over the US High Plains, the control albedo was between 0.07 and 0.17.

Fig. 6.22 shows the change over Africa in the precipitation, soil moisture and ground temperature, and in the vertical velocity at 3 km elevation. The values shown are the averages of the last 60 days of the modified albedo case, minus the ensemble average of the last 60 days of the five control runs. The stippled areas in the diagram show the regions of $r = |\Delta_{ee}|/\sigma_{ee} \geq 3$, where Δ_{ee} is the prescribed change response (i.e., the difference between the 60-day mean in the prescribed change case and the ensemble average of the 60-day means of the five control runs); and σ_{ee} is the standard deviation of the 60-day means of the five control runs. According to Chervin & Schneider (1976), $r \geq 3$ implies an approximately 5% significance level in rejecting the hypothesis that the prescribed change response is the result of random fluctuations and not the result of the prescribed surface albedo change.

The maps in Fig. 6.22 show that the changes are greatest at and near the zone where the albedo is increased from 0.08 to 0.45. In this zone there is a decrease in the average upward motion of the air of about 2 mm/second (200 m/day), with $r > 3$; a decrease in the average precipitation of about 4 mm/day, with $r \geq 2$, [Δ_{ee} $P \approx (4-8)$ mm/day, σ_{ee} $P = 2$ mm/day]; and a decrease in the average soil moisture storage of about 50 mm, with $r > 3$. There is a decrease of the ground-surface temperature, with $r > 3$, over almost all of the region of the albedo change, but not along its southern edge. There, the ground-surface temperature *increases*, by about 0.5°C, with $r > 3$.

The paradoxical rise in the ground-surface temperature, in the region of the largest increase of albedo (the change from 0.08 to 0.45), can be attributed to the fact that in that zone, 7.5–12.5°N, where there is the largest decrease in precipitation, the soil moisture, W, goes down from about 100 mm in the control to 50 mm in the high-albedo case. With $W^* = 150$ mm and $k = 0.75$, this reduces β from 0.9 to 0.45 and, consequently, there is a large reduction in the evapotranspiration and the evaporative cooling of the surface in that zone. There is also a contribution to the

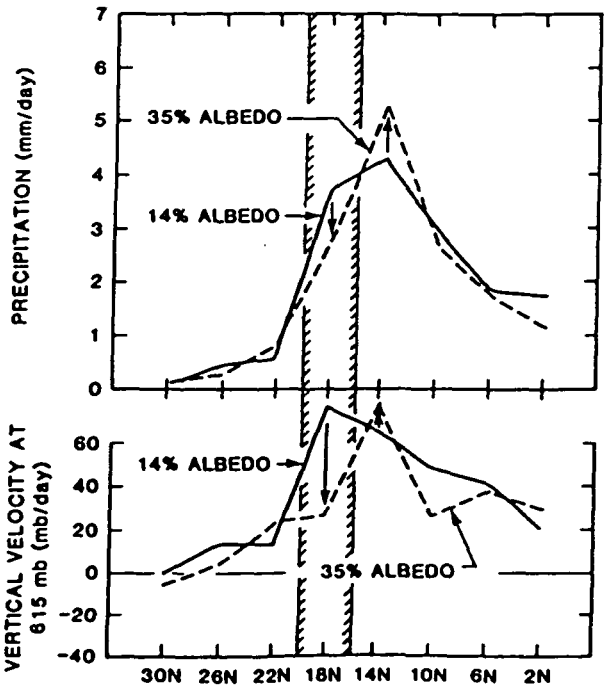

Fig. 6.21. Zonally averaged precipitation (top) and vertical velocity in the middle troposphere (bottom), over Africa, when the albedo in the Sahel (16–20°N) is increased from 0.14 to 0.35. (Figure from Charney, 1975*a*.)

temperature rise from the accompanying reduction of the cloudiness in that zone (R. Chervin, personal communication).

Over the US Great Plain region there was almost no change in the vertical velocity at 3 km elevation; an average decrease of about 1 mm/day in the precipitation, with $r > 3$ over about half of the region; almost no change in the soil moisture storage; and a decrease, averaging about 2°C, with $r > 3$, in the ground-surface temperature.

6.5

(iii) **Hybrid experiments**

6.5.1

Non-interactive v. interactive soil moisture

These are experiments in which a calculation with interactive soil moisture is compared with one in which the prescribed soil moisture is held fixed for the duration of the experiment. If we regard the interactive case as a simulation of nature, then the case with the prescribed, fixed soil moisture can be thought of as showing how the climate would be changed if the land-surface evapotranspiration were to be brought under man's control: as, for example, by large-scale irrigation or by a change or a complete removal of the vegetation cover.

Fig. 6.22. The change in vertical velocity at 3 km elevation (top left), precipitation (top right), ground temperature (bottom left), and soil moisture (bottom right), in the albedo change experiment of Chervin (1979).

6.5.1.1

Manabe (1975)

A massive irrigation simulation experiment was made by Manabe (1975) with one of the Geophysics Fluid Dynamics Laboratory (GFDL) general circulation models. The model used the moist-convective adjustment method for calculating the convective precipitation and the moist-convective heating of the air; solar and long wave radiation transfers calculated with a non-interactive cloud distribution, prescribed as a function of latitude and elevation; and an albedo for ice-free and snow-free land that follows Posey & Clapp (1964).

In the 'natural case' (the interactive soil moisture case) the soil moisture was governed by the equations given at the beginning of Section 6.4, with $W^* = 150$ mm, and $k = 0.75$. In the 'irrigation case' (the non-interactive soil moisture case) β was everywhere held equal to 1.

The natural case simulation produced a rainband across north Africa in which, averaged between 15 and 30°E, there was a rainfall maximum of about 6 mm/day at latitude 5°N. In the irrigation case, the maximum rainfall was about 12 mm/day at latitude 8°N (see Manabe, 1975, Fig. 3).

The solid line in Fig. 6.23 shows the change in the precipitation, the irrigation case minus the natural case. The dashed line shows the corresponding difference in the evapotranspiration. (The reduction in evaporation, between 31 and 37°N, is over the Mediterranean Sea, presumably because the air was more humid from the massive land irrigation.)

Between 18 and 30°N the increase in precipitation is somewhat

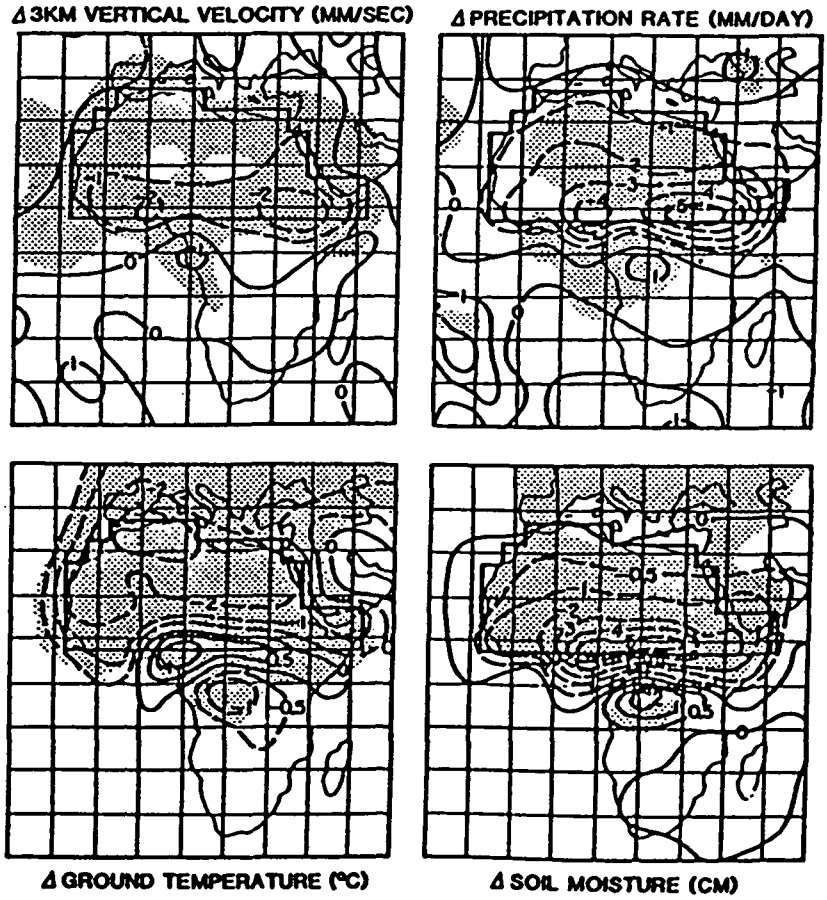

less than the increase in evapotranspiration, while between 12 and 15°N, where the evapotranspiration increases by only about 1.5 mm/day, the precipitation goes up by about 5.5 mm/day. On the other hand, at the equator, where there is an increase of evapotranspiration of 0.7 mm/day, the precipitation *decreases* by 3.5 mm/day. It is obvious, therefore, that there are large changes in the water vapor transport convergence.

Fig. 6.24 shows the circulation in the meridional plane, $(vj + wk)$, averaged between 15 and 30°E (where v is the northward component of the horizontal velocity, w is the vertical velocity, j is unit horizontal vector directed northward, and k is unit vertical vector directed upward). Although the eastward component of the horizontal velocity does not appear here, its divergence, $\partial u/\partial x$, enters into the calculation of the vertical velocity, w.

We see that at the equator there is a change from upward motion to downward motion in the free atmosphere, which must be accompanied by a change from horizontal velocity convergence to horizontal velocity divergence in the boundary layer. It therefore is the decrease in the boundary layer water vapor transport convergence ($-\overline{\nabla \cdot qv} \approx -\overline{q\nabla \cdot v}$) which makes the precipitation decrease by 3.5 mm/day (from 5 to 1.5 mm/day).

Between 12 and 15°N, on the other hand, weak ascending motion changes to very strong ascending motion; and the accompanying large increase in the boundary layer water vapor transport convergence, added to the small increase in evapotranspiration, makes the precipitation increase by 5.5 mm/day (from 0.7 to 6.2 mm/day).

Fig. 6.23. Change in evapotranspiration (broken line) and in precipitation (solid line), averaged between 15 and 30°E, in the hybrid experiment of Manabe (1975).

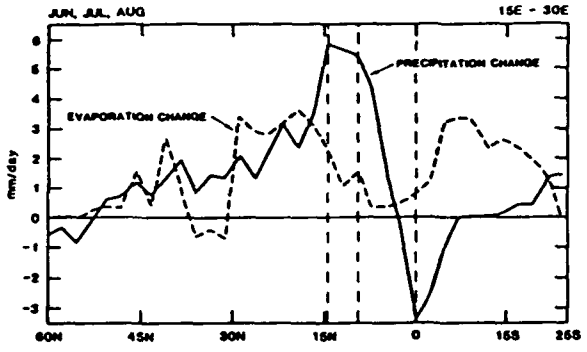

Fig. 6.24. Circulation in the meridional plane, averaged between 15 and 30°E, in the hybrid experiment of Manabe (1975). Top: interactive soil moisture case. Bottom: moist soil case. (Figure by personal communication.)

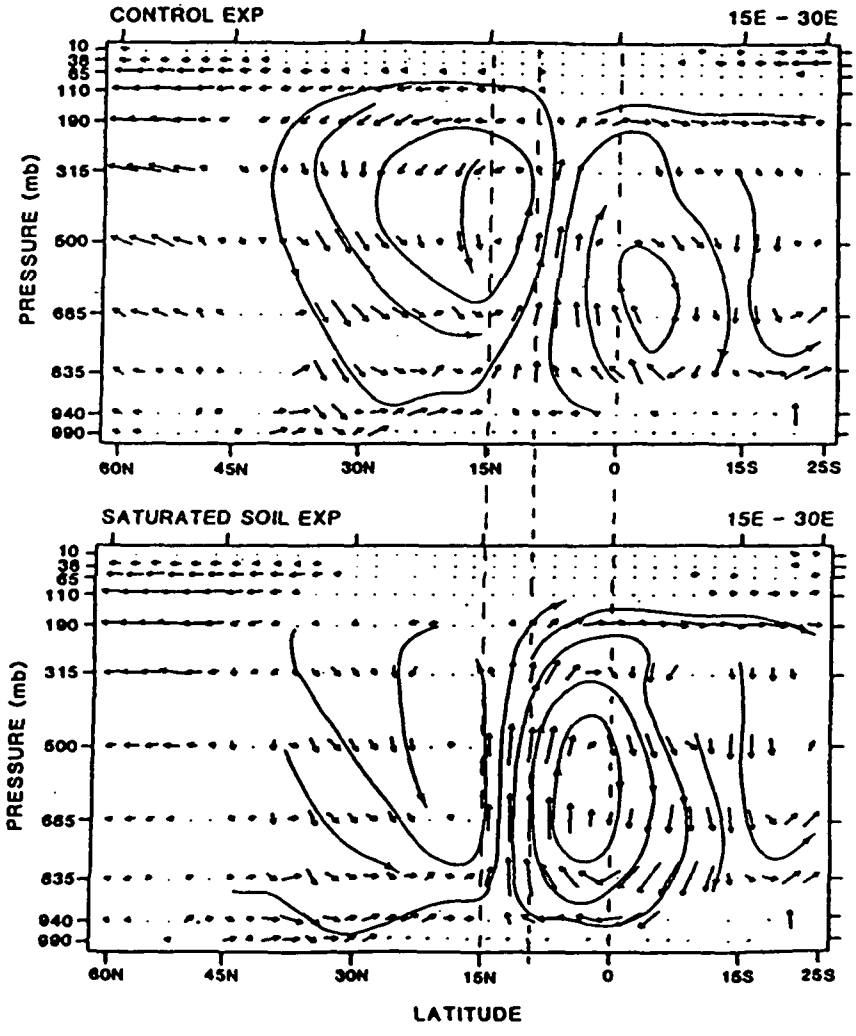

6.5.1.2

Kurbatkin, Manabe and Hahn (1979)

The irrigation experiment (6.5.1.1) (which makes $\beta = 1$ everywhere) is physically realizable in the real world. But it is not so easy to make $\beta = 0$ everywhere in the real world. If the rainfall were to be very constant in time, so that the surface of the earth was always wet, then it would be very difficult (although possible) to prevent evaporation. But where rainfall occurs in an intermittent way, and most of the water infiltrates to a depth of more than a few centimeters, then the removal of the vegetation would stop the transpiration and, thereby, would greatly reduce the transfer of water vapor to the air.

Kurbatkin, Manabe & Hahn (1979) made a hybrid experiment, in which a simulation with $\beta = 0$ everywhere was compared with a simulation with interactive soil moisture. For this experiment they used the M-21 version of the GFDL spectral model (Manabe, *et al.*, 1979), with moist-convective adjustment, prognostic clouds, and a prescribed albedo that follows Posey & Clapp (1964). In the interactive soil moisture case, the soil moisture and evapotranspiration were calculated with the equations given at the beginning of Section 6.4, with $W^* = 150$ mm, and $k = 0.75$.

The integration in the interactive case was over a period of two years and eight months. The results that are shown here are averages for the months of July and August at the end of the integration period. The non-interactive case, with $\beta = 0$, was initialized from the interactive case at the beginning of the last June and run until the end of August.

The top panel in Fig. 6.25 shows the simulated precipitation in the interactive soil moisture case, the center panel shows the precipitation in the no-evapotranspiration case, and the bottom panel shows the difference between the two (no-evapotranspiration case minus interactive case). With no land-surface evapotranspiration, there is less precipitation over the continents and also less precipitation over most of the oceans, with the largest decreases, of up to 5 mm/day, over India, the north Indian Ocean and over the western part of the tropical North Pacific. Only over the

Fig. 6.25. Precipitation (cm/day) averaged for July and August, in experiment of Kurbatkin *et al.* (1979). Top: interactive soil moisture case. Middle: no land-surface evapotranspiration case (contours 0.05, 0.1, 0.2, 0.5, 1.0, 5.0 cm/day. Dotted shading: precip. < 0.1 cm/day; ruled shading: precip. > 0.5 cm/day): Bottom: no-evapotranspiration case minus interactive case (shaded area is negative).

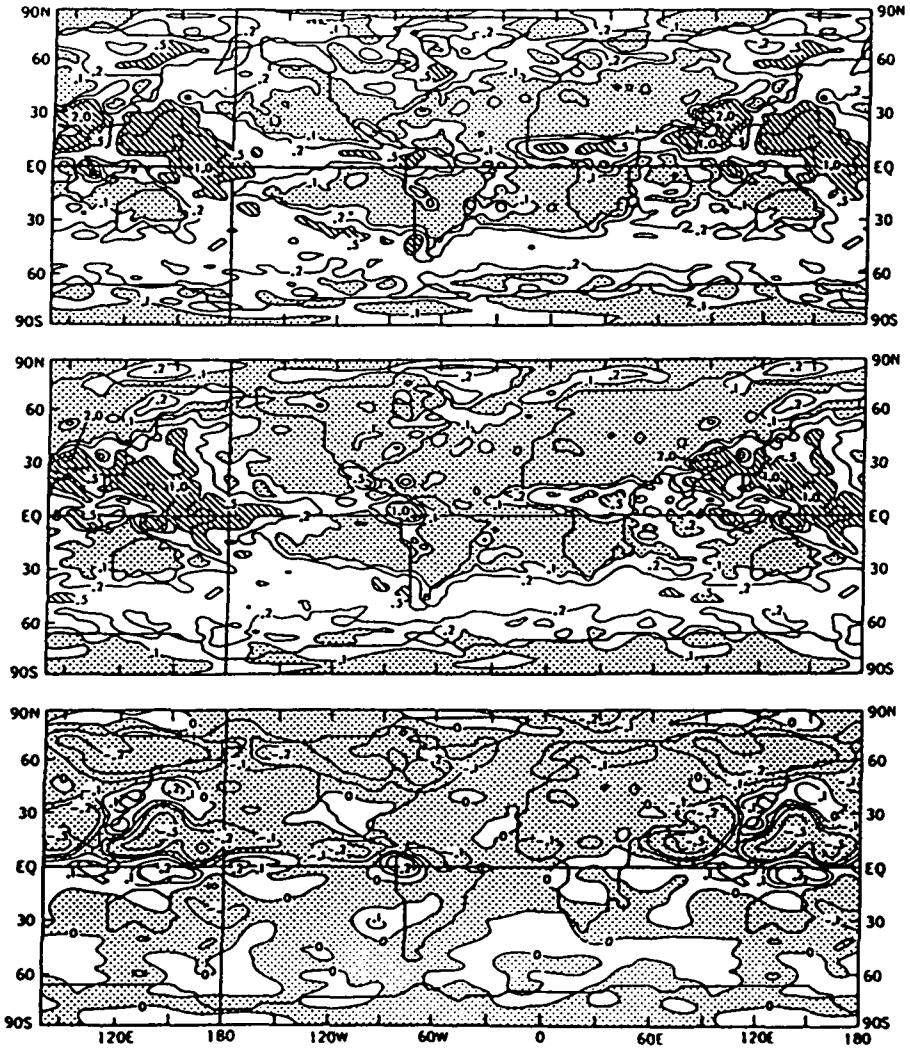

mid-latitude east coast of Asia and the adjacent Pacific, and in some longitudes along the equator (but not over the Atlantic Ocean sector), is the precipitation larger in the $\beta = 0$ case, and by as much as 2 mm/day.

Fig. 6.26 shows the sea-level pressure fields. We see that in the no-evapotranspiration case the pressure is lower over most of the continental areas. But over north-central Asia, over the northeast Atlantic, and especially over the extratropical central and western North and South Pacific Oceans, the pressures are higher in the no-evapotranspiration case. Although only the $\beta = 0$ case has the same evapotranspiration boundary condition that was used in the experiment with the GLAS model (in 6.3.1.1 above), there are many correspondences, as can be seen by comparing the bottom panels of Fig. 6.5 and Fig. 6.26, especially over the central and western North and South Pacific and over the South Atlantic.

The authors show (Kurbatkin *et al.*, 1979, Fig. 4) that in the $\beta = 0$ case there is, on the average, an increase in the large-scale ascending motion in the free atmosphere over the continents; and they remark that in spite of this increased ascending motion there is less cloudiness over the continents, and therefore a greater absorption of solar radiation by the ground and a higher surface temperature than in the interactive soil moisture case. The decrease in the precipitation over the oceans, they point out, is produced by the increase in descending motion (or weakening of ascending motion) over the oceans.

Fig. 6.26. Sea-level pressure (mb), averaged for July and August, in experiment of Kurbatkin *et al.* (1979). Top: interactive soil moisture case. Middle: no land-surface evapotranspiration case. Bottom: *no-evapotranspiration case minus interactive case* (shaded area is negative).

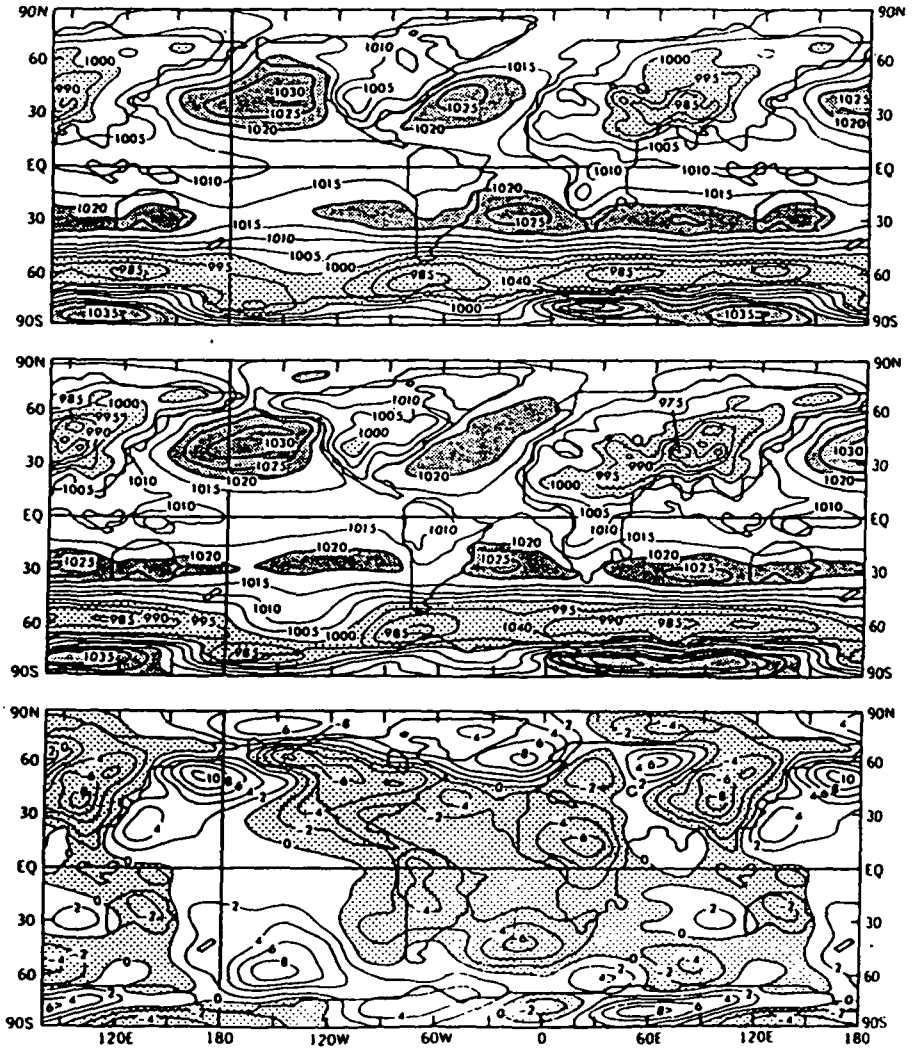

6.6

Summary and conclusions

All of the experiments show that the model simulated climates are sensitive to the land-surface boundary conditions which affect evapotranspiration. When soil moisture availability or surface albedo are changed regionally (or globally), changes in the precipitation, the temperature and the motion field of the atmosphere take place over the corresponding region (or over the globe), which are clearly above the level of the natural variability of the model simulated climates (those which are caused by the shear-flow instabilities of the atmosphere).

(Whether a change in the boundary condition of a given region has a significant effect on the climate of some distant region is not known. Such atmospheric 'teleconnections' are not self-evident in these experiments: and, like other kinds of forcing from

a distance, they require some kind of statistical analysis to separate the signal from the background noise.)

Not only are the regional (local) influences large and consistent from one experiment to another; they are also easily understood, in physical terms, after the analysis has untangled the non-linear interactions. Thus we find, for example, that under some circumstances an increase in the surface albedo reduces the cloudiness and, in that way, increases (not decreases) the ground temperature. Or, as another example, cutting off the evapotranspiration over Asia increases (not decreases) the Indian monsoon rainfall, because it changes the orientation, with respect to the Himalayan mountain barrier, of the moist boundary layer air stream from the ocean. It is this kind of behavior, easily understood after the fact, which is very difficult to anticipate beforehand.

The magnitudes of the changes in climate, which are produced by modifying the soil moisture availability or the surface albedo, as shown in these experiments, are about as large as the changes produced by the seasonal change in the declination of the sun (and, the author hazards the guess, larger than the changes produced by the observed seasonal changes in ocean-surface temperatures and extent of the sea-ice). It is very likely, therefore, that the land-surface evapotranspiration process, whose time scale depends on the magnitude of the soil moisture storage relative to the difference between the precipitation and evapotranspiration rates, is the most important boundary process that can produce anomalies in the time-averaged state of the atmosphere (changes in climate) on the monthly, seasonal and annual time scales.

A shortcoming of all existing general circulation models is that they calculate the potential evapotranspiration with a formulation which is appropriate for evaporation from an open water bucket, but not from a vegetated surface (and, especially, not from tall (forest) vegetation). (See, for example, Shuttleworth & Calder, 1979; and Sellers & Lockwood, 1981.) But, hopefully, this will be corrected and future models will take into account the vegetation influence on the water and energy transfers to the atmosphere in a realistic way.

Acknowledgement

The author thanks the several scientists who provided unpublished or supplementary information about their experiments; Dr J. Shukla and Dr Y. Sud who made helpful comments on the review; and Ms J. Reckley for her extraordinary patience and kindness in the typing, and retyping, of the manuscript.

Since this article was written, four additional papers have appeared, all of which show that the atmosphere is sensitive to the land-surface evapotranspiration.

Rind, D., 1982. 'The influence of ground moisture conditions in North America on summer climate as modeled in the GISS GCM'. *Mon. Wea. Rev.*, **110**, 1487–94.

Rowntree, P. R. & J. A. Bolton, 1983. 'Simulation of the atmospheric response to soil moisture anomalies over Europe'. *Quart. J. R. Met. Soc.*, **109**, 501–26.

Sud, Y. C. & M. Fennessy, 1982. 'A study of the influence of surface albedo on July circulation in semi-arid regions using the GLAS GCM'. *J. Climatology*, **2**, 105–25.

Yeh, T. C., R. T. Wetherald & S. Manabe, 1984. 'The effect of soil moisture on the short-term climate and hydrology change – a numerical experiment'. *Mon. Wea. Rev.* (in press).

References

Arakawa, A. & V. R. Lamb (1977). 'Computational design of the basic dynamical processes of the UCLA general circulation model'. *In: Methods in Computational Physics*, Vol. 17, pp. 173–265, Academic Press, N.Y.

Arakawa, A. & M. J. Suarez (1983). 'Vertical differencing of the primitive equations in sigma coordinates'. *Mon. Wea. Rev.*, **111**, 34–45.

Baumgartner, A. & E. Reichel (1975). *The World Water Balance: Mean Annual Global, Continental and Maritime Precipitation, Evaporation and Runoff*. Elsevier Publishing Co., Amsterdam, 179 pp. and plates.

Benton, G. S., M. A. Estoque & J. Dominitz (1953). *An evaluation of the Water Vapor Balance of the North American Continent*. The Johns Hopkins University Dept. Civil Engineering. Scientific Report No. 1, July 1953, 101 pp.

Budyko, M. I. (ed.) (1963). *Atlas of the Heat Balance of the Earth*. With N. A. Efimova: Maps of the radiation balance for the continents. Plates 14–26. Main Geophysical Observatory, Leningrad, 69 pl.

Carson, D. J. (1981). 'Current parameterization of land surface processes in atmospheric general circulation models. *In: Proceedings of the JSC Study Conference on Land-Surface Processes in Atmospheric General Circulation Models*, Greenbelt, USA, 5–10 January 1981. WMO, Geneva.

Carson, D. J. & A. B. Sangster (1981). 'The influence of land-surface albedo and soil moisture on general circulation model simulations'. GARP/WCRP: *Research Activities in Atmospheric and Oceanic Modelling*. (ed. I. D. Rutherford). *Numerical Experimentation Programme*, Report No. 2, pp. 5.14–5.21.

Charney, J. G. (1975). 'Dynamics of deserts and drought in the Sahel'. *Quart. J. R. Met. Soc.*, **101**, 193–202.

Charney, J. G. (1975*a*). 'Drought, a biophysical feedback mechanism.' *Proceedings of Conference on Weather and Food, Endicott House, Mass. Inst. Tech.* Cambridge, Mass., 9–11 May, 1975, 10 pp.

Charney, J. G., W. J. Quirk, S. H. Chow & J. Kornfield (1977). 'A comparative study of the effects of albedo change on drought in semi-arid regions'. *J. Atmos. Sci.*, **34**, 1366–85.

Chervin, R. M. (1979) 'Response of the NCAR general circulation model to changed land surface albedo'. *Report of the JOC Study Conference on Climate Models: Performance, Intercomparison and Sensitivity Studies*, Washington, DC, 3–7 April, 1978. GARP Publ. Series, No. 22, Vol. 1, pp. 563–81.

Chervin, R. M. & S. H. Schneider (1976). 'On determining the statistical significance of climate experiments with general circulation models'. *J. Atmos. Sci.*, **33**, 405–12.

Corby, G. A., A. Gilchrist & P. R. Rowntree (1977). 'The UK Meteorological Office 5-layer general circulation model. *In: Methods in Computational Physics*, Vol. 17, pp. 67–110.

Denmead, O. T. & R. H. Shaw (1962). 'Availability of soil water to plants as affected by soil moisture content and meteorological conditions'. *Agron. J.*, **54**, 385–439.

Gadd, A. J. & J. F. Keers (1970). 'Surface exchanges of sensible and latent heat in a 10-level model atmosphere. *Quart. J. R. Met. Soc.*, **96**, 297–308.

Korzun, V. I. (ed.) (1978). 'World water balance and water resources of Earth'. *Report of the USSR Committee for the International Hydrological Decade. Studies and Reports in Hydrology*, Vol. 25. Unesco Press, Paris, 663 pp. and plates.

Kurbatkin, G. P., S. Manabe & D. G. Hahn (1979). 'The moisture content of the continents and the intensity of summer monsoon circulation'. *Meteorologiya i Gidrologiya*, **11**, 5–11.

Manabe, S. (1975). 'A study of the interaction between the hydrological

cycle and climate using a mathematical model of the atmosphere'. *Proceedings of Conference on Weather and Food, Endicott House, Mass. Inst. Tech.*, Cambridge, Mass., 9–11 May 1975, 10 pp. (and additional figure by personal communication).

Manabe, S., D. G. Hahn & J. L. Holloway, Jr (1979). 'Climate simulations with GFDL spectral models of the atmosphere: effect of spectral truncation'. *Report of the JOC Study Conference on Climate Models: Performance, Inter-comparison and Sensitivity Studies*, Washington, DC, 3–7 April 1978. GARP Publ. Ser., No. 22, Vol. I, pp. 41–94.

Miyakoda, K., G. D. Hembree & R. F. Strickler (1979). 'Cumulative results of extended forecast experiments. II: Model performance for summer cases'. *Mon. Wea. Rev.*, 107, 395–420.

Miyakoda, K., J. Smagorinsky, R. F. Strickler & G. D. Hebree (1969). 'Experimental extended predictions with a nine-level hemispheric model'. *Mon. Wea. Rev.*, 97, 1–76.

Miyakoda, K. & R. F. Strikler (1981). 'Cumulative results of extended forecast experiment. Part III: Precipitation'. *Mon. Wea. Rev.*, 109, 830–42.

Posey, J. W. & P. F. Clapp (1964). 'Global distribution of normal surface albedo'. *Geophisica Internacional*, 4 (1), 33–48.

Rasmusson, E. M. (1968). 'Atmospheric water vapor transport and the water balance of North America. Part II: Large-scale water balance investigations'. *Mon. Wea. Rev.*, 96, 720–34.

Rowntree, P. R. & J. A. Bolton (1978). 'Experiments with soil moisture anomalies over Europe'. *The GARP Programme on Numerical Experimentation*: Research Activities in Atmospheric and Ocean Modelling (ed. R. Asselin). Report No. 18. WMO/ICSU, Geneva, August 1978, p. 63.

Rutter, A. J. (1975). 'The hydrological cycle in vegetation'. *In Vegetation and the Atmosphere, Vol. II, Case Studies* (ed. J. L. Monteith). Academic Press, New York, pp. 111–54.

Suarez, M. J., A. Arakawa & D. A. Randall (1983). 'The parameterization of the planetary boundary layer in the UCLA general circulation model: formulation and results'. *Mon. Wea. Rev.* (in press).

Schutz, C. & W. L. Gates (1972). *Global Climatic Data for Surface, 800 mb, 400 mb: July*. Rand Report. R-915-ARPA, The Rand Corporation, Santa Monica, Calif., 880 pp.

Sellers, P. & J. G. Lockwood (1981). 'A numerical simulation of the effects of changing vegetation type on surface hydroclimatology'. *Climatic Change*, 3, 121–36.

Shukla, J. & Y. Mintz (1981). 'Influence of land-surface evapotranspiration on the earth's climate'. (Presented at the *JSC Study Conference on Land-Surface Processes in Atmospheric General Circulation Models*, Greenbelt, USA, 5–10 January 1981.) Published in *Science*, 215, 1498–501, 1982.

Shukla, J., D. Randall, D. Straus, Y. Sud & L. Marx (1981). 'Winter and Summer simulations with the GLAS climate model. *NASA Technical Memorandum 83866*, Goddard Space Flight Center, Greenbelt, Md, 282 pp.

Shuttleworth, W. J. & I. R. Calder (1979). 'Has the Priestley–Taylor equation any relevance to forest evaporation? *J. Appl. Meteor.*, 18, 639–46.

Somerville, R. C. J., P. H. Stone, M. Halem, J. E. Hansen, J. S. Hogan, J. Tenenbaum (1974). 'The GISS model of the global atmosphere'. *J. Atmos. Sci.*, 31, 84–117.

Stone, P. H., S. Chow & W. J. Quirk (1977). 'July climate and a comparison of the January and July climates simulated by the GISS general circulation model'. *Mon. Wea. Rev.*, 105, 170–94.

Walker, J. M. & P. R. Rowntree, (1977). 'The effect of soil moisture on circulation and rainfall in a tropical model'. *Quart. J. R. Met. Soc.*, 103, 29–46.

Washington, W. M. & D. L. Williamson (1977). 'A description of the NCAR global circulation models'. *Methods in Computational Physics*, 17, 111–72.

WMO (1979). *Report of the JOC Study Conference on Climate Models: Performance, Intercomparison and Sensitivity Studies. Washington, D.C., 3–7 April 1978.* (ed. L. Gates) GARP Publication Series No. 22. WMO, Geneva.

PRECIPITATION MEASUREMENTS FROM SPACE: WORKSHOP REPORT
D. Atlas and O. W. Theile (editors)
Code 910, NASA/Goddard Space Flight Center, Greenbelt, MD, October 1981

A BRIEF REVIEW OF THE PRESENT STATUS OF GLOBAL PRECIPITATION ESTIMATES

Yale Mintz
Department of Meteorology, University of Maryland, College Park, MD 20742
and
Lab. Atmospheric Sciences, NASA Goddard Space Flight Center, Greenbelt, MD 20771

Introduction

This is a brief review of what is now known about the global distribution of precipitation: both the "normal" distribution (i.e., the precipitation averaged over a number of years) and time-series of the precipitation. Only the most recent studies are explicitly covered. An historical account of earlier studies can be found in Jaeger (1976).

1. Jaeger (1976) produced global maps, and a corresponding machine-readable grided data set, which is the only estimate we have of the normal monthly precipitation over the entire globe.

Over the continents, the inputs were the published national and regional maps of normal monthly precipitation (Jaeger, 1976, Table 3); supplemented, where there were no maps, by station data from the World Weather Records (U.S. Dept. Commerce) and other sources. In so far as the data allowed, the thirty-year period, 1931-1960, was used: but where this was not possible, other time intervals were used. The globe was divided into grid areas of 5° longitude by 5° latitude and, reading from the various sources, the monthly values of the continental precipitation, averaged over the grid areas, were recorded. From these averaged values, plotted in the centers of the squares, the global maps of precipitation were drawn by hand (Jaeger, 1976, Figs. 9-21).

Over the oceans, Jaeger simply took the annual precipitation, as given in the map by Geiger (1965), and distributed that precipitation over the twelve months of the year in proportion to the monthly percentage frequency of observations reporting precipitation, as given, for each 5° by 5° square, in the Marine Climatic Atlas of the World (U.S. Navy, 1955-65). Thus, over the oceans, the annual precipitation is the one given by Geiger (with the exception of some small regions of the oceans adjacent to Indonesia, where Jaeger increased the annual precipitation from about 2000 to 3000 mm/year.)

Geiger's distribution of the annual precipitation over the oceans can be traced back to Schott. For the Atlantic Ocean, Schott (1926) reworked the earlier analysis of Supan (1898) in which the annual frequency of precipitation (the number of days in the year with precipitation), as reported in the logs of a large number of ships crossing the North and South Atlantic and the Indian oceans, was multiplied by an average precipitation intensity (the average amount of precipitation per rainy day) as a function of latitude, as obtained from measurements of rainfall made on a small number of ships.

For the annual precipitation in the Pacific and Indian Oceans, Schott (1933, 1935) used not only the above described frequency of precipitation multiplied by the latitude-dependent intensity of precipitation, but also extrapolated directly to the oceans the observed annual amount of precipitation at the nearest coastal and island stations.

Table 1
Present Status of Global Precipitation Estimates

	Normals			Time Series			
	Monthly	Seasonal	Annual	Weekly	Monthly	Seasonal	Annual
Entire Globe:	1. Jaeger (1976) continents / oceans		2. Baumgartner & Reichel (1975); 3. Korzun, ed. (1974)				
Continents only:		4. Korzun, ed. (1974); 5. Hsu & Wallace (1976)			8. Free Univ. Berlin (1963-1981)		
Oceans only:		6. Reed & Elliott (1979); 7. Dorman & Bourke (1979,1981)		9. Rao et al. (1976) (1972-1975)			

[Jaeger used the same method to divide the annual oceanic precipitation into monthly amounts that Möller (1951) had earlier used to obtain the seasonal (three-monthly) precipitation amounts. Möller had available, at that time, only the seasonal frequencies of oceanic precipitation, as given in the Atlas of Climatic Charts of the Oceans, by MacDonald (1938).]

2. Baumgartner and Reichel (1975) show only the normal annual precipitation over the globe. Over the continents they used about the same input data sources as Jaeger (1976), but they retained in their map much more of the spacial detail of the original sources.

Over the oceans some unspecified combination of the global maps of Albrecht (1960), Knoch (1961) and Drosdov (1964) was used; with an adjustment of the total ocean precipitation to 385 X 10^3 km^3/year. This adjustment was made on the assumption that the total continental precipitation is correct, and the further assumption that the estimate they had made of the total global evaporation is more reliable than any estimate that can be made of the total oceanic precipitation.

3. Korzun (ed., 1974) presents the normal annual precipitation over the continents after correcting for three systematic measurement errors: wind-effect error (which entails the largest correction), rain gauge wetting error, and rain gauge evaporation error. (See, also, Rodda, 1971.) The total correction varies with location, from about 10 mm to 200 mm/year in absolute value, and from about 3% to 70% in relative value (Korzun, ed., 1974, Figs. 19a, 19b.) The mean continental precipitation without the correction was 725 mm/year; and with the correction 800 mm/year. The input data sources were national and regional maps, derived from observations at about 42,000 stations; supplemented by about 18,000 additional stations. Thus, data from about 60,000 land stations entered into the compilation of the global map. Where possible, the data was taken from, or reduced to the 80-year period 1891-1970. The continental precipitation is shown with somewhat less detail than that given by Baumgartner and Reichel (1975). [At the present time, precipitation is measured at about 120,000 (unevenly distributed) land stations over the globe.]

Over the oceans, the annual precipitation was calculated from a new compilation of mean monthly precipitation frequencies, in 5° latitude by 5° longitude squares, taken from records in ships logs (for the period 1900-1964 in the Pacific Ocean, and 1900-1969 in the Atlantic and Indian oceans), multiplied by the mean annual intensity of precipitation (the ratio of the total amount of precipitation to the total duration of precipitation. This field of the mean precipitation intensity, which is shown on a global map (Korzun, ed., 1974, Fig. 121), was made by extrapolating to the ocean from the measured duration and measured (and corrected) amount of precipitation at the nearest of 426 island and coastal stations. [This is essentially the same method that was used by Supan (1898). It implicitly takes into account not only the effect of the spatial variation of the air temperature, but also the effect of the different predominant weather types: giving different weights to the convective showers in the intertropical convergence zone and the western subtropical oceans, drizzle in the eastern subtropical oceans, and rain from the cyclones that move across the middle and high latitude oceans.] In addition to this product of precipitation frequency and precipitation intensity, Korzun (ed. 1974) extrapolated to the ocean directly the measured (and corrected) precipitation amounts at 173 stations on small, low islands. (See, also, Samoilenko, 1966).

4. Korzun (ed. 1974, Figs. 26, 35, 54, 66, 79, 88), using only 523 stations for all of the continents (mostly stations with long-term records), constructed maps of the percentages of the normal annual continental precipitation that occur in the four seasons of the year. Because of the small number of stations used (65 for North America, 133 for Asia), only large scale space variations are shown. Thus, whether it is so in nature or not, according to this analysis the small scale features which are seen on the annual precipitation map are features that persist throughout the year.

5. Hsu and Wallace (1976) have produced an analysis of the normal precipitation over the continents (and many islands of the globe), which shows the normalized amplitude and phase of the first two annual harmonics in the precipitation. They used the precipitation data, for the period 1951-70, at about 700 of the 2000 stations in the World Monthly Surface Climatological Data Set (which they obtained on tape from the National Center for Atmospheric Research, Boulder.)

No information is given by the maps of the two annual harmonics which is not implicit in the maps of monthly precipitation, as given, for example, by Jaeger (1976). But some characteristics of the time-space variation of the precipitation are easier to see (although others are more difficult to see) when the normalized harmonics are displayed in this way.

6. Reed and Elliott (1979) produced maps of the normal seasonal and annual precipitation for the Atlantic and Pacific Oceans north of the equator, using as their input data the monthly precipitation frequencies given in the revised volumes of the Marine Climatic Atlas of the World (U.S. Navy, 1974, 1977). They divided the two oceans into tropical and extratropical domains, with the dividing line at 20°N in the eastern two-thirds, and at 30°N in the western one-third of each ocean. North of this boundary (in the extratropical domain) they used a conversion from monthly precipitation frequency to monthly precipitation amount that changed from 0.31 (cm $month^{-1}\%^{-1}$) in July and August to 0.36 (cm $month^{-1}\%^{-1}$) in December and January; and south of this boundary (in the tropical domain) they used a constant conversion of 1.0 (cm $month^{-1}\%^{-1}$). These conversion factors were derived by Reed and Elliott (1977) and by Reed (1979) mainly from the work of Tucker (1961) on rainfall at land stations in Great Britain, and from measurements of precipitation that were made in the eastern Pacific, between 60°N and 40°N and between 20°N and 2°S,

in 1975-1976, by the ship "Oceanographer". Because of the discontinuity in the conversion factor, the precipitation maps show large discontinuities at the boundaries that separate the two domains.

[When compared with the measured precipitation on ships during GATE, in the summer of 1974, the calculated intertropical precipitation maximum in the eastern Atlantic is about half as large as the measured maximum.]

7. Dorman and Bourke (1979, 1981) give the normal seasonal and annual distributions of precipitation over the Atlantic and Pacific Oceans, from 30°S to 60/70°N, as obtained by the method of Tucker (1961) and a latitude-derived correction for the air temperature.

Tucker's method consists of assigning a given amount of precipitation to the different present weather types (clear sky, drizzle, showers, heavy continuous rain, etc.) that are listed in the synoptic weather code. Tucker derived the precipitation amount, for each category of the synoptic code that is associated with precipitation occurring at the time of observation, by correlating that synoptic code report with the measured precipitation at some stations on the periphery of the British Isles. Dorman and Bourke (1978a) examined the universality of Tucker's coefficients by using also coastal station data along the periphery of the Atlantic and Pacific Oceans, from south of the equator to about 75°N. They found that there was a latitudinal bias related to the local air temperature: i.e., rainfall was increasingly underestimated as air temperature increased. They found that this effect was systematic and could be corrected by empirical formulas for the annual, seasonal and monthly averages. Dorman and Bourke (1979, 1981) use the Tucker method and those correction coefficients to obtain the seasonal and annual precipitation, for 2° latitude by 5° longitude rectangles, over the Pacific and Atlantic oceans. The input data, for "present weather" and air temperature, were the synoptic observations taken by a wide variety of ships of opportunity, for the period 1950-72 in the Pacific and 1950-74 in the Atlantic, as provided by the magnetic tape data file maintained by the North Pacific Experiment (NORPAX) group at Scripps Institution of Oceanography, La Jolla. They also present maps of the normalized amplitude and phase of the first two annual harmonics of the precipitation, as derived from monthly mean precipitation estimates (which are given, for the Pacific Ocean, in Dorman and Bourke, 1978b.) For the Pacific Ocean, some information is also given about the diurnal variation of precipitation.

A detailed intercomparison and critical evaluation of these various estimates of the normal annual and seasonal precipitation distributions, though desirable, is beyond the assigned scope of this review. We should, nonetheless, note that there are large differences in these estimates, over the continents as well as over the oceans. Over large areas of the oceans some of the estimates differ by a factor of two.

8. The Free University of Berlin (1963-1981), Institute of Meteorology, has published an analysis of the precipitation distribution over the northern hemisphere continents (and extending, over Africa, to about 15°S) for each month since the summer of 1963. The field is represented by isolines for seven categories of precipitation derived from a 30-year base period, 1931-1960. (Category 1 denotes that the precipitation for the month is within the range of the amount that fell in the six driest years of the base period; and 5 denotes that it is within the range of the six wettest years of the base period. 0 denotes that it is less, and 6 that it is more than any precipitation that fell during the 30-year base period.)

9. Rao et al. (1976) derived weekly (and also monthly, seasonally and annually) averaged maps of precipitation over the oceans, for the period 11 Dec. 1972 to 28 Feb. 1975, from measurements with the Electrically Scanning Microwave Radiometer on the polar-orbiting Nimbus-5 satellite. The theoretically derived calibration of the precipitation rate as a function of the measured microwave brightness temperature, for different freezing levels, was verified in a ground-based experiment in which upward-viewing microwave brightness temperatures were compared with measured rainfall rates. In calculating the precipitation from the measured brightness temperatures, they used one of three prescribed heights of the 273°K isotherm over the globe.

[The overall pattern and general magnitudes of the seasonal and annual precipitation, as shown in these maps, conform fairly well with the normal seasonal and annual precipitation distributions given by Dorman and Bourke (1979, 1981).]

References

Albrecht, F. 1960: Jahreskarten des Wärme- und Wasserhaushaltes der Ozeane. Ber. Dt. Wetterd., Nr. 66, Offenbach.

Baumgartner, A., and E. Reichel, 1975: The World Water Balance: Mean Annual Global, Continental and Maritime Precipitation, Evaporation and Runoff. Elsevier Publishing Co., Amsterdam/Oxford/New York, 179 pp and plates.

Dorman, C. E., and R. H. Bourke, 1978a: A Temperature Correction for Tucker's Ocean Rainfall Estimates. Quart. J. Roy, Meteor. Soc., 104, pp 765-773.

Dorman, C. E., and R. H. Bourke, 1978b: Maps of Pacific Rainfall, Rep. No. 78-2, Center for Marine Studies, San Diego State University, 14 pp + 34 Figs.

Dorman, C. E., and R. H. Bourke, 1979: Precipitation over the Pacific Ocean, 30°S to 60°N. Mon. Wea. Rev., 107, pp 896-910.

Dorman, C. E., and Bourke, 1981: Precipitation over the Atlantic Ocean, 30°S to 70°N. Mon. Wea. Rev., 109, pp 554-563.

Drosdov, O. A. (ed), 1964: Physical Geographical Atlas of the World. Moscow. Soviet Geography. Review and Translation. Vol. VI. Nos. 5-6, 403 p. Amer. Geogr. Soc. New York.

Free University of Berlin, 1963-1981: Beliage zur Berliner Wetterkarte, Welt-Wetterlage (monthly means). Institute fur Meteorologie der Freien Universitat Berlin.

Geiger, R., 1965: Wandkarten 1:30 Mill., Jahrlicher Niederschlag. Perthes Verlag, Darmstadt.

Hsu, C. F., and J. M. Wallace, 1976: The Global Distribution of the Annual and Semi-annual Cycles in Precipitation. Mon. Wea. Rev., 104, pp 1093-1101.

Jaeger, L., 1976: Monatskarten des Niederschlags für die ganze Erde. Berichte des Deutschen Wetterdienstes, Nr. 139 (Band 18). Offenbach a. M., 38 pp. and plates.

Knoch, K. 1961: Niederschlag und Temperatur (Weltkarten). Welt-Seuchen Atlas III. 5 S., 3 K. Hamburg.

Korzun, V. I. (ed), 1974: World Water Balance and Water Resources of the Earth. Report of the USSR Committee for the International Hydrological Decade. Studies and Reports in Hydrology, vol 25. Unesco Press, Paris, 663 pp, and Atlas with explanatory text (35 pp).

MacDonald, W. F., 1938: Atlas of Climatic Charts of the Oceans. U.S. Weather Bureau, Wash. D.C.

Möller, F., 1951: Vierteljahreskarten des Niederschlags für die ganze Erde. Petermanns Geogr. Mitt., 95, pp, 1-7.

Rao, M. S. V., W. V. Abbott III, and J. S. Theon, 1976: Satellite-derived Global Oceanic Rainfall Atlas (1973 and 1974). X-911-76-116, Goddard Space Flight Center, Greenbelt, Md. 31 pp and weekly, monthly, seasonal, and annual maps.

Reed, R. K., 1979: On the Relationship between the Amount and Frequency of Precipitation over the Ocean, J. Appl. Meteor., 18, pp 692-696.

Reed, R. K., and W. P. Elliott, 1977: A Comparison of Oceanic Precipitation as Measured by Gage and Assessed from Weather Reports, J. Appl. Meteor., 16, pp 983-986.

Reed, R. K., and W. P. Elliott, 1979: New Precipitation Maps for the North Atlantic and North Pacific Oceans, J. Geophys. Res., 84, pp 7839-7846.

Rodda, J. C., 1971: The Precipitation Measurement Paradox-The Instrument Problem. Reports on the WMO International Hydrological Decade Projects, No. 16. WMO No. 316, Geneva, 42 pp.

Samoilenko, V. S., 1966: Moisture Exchange between Ocean and Atmosphere. In: The Pacific Ocean, vol I, Nauka, Moscow, pp 302-310.

Schott, G., 1926: Geographie des Atlantischen Ozeans. Boysen Verlag, Hamburg.

Schott, G., 1933: Die Jahrlichen Niederschlagsmengen auf dem Indischen und Stillen Ozean. Ann. Hydrogr., 61, pp 1-12.

Schott, G., 1935: Geographie des Indischen und Stillen Ozeans. Boysen Verlag, Hamburg.

Supan, A., 1898: Die Jährlichen Niederschlagsmengen auf den Meeren. Petermanns Geogr. Mitt., 44, pp 179-182.

Tucker, G. B., 1961: Precipitation over the North Atlantic Ocean, Quart. J. Roy. Meteor. Soc., 87, pp 147-158.

U. S. Dept of Commerce: World Weather Records. Superintendent of Documents, U.S. Govt. Printing Office, Wash. D.C.

U. S. Navy, 1955-65: Marine Climatic Atlas of the World. Vol. 1-7. NAVAER, 50-1C-528-533. U.S. Govt. Printing Office, Wash. D.C.

U. S. Navy, 1974: Marine Climatic Atlas of the World. Vol. 1, North Atlantic Ocean. U.S. Govt. Printing Office, Wash. D.C.

U. S. Navy, 1977: Marine Climatic Atlas of the World. Vol. 2, North Pacific Ocean. U.S. Govt. Printing Office, Wash. D.C.

PRECIPITATION MEASUREMENTS FROM SPACE: WORKSHOP REPORT
D. Atlas and O. W. Theile (editors)
Code 910, NASA/Goddard Space Flight Center, Greenbelt, MD, October 1981

PRECIPITATION MEASUREMENT REQUIREMENTS FOR GENERAL CIRCULATION CLIMATE MODEL DEVELOPMENT AND APPLICATIONS

Yale Mintz
Department of Meteorology, University of Maryland, College Park, MD 20742
and
Lab. Atmospheric Sciences, NASA Goddard Space Flight Center, Greenbelt, MD 20771

Introduction

A general circulation model is a set of finite-difference analogues of the equations that govern the changes in the state of the atmosphere over the global domain. With given initial state and boundary conditions, these conservation equations (for mass, momentum, energy and water substance) are integrated numerically to obtain the fields of the physical state variables: pressure, velocity, temperature, water vapor and clouds. While doing this, the calculations reveal the mass and momentum transfers, the energy productions and energy conversions, and the compositional change processes that control the distributions of the state variables. [For examples of such general circulation climate models, and of climate simulations made with these models, see, respectively, Chang (ed.), 1977, and WMO/ICSU, 1979].

Precipitation is not one of the physical state variables of the atmosphere. Unlike water vapor and clouds (or snow on the ground and moisture in the soil), it is not part of the atmospheric (or ground) composition field. Precipitation is a process that changes the composition field.

There are two ways in which global precipitation measurements can aid in the development and use of general circulation climate models:

(1) precipitation measurements can verify the calculated precipitation and, thereby, help improve the calculation of the thermal forcing that produces the large scale atmospheric circulation; and

(2) precipitation measurements can be used to initialize one of the very important physical state variables of a climate model, the soil moisture.

1. Global Measurements of Precipitation for Verifying and Improving the Thermal Forcing of the Atmosphere

The large scale motions of the atmosphere are produced by *horizontal differences in the heating of the atmosphere. It is the* horizontal gradient of heating that generates available potential energy, which adiabatic processes convert into the kinetic energy of the large-scale motions (Lorenz, 1955).

Figure 1 shows an example of the time-averaged and zonally-averaged heating in a climate simulation with a general circulation model. The top three panels show, respectively, the heating produced by solar and long wave radiation, by large scale condensation, and by cumulus condensation and convection. The bottom panel shows the heating by all of these processes, together with the sensible heat transfer from the underlying land and ocean.

We see that radiation produces much smaller horizontal gradients of heating than the two kinds of condensation heating. It is especially the strong horizontal gradient of the heating by cumulus condensation and convection in the tropics that forces a strong divergent motion field within the tropics and subtropics. This motion field, by subsidence and horizontal advection of heat into the subtropics, produces the mid-latitude baroclinic zones; and, in turn, these baróclinic zones supply the available potential energy for generating the extratropical wave-cyclones. (What the figure does not show is the very large longitudinal variation of the cumulus condensation heating in the tropics, which also affects the circulation.)

The ability of a general circulation model to simulate (and predict) climate will, therefore, greatly depend on how well the model simulates the heating of the atmosphere; and especially, on how well it simulates the heating by cumulus condensation and convection.

It would be ideal if measurements could reveal how the horizontal distribution of the release of the latent heat of condensation varies with elevation. But even if we can only measure the horizontal distribution of the total latent heat release, as evidenced by the precipitation that reaches the earth's surface, that would be very useful. It would be sufficient to know the precipitation averaged over a day; averaged over areas comparable to the grid-areas of the general circulation models [which presently are about (200 km)^2 to (400 km)^2, but by the end of this decade will probably be (50 km)^2 to (100 km)^2]; and with an accuracy, in this time- and space-average, of about 0.5 mm/day (which, for the regions of above average precipitation, is an accuracy of about 10%).

It would be helpful if, concurrent with the precipitation measurements, there were also measurements of the distribution of the cloud top heights (and, especially, of the cumuliform clouds, which convect the released heat upwards.)

2. Global Measurements of Precipitation for the Initialization of Soil Moisture

A review and intercomparison of a number of climate-sensitivity experiments, made with different general circulation models, shows that the simulated fields of temperature, motion and precipitation greatly depend on the soil moisture, and that this dependence has a time scale of several months (Mintz, 1981.) It is, therefore, of utmost importance for climate simulations and

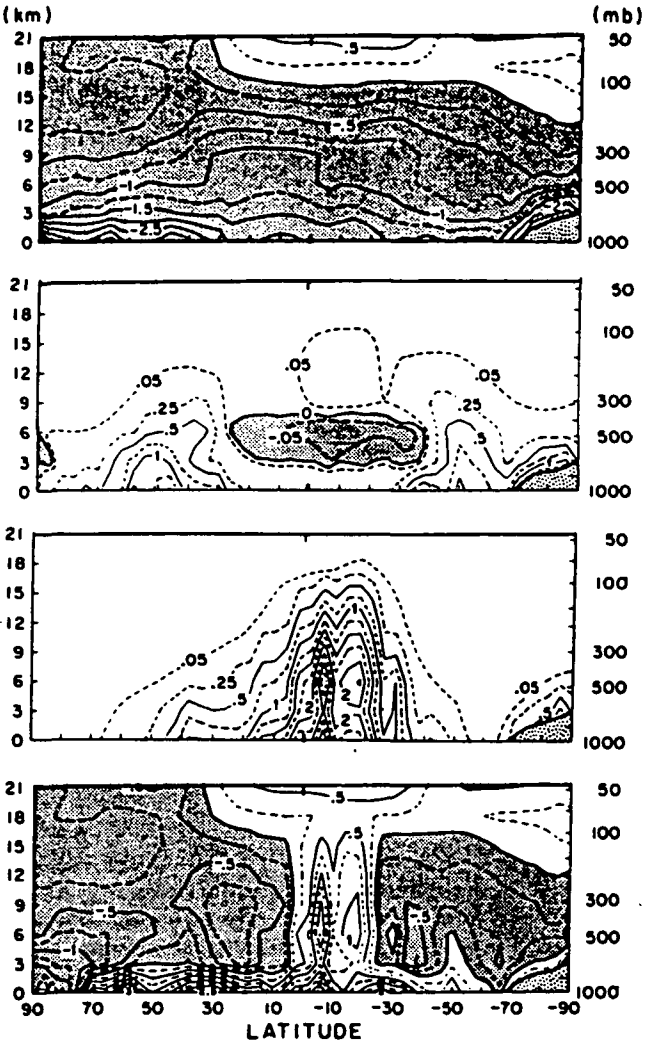

Fig. 1 Zonally-averaged heating of the atmosphere, in January, as calculated in a numerical simulation experiment (Schlesinger and Mintz, 1979). Solid line contour interval is 0.5°C day^{-1}. Top panel: Solar plus longwave radiational heating. Second panel: Large scale condensation heating. Third panel: Heating by cumulus condensation and convection. Bottom panel: Total heating (sum of the first three panels, plus sensible heat transfer from the underlying land and ocean.)

climate predictions to know the amount of moisture in the soil.

One way of determining the amount of moisture in the soil is by integration of the soil moisture continuity equation. In its most simple, but non-trivial form, this can be written

$$\frac{dw}{dt} = P - E, \quad W_{max} = W^* \tag{1}$$

where

$$E = \beta E_p \tag{2}$$

$$\beta = \beta(W, W^*) \tag{3}$$

and

$$E_p = E_p(T). \tag{4}$$

Here, W is the amount of evapotranspiration-available moisture in the soil, W* is the maximum available moisture that the soil can hold, P is the precipitation rate, E is the rate of evapotranspiration, β is the evapotranspiration coefficient, E_p is the rate of potential evapotranspiration, and T is the temperature of air near the surface.

Figure 2 shows an example of the calculated soil moisture obtained by cyclic integration of equation (1) over the year, when P is the normal observed precipitation; W^* is 15 gm/cm^2; $\beta = 1 - \exp^{-6.8(W/W^*)}$ when $P < E_p$, and $\beta = 1$ when $P \geq E_p$; and E_p is obtained from the empirical formula of Thornthwaite, using the normal observed surface air temperature. (See Mintz and Serafini, 1981).

One can also use this method to initialize the soil moisture distribution in real time. [See, for example, Louie and Pugsley, 1981.] The global precipitation measurements that are required are a continuous time series of the measured daily (or weekly) precipitation, averaged over the computational grid areas, and with about 10% accuracy in the time and space averages. This precipitation, together with the calculated potential evapotranspiration, will produce a real-time distribution of the soil moisture.

3. Global Measurements of Detained Surface Water, for the Initialization of Soil Moisture

In the preceding section, the measured precipitation was used to obtain the infiltration of water into the soil. But there may be a better way of determining the infiltration.

Consider the water balance for the small horizontal region shown in Figure 3, where z_0 denotes a level that is a few centimeters below the surface of the soil. Then we can write,

$$\frac{d}{dt}(W_{>z_0}) = P - I_{z_0} - R_{>z_0} - E_{>z_0} \,. \qquad (4)$$

where $W_{>z_0}$ is the amount of moisture in the soil above the level z_0, together with any water that is on the surface; P is the rate of precipitation; I_{z_0} is the rate of infiltration at the level z_0; $R_{>z_0}$ is the rate of runoff above the level z_0; and $E_{>z_0}$ is the rate of evaporation of the soil moisture and water that are above the level z_0. ($E_{\lesssim z_0}$ is the rate of evapotranspiration of the soil moisture that is below the level z_0; and which, for the most part, is removed by the vegetation.) $R_{>z_0}$ is the surface runoff into rills whose horizontal spacing is several times larger than the depth of the plant root zone. This is water which will not be available for evapotranspiration.

We will call $W_{>z_0}$ the "detained surface water". (It is the water that gets your shoes wet when you walk across a field after the rain has stopped.) It is, perhaps, the water that can be measured from space by microwave radiometry (Schmugge, 1980).

Although $R_{>z_0}$ and $E_{>z_0}$ are functions of $W_{>z_0}$, for the purpose at hand we need only be concerned with the dependence of I_{z_0} on $W_{>z_0}$. For example, if the measured $W_{>z_0}$ is less than the field capacity of the soil above level z_0, there will be no infiltration. If the measured $W_{>z_0}$ is larger than field capacity, there will be infiltration. The task will be to measure $W_{>z_0}$ and to know the function

$$I_{z_0} = I_{z_0}(W_{>z_0}, \ldots) \,. \qquad (5)$$

as I_{z_0} will depend not only on $W_{>z_0}$ but also on the properties of the soil and its antecedent wetting.

In other words, the surface of the earth and the top few centimeters of the soil would be used as a remotely-sensed "leaky rain gauge". There will be a discontinuity in the "leakage rate" when $W_{>z_0}$ changes from being less than to being greater than the field

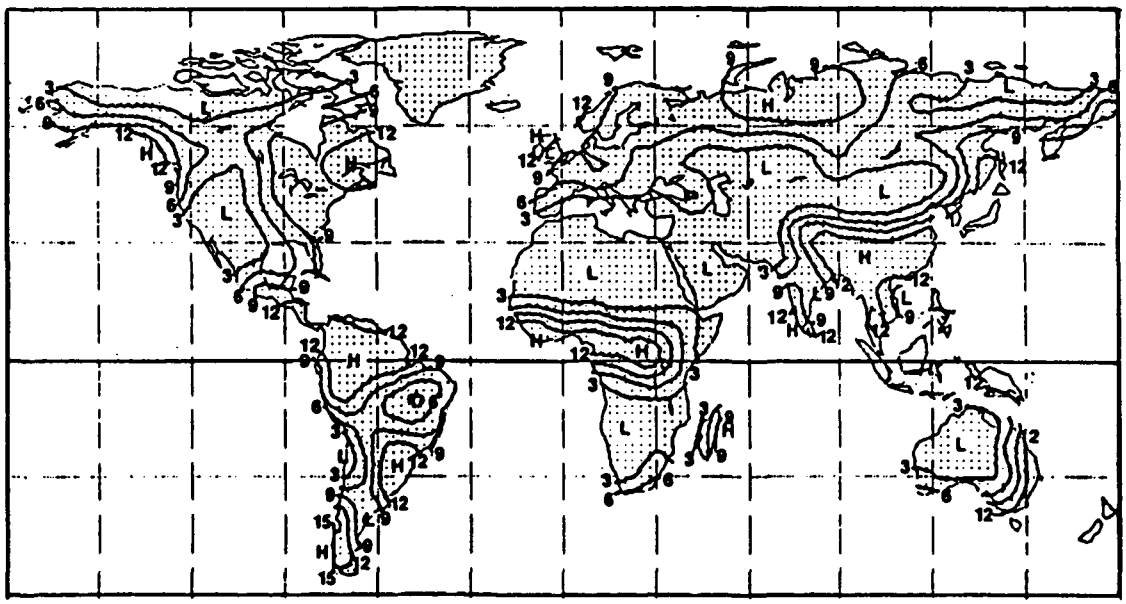

Fig. 2 Soil moisture available for evapotranspiration, in mid-July, as calculated from the observed antecedent rainfall and estimated potential evapotranspiration (Mintz and Serafini, 1981). Units: gm/cm^2. Maximum= 15gm/cm^2 (=150mm depth of water.)

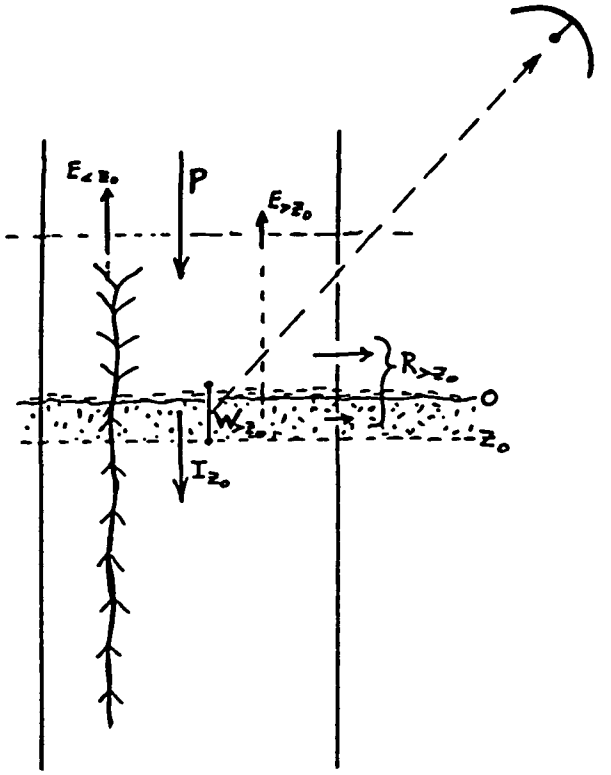

Fig. 3 Concept of the remote sensing of the earth's surface, treated as a "leaky rain gauge". Measurement of the transient water within the top few centimeters of the soil is used to calculate the infiltration into the underlying soil.

capacity of the soil above level z_o. In addition, if we measure the time rate of change of $W_{>z_o}$, as well as $W_{>z_o}$ itself, on some occasions immediately subsequent to rainfall events, but at times of the day when the evaporation is negligibly small, and under various conditions for the ratio $(I_{>z_o}/R_{>z_o})$, we may be able to determine the function $I_{z_o}(W_{>z_o}, \ldots)$.

The requirement will be to measure $W_{>z_o}$ accurately enough, and frequently enough, to determine the total daily area-averaged infiltration with an accuracy of about 10%. In this respect, there may be a practical advantage in measuring the detained surface water, $W_{>z_o}$, instead of measuring the precipitation, P. To obtain the daily precipitation to an accuracy of 10% may require measurements of the precipitation every few minutes. But to obtain the daily infiltration to an accuracy of 10% may require measurements of $W_{>z_o}$ only every few hours.

Addendum

The above discussion was addressed to general circulation model development and the use of such models for climate simulations and climate predictions. It was not addressed to the use of general circulation models for short and medium range weather predictions, where the accuracy of the initial state of the motion field is important.

Dr. Norman Phillips has pointed out that global measurements of the precipitation, which would provide information about the horizontal distribution of the condensation heating, may make it possible to use the method of nonlinear normal mode initialization to obtain the motion field in the tropics, where there is a strong interaction between the low level velocity convergence and the heating by cumulus condensation and convection. This, in turn, will influence the prediction of the motion and weather fields in the extratropics.

It may also be possible to do this when the initialization method is four-dimensional data assimilation. (See, for example, Miyakoda et al., 1976; Ghil, et al., 1979). At present, because of inadequate wind observations in the tropics, it is largely the model predicted heat of condensation that forces the circulation and is the main factor in initializing the motion field in the tropics. With measurements of precipitation, we would replace the model produced condensation heating with the true condensation heating and, thereby, obtain a better initialization of the tropical motion field.

Whichever initialization method is used, the requirements are not less than 12-hourly (and preferably 3-hourly) measurements of the precipitation, averaged over the computational grid areas, and with an accuracy of about 10%. If there must be a choice (as in the satellite orbit) between 12-hourly global coverage and 3-hourly tropical coverage, it is the latter that is to be preferred for the motion field initialization.

References

Chang, J. (ed.), 1977: General Circulation Models of the Atmosphere. Methods in Computational Physics, Vol. 17, Academic Press, New York/San Francisco/London, 337 pp.

Ghil, M., M. Halem and R. Atlas, 1979: Time-Continuous Assimilation of Remote-Sounding Data and Its Effect on Weather Forecasting. Mon. Wea. Rev., 107, pp 140-171.

Lorenz, E. N., 1967: The Nature and Theory of the General Circulation of the Atmosphere. Tech. Note No. 218, TP 115, WMO, Geneva, 161 pp.

Louie, P. Y. T. and W. I. Pugsley, 1981: Application of Near Real-Time Water Budgets in Monitoring Climate-Related Events. Proceedings of the Fifth Annual Climate Diagnostics Workshop, University of Washington, Seattle, October 22-24, 1980. U.S. Dept. Commerce/NOAA, Wash. D.C., pp. 158-166.

Mintz, Y., 1981: The Influence of Land-Surface Evapotranspiration on Rainfall and Circulation: A Review of Simulation Experiments. Land-Surface Processes in Atmospheric General Models. Proceedings of the Study Conference on Land Surface Processes, Greenbelt, Maryland, 5-10 Jan. 1981. GARP Publications Series, WMO, Geneva. (in press).

Mintz, Y., and M. E. Schlesinger, 1979: Numerical Simulation of Ozone Production, Transport and Distribution with a Global Atmospheric General Circulation Model. J. Atm. Sci., 36, pp. 1325-1361.

Mintz, Y., and V. Serafini, 1981: Global Fields of Moisture and Land-Surface Evapotranspiration. Paper submitted to Symposium on Variations in the Global Water Budget, Oxford, 9-15 August 1981.

Miyakoda, K., L. Umscheid, D. H. Lee, J. Sirutis, R. Lusen and F. Pratte, 1976: The Near-real-time, Global Four-dimensional Analysis Experiment During the GATE Period, J. Atmos. Sci., 33, 561-591.

Schmugge, T., 1980: Soil Moisture Sensing with Microwave Techniques. Proc. 14th Int. Symp. for Remote Sensing of Environment, San Jose, Costa Rica, 23-30 Apr. 1980. Environmental Res. Inst. of Michigan, Ann Arbor, pp. 487-505.

WMO/ICSU, 1979: Report of the JOC Study Conference on Climate Models: Performance, Intercomparison and Sensitivity Studies. GARP Publication Series No. 22, Vol. I, World Meteor. Organization, Geneva, 606 pp.

GLOBAL FIELDS OF MONTHLY NORMAL SOIL MOISTURE, AS DERIVED FROM OBSERVED PRECIPITATION AND AN ESTIMATED POTENTIAL EVAPOTRANSPIRATION

by Y. Mintz[1,2] and Y. Serafini[2]

[1]Department of Meteorology
University of Maryland
College Park, Maryland 20742

[2]Laboratory for Atmospheric Sciences
NASA Goddard Space Flight Center
Greenbelt, Maryland 20771

June 1984

ABSTRACT

Monthly normal soil moisture is obtained from the time integral of

$$\frac{dW}{dt} = P - E \,, \qquad W_{max} = W^* \,,$$
$$E = \beta E_p \,.$$

where W is soil moisture and E is evapotranspiration. P is observed monthly normal precipitation; E_p is the potential evapotranspiration rate as estimated from observed monthly normal surface air temperature, using the method of Thornthwaite (1948); and W^* is the maximum available moisture that the soil can hold, taken as 150 mm (in equivalent water depth.) β is an empirical function which relates the evapotranspiration ratio (E/E_p) to the soil moisture ratio (W/W^*), and is taken as $\beta = 1 \exp^{-6.8(W/W^*)}$, as adapted from Nappo (1975.)

Starting from an initial state in which W is zero on an arbitrary calendar day of the year, the governing equation is integrated forward in time until a steadily seasonally varying state is reached. The calculation is made at intervals of 5° of longitude and 4° of latitude; and the resulting field of soil moisture is shown on global maps, and in tables, for the middle of each calendar month. (The values of W and E at the beginning and in the middle of each month, as well as the input parameters, monthly mean P and E_p, are available on magnetic tape.)

1.1 Governing equation for soil moisture.

The calculation of soil moisture from observed precipitation and an estimated potential evapotranspiration was first proposed and carried out by Thornthwaite (1948). Expressed in our present notation, he did this by taking the time integral of

$$\frac{\partial W}{\partial t} = P - E \ , \quad W_{max} = W^* \ , \tag{1}$$

where

$$E = E_p \times \beta \ (W, W^*) \ , \tag{2}$$

and

$$E_p = E_p \ (T_A, h) \ , \tag{3}$$

where W is the available moisture in the root zone of the soil (the moisture in excess of the amount at the wilting point of the vegetation); W* is the difference betwen the soil moisture at field capacity and at the wilting point; P is the rate of precipitation; E is the rate of evapotranspiration; E_p is the potential evapotranspiration (the evapotranspiration when the vegetation is not under any water stress); β is the function which relates the ratio (E/E_p) to W and W*; T_A is the surface air temperature, averaged for a day or more; and h is the duration of daylight.

1.2 Potential evapotranspiration, E_p.

Thornthwaite knew that the potential evapotranspiration is principally dependent on the net radiational heating of the vegetation and, to a lesser extent, on the drying power of the air (its wind speed, temperature and relative humidity.) He believed, however, that it would be a very long time before either measurements or dependable calculations of the radiational heating would be available from more than just a few experimental sites and, therefore, that the

required information on the radiational heating would simply not be available for a climatology of the terrestrial water cycle.

25 years later, De Jong (1973) made a comprehensive review of what is known about the net radiational heating of the earth's surface and reached the same conclusion: namely, that the existing radiation measurements and radiation calculations were insufficient for calculating the surface water balance over the global (or even single continental) domain(s).

Priestley and Taylor (1972) made a strong recommendation that the mapping of daily net radiation at the surface of the earth, on a space scale of several hundred kilometers, be made part of the Global Atmospheric Research Program (GARP). This would not be difficult, they said, because "the problem of sampling and representativeness of net radiation is not different in kind from those encountered with the accepted basic elements near the surface (temperature, wind, rainfall, etc.) and the typical accuracy of a good net radiometer, about 5 percent for daily totals, is more than adequate." But, unfortunately, this was not included in the First GARP Global Experiment (FGGE).

As a substitute for making the potential evapotranspiration depend on the net radiation at the surface, Thornthwaite (1948) proposed that E_p be made a function of the surface air temperature, which is a widely available measurement, and the duration of daylight. To this end, he compared the measured monthly evapotranspiration with the measured monthly mean surface air temperature at a number of well-watered drainage basins and grass-covered lysimeters in the central and eastern U.S., and obtained as the regresion of E_p upon T_A,

$$E_p \text{ (mm/month}^{-1}\text{)} \begin{cases} = 0 , & \text{when } T_A < 0°C \\ = 16\ L\ (10\ T_A/I)^a , & 0 \leq T_A < 26.5°C \\ = -415.85 + 32.25\ T_A - 0.43\ T_A^2 , & T_A > 26.5°C \end{cases} \quad (4)$$

where $$I = \sum_{1}^{12} (T_A/5)^{1.514} ,$$

$$a = (6.75 \times 10^{-7}\ I^3) - (7.71 \times 10^{-5}\ I^2) + (1.79 \times 10^{-2}\ I) + 0.49 ,$$

and $$L = (D/30)(h/12) ,$$

where D is the number of days in the month and h is the number of hours of daylight. (When used to evaluate I, T_A is the mean temperature in each month of the year.)

This way of determining the potential evapotranspiration, wrote Thornthwaite and Hare (1965), is "... only an approximation, to be replaced whenever a fully rational predictor of E_p becomes available. Its success depends on the fact that the mean air temperature does, to a considerable extent, serve as a parameter of the net radiation ...".

Comparison field studies, as reported by Makkink (1957), Pelton, King and Tanner (1960), Stanhill (1961), Stephens and Stewart (1963), Smith (1964), Stern and Fizpatrick (1965), Jensen (1966), Jones (1966), Omar (1968), and McGuiness and Bordne (1972), show that the monthly potential evapotranspiration calculated with Eq. (4) does not greatly differ from the potential evapotranspiration which is calculated from a local radiation measurement, or which is obtained from a lysimeter measurement.

1.3 Evapotranspiration coefficient, β.

Thornthwaite (1948) initially assumed that the evapotranspiration rate would be the same as the potential rate as long as there is any extractable moisture in the soil, at which point the evapotranspiration would abruptly stop, or

$$\beta \begin{cases} = 1, & \text{when } W > 0 , \\ = 0, & \text{when } W = 0 . \end{cases} \tag{5}$$

Later, Thornthwaite and Mather (1955) assumed that the ratio of E to E_p varies linearly with the amount soil moisture, or

$$\beta = \frac{W}{W^*} . \tag{6}$$

For the present study, we will use the relationship between (E/E_p) and (W,W^*) which we have taken from the analysis by Nappo (1975) of field measurements made by Davies and Allen (1973). In the field study, during a summer in southernmost Ontario (44°N), the energy balance/Bowen ratio method was used to obtain the rates of evapotranspiration from two adjacent (122 m x 67 m) plots of perennial rye grass, growing in a sandy loam soil. One of the plots was irrigated and, therefore, the moisture in its soil taken to be at field capacity. Nappo let the ratio of the evapotranspiration from the nonirrigated field to that from the irrigated field, both taking place under the same atmospheric conditions, be (E/E_p), and plotted this ratio against η, the measured volumetric soil moisture content in the upper 5 cm of the non-irrigated field. This is shown by the data points, and with his exponential curve of best fit, in Fig. 1. What we have done is to assume that the grass cover, by shielding the soil from the sun, has made the soil moisture density constant with depth over the root zone and, therefore, that $(W/W^*) = (\eta/\eta_{max})$, as shown along the upper abscissa of the figure, which gives us

Fig. 1

$$\beta = 1 - e^{-6.8(W/W^*)} . \tag{7}$$

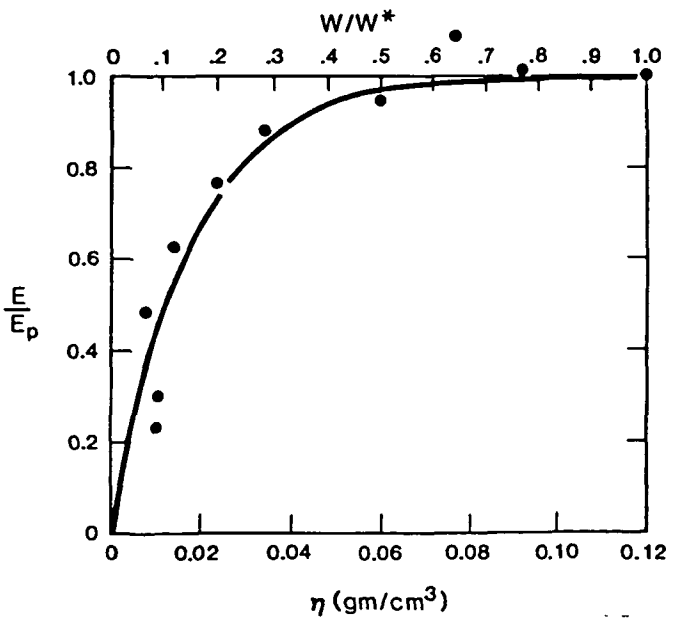

Fig. 1 Evapotranspiration ratio, E/E_p, as a function of the soil moisture ratio, W/W*.

Data points and exponential curve of best fit, $E/E_p = 1 \exp^{-56.6\eta}$, from Nappo (1975), was obtained from measurements of E, E_I and η by Davies and Allen (1973). Relationship assumed for the present study is $E/E_p = 1 - \exp^{-6.8(W/W^*)}$.

Measurements were made in adjacent non-irrigated and irrigated fields of perennial rye grass, in southern Ontario (42°N), in June-September 1971. λE of the non-irrigated field and λE_I ($= \lambda E_p$) of the irrigated field were obtained from the measured radiation, air temperatures and humidities, using the energy balance/Bowen ratio method. η is the volumetric soil moisture content of the non-irrigated field and was obtained by weighing samples form the upper 5 cm of the soil.

(Figure after Nappo 1975.)

Fig. 2 Fig. 2 shows that the evapotranspiration coefficient, β, given by Eq. (7), is closer to Thornthwaite's initial (1948) assumption than to his later assumption. That evapotranspiration remains close to the potential rate over some broad range of the soil wetness, W/W*, is now generally accepted (see, for example, Miller, 1977, 1981; Shuttleworth, 1979; Brutsaert, 1982).

1.4 Soil moisture storage capacity, W*.

a. W* from the soil properties and depth of the plant roots.

The soil moisture storage capacity, W*, can be obtained by taking the vertical integral of the volumetric soil moisture storage capacity, w*, over the effective depth of the roots of the plants.

Table 1 Table I shows the volumetric field capacity, w_{fc}; volumetric wilting point, w_{wp}, and volumetric soil moisture storage capacity, $w^* (= w_{fc} - w_{wp})$, of the different soil types, arranged in order of decreasing soil particle sizes (from Smith and Ruhe, 1955.) We see that w* is about (0.15 ± 0.03) gm/cm^3 for all soil types except fine sand (which, in any event, rarely is found with naturally growing vegetation.)

What has a larger variation with space (and, in the case of the annual plants, also a large variation with time) is the effective depth of the plant roots.

Fig. 3 Figure 3 shows the soil moisture sampled across a line of oak trees in a fallow field (from Miller, 1977; after Rode, 1969.) Away from the trees, the soil moisture is depleted to a depth of about 30 cm. Under the trees, the moisture is depleted to a depth of about 150 cm. Therefore, if $w^* \approx 0.15$ gm/cm^3, W* will be about 45 mm (in water depth equivalent) away from the trees, and 225 mm under the trees. These are also characteristic of the values of W* for very short (herbacious) vegetation and for tall (woody) vegetation, generally.

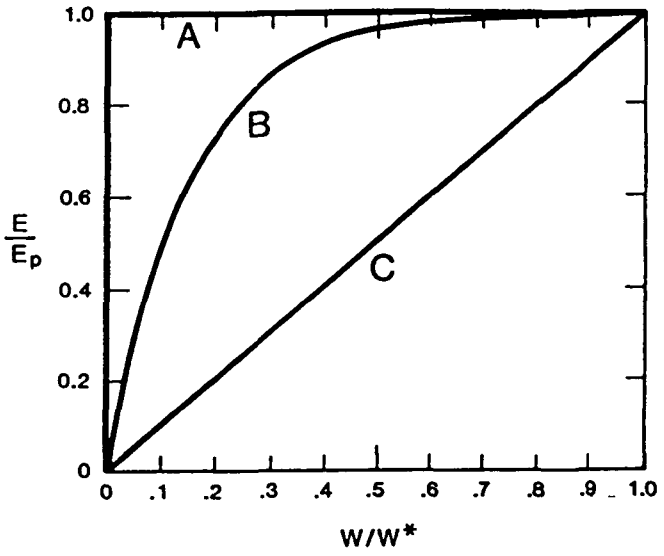

Fig. 2 Evapotranspiration ratio, E/E_p (= β), as a function of the soil moisture ratio, W/W*:

A: Thornthwaite (1948.)
B: Thornthwaite and Mather (1955.)
C: Present study.

TABLE I

Water Holding Properties of the Soils (gm/cm^3)

Soil type	w_{fc}	w_{wp}	$w^* = (w_{fc} - w_{wp})$
fine sand	0.125	0.033	0.092
fine sandy loan	0.217	0.067	0.150
loam	0.267	0.100	0.167
silt loam	0.292	0.117	0.175
clay loam	0.317	0.150	0.167
clay	0.333	0.208	0.125

Average w^* for all soil types = 0.146

w_{fc}: volumetric field capacity. (Maximum amount of moisture that can be held in the soil against the force of gravity.)

w_{wp}: volumetric wilting point. (Value below which moisture cannot be extracted from the soil by the roots of plants.)

$w^* = w_{fc} - w_{wp}$): volumetric soil moisture storage capacity. (Maximum available soil moisture.)

from Smith and Ruhe (1955)

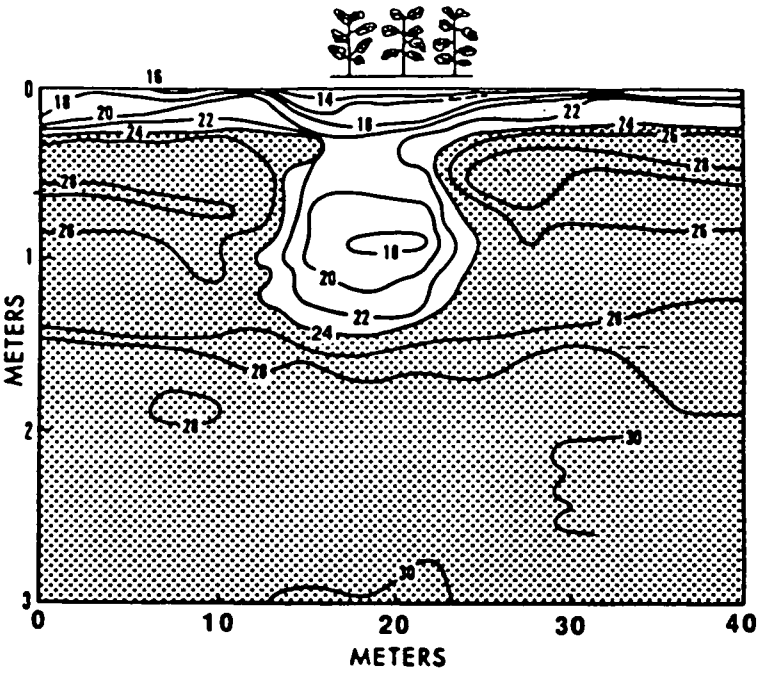

Fig. 3 Soil moisture (percent) sampled across a line of oak trees in a fallow field. (From Miller, 1977; after Rode, 1969.)

"Depletion of soil moisture by woody vegetation, which usually is deep rooted, reaches a large total over a year because the trees or shrubs experience fewer days of limited moisture supply than does herbacious vegetation. Green trees amid an expanse of baked, sundried grass are a familiar sight, representing continued availability of soil moisture at depth greater than grass roots can reach". (Miller, 1977, p 224).

The depth to which roots extract soil moisture is greater than what one might think by just looking at the vertical profile of the root length density. This Fig. 4 can be seen in Fig. 4, which shows the results of a numerical simulation of the extraction of soil moisture by roots (Hillel, 1977, pp 168-189.) In the simulation, the transpiration rate was prescribed as 10 mm/day, with a sinusoidal diurnal variation; the surface evaporation rate as 2 percent of the transpiration rate; the initial volumetric soil miosture as equal to 0.25 gm/cm^3 at all depths (which is the volumetric field capacity of a loam soil): the total root length as 10,000 m of roots per m^2 of field, with the vertical distribution as shown on the left in Fig. 4; and a state of stress on the hypothetical plant, producing wilting, when the crown potential falls to -30 bars.

The curves on the right, in Fig. 4, show the depletion of the soil moisture from 0 to the end of the 10th day. On the 11th day, wilting began. We see that about 95% of the roots are less than 30 cm deep, but about half of the moisture extracted by the roots is from below 30 cm; which is to say that the "effective depth" of the roots is about twice as large as their apparent depth. W* is about 100 mm, even though most of the roots are less than 30 cm cm deep.

b. W* from the drawdown to the wilting point.

There have been a few field studies where the soil moisture budget equation, Eq. (1), was used to obtain W*.

When we take the integral of Eq. (1) from a time t_o, when W = W*, until a

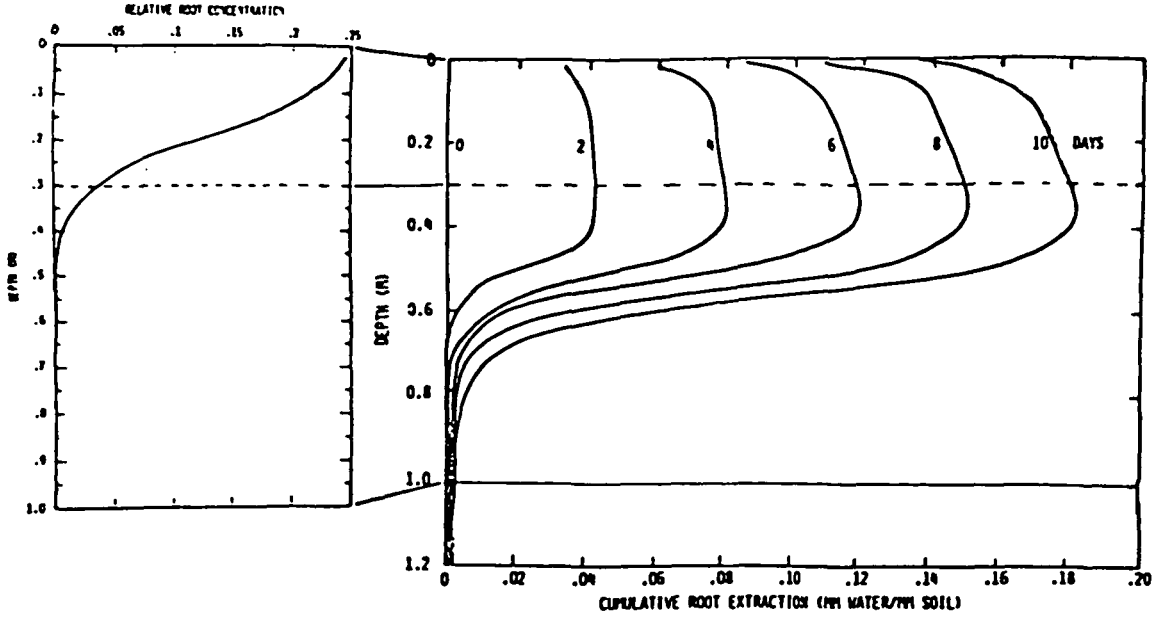

Fig. 4 Numerical simulation of the extraction of soil moisture by the roots of a field crop.

Panel on the left: prescribed root length density as a function of depth.

Panel on the right: cumulative extraction of soil moisture as a function of depth, at intervals of 2 days. Wilting phase started on the 11th day.

(From Hillel, 1977.)

time t_1, when E = 0 (and, therefore, W = 0), we obtain

$$0 - W^* = \int_{t_o}^{t_1} (P - E)\ \delta t\ . \qquad (6)$$

The starting time, t_o, must be one preceeding which there has been sufficient rainfall (or irrigation) to assure us that W = W*, and there must be reliable measurements of P and E.

An example of this kind of running budget of soil moisture is shown in Fig. 5 Fig. 5 (from Miller, 1977; after Chang, 1963.) For example, on 14 September the field of sugarcane was irrigated, making W = W*, and on 7 October the measured evapotranspiration became zero. Over that time period, therefore,

$$W^* = \int_{t_o}^{t_1} (E - P)\ \delta t \approx 62 \text{ mm},$$

as also over the other periods shown in the figure. In this example, the measured rate of evapotranspiration (of 4 to 5 mm/day) remains almost constant while approaching the zero value of W. This means that the evapotranspiration coefficient, β, is more like curve A than curve C of Fig. 2.

Priestley and Taylor (1972) give other examples of W* obtained in this way with field crops; with W* varying from about 95 mm to 230 mm (all of the values being larger than what one would expect from the apparent depth of the roots of those crops.)

W* has not been obtained for tall (forest) vegetation in this way because there have been no realiable measurements of the evapotranspiration from a forest over a drawdown to the wilting point.

For the present study, we will use W* = constant = 150 mm; this being about the average value for all kinds of vegetation. It is also the value of W* that is used in many atmospheric general circulation models with interactive soil moisture (Carson, 1981.) Initially, Thornthwaite (1948) used W* = 100 mm;

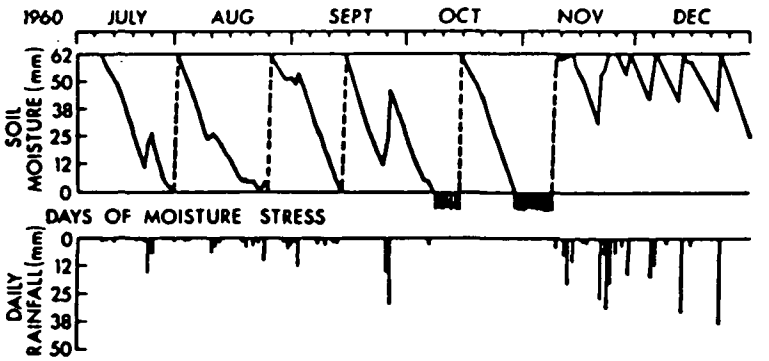

Fig. 5 Drawdown of soil moisture at Waipio, Oahu.

Daily rainfall is shown on the lower graph. Replenishment of soil moisture, by irrigation, is shown by the vertical dashed lines on the upper graph. Days of moisture stress (in October and November) indicate zero available soil moisture.

(From Miller, 1977; after Chang, 1963.)

later, Thornthwaite and Mather (1955) used 300 mm. Louie and Pugsley (1981), who have been producing time-series of weekly soil moisture maps for Canada, let W* vary with location. Their values of W* range from 100 mm to 280 mm; which they make depend not on the type of vegetation, but on the type of soil.

1.5 Calculation procedure.

In our calculation of the evapotranspiration and the soil moisture, we use the monthly mean values of P and E_p (expressed in units of mm/day) in the following finite-difference analog of Eq. (1),

$$W_d = W_{d-1} + P - E_d) \ , \quad W_d \leq W^* \tag{7}$$

$$E_d = E_p \ [1 - e^{-6.8(W_{d-1}/W^*)}] \ , \tag{8}$$

where W_d is the soil moisture at the end of day d, W_{d-1} is the soil moisture at the end of the preceding day; E_d is the evapotranspiration during day d, and P and E are the monthly means of the observed precipitation and estimated potential evapotranspiration (expressed in units of mm/day.)

If at the end of day d W_d exceeds W*, then W_d is set equal to W* and the surplus is set aside as that day's contribution to the annual runoff. Fig. 6 is a schematic of how W and E depend on P and E_p, and on each other.

Fig. 6

The soil moisture was initialized by assuming that, at every gridpoint, W_{d-1} was equal to zero on 1 January of an arbitrary year. Using the fields of P and E_p described in the next section, the calculation with Eqs. (7) and (8) was carried forward, in one day time steps, until at every gridpoint the difference between W_d on the same calendar day of two successive years was smaller than 0.01 mm. The convergence of the solution was acheived when the calculation had gone through seven annual cycles.

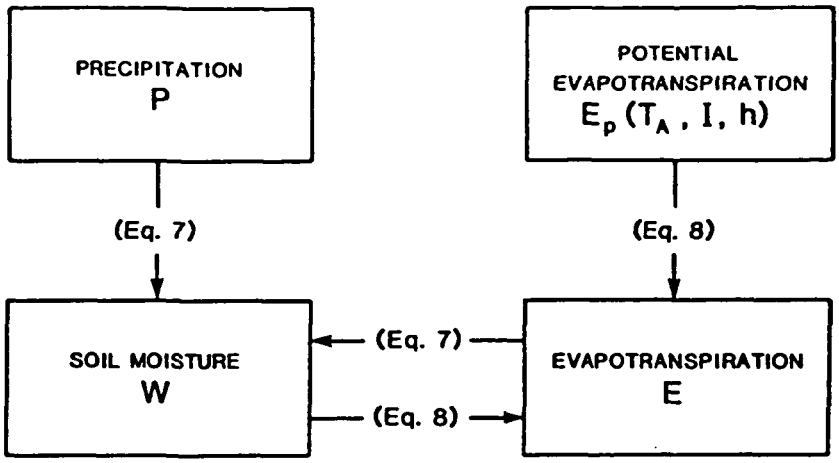

Fig. 6 Schematic of the relationships between the governing equations and the parameters

P: precipitation,
$E_p(T_A,I,h)$: potential evapotranspiration ,
E: evapotranspiration,
W: soil moisture.

1.6 The prescribed forcing fields, P and E_p.

a) Precipitation, P.

For precipitation we used the normal monthly mean precipitation given by Jaegger (1976). From each of his monthly maps he obtained, and has kindly made available in machine readable form, the average precipitation for each 5° latitude by 5° longitude square. We have interpolated the precipitation values from the 5° by 5° grid to the 4° latitude by 5° longitude grid, which is the grid used by the GLAS atmospheric general circulation model. The precipitation fields for January, April, July and October, as machine analyzed from the 4° by 5° data set, are shown in Fig. 7.

Fig. 7

b. Potential evapotranspiration, E_p.

E_p was derived from the normal monthly mean surface air temperatures, using Eq. (4). The temperatures were obtained by interpolation from the NCAR (197_) global data set of monthly normal surface air temperatures, averaged for 5° latitude by 5° longitude areas. The potential evapotranspiration fields for January, April, July and October are shown in Fig. 8.

Fig. 8

1.7 The calculated fields, E and W.

a. Evapotranspiration, E.

The calculated evapotranspiration fields for mid-January, -April, -July and -October are shown in Fig. 9.

Fig. 9

b. Soil moisture, W.

The calculated fields of soil moisture, expressed as the soil wetness ratio, (W/W*), are shown for mid-January, -April, -July, and -October in Fig. 10. The mid-monthly fields of (W/W*), for all months of the year, are given in numerical form in the Appendix, Tables A.I through A.XII.

Fig. 10

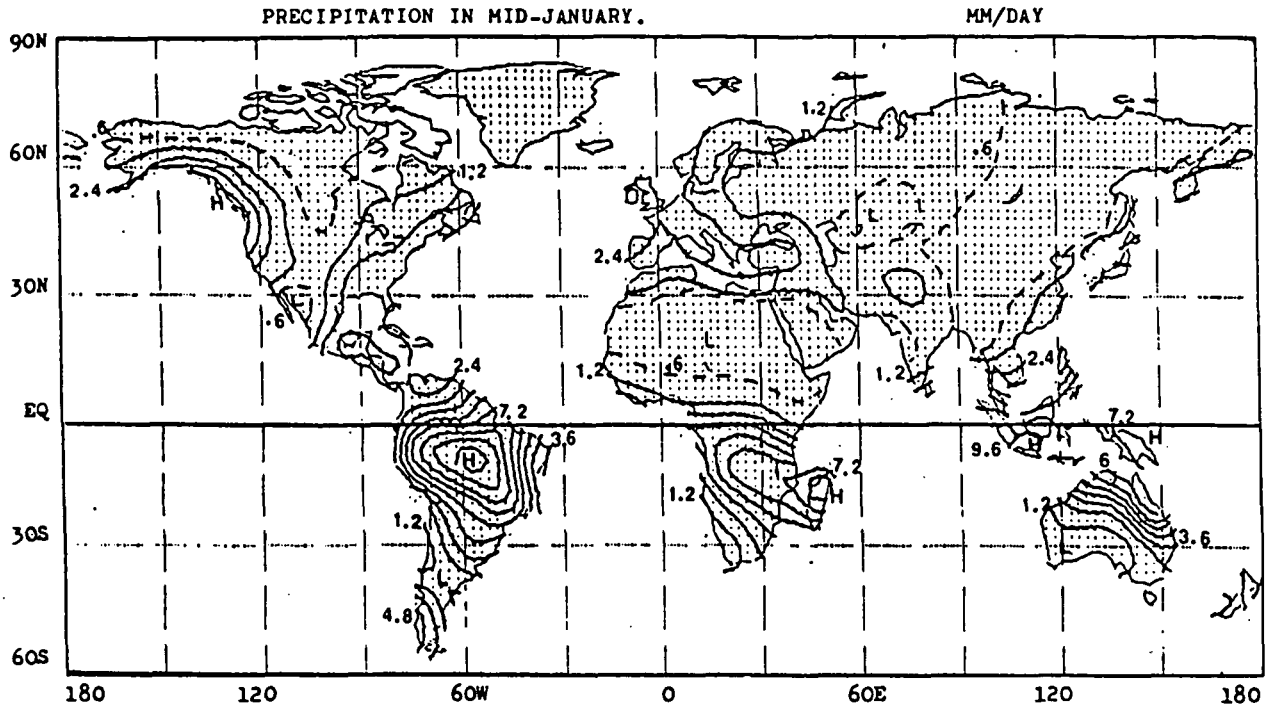

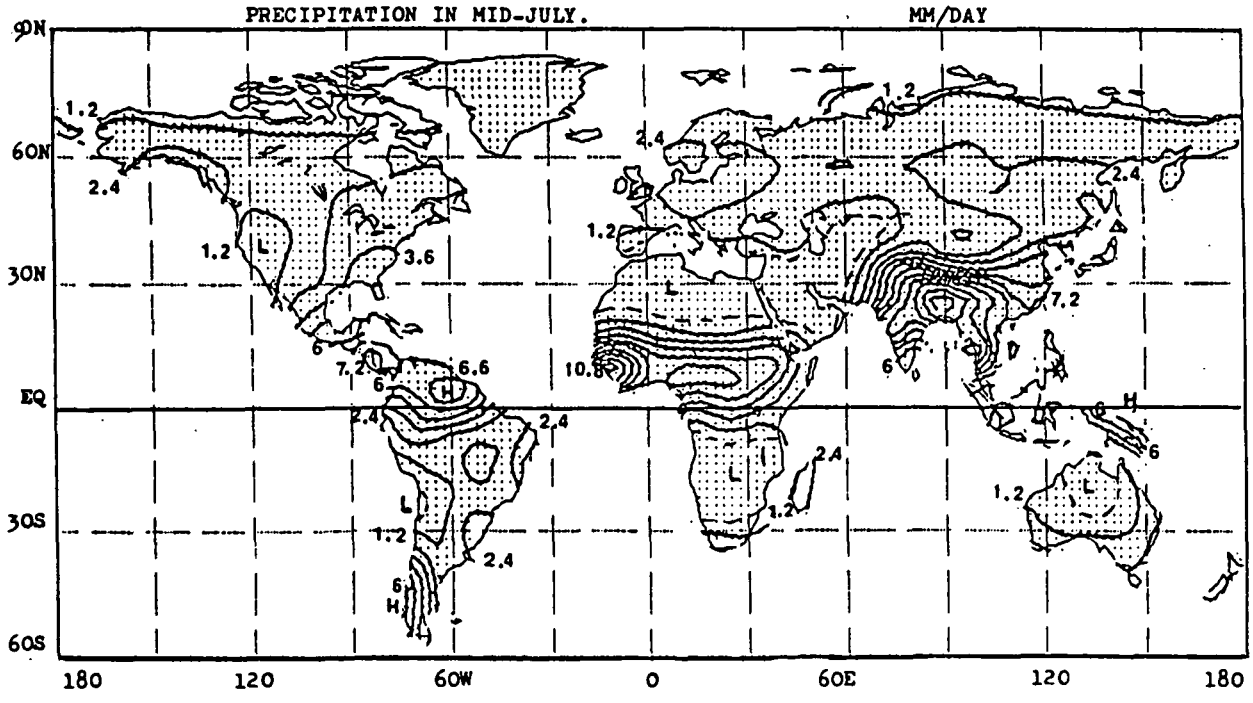

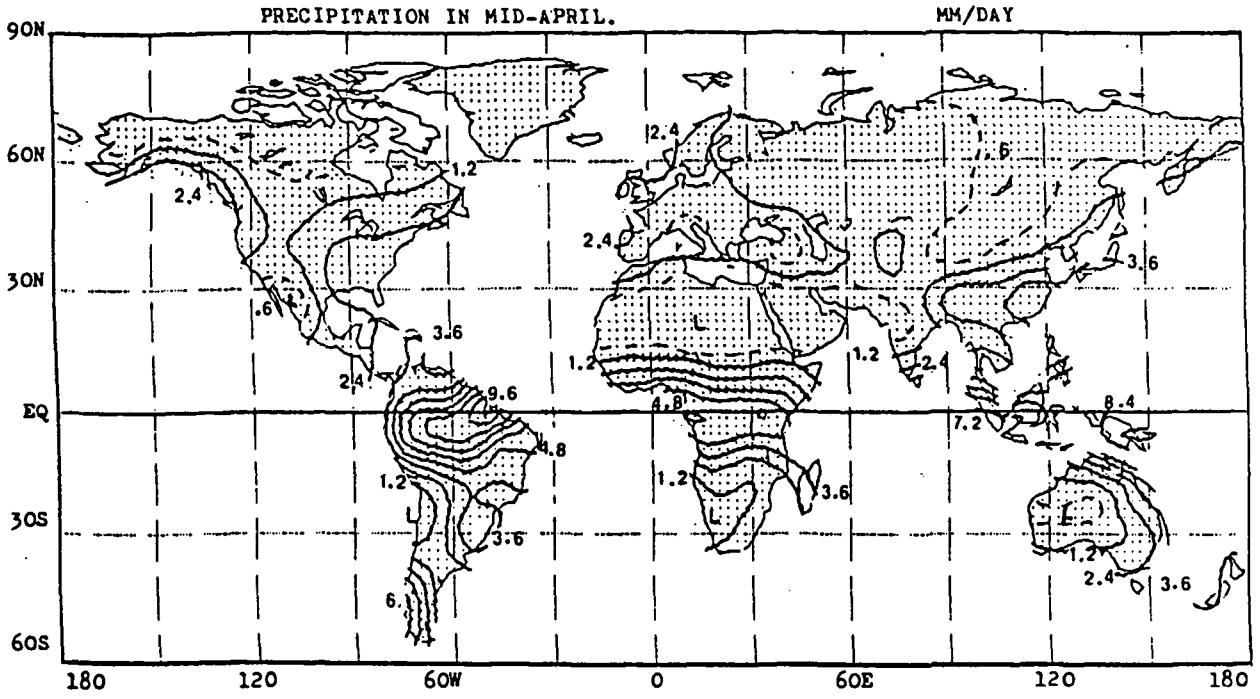

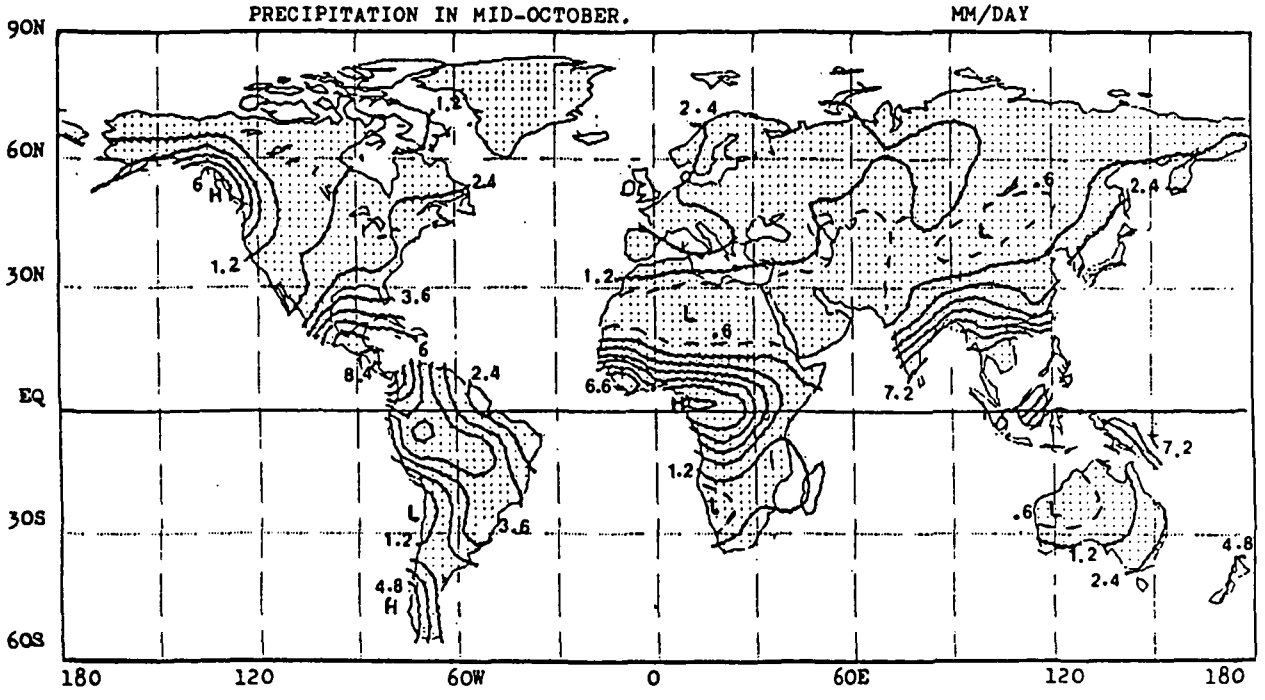

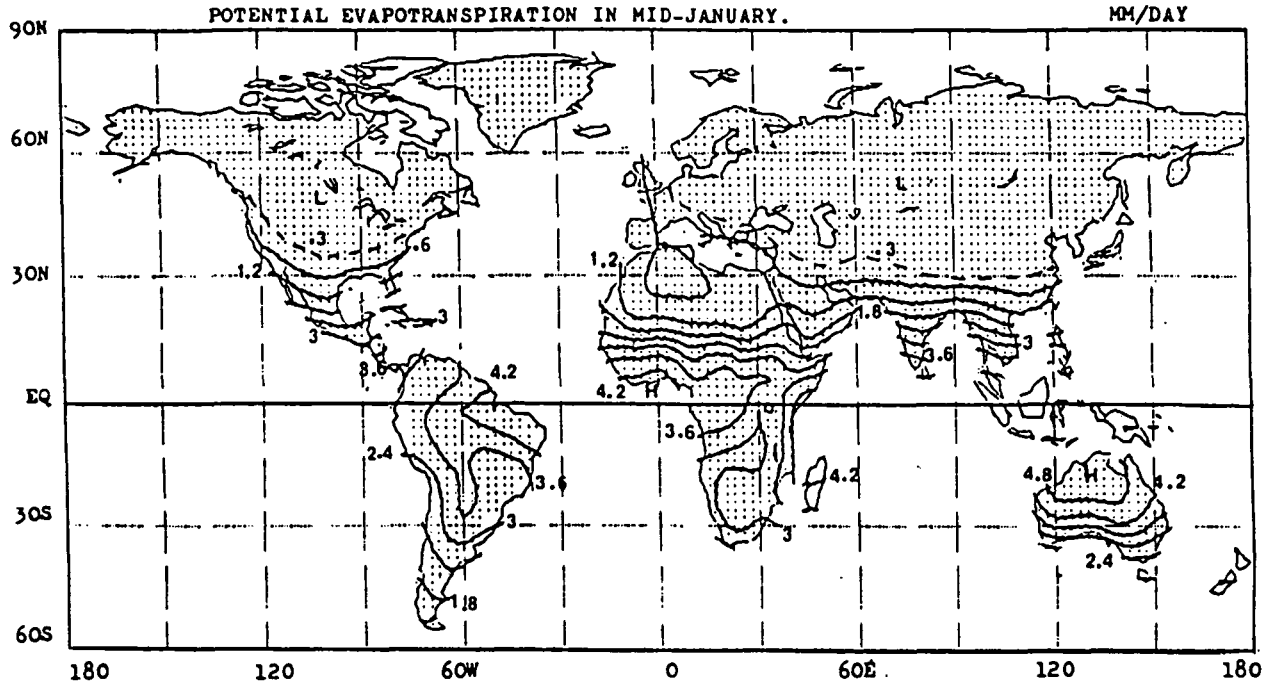

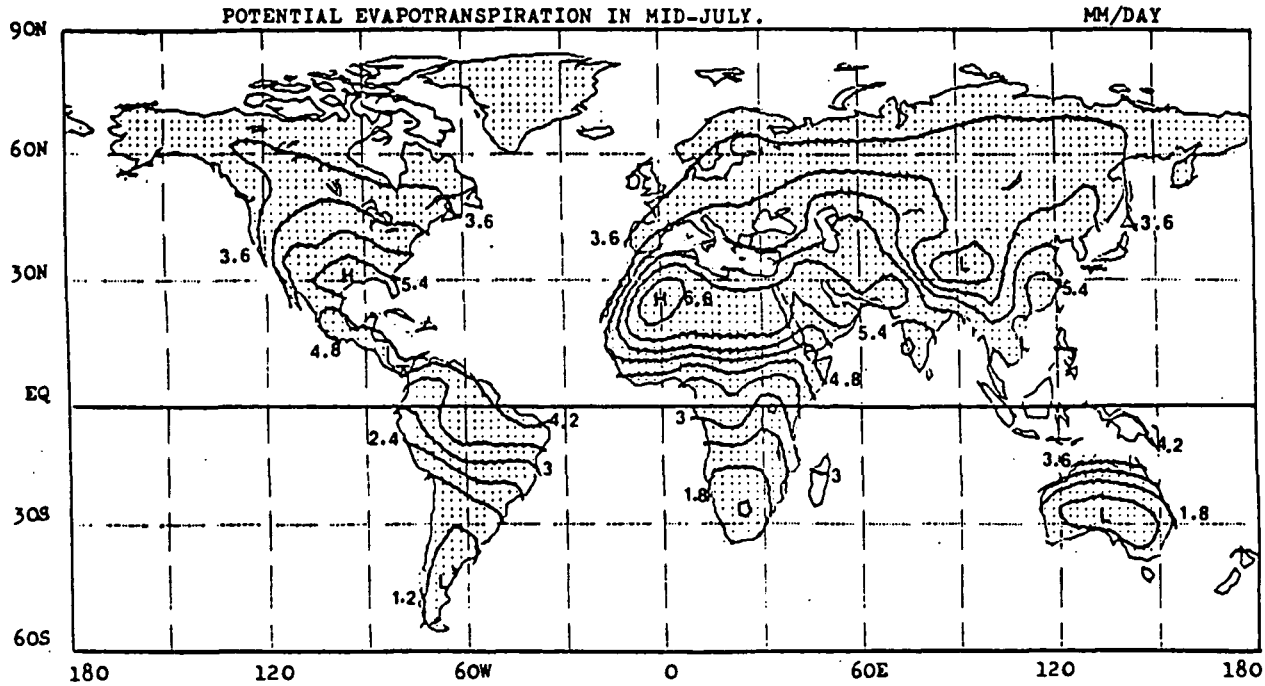

POTENTIAL EVAPOTRANSPIRATION IN MID-APRIL. MM/DAY

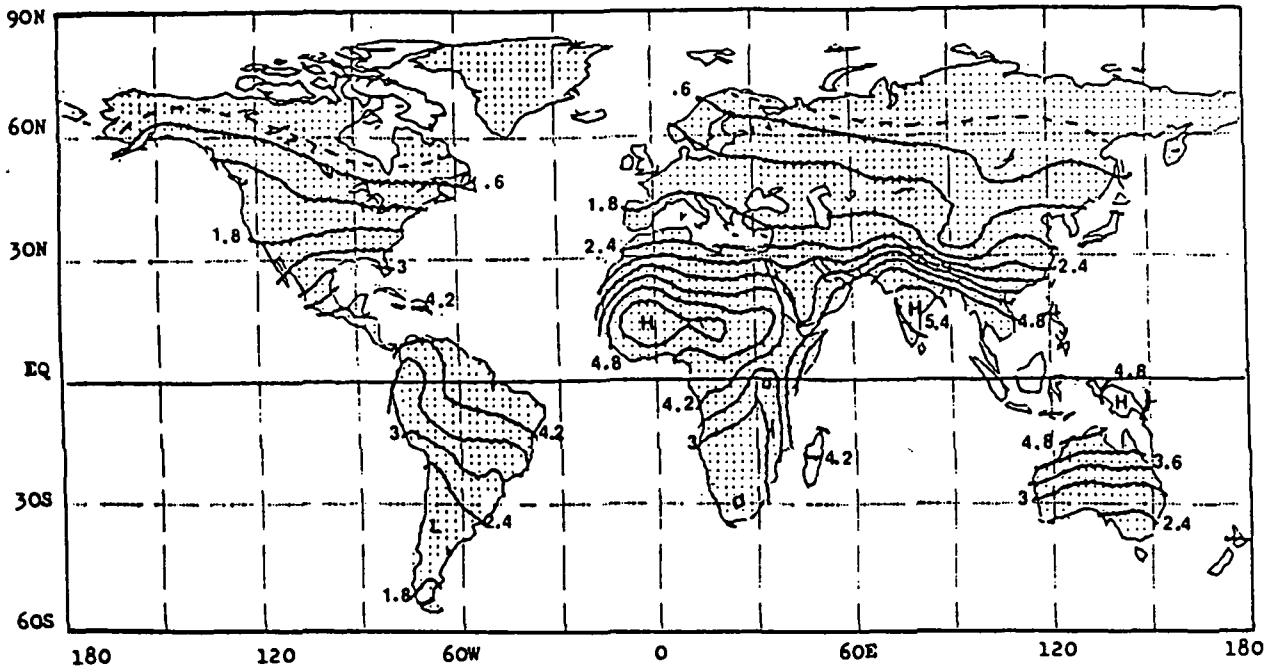

POTENTIAL EVAPOTRANSPIRATION IN MID-OCTOBER. MM/DAY

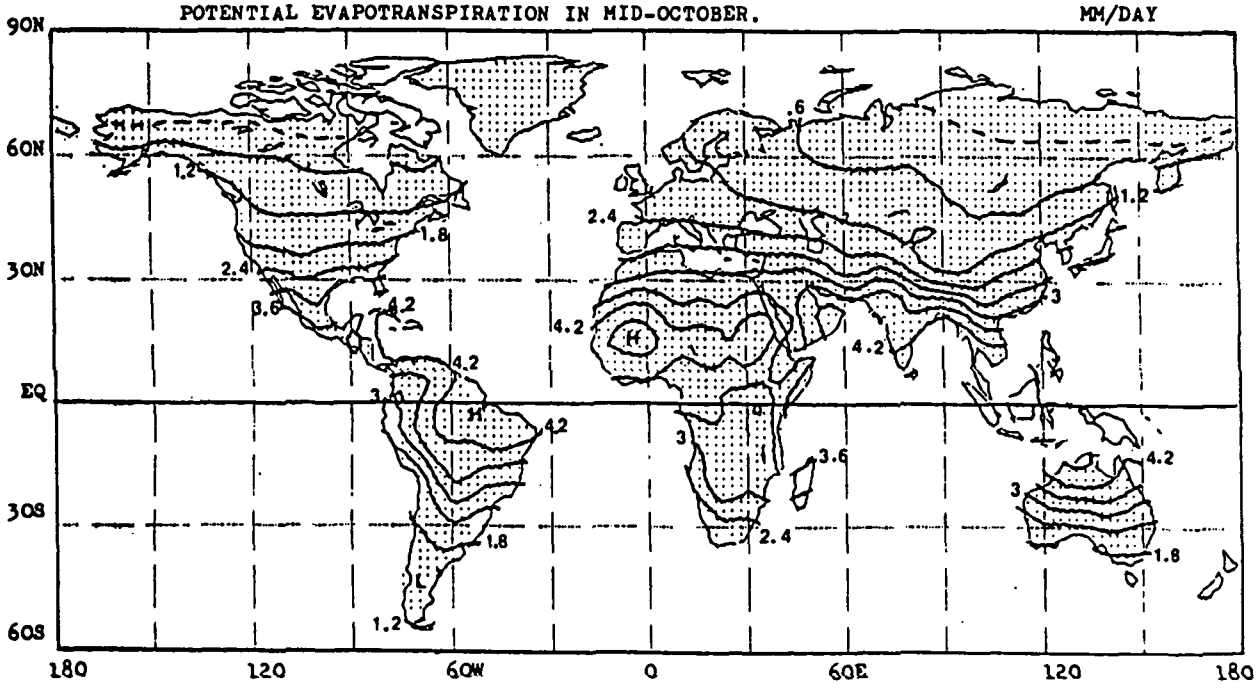

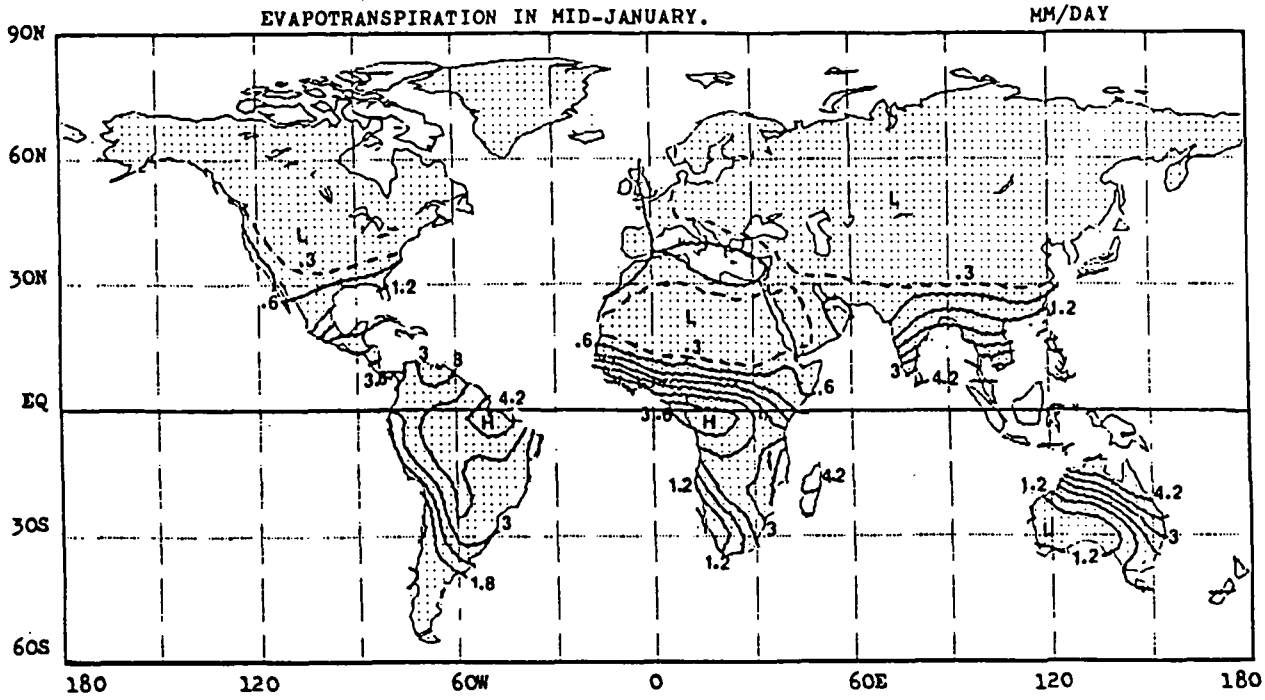

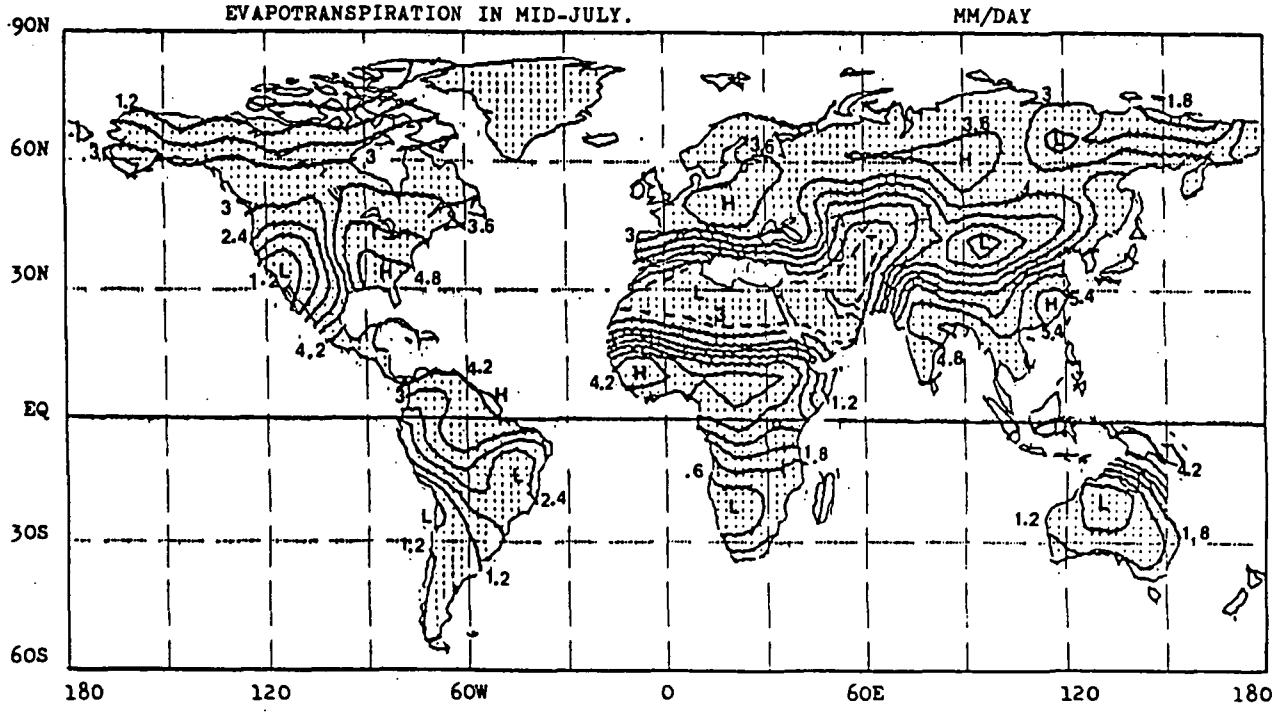

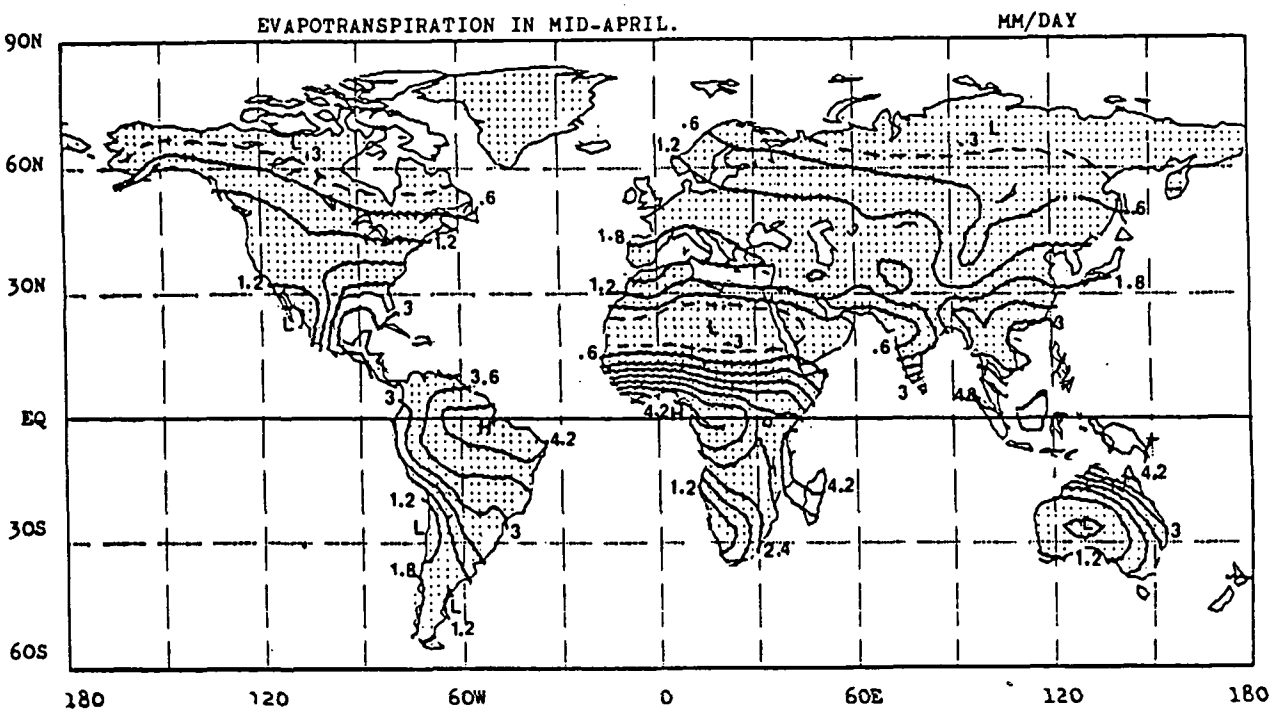

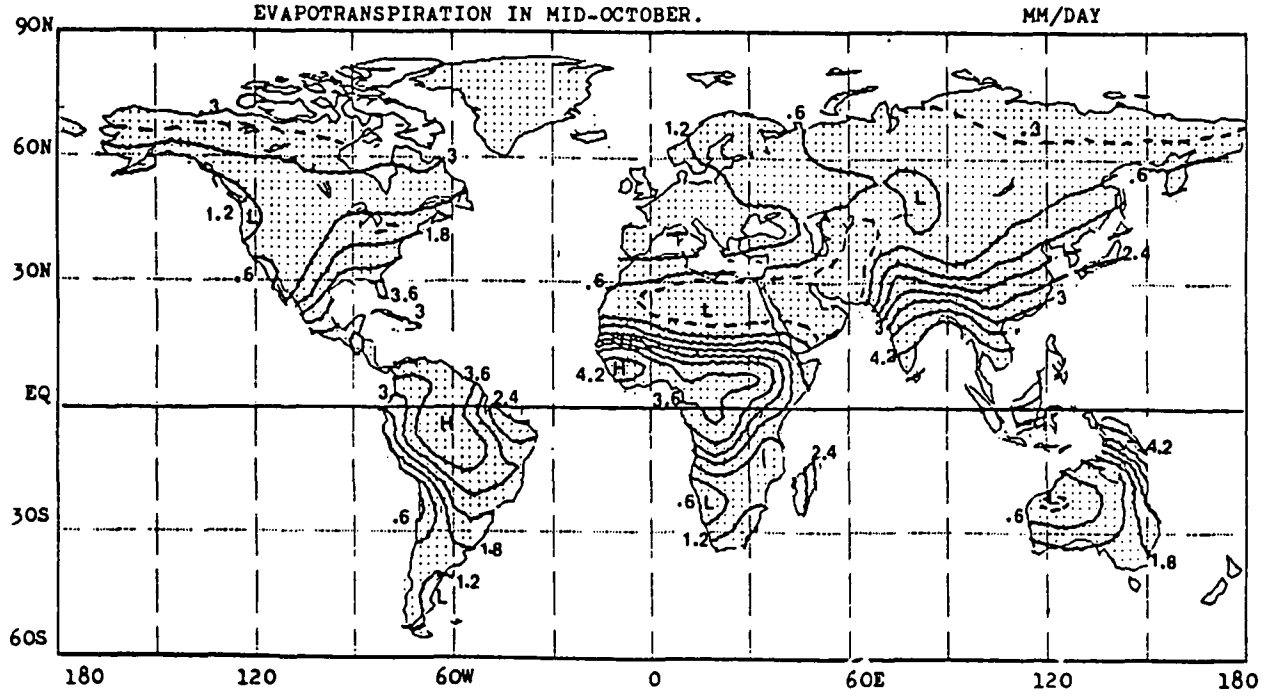

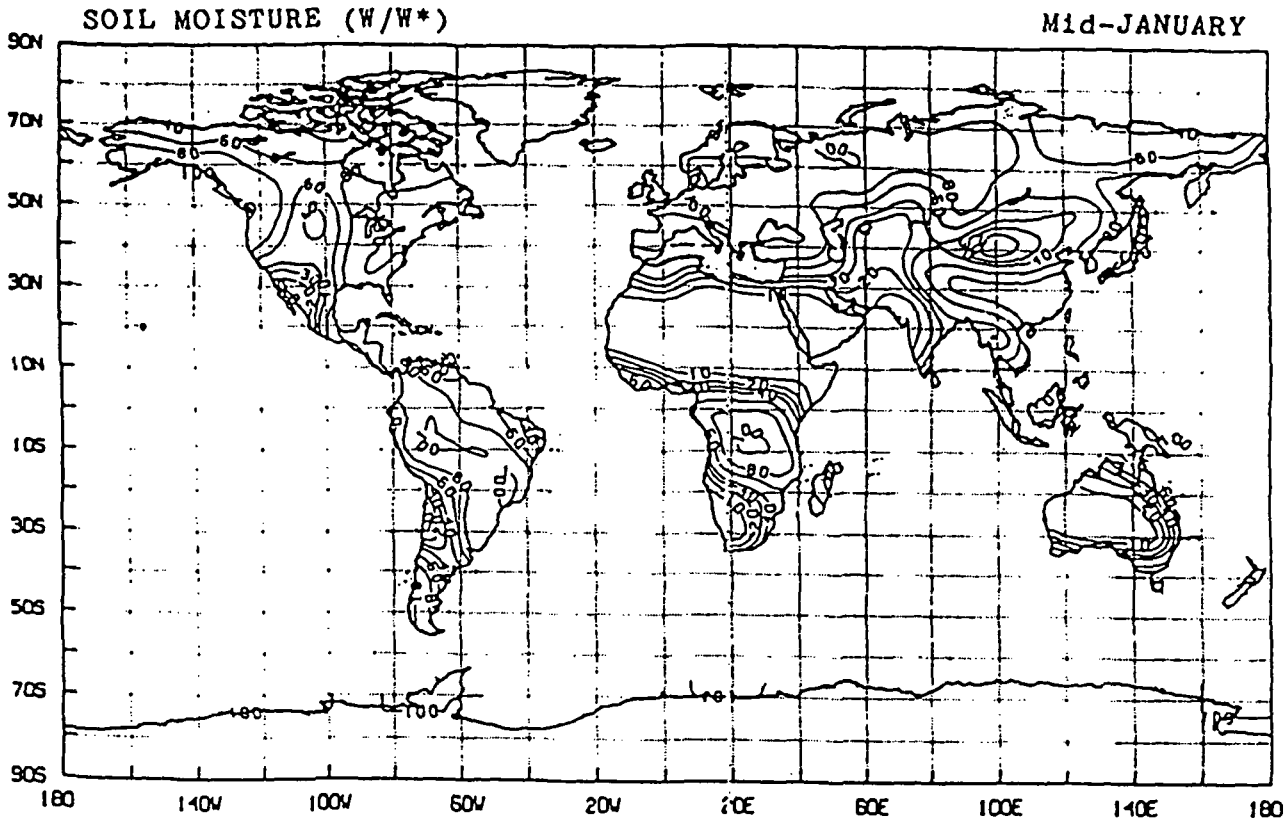

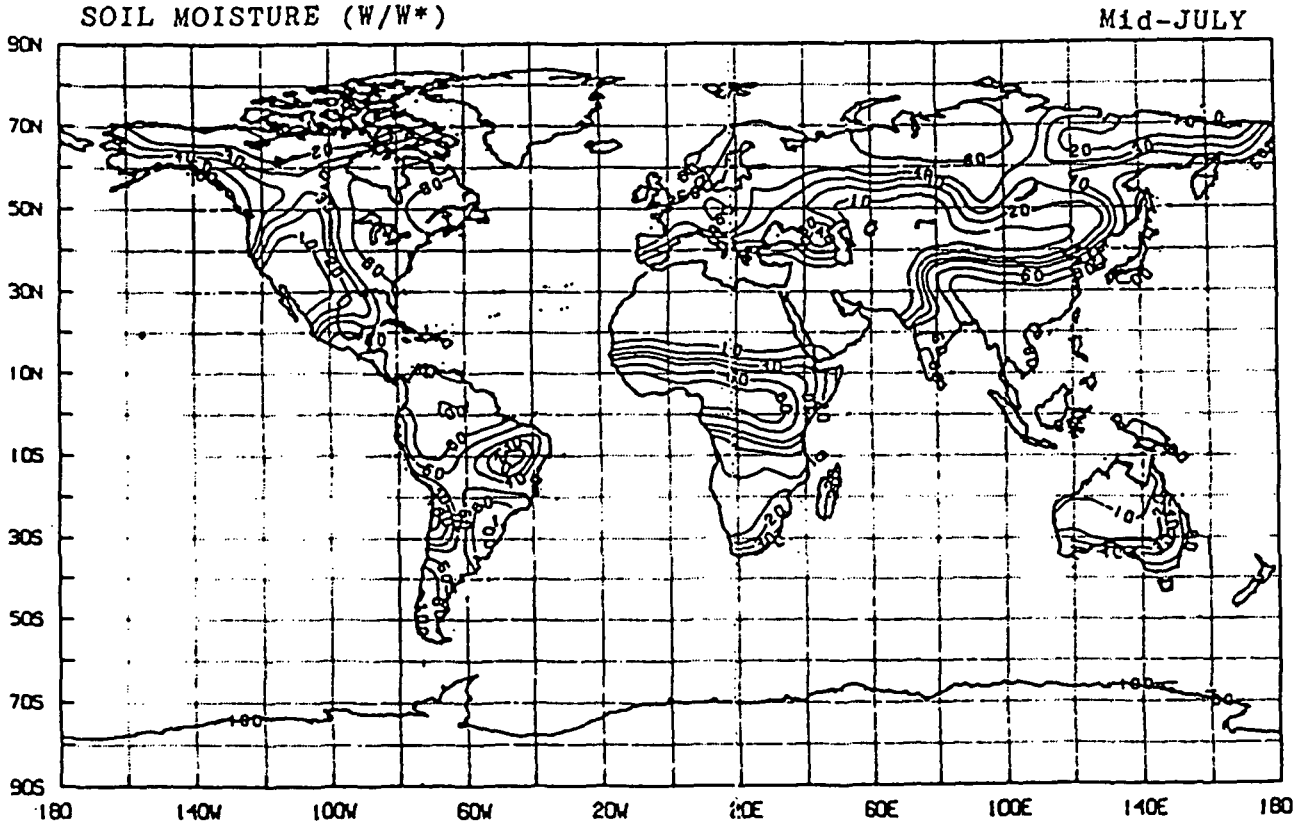

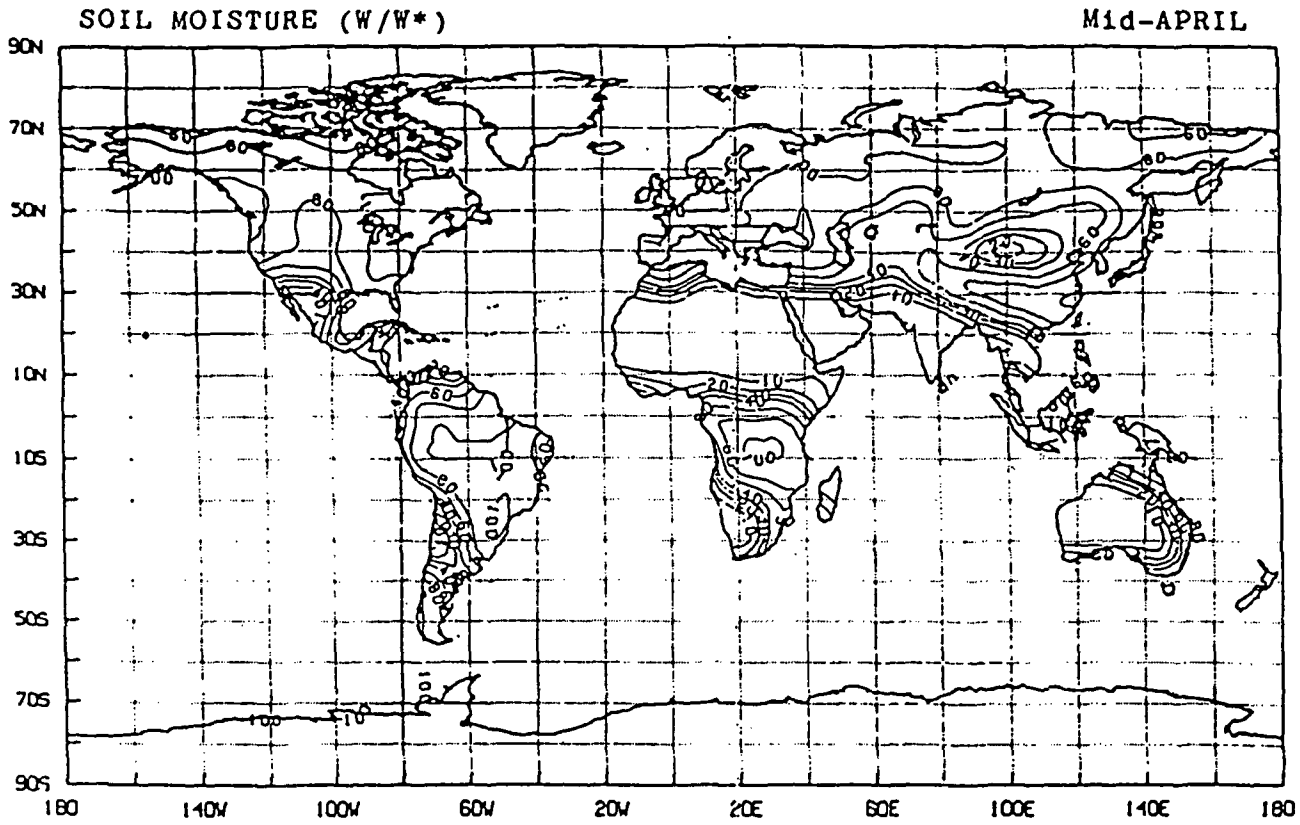

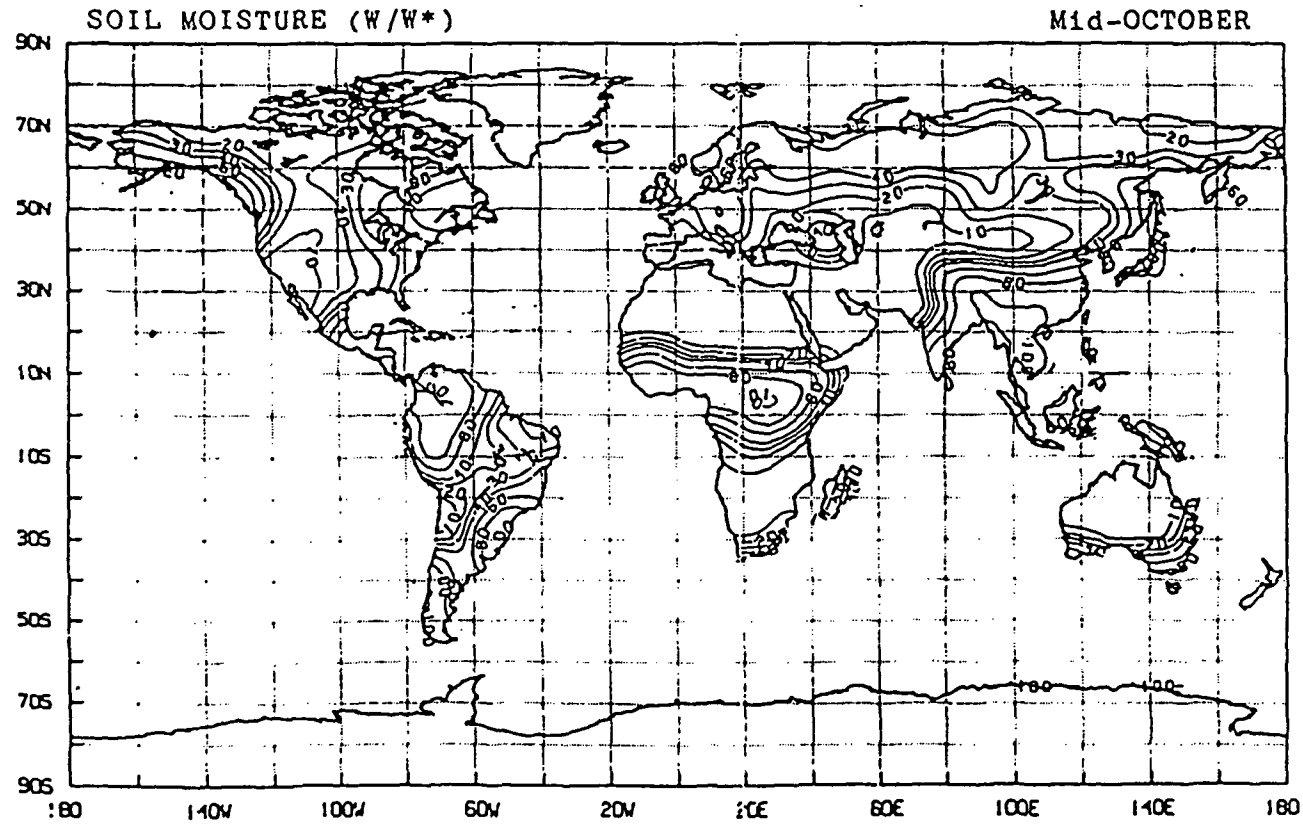

(W/W*), at the beginning of each month and at the middle of each month, has also been recorded on magnetic tape; together with the evapotranspiration rate, E, at the beginning and at the middle of each month. Also on the tape are the monthly mean forcing fields: P, T_A, and E_p (T_A, I, h). Copies of the tape can be obtained from the Branch Head, Global Modelling and Simulation Branch (Code 911), Laboratory for Atmoshperic Sciences, NASA Goddard Space Flight Center, Greenbelt, MD, 20771. Tel: (301) 344-7482.

REFERENCES

Brutsaert, W. H., 1982: Evaporation Into the Atmosphere. Reidel Pub. Co., Dordrecht/Boston/London. 299 pp.

Carson, D. L., 1981: Current Parameterizations of Land-Surface Processes in Atmospheric General Circulation Models. In Proceedings of the JSC Study Conference on Land Surface Processes in Atmospheric General Circulation Models, Greenbelt, Maryland, January 1981.

Chang, J.-H., 1963: The Role of Climatology in the Hawaiian Sugar-cane Industry: An Example of Applied Agricultural Climatology in the Tropics. Pac. Sci., 17, 379-397.

Davies, J. A. and C. D. Allen, 1973: Equilibrium, Potential and Actual Evaporation from Cropped Surfaces in Southern Ontario. Journ. Applied Meteor., 12, 649-657.

De Jong, B., 1973: Net Radiation Recieved by a Horizontal Surface of the Earth: A Literature Study Directed To Evaporation Calculations. Sijthoss and Noordhoff. 52 pp and 62 maps.

Hillel, D., 1977: Computer Simulation of Soil-Water Dynamics: A Compendium of Recent Work. International Development Research Centre, Ottawa, Canada. 214 pp.

Jaeger, L., 1976: Monatskarten des Niederschlages für die ganze Erde. Berichte Deutscher Wetterdienst, Nr 139, Offenbach. 38 pp. and 13 plates.

Jensen, M. E., 1966: Empirical Methods of Estimating or Predicting Evapotranspiration Using Radiation. In Proceedings of the Conference on Evapotranspiration and its Role in Water Resource Management. Amer. Soc. Agr. Engin. 1964. 49-53.

Jones, D. M. A., 1966: Variability of Evapotranspiration in Illinois. Illinois State Water Survey, Circ. 89, 13 pp.

Louie, P. Y. T. and W. I. Pugsley, 1981: Application of Near Real-Tme Water Budgets in Monitoring Climate-Related Events. Proceedings of the Fifth Annual Climate Diagnostice Workshop, University of Washington, Seattle, 22-24 October 1980. NOAA, U.S. Dept Commerce, March 1981, pp. 158-166.

Makkink, C. F., 1957: Testing the Penman Formula by Means of Lysimeters. Jour. Inst. Water Engin., 11, 277-288.

McGuinness, J. L. and E. F. Bordne, 1972: A Comparison of Lysimeter-Derived Potential Evapotranspiration with Computed Values. Agricultural Research Service, Technical bulletin No. 1452, U. S. Dept. Agr., Wash. D.C., 71 pp.

Miller, D. H., 1977: Water at the Surface of the Earth. Academic Press, New York/ San Francisco/ London. 557 pp.

Miller, D. H., 1981: Energy at the Surface of the Earth. Academic Press New York, San Francisco/London/Sydney. 516 pp.

Nappo. C. J., 1975: Parameterization of Surface Moisture and Evaporation Rate in a Planetary Boundary Layer Model. Journ. Applied Meteorol., 14, 289-296.

Omar, M. H., 1968: Potential Evapotranspiration in a Warm Arid Climate. In Agroclimatological Methods, Proc. of the Reading Symp., Nat. Resources Res. Pub. 7, UNESCO, Paris, 347-353.

Pelton, W. L., K. M. King and C. B. Tanner, 1960: An Evaluation of the Thornthwaite Method for Determining Potential Evapotranspiration. Agron. Jour., 52, 387-395.

Priestley, C. H. B. and Taylor, R. J., 1972: On the Assessment of Surface Heat Flux and Evaporation Using Large-scale Parameters. Mon. Wea. Rev., 100, 81-92.

Rode, A. A., 1969: Osnovy Ucheniia o Pochvennoi Vlage, Tom II. Metody Izucheniia Vodnogo Rezhima Pochv. Gidrometeorologischeskow Izdatel'stvo, Leningrad, 287 pp.

Shuttleworth, W. J., 1979: Evaporation. IH Report No. 56. Institute of Hydrology, Wallingford, Oxon., UK. 61 pp.

Smith, K., 1964: A Long-Period Assessment of the Penman and Thornthwaite Potential Evapotranspiration Formulae. Jour. Hydrol., 2(4), 277-290.

Smith and Ruhe, 1955: Water; Yearbook of Agriculture, 1955. U.S. Gov't. Printing Office, Washington D.C., 751 pp.

Stanhill, G., 1961: A comparison of Methods of Calculating Potential Evapotranspiration from Climatic Data. Israel Jour. Agr. Res., 11 (3-4), 157-171.

Stephens, J. C. and E. H. Stewart, 1963: A Comparson of Procedures for Computing Evaporation and Evapotranspiration. Publ. 62, Internatl. Assoc. Sci. Hydrol., International Union of Geodesy and Geophysics, Berkeley, Calif, 123-133.

Stern, W. R. and E. A. Figzpatrick, 1965: Calculated and Observed Evaporation in a Dry Monsoonal Environment. Jour. Hydrol, 3, 297-311.

Thornthwaite, C. W., 1948: An Approach Toward a Rational Classification of Climate. Geographical Review, 38, 55-94.

Thornthwaite, C. W. and F. K. Hare, 1965: The loss of Water to the Air. Meteorol. Monographs, 28, No. 6, 163-180.

Thornthwaite, C. W. and J. R. Mather, 1955: The Water Balance. Publ. Climatol., 8, No. 1, 104 pp.

Willmott, C. J.. J. R. Mather and C. M. Rowe, 1981: Average Monthly and Annual Surface Air Temperature and Precipitation Data for the World. Part 1: The Eastern Hemisphere. Part 2: The Western Hemisphere. Elmer, New Jersey: C. W. Thornthwaite Associates (Publications in Climatology, Vol. 34, Nos. 1 and 2).

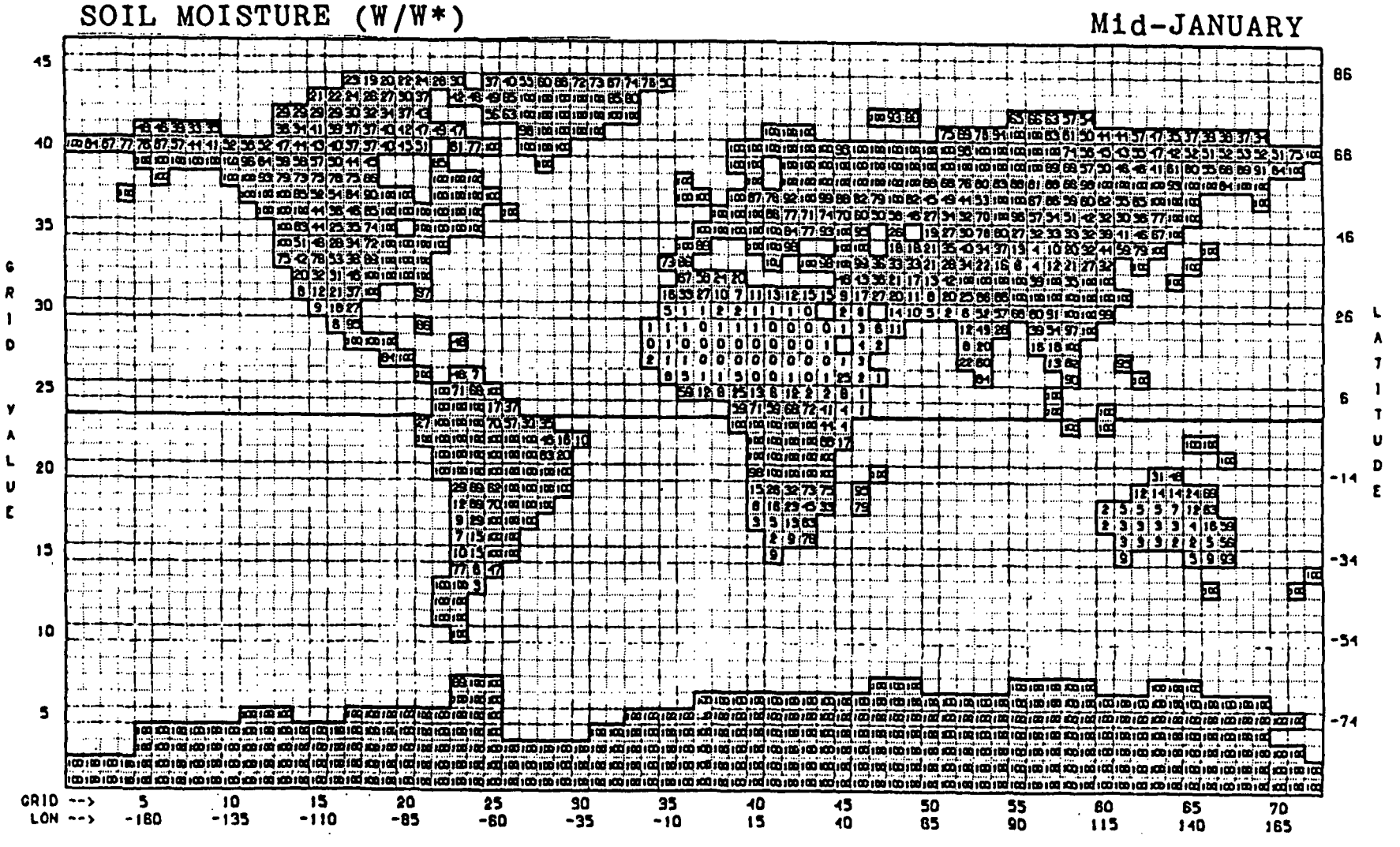

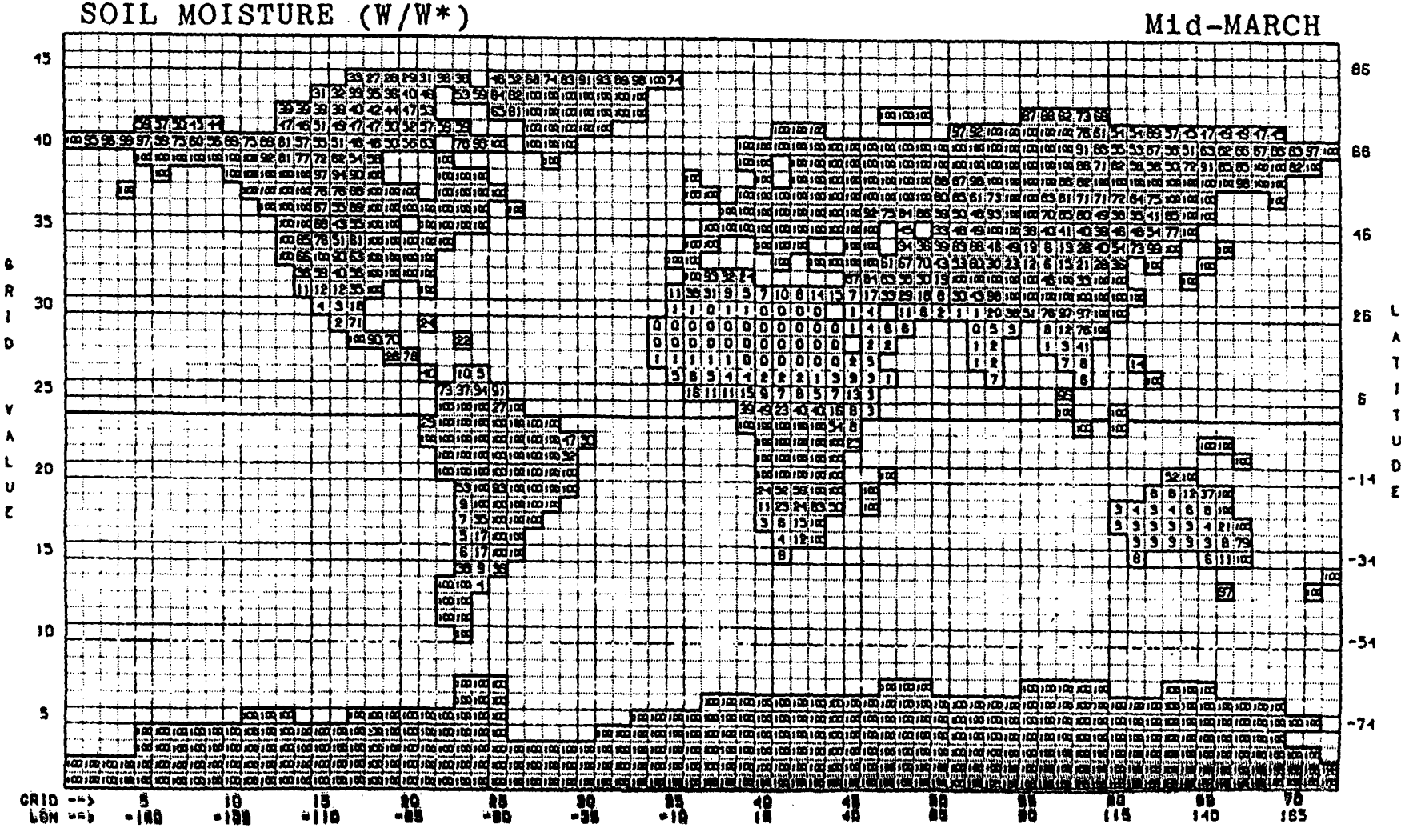

ORIGINAL PAGE IS
OF POOR QUALITY

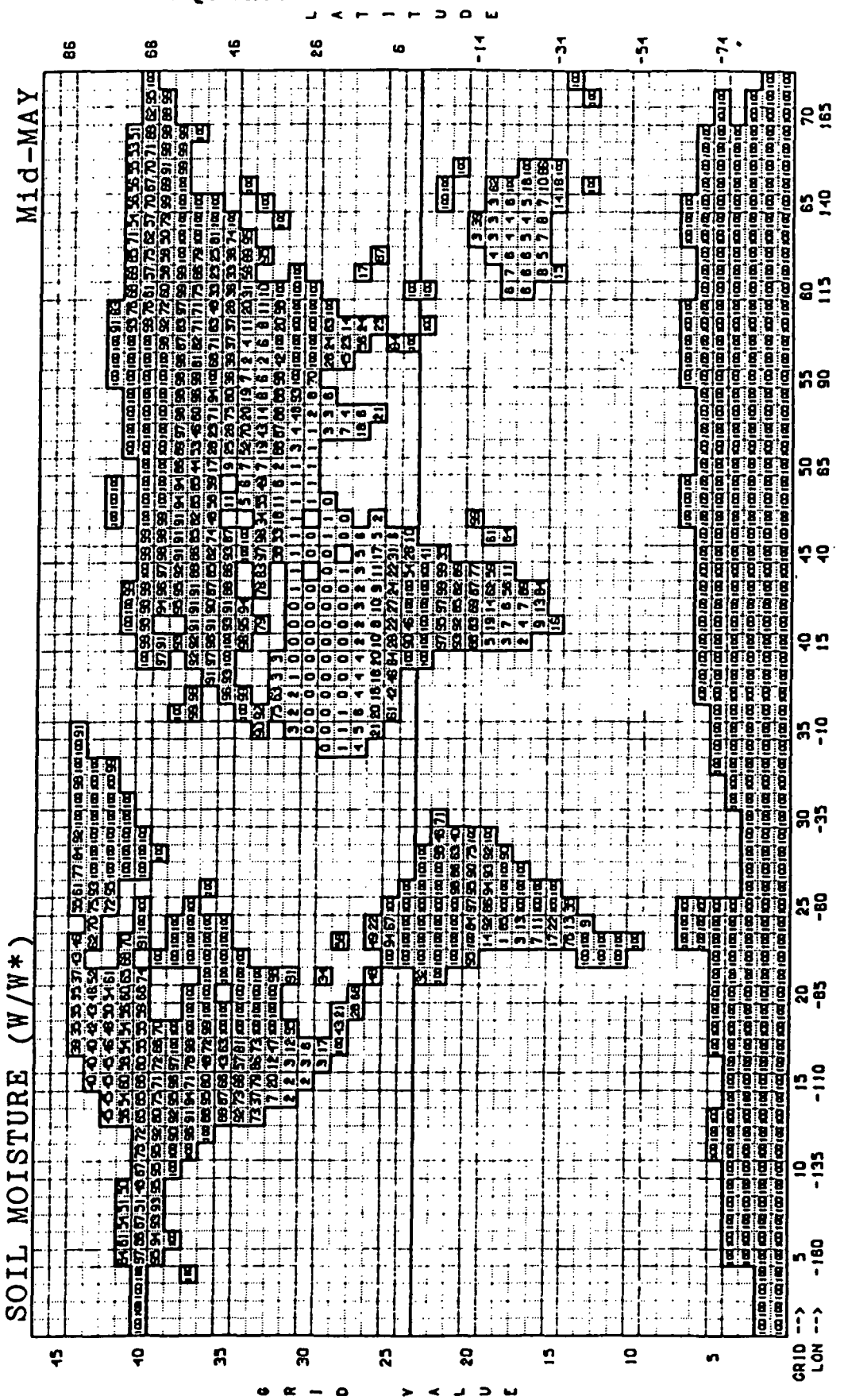

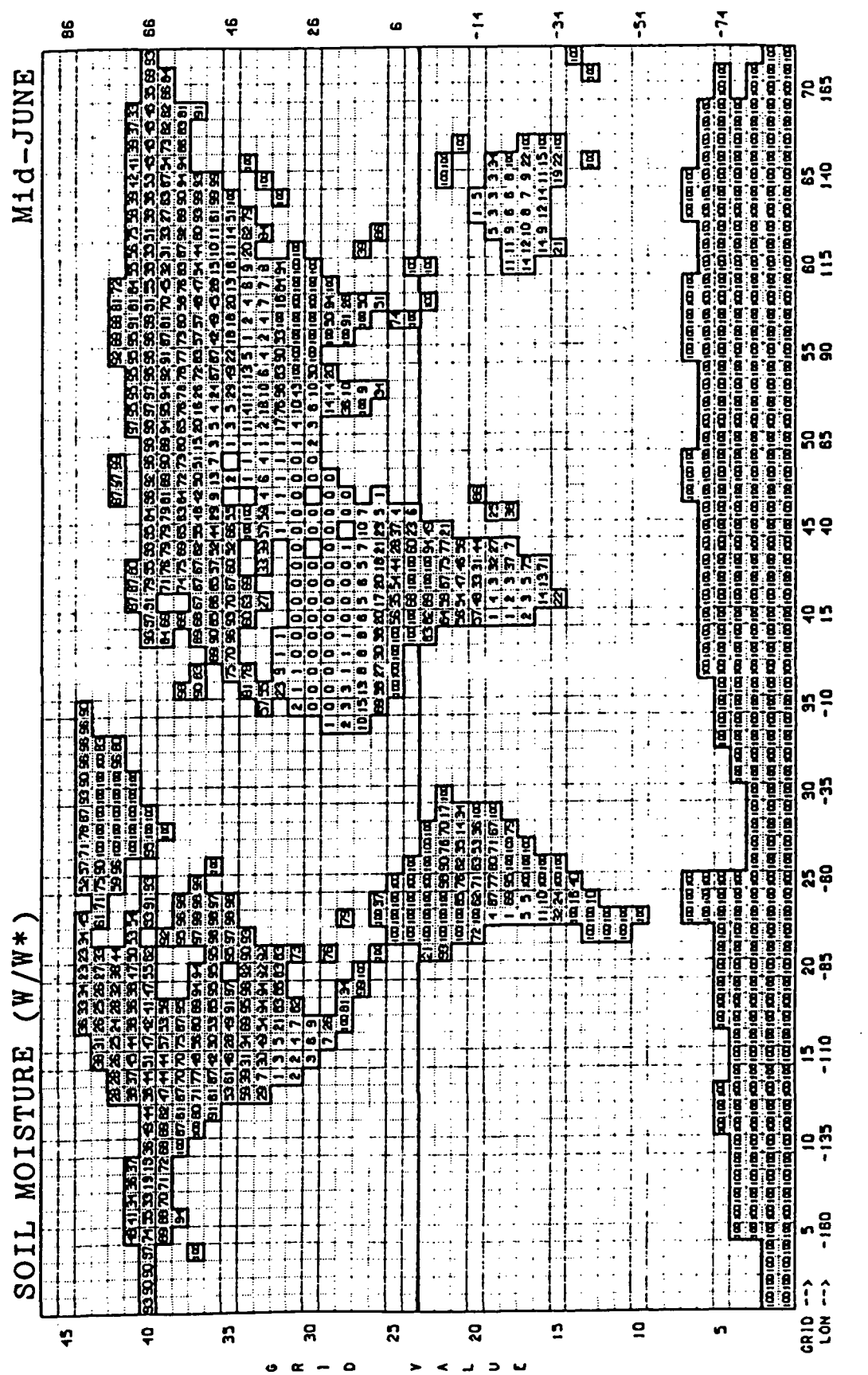

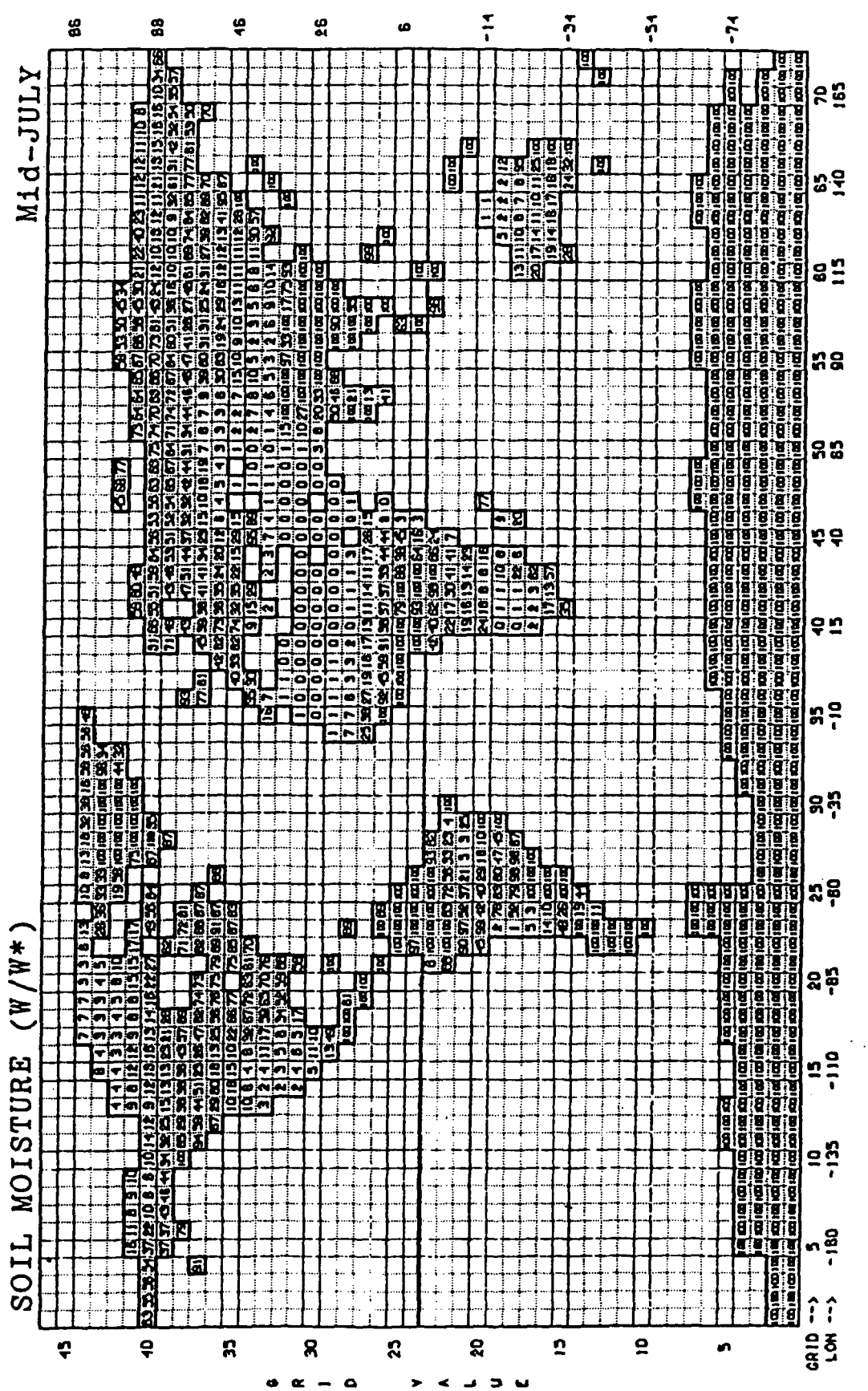

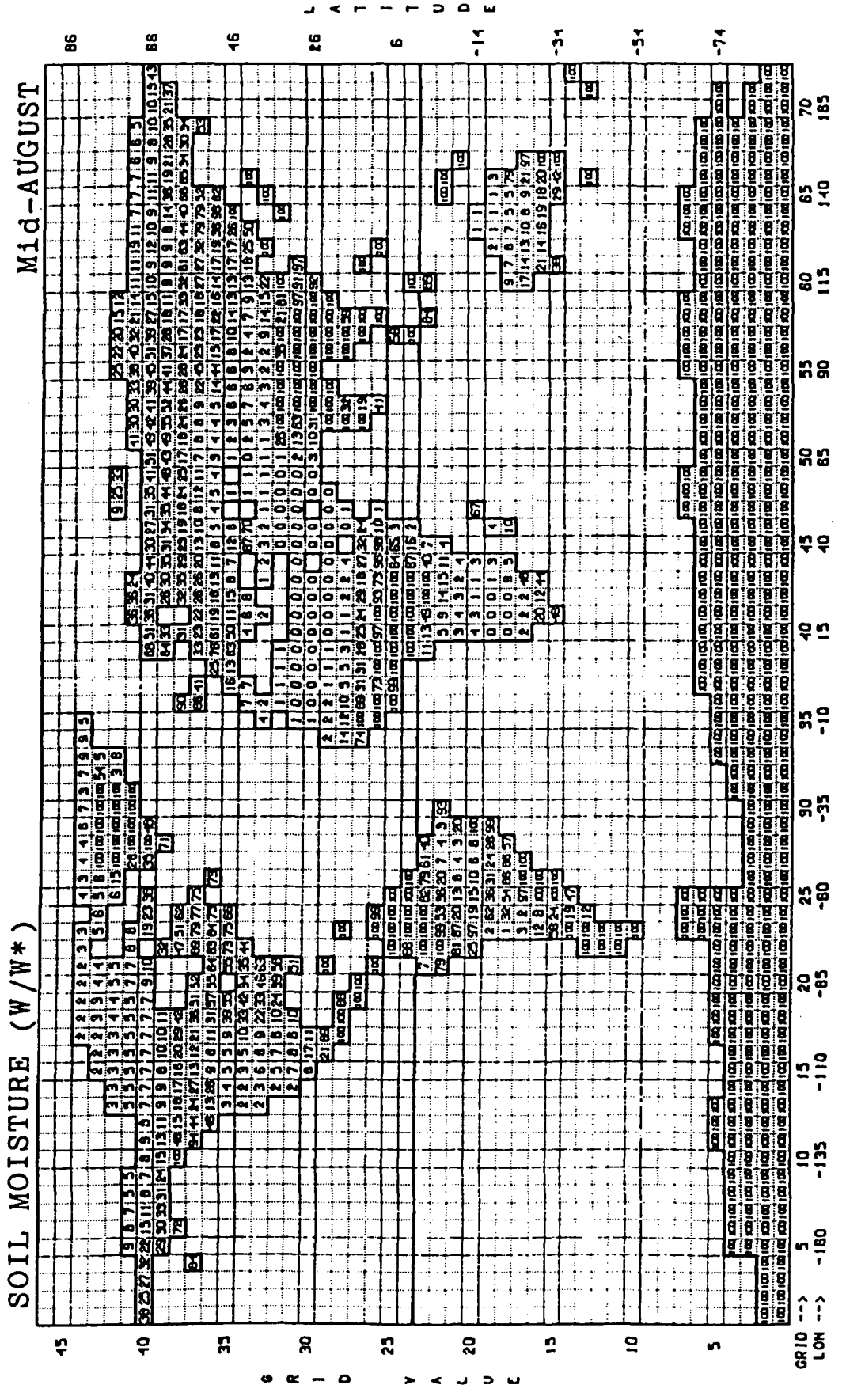

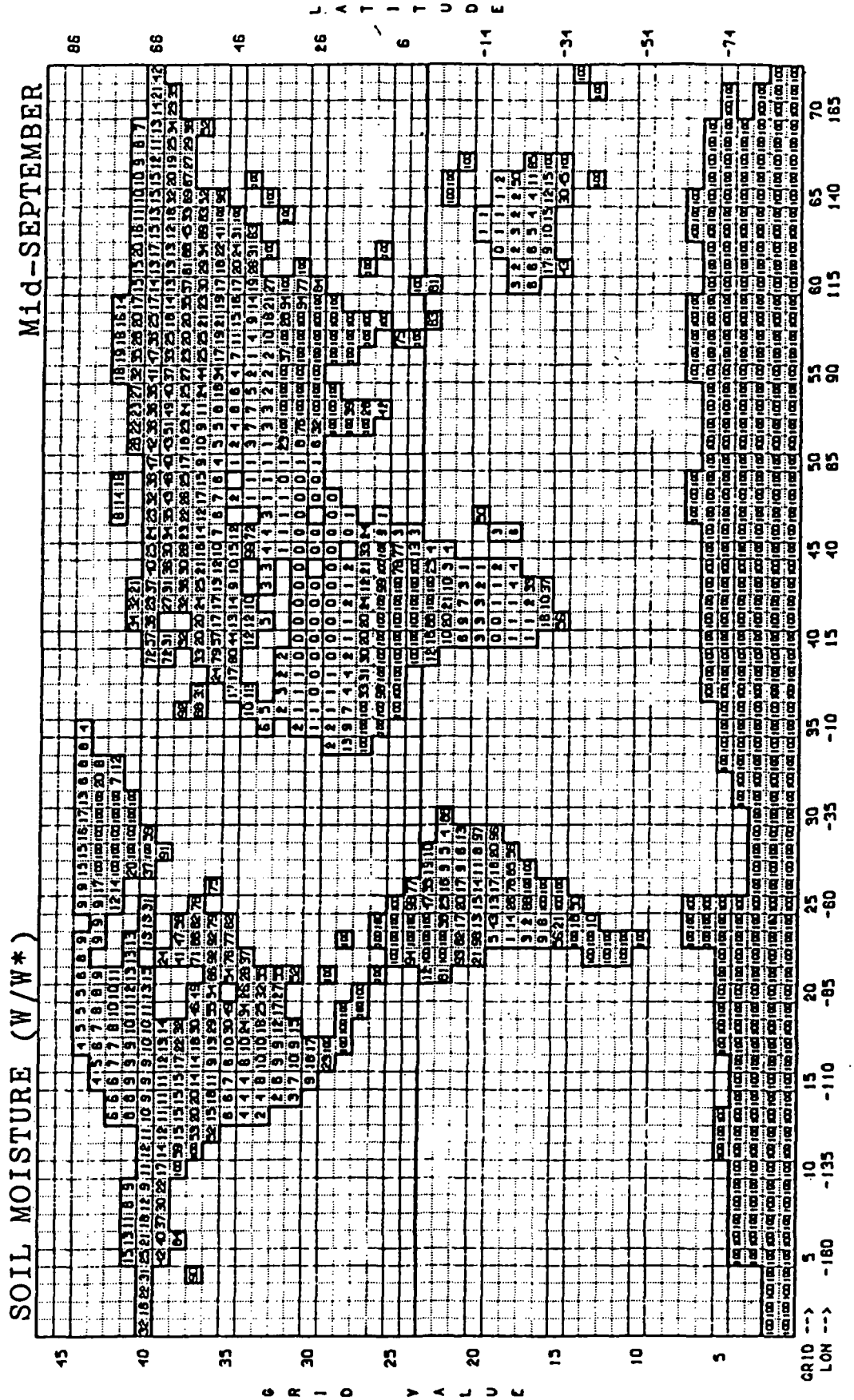

ORIGINAL PAGE IS
OF POOR QUALITY

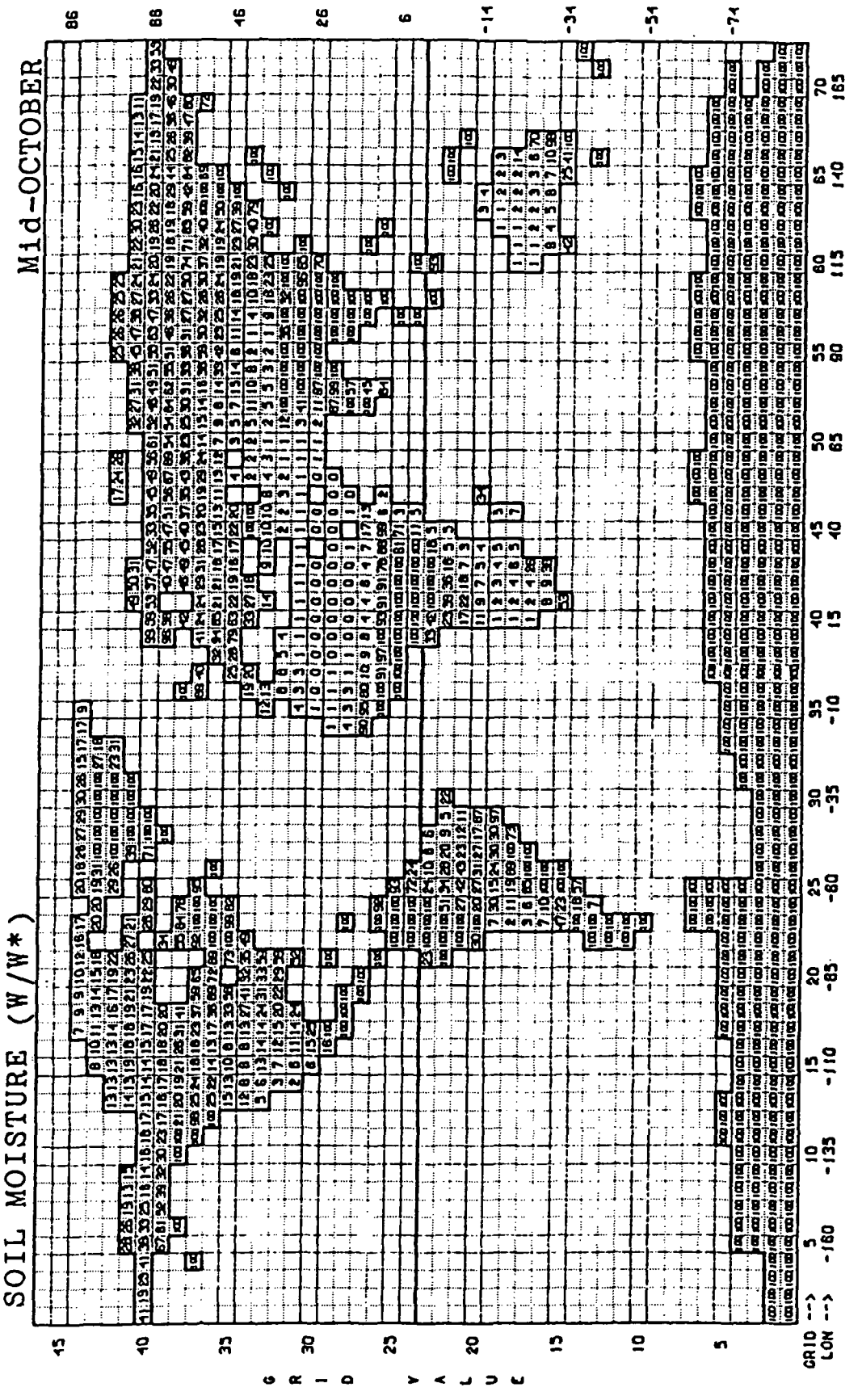

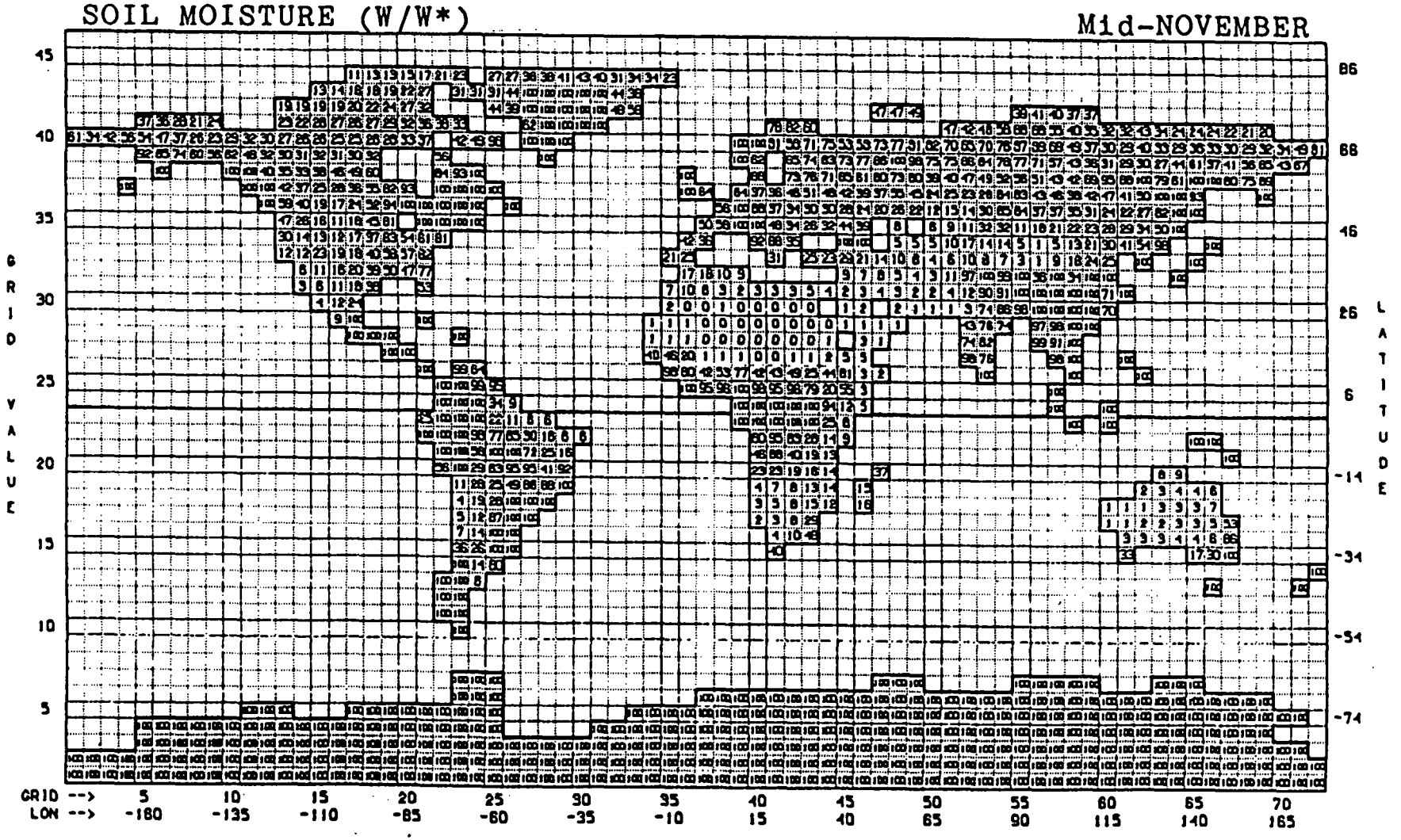

ORIGINAL PAGE IS
OF POOR QUALITY

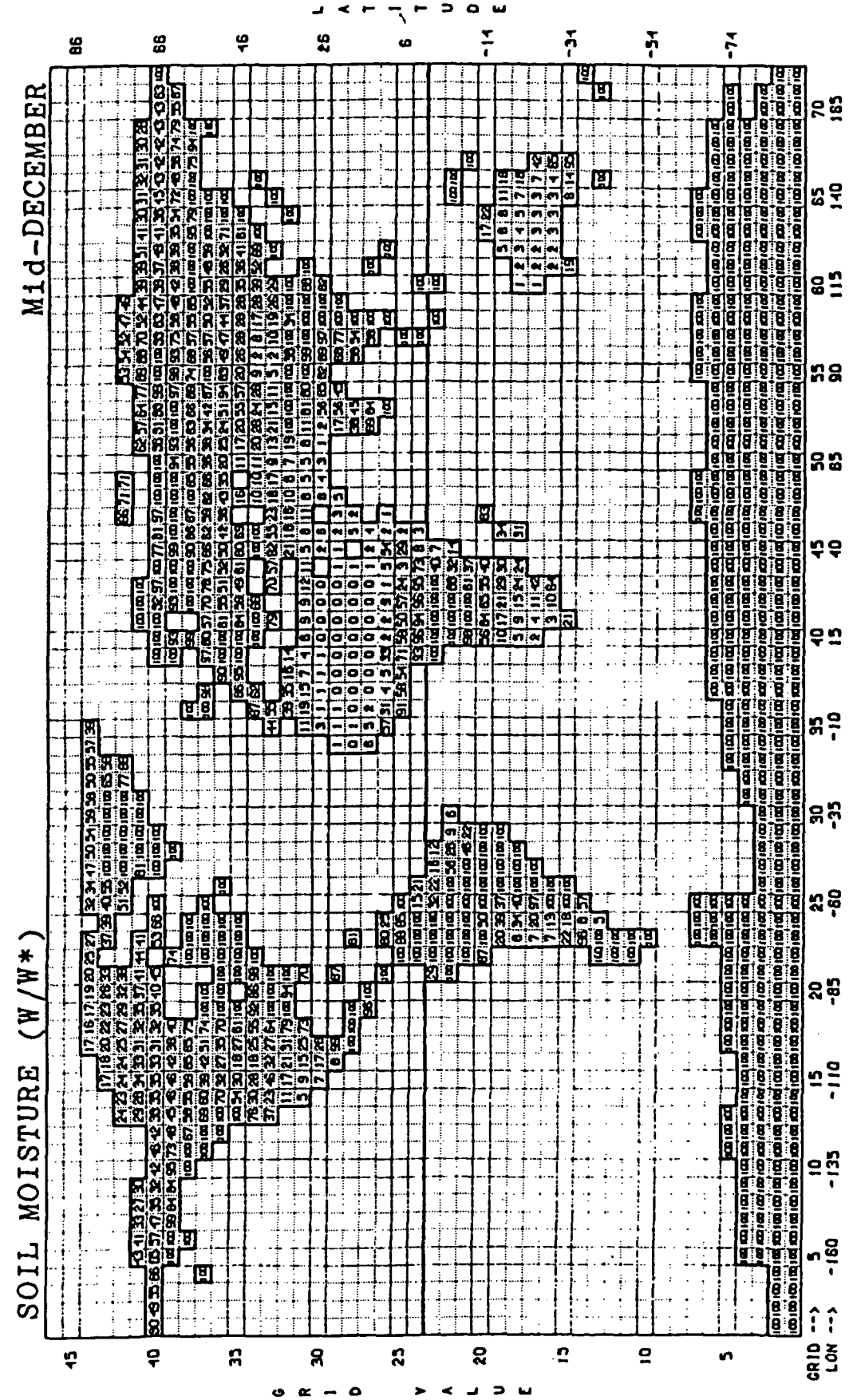

CLIMATOLOGY OF THE TERRESTRIAL SEASONAL WATER CYCLE

by

Cort J. Willmott & Clinton M. Rowe

Center for Climatic Research
Department of Geography
University of Delaware
Newark, Delaware 19716

and

Y. Mintz

Department of Meteorology
University of Maryland
College Park, Maryland 20742

Laboratory for Atmospheric Sciences
NASA Goddard Space Flight Center
Greenbelt, Maryland 20771

June 1984

ABSTRACT

The spacial and seasonal variations of the continental fields of snowcover, soil moisture and evapotranspiration are presented and interpreted. The fields were obtained from a water budget analysis that is based on observed monthly normal precipitation and an estimate of potential evapotranspiration derived from observed monthly normal surface air temperature, following the method of Thornthwaite. The month-by-month local water budget analysis was made for 13,332 station records over the globe, and then spacially interpolated to regular grids at 1° by 1° and at 4° by 5° latitude-longitude intervals. From the monthly fields in the 4° by 5° grid the annual mean and the first and second annual harmonics were extracted and are displayed on global maps. Of the three fields, the soil moisture has the largest space-time variation; the snowcover depth the most coherent distribution; and the evapotranspiration an intermediate level of variation.

Table of Contents

I. THEORY, CALCULATION PROCEDURE, AND INPUT DATA

1.1 Soil moisture budget, and potential evapotranspiration as a function of surface air temperature, following Thornthwaite.

1.2 Evapotranspiration coefficient, β; and soil moisture storage capacity, W*.

1.3 Snowcover budget, and rate of snowmelting.

1.4 Calculation procedure.

1.5 Global records of monthly normal precipitation and surface air temperature.

II. SEASONAL WATER CYCLE

2.1 Snowcover depth.

2.2 Soil moisture.

2.3 Evapotranspiration.

I. THEORY, CALCULATION PROCEDURE, AND INPUT DATA

1.1 Soil moisture budget, and potential evapotranspiration as a function of surface air temperature, following Thornthwaite.

Almost four decades ago, Thornthwaite (1948) formulated a fairly simple way of estimating the soil moisture and evapotranspiration from observed precipitation and a potential evapotranspiration which depends on observed surface air temperature; and, a few years later, he began the collection of a global data set of observed normal monthly precipitation and surface air temperature from which the terrestrial seasonal water cycle could be calculated.

When expressed in the notation we use today, Thornthwaite's governing equations for the soil moisture and evapotranspiration were

$$\frac{\partial W}{\partial t} = P - E \quad , \qquad W_{max} = W^* \quad , \tag{1}$$

$$E = E_p \times \beta\,(W, W^*) \quad , \tag{2}$$

$$E_p = E_p\,(T_A, h) \quad , \tag{3}$$

where W is the available moisture in the root zone of the soil (the moisture in excess of the amount at the wilting point of the vegetation); W* is the difference between the soil moisture at field capacity and at the vegetation wilting point; P is the rate of precipitation; E is the rate of evapotranspiration; E_p is the potential evapotranspiration (the evapotranspiration when the vegetation cover is not under any water stress); β is the function which relates the ratio (E/E_p) to W and W*; T_A is the surface air temperature, averaged for a day or more; and h is the duration of daylight.

Thornthwaite proposed that E_p be made a function of the surface air temperature, which is a widely available meterological measurement, and the duration of daylight. To this end, he compared the measured monthly evapotranspiration with the measured monthly mean surface air temperature at a number of well-watered drainage basins and grass-covered lysimeters in the central and eastern U.S., and obtained as the regression of E_p upon T_A,

$$E_p \text{ (mm month}^{-1}\text{)} \begin{cases} = 0 , & \text{when } T_A < 0°C \\ = 16\, L\, (10\, T_A/I)^a , & 0 \leq T_A < 26.5°C \\ = -415.85 + 32.25\, T_A - 0.43\, T_A^2 , & T_A > 26.5°C \end{cases} \quad (4)$$

where $$I = \sum_1^{12} (T_A/5)^{1.514} ,$$

$$a = (6.75 \times 10^{-7}\, I^3) - (7.71 \times 10^{-5}\, I^2) + (1.79 \times 10^{-2}\, I) + 0.49 ,$$

and $$L = (D/30)(h/12) ,$$

where D is the number of days in the month; h is the number of hours of daylight; and, when used to evaluate I, T_A is the monthly mean temperature of each month of the year.

1.2 Evapotranspiration coefficient, β, and soil moisture storage capacity, W*.

Thornthwaite (1948) initially assumed that $\beta = 1$, $(E = E_p)$, as long as there is any available soil moisture, and that $\beta = 0$, $(E = 0)$, when the soil moisture is at the vegetation wilting point. He also assumed, initially, that W*, the maximum moisture storage capacity of the soil, was effectively constant with respect to the various plant and soil type combinations, with W* = 100 mm of equivalent water depth.

Later, Thornwaite and Mather (1957) assumed that $E = E_p\ (W/W^*)$; and they let W^* vary from 50 to 400 mm, depending on soil and vegetation.

In the present study, we will follow Mintz and Serafini (1984), and let

$$E = E_p\ (1 - e^{-6.8(W_{D-1}/W^*)}), \tag{5}$$

where the subscript D denotes the day of the month, and $W^* = 150$ mm.

1.3. Snowcover budget, and rate of snowmelting.

Thornthwaite treated all precipitation as if it were immediately available for storage in the soil and, therefore, he did not keep a separate budget for snowcover. In the present study, we maintain a separate budget for the snowcover in the following simple way.

When the monthly mean surface air temperature, T_A, is equal to or warmer than -1°C, the precipitation for the month is taken as rainfall, $P = P^r$. When T_A is colder than -1°C, the precipitation for the month is taken as snowfall, $P = Ps$. Because our records are of monthly precipitation and monthly mean temperature, we take P^r and P^s as constant over the month; and for the day-to-day calculation of the snowcover and the soil moisture, we let P^s_d and P^r_d be the monthly mean precipitation rates (in units of mm/day.)

We take the daily snowmelt, in mm/day, as

$$M_D = 2.63 + 2.55\ T_A + 0.0912\ T_A\ P^r_d, \qquad M_{D,min} = 0$$
$$M_{D,max} = (W^s_{d-1} + P^s_\partial)\ , \tag{6}$$

where T_A is in °C.

Comparison of Eq. (6) with the data from which it was derived -- data from three dissimilar drainage basins and 113 sets of observations, Anderson (1973), Pysklywec et al. (1968), and Storr (1978) -- shows a moderately good fit: RMS error = 6.62 mm/day and $r^2 = 0.59$.

The snowcover depth at the end of day D (in equivalent depth of liquid water) is

$$W_D^S = W_{D-1}^S + P_d^S - M_D \quad (mm), \tag{7}$$

where W_{D-1}^S is the snowcover depth at the end of the previous day.

1.4 Calculation procedure.

The calculation begins with Eqs. (6) and (7), the calculation of the snowmelt and snowcover depth. Then, the finite difference form of Eq. (1) is used, with P_d^r plus M_D replacing P, to obtain the soil moisture,

$$W_D = W_{D-1} + (P_d^r + M_D) - E_{pd}\,(1 - e^{-6.8(W_{D-1}/W^*)}), \quad W_{Dmax} = W^*. \tag{8}$$

Whenever W_D exceeds W*, the excess is set aside as the surplus (S_D) for day D.

The soil moisture was initialized as being zero, everywhere, on 1 January, and the calculation, with Eqs. (6), (7), and (8), carried forward in time, by iteration, until the change from year to year (from one January 1st to the next January 1st) became negligibly small. The snowcover and the soil moisture values that are recorded are those at the end of the fifteenth day of each month. The evapotranspiration, E_D, that is recorded (the last term in Eq. 8) is the total for the month.

1.5 Global records of monthly normal precipitation and surface air temperature.

The collection of records of observed monthly precipitation and monthly mean surface air temperature that was begun by Thornthwaite, was continued by Mather and Willmott. This data set provides the normal monthly values of precipitation and surface air temperature at 13,332 locations over the globe (Willmott et al., 1981). The station locations are shown in Fig. 1.

Fig. 1

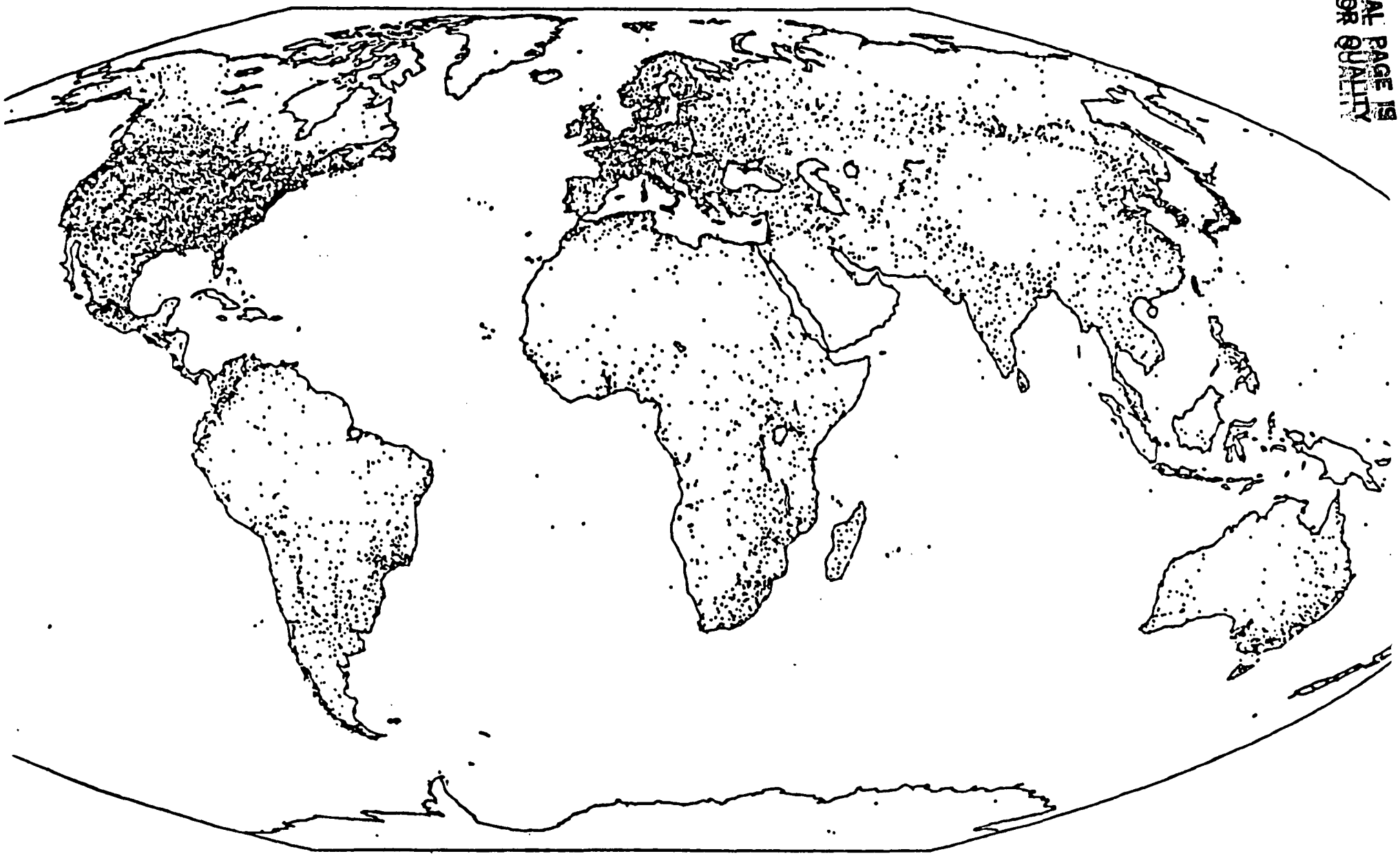

Fig. 1 Distribution of stations in the Thornthwaite/Mather/Willmott data set of monthly normal precipitation and surface air temperatures.

II. SEASONAL WATER CYCLE

From the solutions at each of the 13,332 station locations, W_D^S, W_D, and E_D were spacially interpolated to the nodes of the 1° latitude by 1° longitude grid. The interpolation was made using the method described by Willmott et al. (1984), except that the number of stations which influenced a grid point was held constant at 10. This damps the spatial variance where the stations are widely separated, and accentuates the variance where the stations are close together. Here, to preserve map clarity, we show the fields only for the subset of the interpolations at the nodes of the 4° latitude by 5° longitude grid.

2.1 Snowcover depth.

Fig. 2 As seen in Fig. 2.A, the annual mean snowcover depth $\overline{W^S}$ (given in mm water depth equivalent), shows a general increase with latitude. Over eastern North America, there is a greater than average depth for the latitude as a consequence of its large precipitation and low monthly mean air temperature in winter. Over the Rocky and Ural mountains, one sees the effect of the enhanced orographic precipitation combined with low air temperature.

The root-mean-square of the deviation of the monthly mean snowcover depth from the annual mean in shown in Fig. 2.B. Over most of the northern hemisphere, the snowcover completely melts in summer and, therefore, $\hat{\sigma}^S$ is roughly colinear with $\overline{W^S}$, because $W^S{}_D$ is bounded on the low end by zero. Along the east coast of North America, the seasonal variance increases with latitude to about 50°N, and then σ^S begins to lessen with the latitudinal decrease in the winter precipitation and the shortening in the length of the melting season. The northern hemisphere mountain regions also show large seasonal variances in $\hat{\sigma}^S$.

Most of the seasonal variation in the snowcover depth is accounted for by the first two annual harmonics, which are shown in Figs. 2.C and 2.D. Over

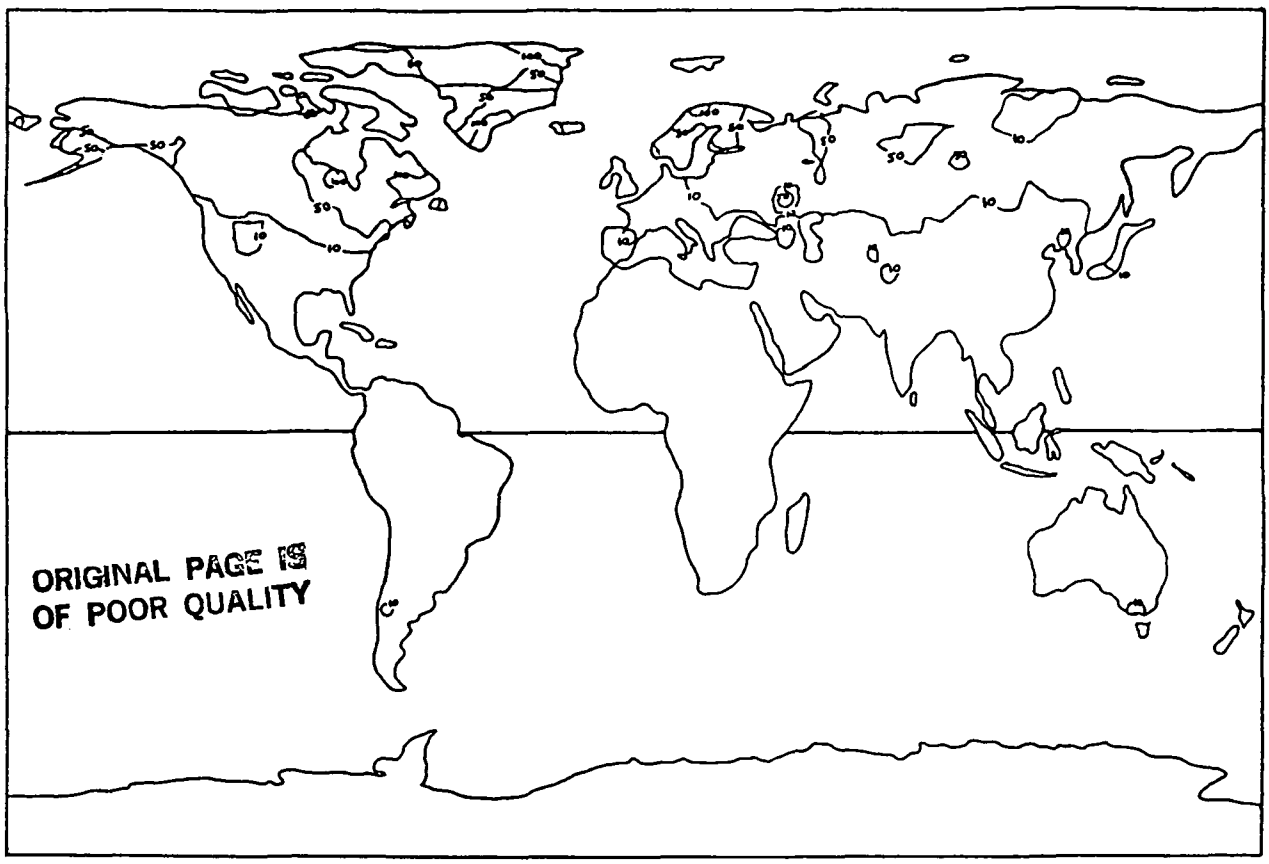

Fig. 2.A Annual mean snowcover depth (in mm equivalent water.)

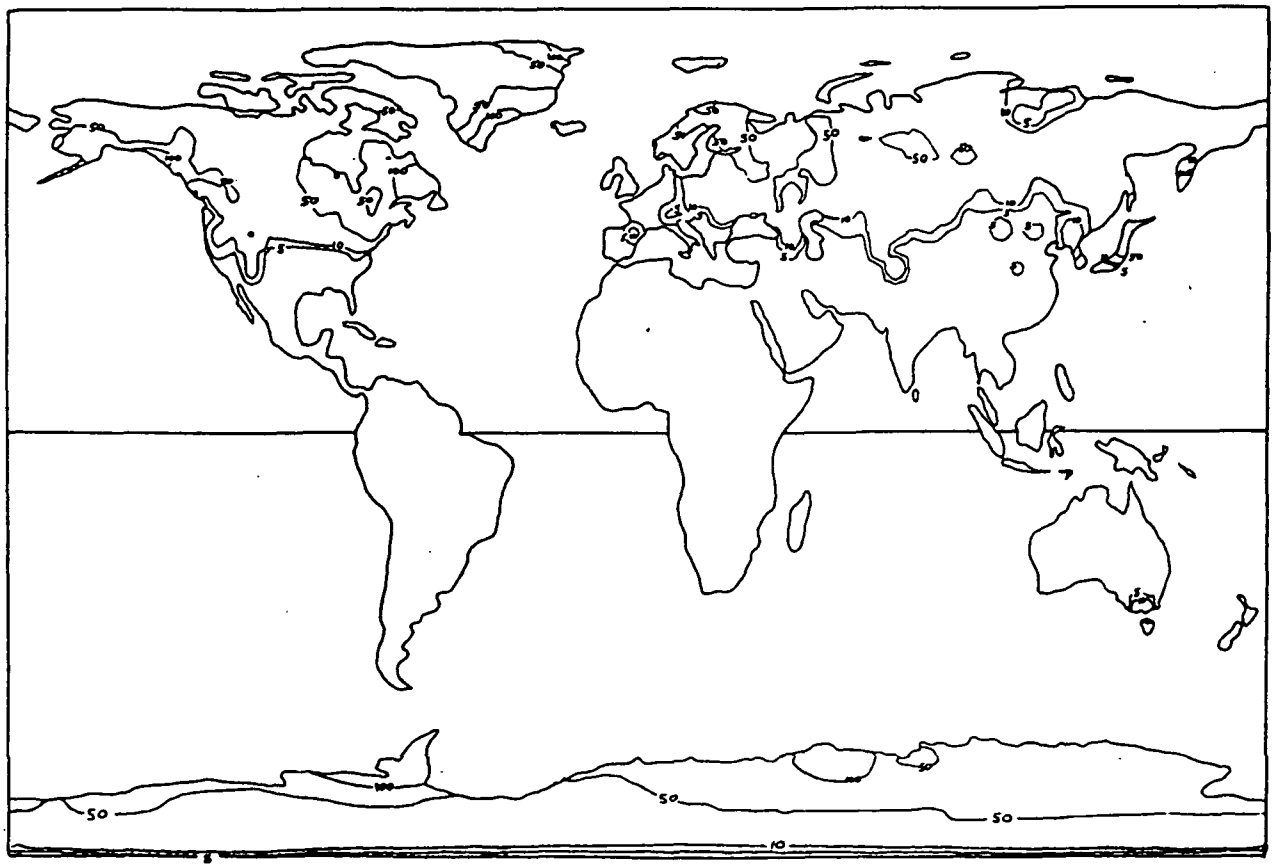

Fig. 2.B Root-mean-square of the deviations of mid-monthly snowcover depth from the annual depth (in mm equivalent water.)

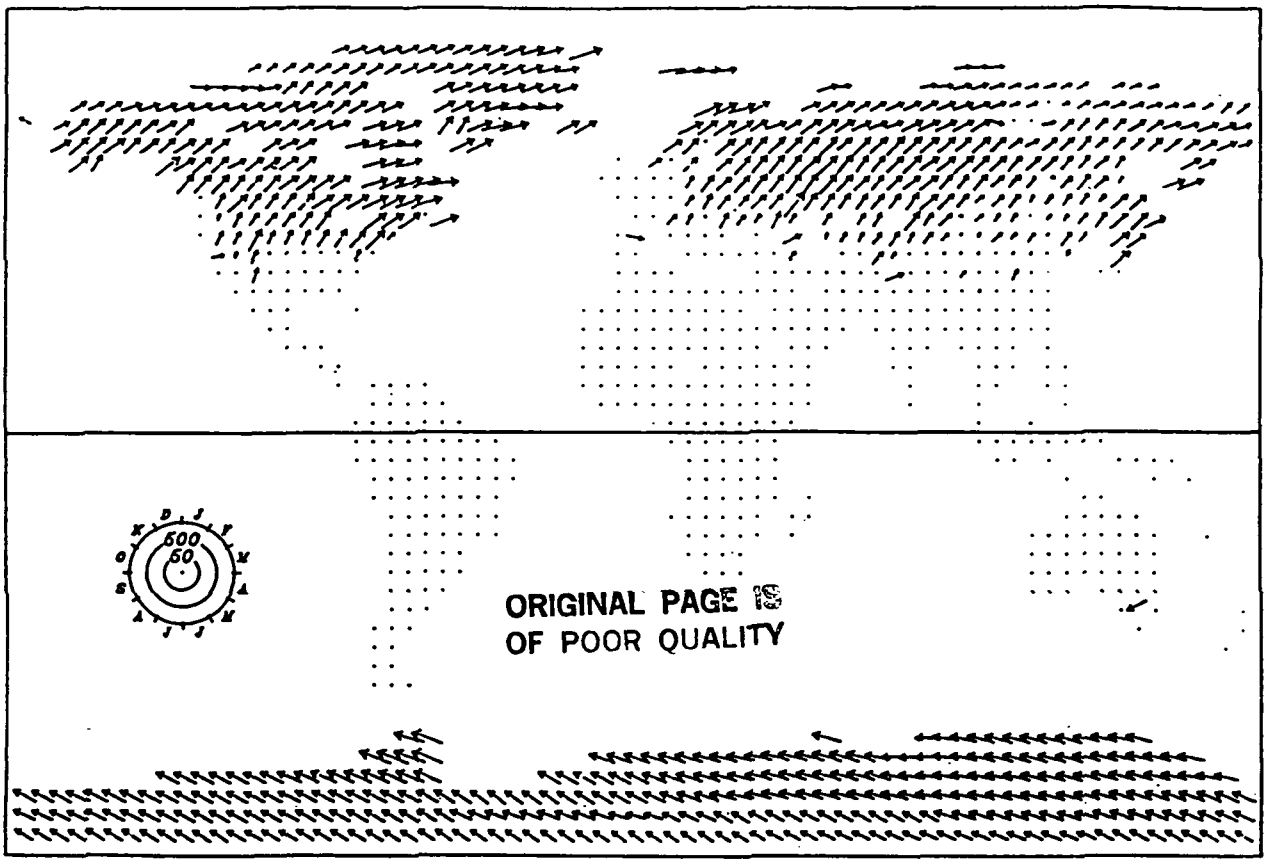

Fig. 2.C First annual harmonic of snowcover depth (in mm equivalent water.)

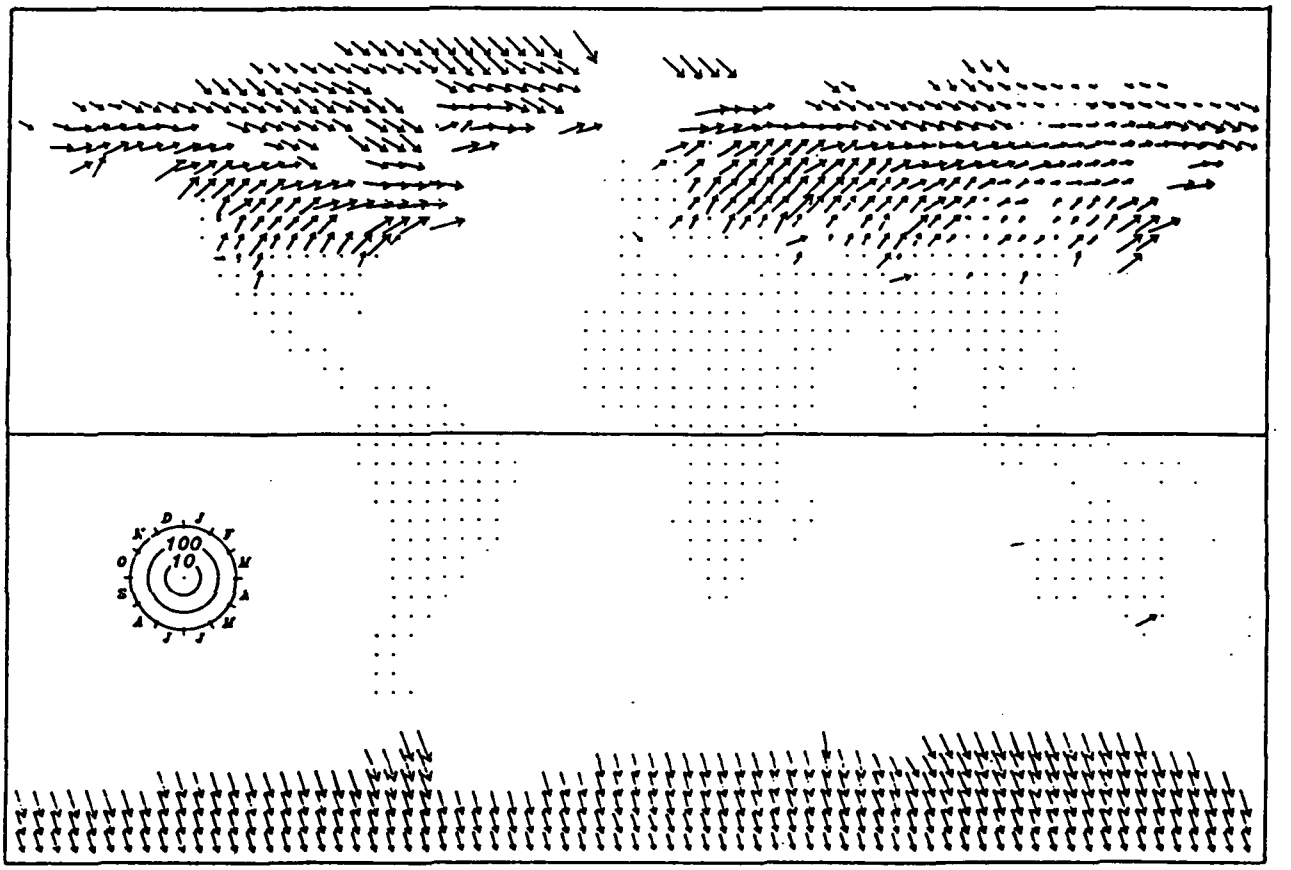

Fig. 2.D Second annual harmonic of snowcover depth (in mm equivalent water.) Note that the amplitude scale differs from that of the first harmonic by a factor of five.

almost all of the continents, the root mean square of the monthly residuals is no more than about 10 mm.

The phase angle (the time of maximum) of the first annual harmonic, represents the end of the accumulation season and the onset of melting. A clockwise shift, from January and February near the snowline, to March and April in the higher latitudes, is evident over North America and Eurasia. Eastern North America, shows an extended accumulation season. Increases in the length of the accumulation season also appear in the mountain regions (e.g., the Sierra Nevada, the Pyrenees and the Himalayas). Over Antarctica, the phase is shifted by four to five months.

Fig. 2.D shows the phase and amplitude of the second annual harmonic of the snowcover depth. Near the equatorial limit of the snowcover, the phase of the second annual harmonic is about the same as the that of the first harmonic; but with increasing latitude the phase shifts clockwise with respect to that of the first harmonic. When comparing the amplitudes of the first and second annual harmonics, note that the scales in the two representations differ by a factor of five. [Note, also, that α_2 and $(\alpha_2 + 180°)$ are equivalent.]

2.2 Soil moisture.

The soil moisture is spatially more variable than the snowcover. As we see in Fig. 3.A, for example, eastern North America, has large soil moisture throughout the year, as manifested by annual averages that are only a little less than the assumed soil moisture storage capacity of 150 mm. By contrast, the mountain states and the southwest U.S. have annual means of only about 25 mm. The year round onshore orographic precipitation along the northwest coast is the reason for its soil moisture being larger than in the plateau region to the east.

Fig. 3

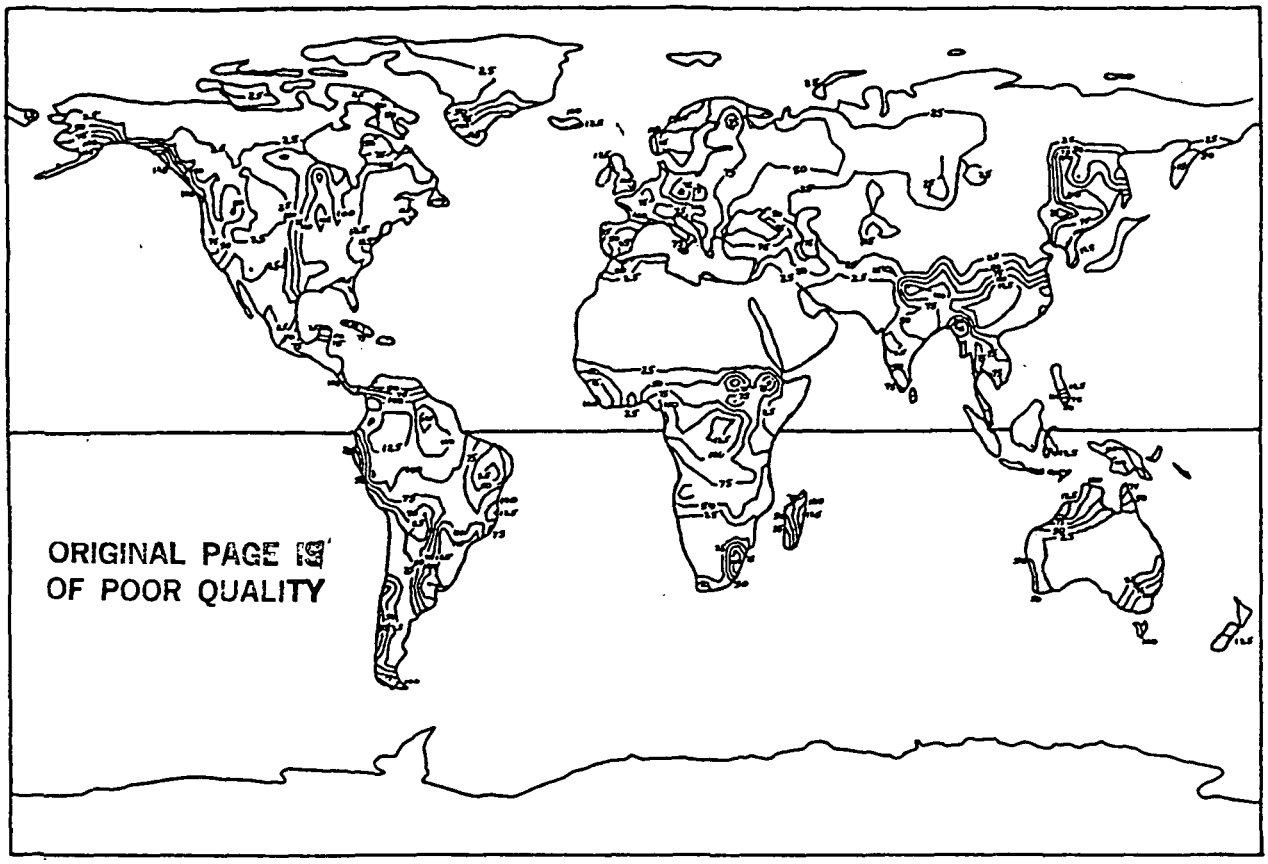

Fig. 3.A Annual mean soil moisture (in mm.)

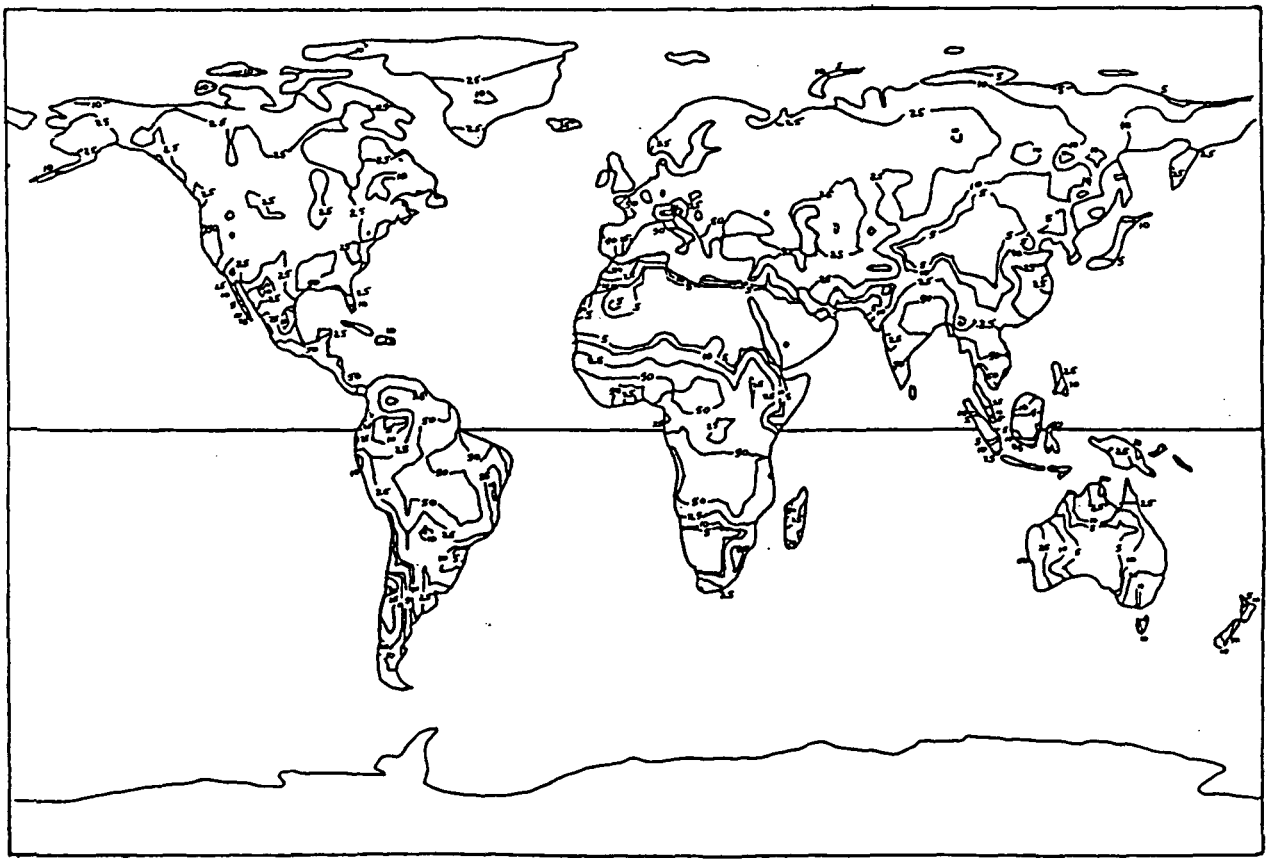

Fig. 3.B Root-mean-square of the deviations of mid-monthly soil moisture from the annual mean moisture (in mm.)

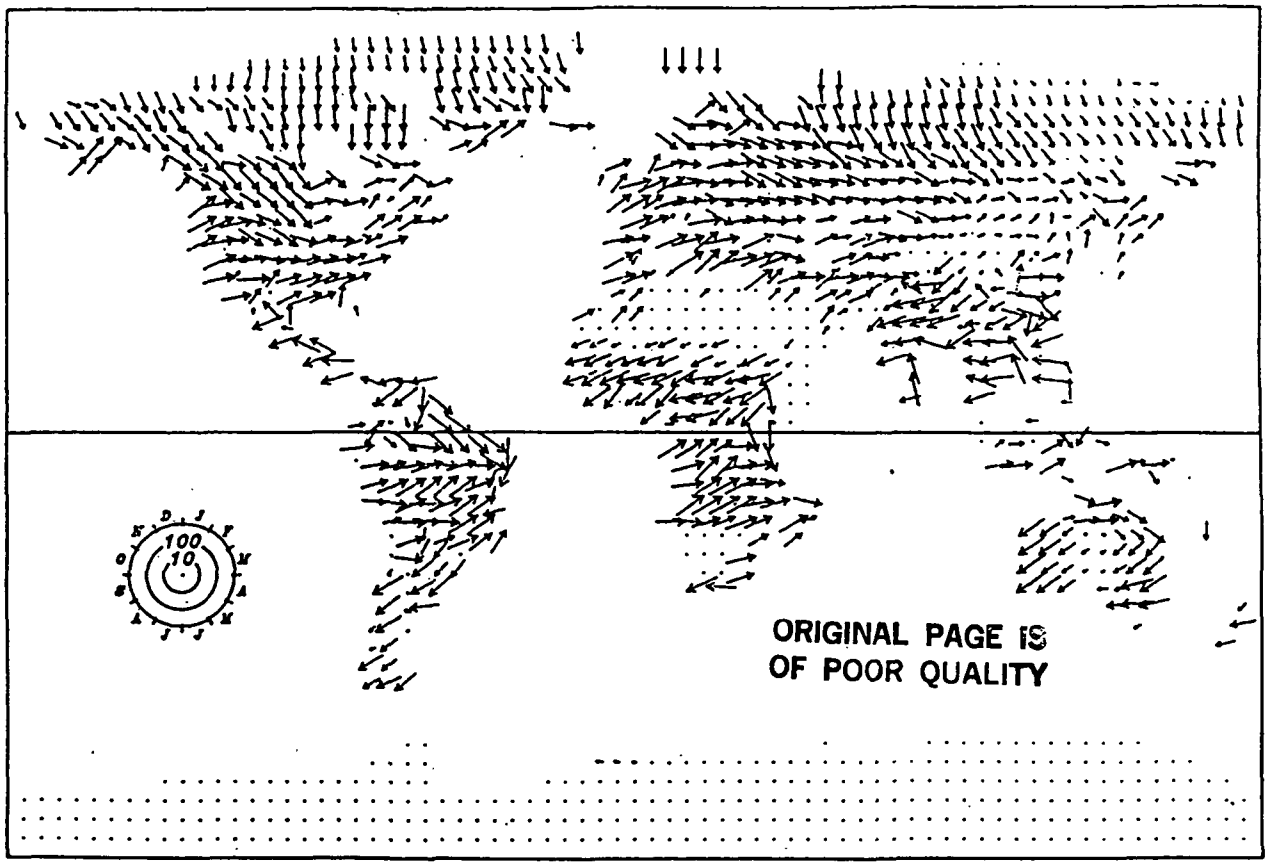

Fig. 3.C First annual harmonic of soil moisture (in mm.)

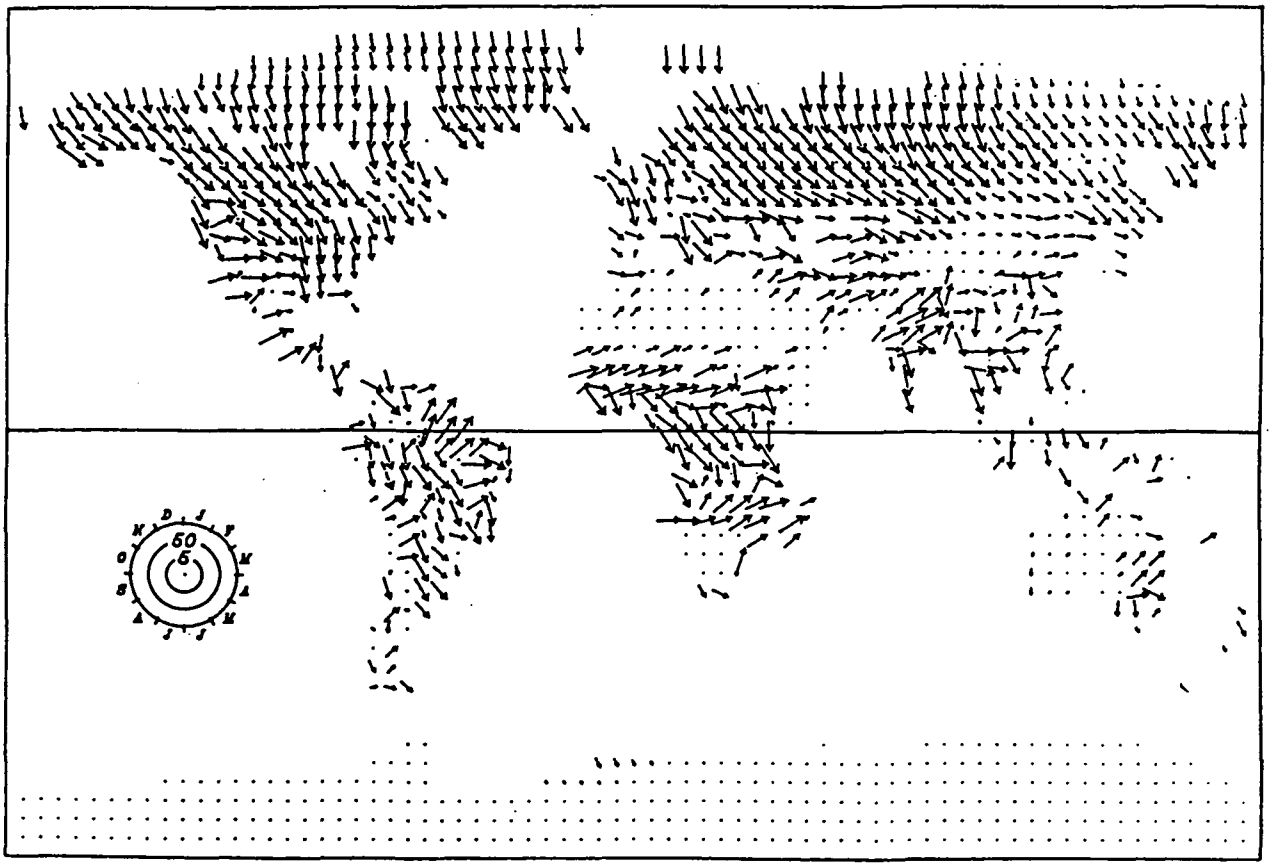

Fig. 3.D Second annual harmonic of soil moisture (in mm.) Note that the amplitude scale differs from that of the first harmonic by a factor of two.

South America, too, shows large variations. In the tropical eastwind zone very dry soil ($\overline{W} < 25$ mm) extends along the west coast from northern Peru to central Chile. But in the extratropical westwind zone, the dry soil region crosses into Patagonia, which is in the rainshadow of the southern Andes. On the windward side of the southern Andes the soil is very moist. Within the tropics, east of the Andes, there is large annual mean soil moisture.

The annual mean soil moisture is high over most of Europe. But from Ural mountains and the Caspian Sea, and extending eastward over most of Asia, the soil is very dry. Only along the east coast of Asia and over southeast Asia is the soil moisture high ($W > 125$ mm).

In Africa, what is most conspicuous is the vast subtropical expanse of the dry soil of the Sahara, with a smaller, corresponding dry soil region in south Africa. Over most of central Africa and the Ivory coast the average annual soil moisture is high.

Australia has dry soil over most of its interior ($\overline{W} < 25$ mm) and only a narrow band along the northern, eastern and southern coasts has moist soil. The west coast, like the interior, has dry soil.

Fig. 3.B shows the RMS of the monthly deviations from the annual mean soil moisture. The deviations are large, as we expect, in the regions where there is a large seasonal variation in precipitation. There, the RMS deviations can exceed 50 mm. This is true in Brazil, north and south Africa, the Mediteranean region, the southwest coastal area of U.S., and the monsoon regions of Asia. But, overall, there is a general decrease in the magnitude of $\hat{\sigma}(W)$ with latitude.

Figs. 3.C and 3.D show the first two annual harmonics of the soil moisture. These two harmonics represent most of the seasonal soil miosture variation, with the RMS of the residuals being generally less than about 10 mm.

Although the scale of the vectors for the two harmonics differ by a factor of two, we can see that both harmonics are significant. From the middle to the high latitudes of the Northern Hemisphere there is a general clockwise rotation of the phase angles with increasing latitude. Over mid-latitude North America and Eurasia, the soil moisture maximum is in March or April, and over northern North America and northern Eurasia, it is in May or June. This shows the increasing time lag in the snowmelting, as the latitude increases. Mountain and inland regions also have an enhanced delay in the time of maximum soil moisture, relative to other regions in the same latitude, and we see this in the northern Rocky Mountains and northern Great Plains. In the high latitudes, the effect of the late springtime snowmelting is reinforced by the lag in the springtime potential evapotranspiration after the snow has gone.

Equatorward of the snow line, the time of the soil moisture maxima will not depend on snowmelting. There, the maxima are at the end of the seasons during which precipitation exceeds evapotranspiration. Thus, where the source of the soil moisture is the migrating belt of intertropical convergence rain, in northern South America, the Sahel of Africa, India, and southeast Asia, the maxima in the first annual harmonic of the soil moisture is August-September; and in Argentina, south-central Africa, and Indonesia it is February-March. In the Mediterranean region and southwestern U.S., the time of maximum soil moisture is also February-March, which is when their seasonal rains end.

In the higher latitudes of the northern hemisphere, the second harmonic of the soil moisture has about the same phase as the first harmonic, as we see in Fig. 3.D. This again shows the dominance of the snowmelting effect. But in the middle latutudes of the northern hemisphere, the phase of the second harmonic is rotated clockwise with respect to the first harmonic. This represents a lag in the accumulation of soil moisture because the potential evapotranspiration is smaller in the spring than in the fall.

2.3 Evapotranspiration.

Where there is sufficient soil moisture, the evapotranspiration follows the potential evapotranspiration, which covaries with the air temperature.
Fig. 4 Therefore, as Fig. 4.A shows, there is a general decrease of the annual mean evapotranspiration with latitude; upon which is superposed the variation caused by the soil moisture deficits.

Where there is ample soil moisture, the annual mean evapotranspiration is about 100 mm/month near the equator and 25 mm/month in the polar region. But $\overline{E}$ is also 25 mm/month and less over the subtropical west coasts and across the Sahara, Arabia, and central Asia.

The RMS of the deviation of the monthly evapotranspiration from the annual mean, shown in Fig. 4.B, is comparable in magnitude to the annual mean wherever the annual mean is small: in the high latitudes, where the available energy for evapotranspiration changes by a large amount during the year; and in those low latitude regions where the precipitation, and therefore the soil moisture, has a large annual variation.

Most of the seasonal variation in evapotranspiration is in the first two annual harmonics, shown in Figs. 4.C and 4.D. In these figures the two amplitude scales are the same. The RMS residuals from the first two harmonics are only about 5 to 10 mm/month.

As Fig. 4.C shows, in the high and middle latitudes the phase of the first annual evapotranspiration harmonic coincides with the time of temperature maximum: July in the northern hemisphere and January in the southern hemisphere. Thus, the evapotranspiration phase coincides with the soil moisture phase in the high latitudes. But it is about three months later than the phase of the soil moisture maximum in the middle latitudes. Within the tropics, in Mexico, Central America, Africa, and South-southeast Asia, where there is no large

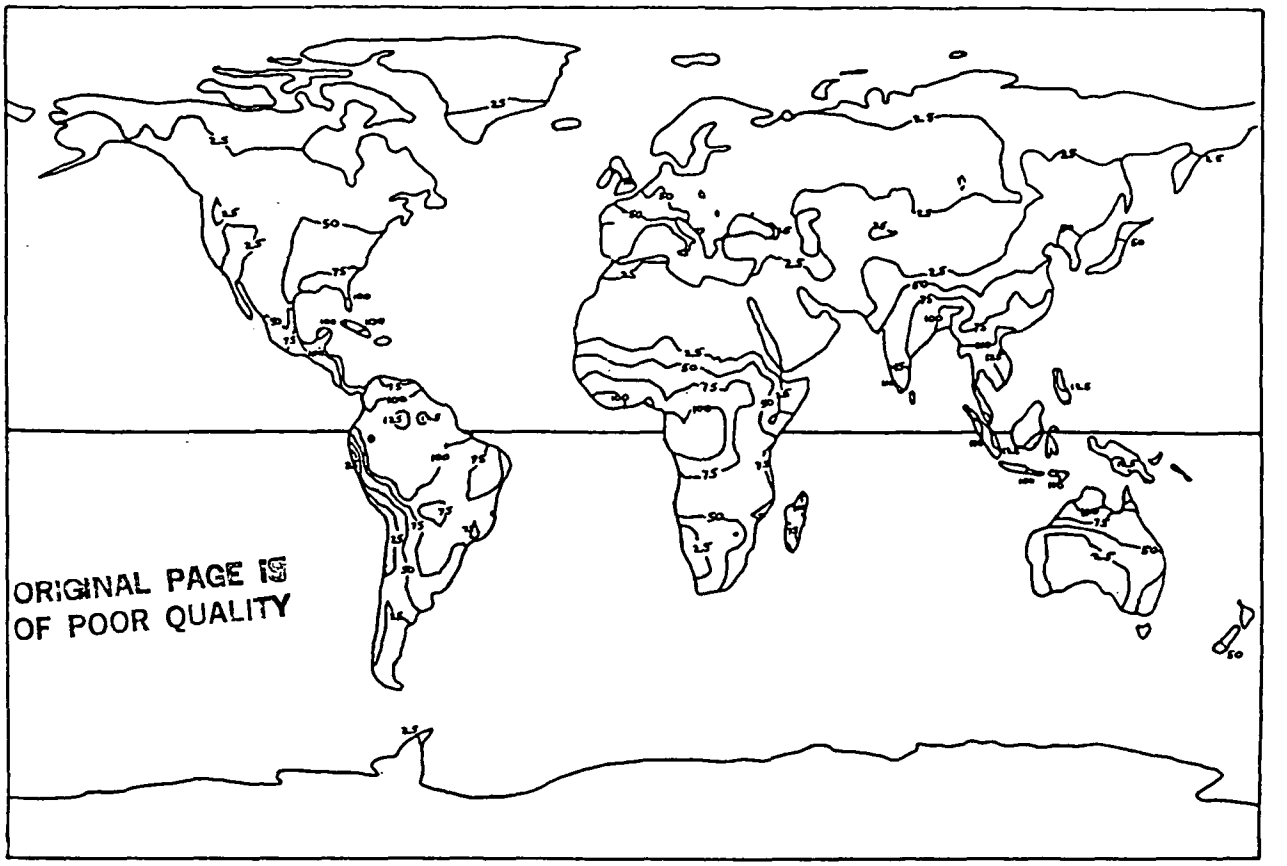

Fig. 4.A Annual mean evapotranspiration rate (in mm/month.)

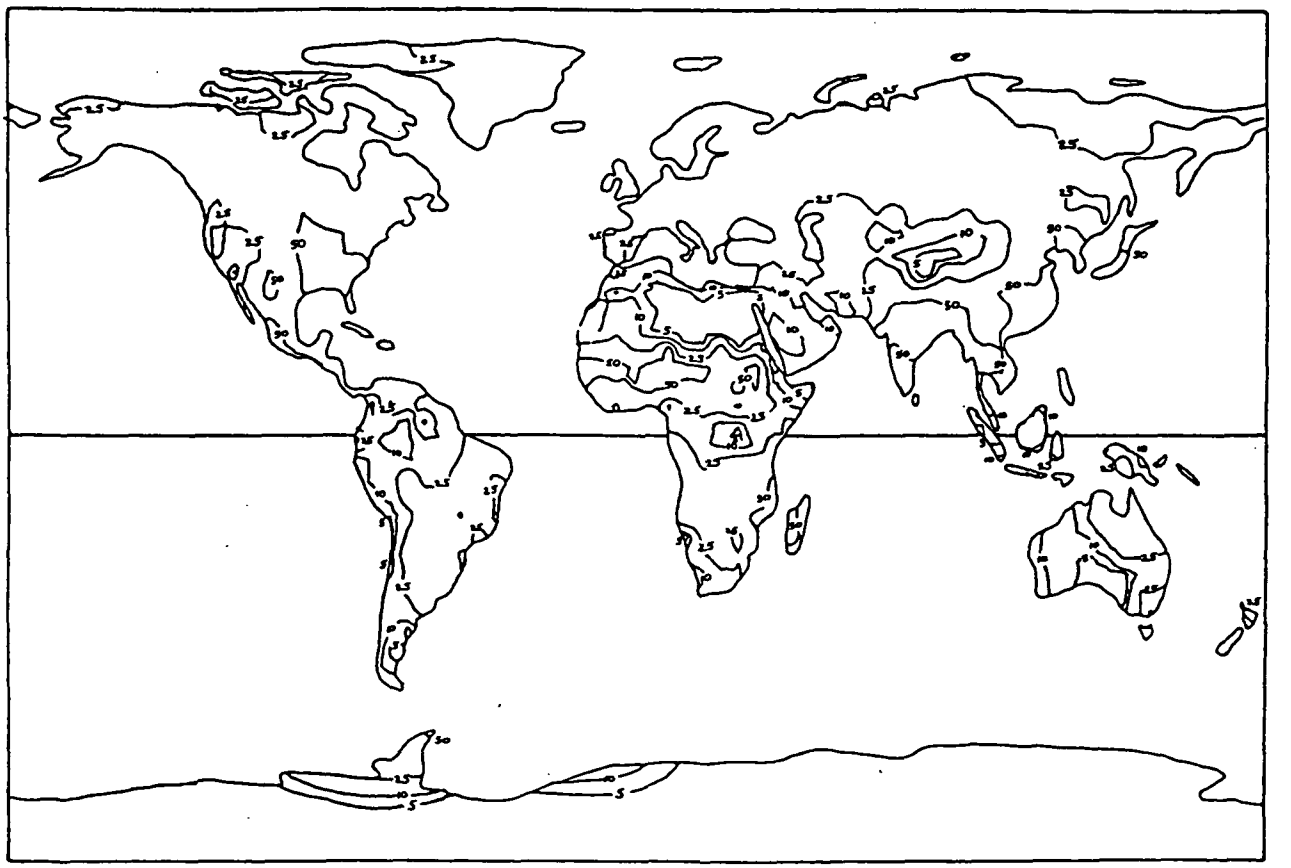

Fig. 4.B Root-mean-square of the deviations of monthly evapotranspiration from the annual mean (in mm/month.)

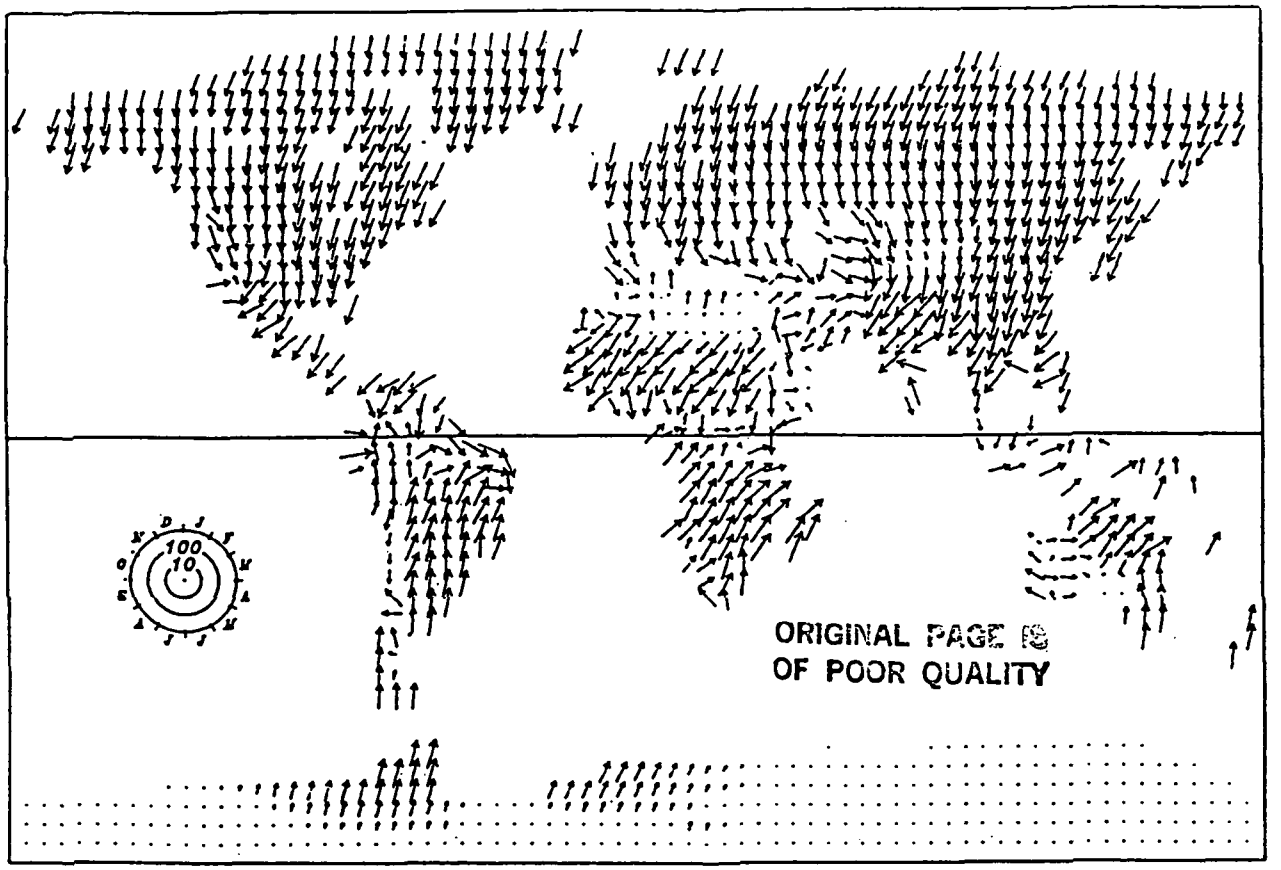

Fig. 4.C First annual harmonic of monthly evapotranspiration (in mm.)

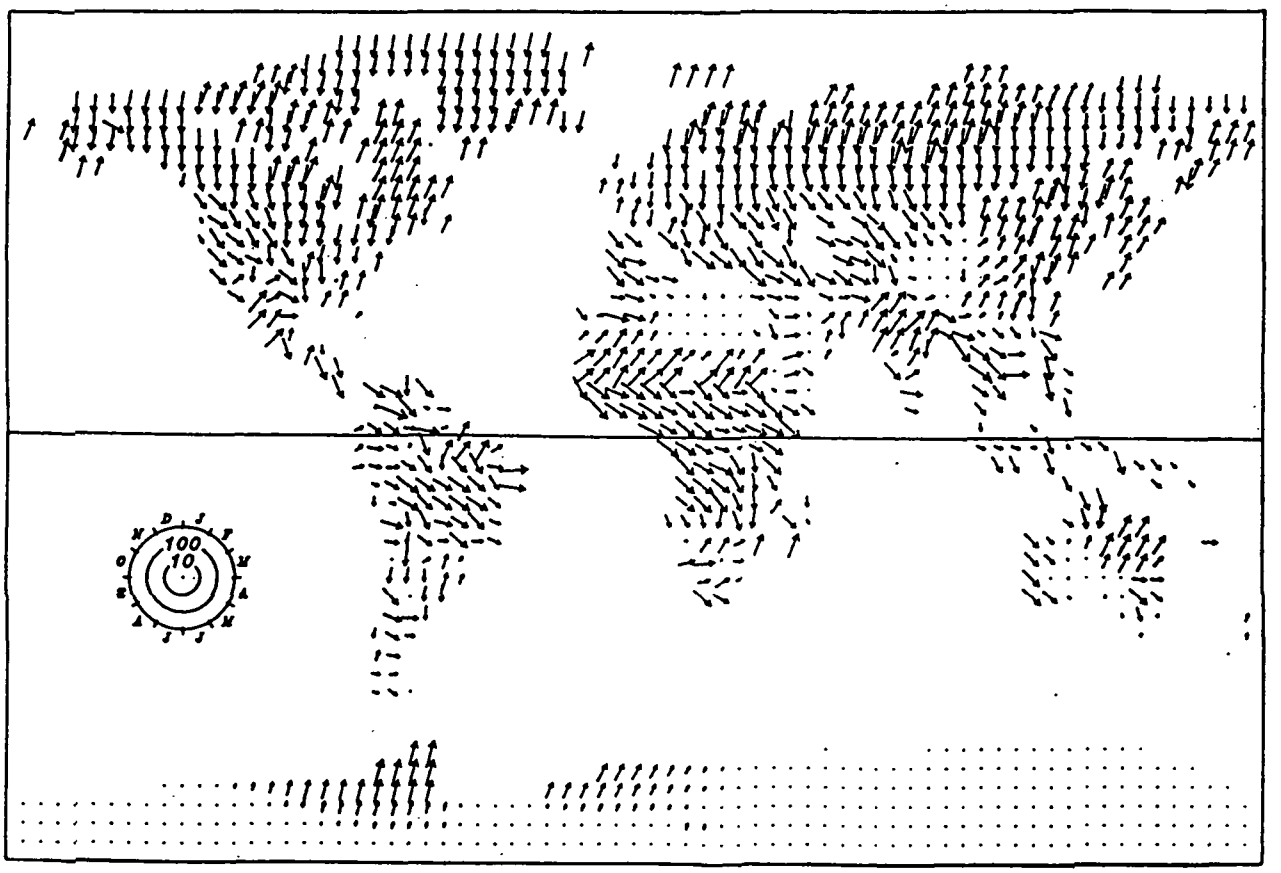

Fig. 4.D Second annual harmonic of monthly evapotranspiration (in mm.) The amplitude scale is the same as for the first harmonic.

seasonal temperature change, the evapotranspiration maximum occurs near the time of the soil moisture maximum, in August-September.

The phase of the second annual harmonic of the evapotranspiration is almost everywhere about the same as that of the soil moisture.

REFERENCES

Anderson, E. A., 1973: National Weather Service River Forecast System - Snow Accumulation and Ablation Model. Silver Spring, Maryland. NWS, USDOC (NOAA Tech. Memo. NWS HYDRO-17), 217 pp.

Mintz, Y. and Y. Serafini, 1984: Global Fields of Monthly Normal Soil Moisture, as Derived from Observed Precipitation and an Estimated Potential Evapotranspiration. Final Scientific Report under NASA Grant No. NAS5-26, Part V.

Pysklywec, D. W., K. S. Davar and and D. I. Bray, 1968: Snowmelt at an Index Plot. Water Resources Research, 4, pp 937-946.

Storr, D., 1978: A Comparison of Daily Snowmelt Calculated by the U.S. Corps of Engineers Theoretical Model with Measured Amounts on a Snowpillow. Ganges; British Columbia: Storm Water Resources Consulting Service.

Thornthwaite, C. W., 1948: An Approach Toward a Rational Classification of Climate. Geographical Review, 38, pp 55-94.

Thornthwaite, C. W. and J. R. Mather, 1955: The Water Balance. Publ. Climatol., 8, No. 1, 104 pp.

Willmott, C. J., J. R. Mather and C. M. Rowe, 1981: Average Monthly and Annual Surface Air Temperature and Precipitation Data for the World. Part 1: The Eastern Hemisphere. Part 2: The Western Hemisphere. Elmer, New Jersey: C. W. Thornthwaite Associates (Publications in Climatology, Vol. 34, Nos. 1 and 2).

Willmott, C. J., C. M. Row and W. D. Philpot, 1984: Small-scale Climate Maps: A Sensitivity Analysis of Some Common Assumptions Associated with Grid Point Interpolation and Contouring. Annals of the Association of American Geographers. (Submitted for publication.)

JSC Study Conference on the Physical Basis for Climate Prediction on Seasonal, Annual and Decadal Time Scales, Leningrad, 13-17 September 1982.

Influence of the Vegetation Structure on the Thermal Forcing of the Atmosphere

by

Yale Mintz

Department of Meteorology
University of Maryland, College Park, MD 20742

and

Laboratory for Atmospheric Sciences
NASA Goddard Space Flight Center, Greenbelt, MD 20771

ABSTRACT

It is shown that the vertical structure of the earth's vegetation cover has a strong influence on the transfers of latent and sensible heat to the atmosphere; and a strategy is proposed for incorporating vegetation into numerical general circulation models.

		page
I.	Influence of land-surface evapotranspiration on the atmosphere.	1
II.	Evapotranspiration from low (herbacious) vegetation versus evapotranspiration from tall (forest) vegetation.	2-6
III.	A strategy for incorporating vegetation into numerical general circulation models.	7-11

I. Influence of land-surface evapotranspiration on the atmosphere.

Many sensitivity experiments have been made, with numerical general circulation models, which show that the simulated precipitation, temperature and motion fields of the atmosphere are greatly influenced by the land-surface evapotranspiration. The review paper by Mintz (1982) describes and compares eleven such experiments.

These experiments show that not only does the available soil moisture and the surface albedo (which affects the energy used for evapotranspiration) influence the local precipitation; but that, by changing the ratio of the sensible heat transfer to the latent heat transfer to the atmosphere (changing the Bowen ratio, H/LE), large changes are produced in the circulation of the atmosphere. The reason for this is that the sensible heat transfer immediately and locally warms the atmospheric planetary boundary layer; whereas the latent heat transfer, LE, (whether it is realized immediately and locally, or, by transport of the water vapor, is realized at some later time and distant place), heats the free atmosphere, from the top of the boundary layer to the tropopause. It is this difference in the vertical distribution of the diabatic heating (as well the possible difference in the horizontal distribution of the realized heating) which makes the circulation sensitive to the Bowen ratio.

However, it is not only the soil moisture availability and the surface albedo which are important. Given the same soil moisture and albedo, the different kinds of vegetation structures can produce large differences in evapotranspiration and Bowen ratio.

II. Evapotranspiration from low (herbacious) vegetation versus evapotranspiration from tall (forest) vegetation.

• The general experience with measurements of evapotranspiration from a grass-cover and from other low-growing vegetation which is not under water stress is that the evapotranspiration depends almost entirely on the radiational energy absorbed by the surface. This finds expression, for example, in the widespread and growing practical use of the equation of Priestly and Taylor (1972),

$$E_{PT} = \frac{\alpha}{L} \frac{\Delta}{\Delta+\gamma} (R_N - G) \quad ,$$

where R_N is the net radiational heating of the surface, G is the heat flux into the soil, Δ is the gradient of saturation vapor pressure with temperature (which is a function of temperature), L is the latent heat coefficient, γ is the psychrometric constant, and $\alpha = 1.26$ is an empirical constant. (Averaged over 24 hours, G is much smaller than R_N and is usually neglected). An example of how well this works is given in Fig. 1 (from Davis and Davies, 1981).

Fig. 1

The reason why the Priestly-Taylor equation works so well, for this kind of surface, is that with low-growing vegetation which is not under water stress the aerodynamic resistance to the transfer of water vapor is as large as the biological (stomatal) resistance; and hence the vapor pressure gradient near the surface of plants has the same sign as the temperature gradient. It is this which makes the Bowen ratio a function of temperature only. (see Davies and Allen, 1973, Fig. 5).

A good field example, which shows that close to the surface of short vegetation the vapor pressure gradient has the same sign as the temperature gradient, is given in Fig. 2 (from Penman and Long, 1976). The arrows added to the figure show that the down-gradient transfers of water vapor and sensible

Fig. 2

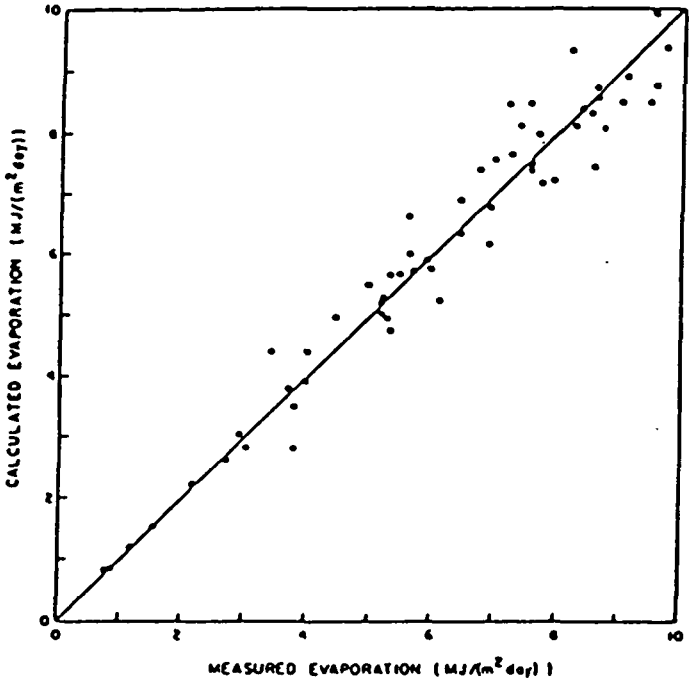

Fig. 1. Measured daily evapotranspiration from a grass-cover, compared with evapotranspiration calculated with the Priestley-Taylor equation. (Davis and Davies, 1981) (1 MJ m^{-2} day^{-1} = 0.4 mm/day evapotranspiration)

[The measured latent heat transfer and sensible heat transfer were obtained by the Bowen ratio/energy balance method, in which: 1) $H/LE \approx \Delta T/\Delta e$, and 2) $H + LE = (R_N + G)$, where ΔT was the measured temperature difference between 75 cm and 175 cm above the ground, Δe was the measured vapor pressure difference between 75 cm and 175 cm (obtained from the measured wet bulb temperatures), R_N was the measured net downward radiation flux at 100 cm above the ground, and G was the measured net conductive heat flux into the ground. The measurements were made at 15 minute intervals, and the Priestley-Taylor calculations were made at 30 minute intervals, and summed for the day between sunrise and sunset. (The Bowen ratio/energy balance results were also checked against, and gave good agreement with, lysimeter measurements.) The location was at Sunset Prarie, British Columbia (56°N); and the period was mid-May to late August in the wet summer of 1977. The surface was a grazed pasture of grasses and clover, covering the ground and freely transpiring. The measured volumetric soil moisture content of the root zone always exceeded 0.32, thus ensuring transpiration at the potential rate. The large range in evapotranspiration that we see in the figure was caused by variations in the cloud cover.]

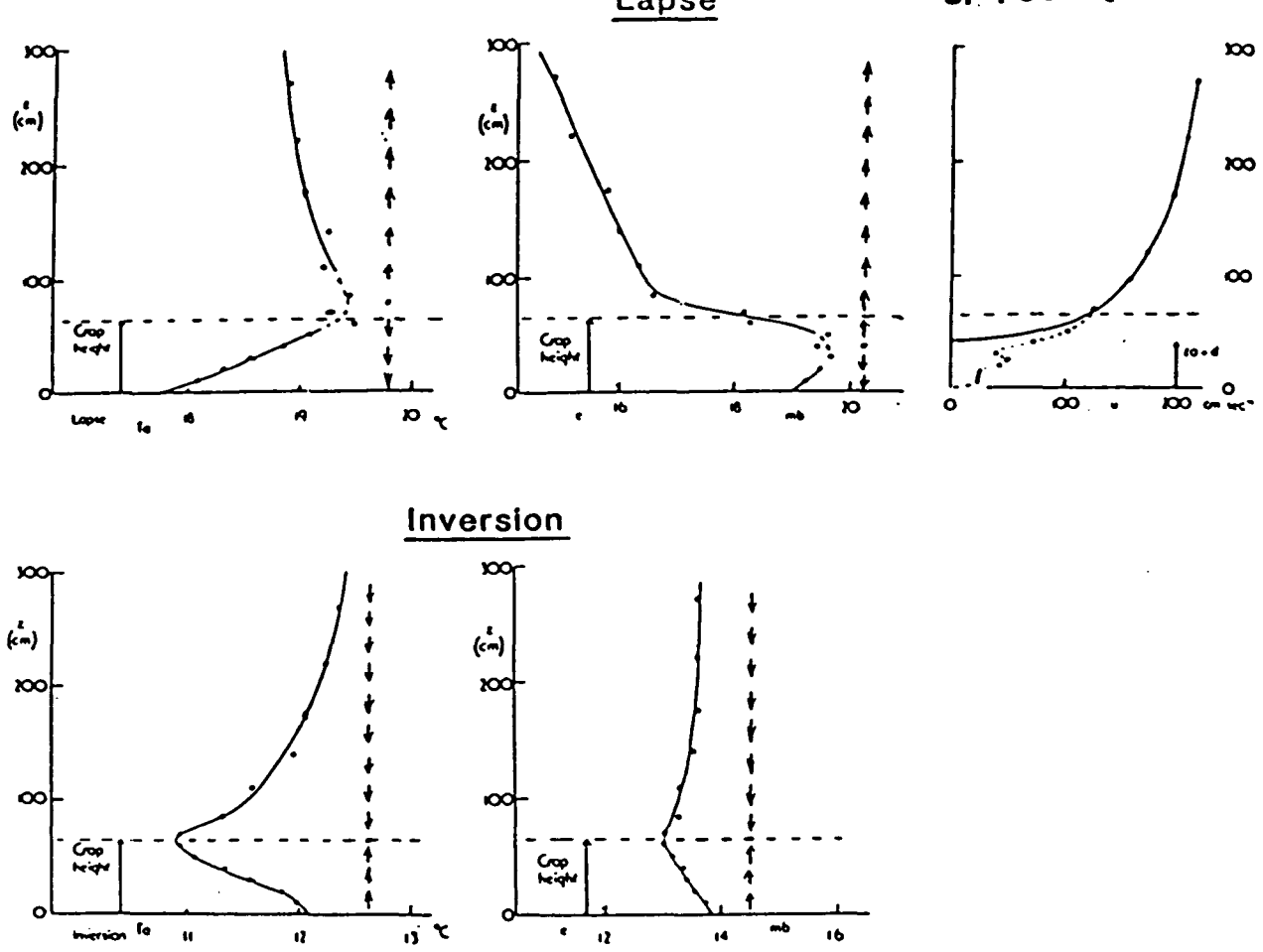

Fig. 2 Profiles of temperature, vapor pressure, and wind speed, above growing kale, during 20–24 July 1971. (Penman and Long, 1976)

Top: average of the hour in each of the five days which had the maximum temperature lapse rate between 85 cm and 270 cm.

Bottom: average of the hour in each of the five days which had the minimum temperature lapse rate (the maximum temperature inversion) between 85 cm and 270 cm.

[Measurements made with wet-bulb and dry-bulb resistance thermometers, and with hot-bulb anemometers, at the indicated elevations. Rothamstead Experimental Station, Harpenden, U.K.]

heat are in phase and, therefore, that the sensible heat transfer is not a source of energy for the evapotranspiration.

Furthermore, and of considerable importance for the modeling and simulation of evapotranspiration, is the fact that the wetting of the surface of a grass-cover, (which reduces the surface resistance to zero and shuts off the transpiration), has little or no effect on the evapotranspiration rate. The field
Fig. 3 evidence for this is shown in Fig. 3 (from McMillan and Burgy, 1960). It tells us that with a grass cover it is only the radiational heating, and not the state of the surface of the vegetation, which determines the evapotranspiration.

As a consequence, with this type of vegetation and moisture available in the root zone, one does not need to know whether the surface of the vegetation is wet or dry in order to calculate the evapotranspiration. Because the moisture storage capacity in the root zone is of the order of 150 mm, and evapotranspiration is of the order of a few mm/day, it follows that the GCM grid-area averaged rainfall (even if it is daily, weekly or monthly time-averaged) will suffice to calculate the evapotranspiration and soil moisture storage.

•• Tall (forest) vegetation behaves differently. The canopy has about the same total leaf area (three to five times the ground area) as lower vegetation; but it is spread over a layer which is several meters, not a few centimeters, thick; and it is in an elevated position. Both the large volume occupied by the leaves and its elevated position make for good ventilation; and, as a consequence (unlike the low vegetation, where the areodynamic resistance and the stomatal resistance have about the same magnitude), the aerodynamic resistance to the transfer of water vapor is one to two orders of magnitude smaller than
Fig. 4 the biological resistance. An example of this is shown in Fig. 4 (from Szeicz et al., 1969).

As a consequence of the small aerodynamic resistance, which affects the

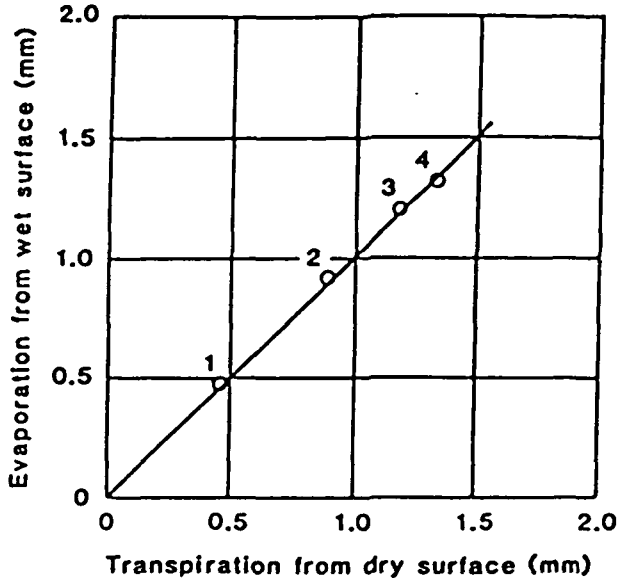

Fig. 3. Comparison of measured evapotranspiration, from growing rye-grass, when the surface of the grass is wet and when it is dry. Averages of cumulative amounts during 1, 2, 3 and 4 hours subsequent to mid-day wetting. (McMillan and Burgy, 1960)

[Measurements made with vigorously growing ryegrass in a pair of floating lysimeters. By sprinkling, the surface of the grass was alternately wetted on one of the lysimeters and not on the other. The numbered points show the averages for 25 runs, between 1 September and 31 January, at Davis, California.]

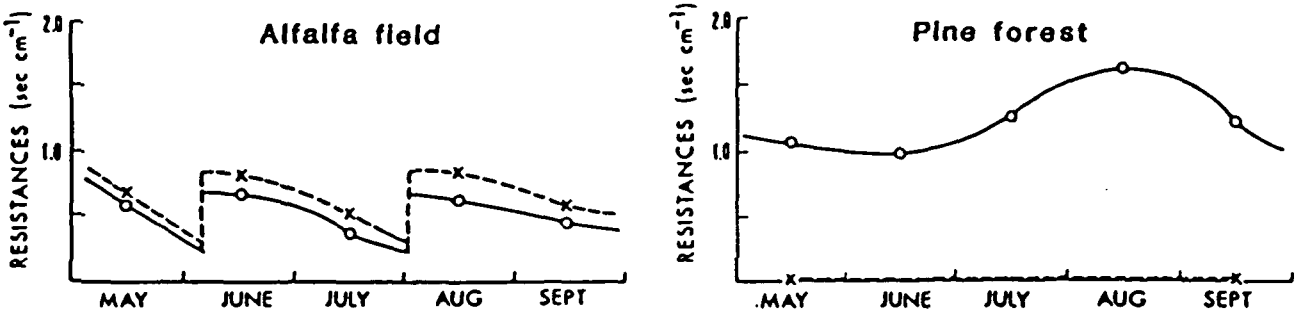

Fig. 4. Variation with time of the surface resistances (solid lines) and the aerodynamic resistances (dashed lines) to water vapor diffusion, for two types of vegetation. (Szeicz et al., 1969)

[The alfalfa (lucerne) grew to 60 cm in height, and was cut back to 10 cm on June 8 and August 5. The pine trees had a mean height of 27.2 m, and covered about 90% of the surface.]

[For the method of obtaining the aerodynamic and stomatal (surface) resistances, see Szeicz et al., 1969.]

sensible heat transfer as well as the water vapor transfer, with tall vegetation the radiational heating is not the only important source of energy for evapotranspiration. Depending on the wind speed and the vapor pressure deficit in the air, water vapor can be transferred from the vegetation to the air while at the same time sensible heat is transferred in the opposite direction (the temperature gradient and the vapor pressure gradient then having opposite signs), so that the Bowen ratio is negative. Moreover, unlike a grass cover, where the rates are the same, the rate of evaporation from a wet forest canopy can be several times larger than the rate of transpiration of water removed from the root zone.

Fig. 5 A good example of this is shown in Fig. 5 (from Shuttleworth and Calder, 1979), where the evapotranspiration measured with a "natural" lysimeter in the Severn forest in Plynlimon, Wales, U.K., is compared with the evapotranspiration calculated with the Priestly-Taylor equation. The measurements and the calculations were done separately for the times when the surfaces of the trees were wet (upper left panel) and for when they were dry (upper right panel).

We see that when the surface of the forest canopy was wet the measured water loss, E_M, was about eight times larger than the Priestly-Taylor calculation, E_{PT}.

On the other hand, when the surface was dry E_M was about 40% smaller than E_{PT}. This is because of the large biological resistance to transpiration of spruce trees, and not because of soil moisture stress. (Even for the summer of 1976, which was the driest period on record, and when the soil moisture in the forest as measured by neutron probe was 200 mm below field capacity (Calder, 1978), the curve in the upper right panel has the same slope as at other times.)

The bottom panel of Fig. 5 shows that the total measured evapotranspiration from the forest is about 1.4 times larger than the Priestly-Taylor calculation. In the mid-winter months, the ratio of E_M to E_{PT} is more than 10 to 1. It is obvious that the forest removes large amounts of sensible heat from the air and

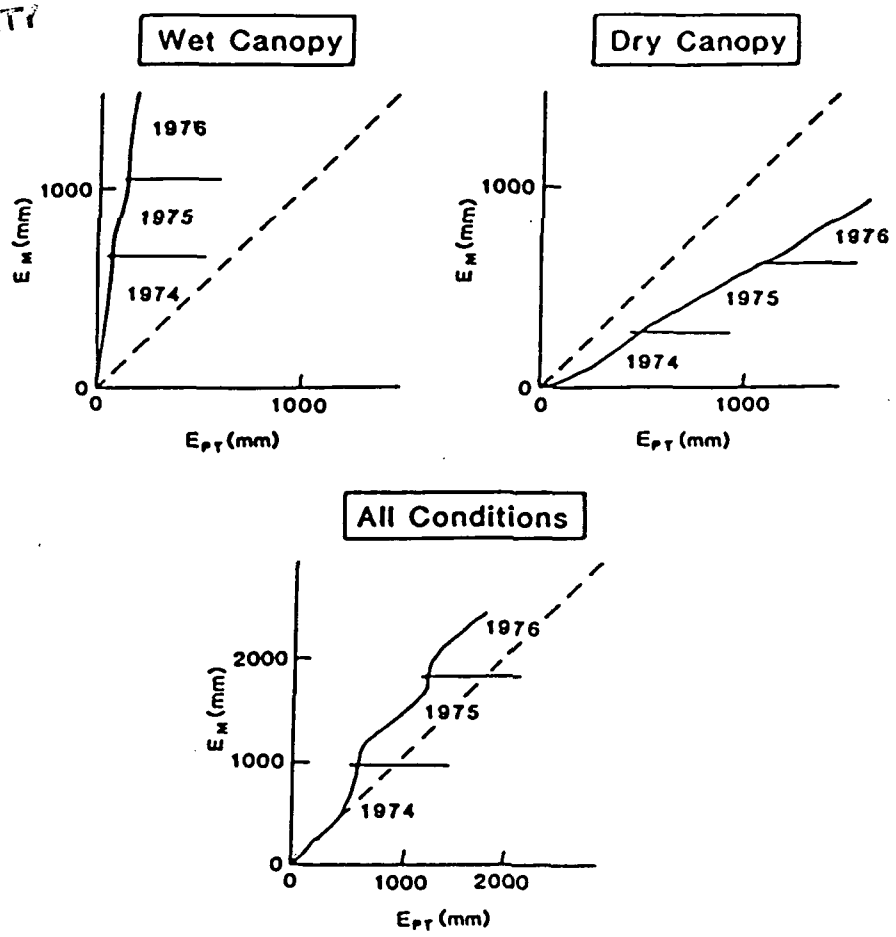

Fig. 5 Comparisons between cumulative evapotranspiration in the Severn forest as measured with a "natural" lysimeter, E_M, and as calculated with the Priestly-Taylor formula, E_{PT}. (Shuttleworth and Calder, 1979)

[The "natural" lysimeter consisted of 26 spruce trees about 10 m in height, growing in a peat soil over an impervious layer of clay, which were cut off from lateral water exchange with the rest of the forest by a dug-in wall of corrugated iron sheets grouted into the clay. E_T was obtained by measuring the rainfall beneath the canopy (measuring the throughfall and stemflow), subtracting the water draining from the peat soil plus the surface runoff at the downslope end of the pen, and subtracting the water stored in (or removed from) the soil as measured with a neutron probe. E_I was obtained by measuring the rainfall above the canopy and subtracting the measured rainfall beneath the canopy. $E_M = E_T + E_I$.

[For calculating E_{PT}, R_N was obtained in the early part of the experiment from the measured net radiation over a small grassland clearing, 400 m from the lysimeter, multiplied by 1.1. In the latter part of the experiment, R_N was measured above the forest canopy. The soil heat flux, G, was assumed to be negligible. The calculation of E_{PT} was carried out, on an hourly basis, for only the daylight hours (net radiation positive), as this reduces the difference with the measured evapotranspiration. If the night-time hours were to be included, E_{PT} would be diminished by 10 to 15%, which would increase the difference with the measured evapotranspiration.

[For the separate accumulations shown in the two upper panels, the determinations of the wet and dry canopy periods were made according to whether or not there was rainfall in the preceding 3 hours.]

uses that energy for evapotranspiration.

Shuttleworth and Calder (1979, p. 642) remark that ". . . meteorologists unfamiliar with forest micrometeorology . . . might be surprised by the . . . observation of sensible heat [transfer] to a wet forest. The conventional attitude, that evaporation is largely a radiation-controlled process, is of course easily justified for short vegetation from more fundamental descriptions such as those provided by Monteith (1965) or Shuttleworth (1976, 1978). At the same time and on the same basis, it is also fairly easy to understand why evaporation from tall vegetation, with large atmospheric exchange coefficients, is more intimately related to the atmospheric vapor pressure deficit (e.g., Stewart and Thom, 1973; Thom and Oliver, 1977). Indeed, for basic theoretical reasons, the simple experimental observation of a finite atmospheric humidity deficit near the surface of forest vegetation in wet canopy conditions very often implies the presence of sensible heat (transfer), since the incident radiation is often low at such times."

••• A good field example, which compares evapotranspiration from a forest with evapotranspiration from a grass-cover, under the same climatic conditions, is given in Fig. 6. This shows the water budgets, averaged over eight years (1968-1975), for the Severn catchment and for the adjacent Wye catchment in Plynlimon, Wales (Calder and Newson, 1979). The Severn catchment $(2.9\ km)^2$ has a mixed coniferous forest over two-thirds of its area. The Wye catchment $(3.2\ km)^2$ is completely grass covered. Averaged over the eight year period, the measured precipitation rates were, respectively, 6.1 and 6.4 mm/day (a difference of only 0.3 mm/day, or 5%). Subtracting the respective measured runoffs of 3.7 and 5.3 mm/day, gives us an evapotranspiration of 2.4 mm/day from the forest catchment and 1.1 mm/day from the grass-covered catchment (a difference of 1.3 mm/day, which is more than a factor of 2). If we assume that the ratio of E_I to E_T in the Severn catchment, for the eight year period (1968-1975), was

Fig. 6

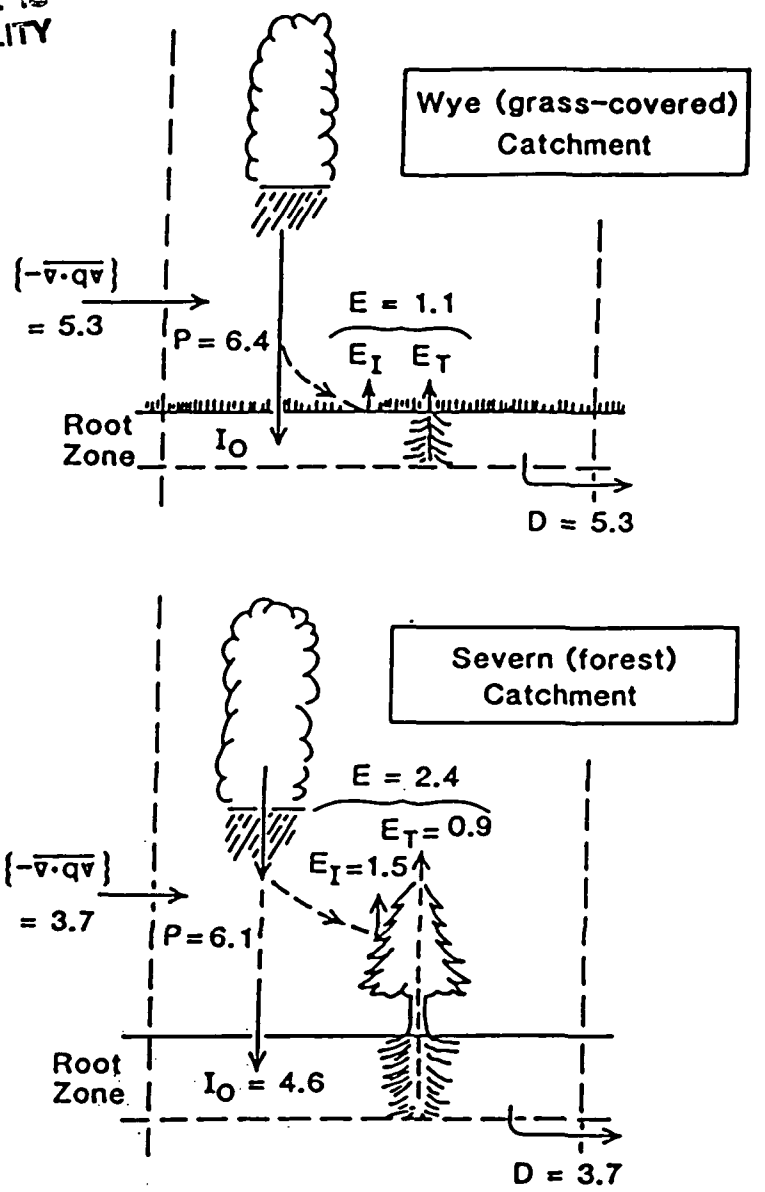

Fig. 6. Comparison of the water budgets in the Severn (forest) catchment and the Wye (grass-covered) catchment, Plynlimon, Wales, U.K. (Calden and Newson, 1979).

(For definitions of symbols, see legend to Fig. 7.)

the same as the ratio of the measured interception loss, 1580 mm (1.63 mm/day), to the measured transpiration loss, 901 mm (0.93 mm/day), as given by the "natural" lysimeter in the Severn forest for the three years (1974-1976), we obtain the values of E_I and E_T that are shown in Fig. 6.

In the Wye (grass-covered) catchment, 17% of the precipitation is returned to the air by evapotranspiration. In the Severn forest catchment, 40% is returned. Of this, 62% is given to the air by evaporation of intercepted precipitation and 38% by transpiration of water taken from the root zone of the soil.

[As we expect for neighboring regions of such small size, the one with the smaller evapotranspiration has the larger atmospheric water vapor transport convergence. As discussed in Attachment A (Mintz, 1982, pp. 4-5), it is only in large regions that a reduction in evapotranspiration diminishes precipitation.]

Fig. 7 •••• Figure 7 compares the water and energy budgets of a forested and a grass-covered region, when the atmospheric forcing parameters of precipitation and radiational heating are like the average conditions in England and Europe.

Here the mean annual precipitation is taken as 2.5 mm/day (Jaeger, 1976, Fig. 21) and the net radiational heating of the surface as 50 watt/m^2 (Budyko, 1963, Plate 14). The ratio of E_I to P is taken as 0.40, which is an average value for the English forests (Calder and Newson, 1979, Fig. 1). The Bowen ratio for the grass-cover is taken as 0.25.

The two regimes shown in Fig. 7 differ not only in that the evapotranspiration from the forest is greater than from the grass-cover, but that the grass-cover adds sensible heat to the boundary layer of the atmosphere, whereas the forest removes sensible heat from the boundary layer. In effect, the forest cools the boundary layer of the atmosphere and (either at the same location and at the same time, or in some distant place at a later time) uses that energy to warm the free atmosphere. Because of this, the vertical structure of the vegetation can have a large influence on the atmospheric circulation.

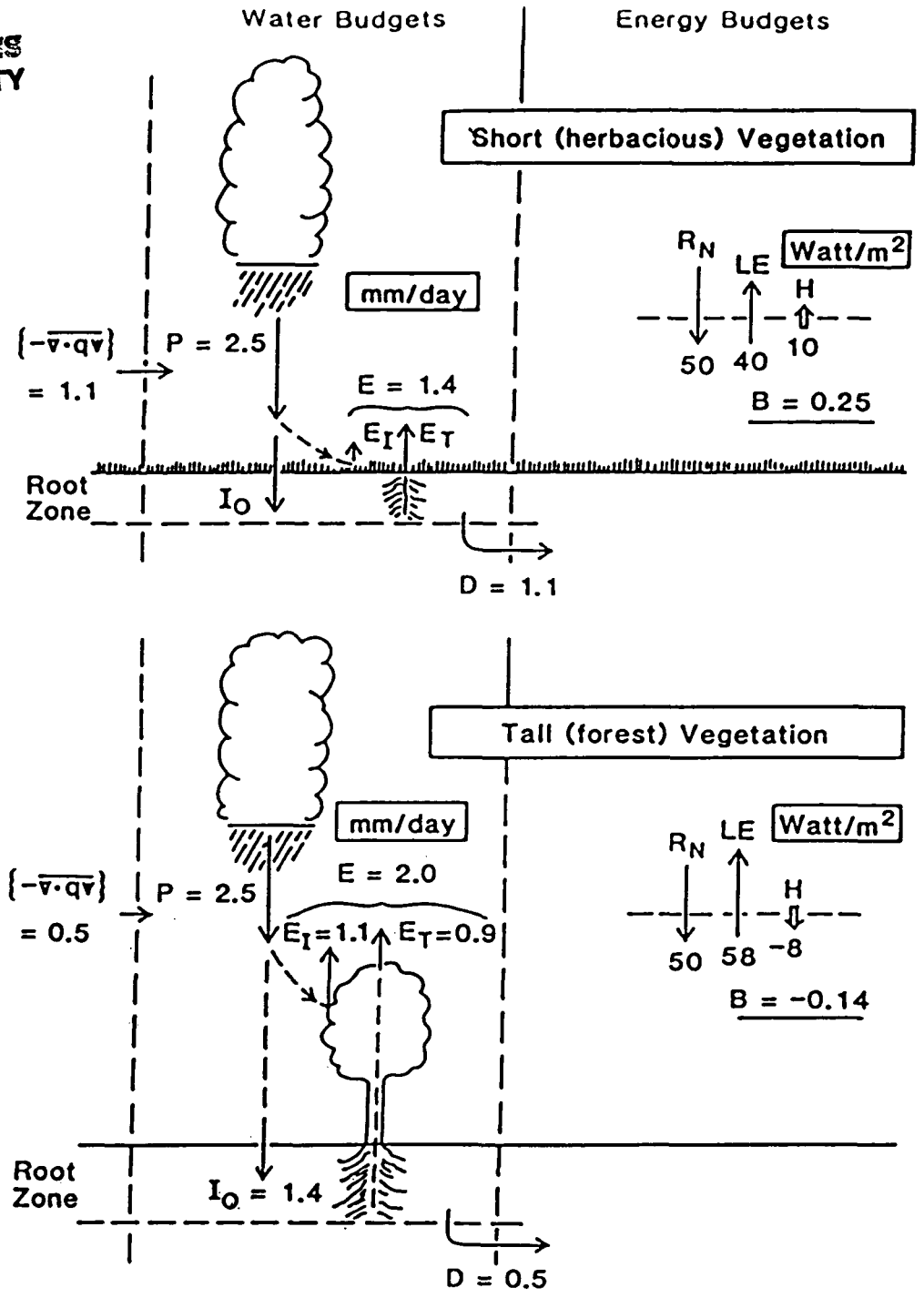

Fig. 7. Comparisons of water and energy budgets of short (herbacious) vegetation and tall (forest) vegetation.

P: precipitation.

I_O: surface infiltration.

D: runoff.

$(-\overline{\nabla \cdot q \psi})$: atmospheric water vapor transport convergence.

E_I: evaporation of intercepted water.

$E = (E_I + E_T)$: evapotranspiration.

R_N: net radiational heating of surface.

LE: latent heat transfer to atmosphere.

H: sensible heat transfer to atmosphere.

$B = (H/LE)$: Bowen ratio.

E_T: transpiration.

III. A strategy for incorporating vegetation into numerical general circulation models.

A practical strategy for incorporating the different kinds of vegetation into numerical general circulation models is to separate the vegetation properties which change on a time scale of the order of a year and less, such as leaf area density, albedo, stomatal resistance and root structure (of herbacious vegetation), i.e., the phenological changes (those which depend on the seasonal changes in climate), from those properties which change on a time scale of the order of 10^1 years and more, such as the gross vertical structure (the morphology) of the vegetation, and the vegetation and climate influenced properties of the soil.

If this separation is made, then, when the general circulation model is used for simulations and predictions of climate (the time-averaged weather) on the time scales of a season or a year, only the phenologically changing vegetation properties will need to be modeled as interactive components of the system. The gross vertical structure of the vegetation (and the soil properties) can then be prescribed.

It is only when we shall make integrations over the order of 10^1 or 10^2 years or more (as we can now do with models that have a high degree of space truncation), that we will need to specify the physical-physiological laws which govern the slowly changing vegetation structure and soil properties. Within the biological-ecological sciences there already exists the background knowledge that we need to model the interactive properties of the vegetation on these two different time scales; and, indeed, a good deal of vegetation modeling, especially phenological modeling, has already been done. (See, for example, Leith, ed., 1974).

For the modeling of the momentum, heat and water transfers between the

atmosphere, vegetation and soil, there are many studies to draw upon, in particular: Cowan (1965), Waggoner et al. (1969), Vowinckel and Orvig (1972), Shuttleworth (1976, 1978), Goudrian (1977), Hillel (1977), Federer (1979) and Sellers (1981).

. . . . . .

In order to calculate the interception storage and the evaporation of the intercepted water, it will be necessary to modify the precipitation output of the existing general circulation models. This follows from the relative magnitudes of the different water storage and water transfer terms in the vegetation-soil system.

Fig. 8 As shown, schematically, in Fig. 8 (from Rutter, 1975), the available water storage capacities on the surface of the plants, within the plants and within the plant root zone of the soil, are of the order of 1, 10 and 100 mm, respectively. But, although the interception storage capacity on the plant surface is two orders of magnitude smaller than the soil storage capacity, the interception loss by evaporation is comparable in magnitude to the transpiration of water taken from the root zone of the soil. It follows, therefore, that to calculate the interception storage and interception loss (which must be done with tall vegetation), the precipitation rate must be known at about half-hourly to hourly intervals.

The existing general circulation models calculate precipitation about every half hour; but it is precipitation averaged over the model grid-area, which is of the order of $(100\ km)^2$ to $(400\ km)^2$. This area-averaging so reduces the precipitation intensity that, if intercepted by vegetation, none of it may get through to the soil. It will therefore be necessary either to parameterize the half-hourly grid-point precipitation, such that a time-average of the grid-point precipitation will equal the time-average of the calculated

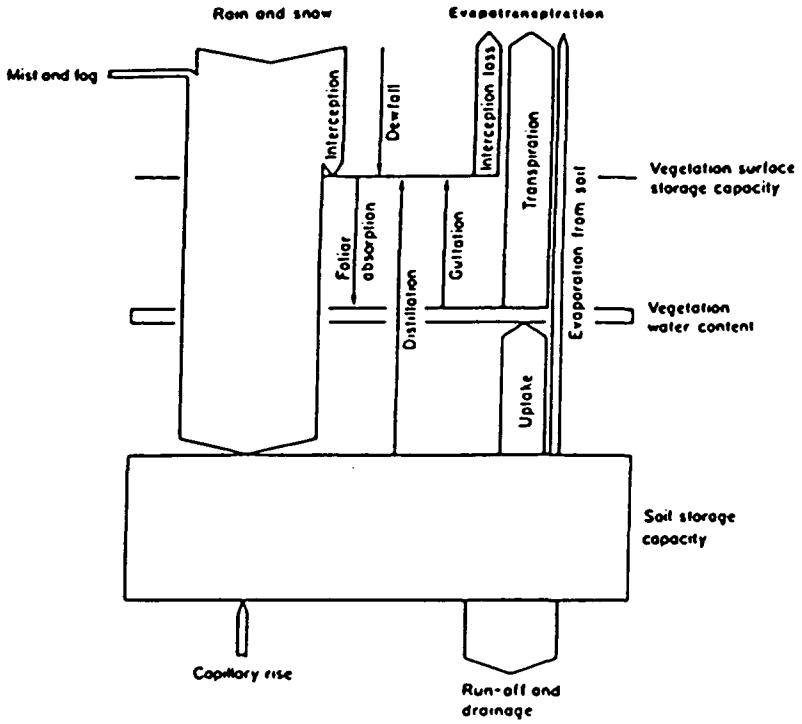

Fig. 8. Water budget of the vegetation-soil system. Components approximately to scale for rainfall of 1000 mm/year (2.8 mm/day) and evapotranspiration of 500 mm/year (1.4 mm/day). (From Rutter, 1975)

grid-area precipitation; or else to subdivide the half-hourly calculated grid-area averaged precipitation into a number of representative subdivisions of the grid-area, with each subdivision having its own water and energy budget calculation. In the former case the time-spectrum of the precipitation, and, in the latter case, the space-spectrum of the precipitation will need to be related to the parameters which control the convective part of the precipitation in the general circulation model.

References

Budyko, M. I. (editor), 1963: Atlas of the Heat Balance of the Earth. With N. A. Efimova: Maps of the radiation balance for the continents. Plates 14-26.

Calder, I. R., 1976: The Measurement of Water Losses from a Forested Area Using a "Natural" Lysimeter. J. Hydrol., 30, pp. 311-325.

Calder, I. R., 1978: Transpiration Observations from a Spruce Forest and Comparisons with Predictions from an Evaporation Model. J. Hydrol., 38, pp. 33-47.

Calder, I. R. and M. D. Newson, 1979: Land Use and Upland Water Resources in Britain - A Strategic Look. Water Resources Bulletin, American Water Resources Assoc., 15, pp. 1628-1639.

Cowan, I. R., 1965: Transport of Water in the Soil-Plant-Atmosphere System. J. Appl. Ecol., 2, pp. 221-239.

Davies, J. A., and C. D. Allen, 1973: Equilibrium, Potential and Actual Evaporation from Cropped Surfaces in Southern Ontario. J. Appl. Meteor., 12, 649-657.

Davis, R. L., and J. A. Davies, 1981: Potential Evaporation in the Place River Region of British Columbia. Atmosphere-Ocean, 19, pp. 251-260.

Federer, C. A., 1979: A Soil-Plant-Atmosphere Model for Transpiration and Availability of Soil Water. Water Resources Res., 15, pp. 555-562.

Goudriaan, J., 1977: Crop Micrometeorology: A Simulation Study. Wageningen Center for Agricultural Publishing and Documentation. Wageningen, The Netherlands. pp.

Hillel, D., 1977: Computer Simulation of Soil Water Dynamics. International Development Research Centre, Ottawa. pp.

Jaeger, L., 1976: Monatskarten des Niederschlags fur die Ganze Erde. Berichte des Deutchen Wetterdienstes, Nr. 139, (Band 18). Offenbach a.M., 38 pp. and plates.

Leith, H. (ed.), 1974: Phenology and Seasonality Modeling. Springer-Verlag, N. Y./Heidelberg/Berlin. 444 pp.

McMillan, W. D. and R. H. Burgy, 1960: Interception Loss from Grass. Jour. Geophys. Res., 65, pp. 2389-2398.

Mintz, Y., 1982: The Sensitivity of Numerically Simulated Climates to Land-Surface Conditions. (Presentation at JSC Study Conference on Land-Surface Processes in Atmospheric General Circulation Models, Greenbelt, USA, 5-10 January 1981). (Submitted for publication). 55 pp. plus 26 figures.

Moneith, J. L., 1965: Evaporation and Environment. Symp. Soc. Exp. Biol., 19, pp. 205-235.

Penman, H. L. and I. F. Long, 1976: Profiles and Evaporation. Quart. Jour. Roy. Met. Soc., 102, pp. 841-855.

Priestley, C. H. B. and R. J. Taylor, 1972: On the Assessment of Surface Heat Flux and Evaporation Using Large Scale Parameters. Mon. Wea. Rev., 100, pp. 81-92.

Rutter, A. J., 1975: The Hydrological Cycle in Vegetation. In Vegetation and the Atmosphere, Vol. 1. (ed. J. Monteith). Academic Press, London/ New York/San Francisco. pp. 111-154.

Sellers, P. J., 1981: Vegetation Type and Catchment Water Balance: A Simulation Study. Ph.D. Thesis, University of Leeds, Leeds, U.K 836 pp.

Shuttleworth, W. J., 1976: A One-Dimensional Theoretical Description of the Vegetation-Atmosphere Interaction. Bound. Layer Meteor., 10, pp. 273-302.

Shuttleworth, W. J., 1978: A Simplified One-Dimensional Description of the Vegetation-Atmosphere Interaction. Bound. Layer Meteor., 14, pp. 3-27.

Shuttleworth, W. J. and I. R. Calder, 1979: Has the Priestley-Taylor Equation Any Relevance to Forest Evaporation? J. Appl. Meteor., 18, pp. 639-646.

Stewart, J. B., and A. S. Thom, 1973: Energy Budgets in a Pine Forest. Quart. J. Roy. Met. Soc., 99, pp. 154-170.

Szeicz, G., G. Endrodi and S. Tajchman, 1969: Aerodynamic and Surface Factors in Evaporation. Water Resources Res., 5, pp. 380-394.

Thom, A. S., and H. R. Oliver, 1977: On Penman's Equation for Estimating Regional Evaporation. Quart. J. Roy. Met. Soc., 101, pp. 93-105.

Vowinckel, E. and S. Orvig, 1972: EBBA: An Energy Budget Programme. Publs. in Meteorology, No. 105, McGill University, Montreal. 50 pp.

Waggoner, P. E., G. M. Furnival and W. E. Reifsnyder, 1969: Simulation of the Microclimate in a Forest. Forest Sci., 15, pp. 37-45.

NASA

Technical Memorandum 84973

On the Design of an Interactive Biosphere for the GLAS General Circulation Model

Yale Mintz, Piers J. Sellers and Cort J. Willmott

January 1983

Laboratory for Atmospheric Sciences
Modeling and Simulation Facility

National Aeronautics and
Space Administration

Goddard Space Flight Center
Greenbelt, Maryland 20771

ON THE DESIGN OF AN INTERACTIVE BIOSPHERE FOR THE GLAS GENERAL CIRCULATION MODEL

by

Y. Mintz

Dept. Meteor., Univ. Maryland, College Park MD 20742, and
Lab. Atm. Sci., Code 911, NASA/Goddard Space Flight Center,
Greenbelt, MD 20771

P. J. Sellers

Resident Research Associate, National Research Council and
Hydrological Sciences Branch, Code 924,
NASA/Goddard Space Flight Center, Greenbelt, MD 20771

and

C. J. Willmott

Dept. Geography, Univ. Delaware, Newark, DE 19771.

January 1983

Abstract

The purpose of adding an interactive biosphere to the GLAS general circulation model is to make the calculation of land-surface evapotranspiration and sensible heat flux more realistic and, therefore, more accurate. This is important because sensitivity experiments with general circulation models have shown that the large scale fields of rainfall, temperature and motion of the atmosphere are highly sensitive to the transfers of latent and sensible heat at the land surface.

Water and energy transfers at the land surface depend on vegetation morphology and physiology. In the proposed model biosphere, the vegetation morphology will control these transfers through the leaf area density as a function of height, $L_D(Z)$, and through the root length density as a function of depth, $RT_D(Z)$, as expressed in a discretized form for each of the model grid areas. $L_D(Z)$ will influence (a) the aerodynamic resistance to the latent and sensible heat transfers; (b) the transmission, absorption and emission of radiation energy by the canopy and underlying ground; and (c) the interception, evaporation and throughfall of rain and snow. The vegetation physiology will control the transfers of water and energy through the stomatal resistance, the xylem resistance of the stems, and the root cortex resistance. The stomatal resistance will be a function of the leaf water potential, short-wave radiation intensity, leaf temperature, and humidity of the air.

In the initial formulation, $L_D(Z)$ and $RT_D(Z)$ will be prescribed as functions of latitude and longitude and the season of the year, as known from ecological observations in the various vegetation formations. Later, the phenological changes of $L_D(Z)$ and $RT_D(Z)$ in the deciduous forests and grasslands will be made interactive with the atmospheric variables and the soil moisture as calculated by the GCM. Finally, the vegetation formations themselves will be made interactive with the atmospheric and soil moisture conditions.

The realism of the model biosphere will be evaluated (1) through short period one-dimensional comparisons with measured values of the local atmospheric forcing and measured values of the vertical fluxes of water and energy; (2) through long period comparisons of simulated and observed catchment water budgets; and (3) through comparisons of the simulated and observed surface temperatures, surface albedos, snow cover, live biomass, and the water balances of the large river basins, when the model biosphere is forced with atmospheric variables taken from the FGGE level 3-B and 2-C data sets.

Table of Contents

	Page
Introduction: The need for an interactive biosphere in general circulation models.	3
A. Goals of the proposed research.	11
B. Overview of the proposed biosphere.	13
1. Governing equations for	
i. Transpiration and water uptake by roots.	13
ii. Rainfall interception and interception loss.	22
iii. Snowfall interception and disposal.	25
iv. Water and heat budget of the soil.	26
2. The multilayer vegetation model.	
i. Definition and advantages of a multilayer model.	28
ii. Distribution of the observed vegetation formations.	31
iii. Specification of the multilayer model.	35
3. Comparisons of the model performance with observations:	
i. Field measurements.	44
ii. Water balances in catchments.	44
iii. Specification of the multilayer model.	45
4. Numerical simulation of the vegetation formations.	47
C. Notation.	51
D. References.	55

Introduction: The need for an Interactive Biosphere in General Circulation Models.

Importance of Evapotranspiration.

The sensitivity of weather and climate to land-surface evapotranspiration is difficult to determine from observations, but has been revealed in experiments with numerical general circulation models. (See Shukla and Mintz, 1982; and the paper by Mintz, 1982, in which eleven such experiments are reviewed.) In each experiment two calculations were made, which started from the same initial atmospheric state and had the same sea surface temperatures and sea-ice extent, but with land-surface conditions that produced different evapotranspirations. In every case the result was a large difference in the calculated precipitation, temperature and motion field of the atmosphere.

A decrease in latent heat transfer from the land to the atmosphere is approximately balanced by an increase in the sensible heat transfer. The sensible heat transfer, however, warms the air within the relatively shallow planetary boundary layer, and it does so locally in space and time. The latent transfer, by contrast -- if realized as heating through the convective condensation process -- warms the air in the free atmosphere up to the tropopause level. Moreover, because of water vapor advection, the realization of the heating may be at some distant place and a later time. It is the difference in the vertical distribution of the two kinds of heating, as well as the possible shift in their horizontal distributions, which makes the general circulation (the thermally-forced large scale atmospheric circulation) sensitive to land-surface evapotranspiration.

Importance of Vegetation.

Because numerical weather predictions and predictions of climate anomalies with general circulation models will be sensitive to the land-surface evapotranspiration, great care must be used in the way in which the evapotranspiration is calculated.

In almost all existing general circulation models (see the review by Carson, 1982), an "open bucket" formulation is used to calculate the transfer of water vapor from the land to the atmosphere. The level of the water in the bucket is lowered when evaporation is larger than precipitation; and the level is raised when precipitation is larger, up to the point at which the bucket overflows and produces "runoff". Over some broad range in the level of the water in the bucket (which varies somewhat from model to model), the rate of evaporation is taken as equal to (or nearly equal to) the evaporation from a free water surface; and only when the water level is low is the evaporation rate made less than that from a free water surface. But this is hardly the way in which water vapor is transferred from the land to the atmosphere in the real world.

A more realistic representation of how water is exchanged between the land and atmosphere is shown in Fig. 1 (from Rutter, 1975). Here the atmosphere is insulated from the water in the soil by a vegetation layer; and the largest part of the water transfer to the atmosphere is the transpiration of water which the roots of the plants take up from the soil. Another large part of the precipitation (and under some vegetation and precipitation conditions the largest part) never enters the soil at all, but is intercepted by and stored on the surface of the plants and from there evaporated into the air. The third transfer process, the

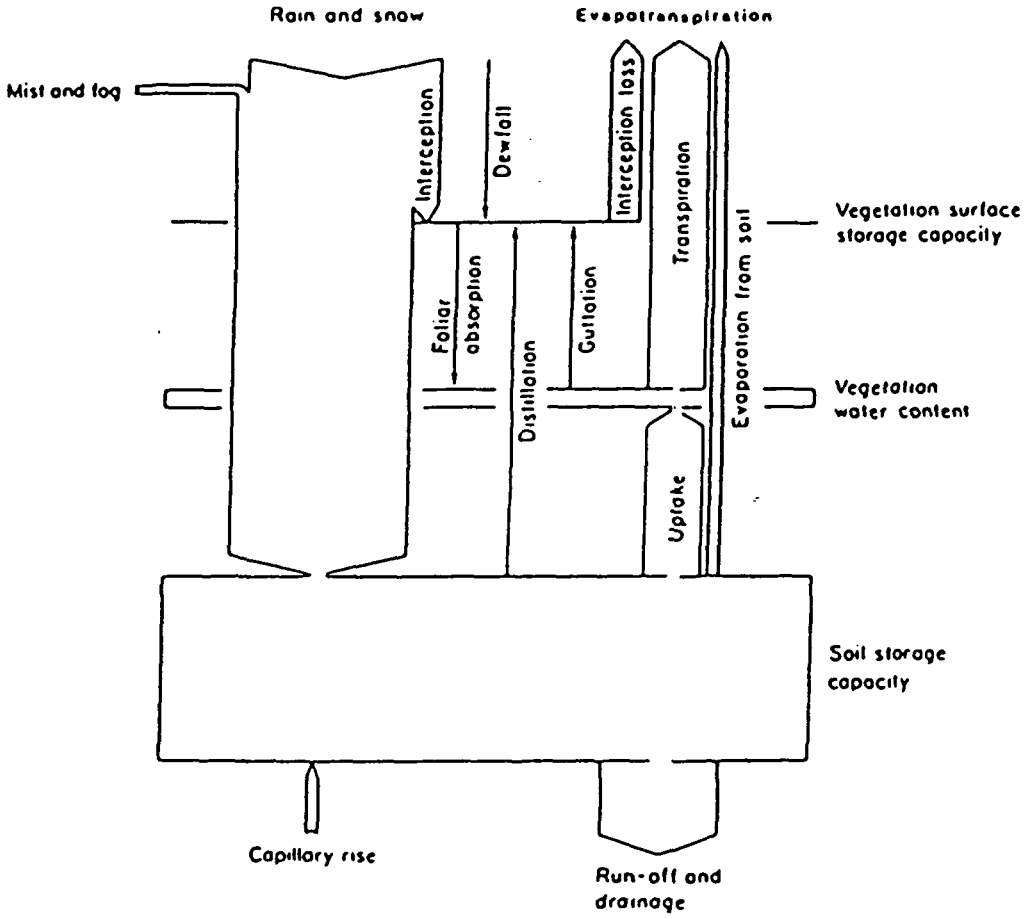

Fig. 1 Water transfers and water stores in the vegetation-soil system (after Rutter, 1975).

evaporation of water from the pores of the soil, is generally much smaller than the other two transfers.

The water storage capacities on the surface of the plants, within the plants and within the plant root zone of the soil, are of the order of 1, 10 and 100 mm, respectively. Inasmuch as both the interception loss and the transpiration are of the order of a few mm per day, the characteristic recycling time for the intercepted water is of the order of a few hours, and for the soil moisture store it is of the order of a month.

The 100 mm of water which the vegetation can remove from the soil is only a small fraction of the total water in the ground. Similarly, of the total of about 30 mm of water vapor held in an atmospheric column, only about 3 mm, out of about the 10 mm in the planetary boundary layer, can be removed from the atmosphere by the convective precipitation process. (Reducing the relative humidity in the PBL by more than about 30% shuts off the convection.) Thus, if not renewed, water vapor in the atmosphere can provide only about 1 day's worth of space-averaged convective precipitation. Soil moisture, however, even when not renewed, can maintain the average rate of evapotranspiration for about a month. It is this which makes the soil moisture store more important than the atmospheric water vapor store for numerical weather predictions and predictions of monthly and seasonal anomalies of climate.

Vegetation exerts physiological and morphological controls over evapotranspiration. Because transpiration is associated with photosynthesis, it is usually confined to the daylight hours; unlike the open bucket formulation, which can produce appreciable evaporation at night. Moreover, when water is available, the rate of the bucket evaporation is limited only

by the atmospheric factors of radiation, wind speed and air humidity; and the daytime rate, especially in semi-arid regions, can be very large. But with plants there is also a daytime limit to the transpiration rate, because there is a constraint on the rate at which water can flow through the plants.

The morphology (the vertical structure) of the vegetation has a large influence on the rate of interception loss. With tall (forest) vegetation, the elevated and dispersed surfaces of the leaves are more strongly ventilated than are the surfaces of the leaves in short (herbacious) vegetation. When the leaf surfaces are wet, therefore, the interception loss from tall vegetation is much greater than that from short vegetation. But when the leaf surfaces are dry, the greater ventilation of tall vegetation is generally compensated by its larger stomatal resistance; so that (under the same atmospheric conditions) the transpiration losses for tall and short vegetation are not very different.

The interception loss rate from short vegetation is not much larger than its transpiration rate; but with tall vegetation, the interception loss rate can be 5 to 10 times larger than the transpiration rate. Even though the vegetation surface storage capacity is small, the time-integrated interception loss from tall vegetation can be very large.

Fig. 2 is an example of the mean annual water and energy balances of short and tall vegetation, as derived from measurements in two adjacent catchments which have nearly the same atmospheric conditions. The total evapotranspiration loss from the forest catchment is more than twice as large as that from the grass-covered catchment. With the grass-cover, 58% of the net radiational heating of the surface is used for evapotranspiration, and 42% for the sensible heating of the atmospheric boundary layer. But

with the forest cover, the energy used for evapotranspiration exceeds the radiational heating by 15%, and this results in a removal of sensible heat from the boundary layer (there is a negative Bowen ratio, -0.13). In the forest case it was possible to measure the two components of the evapotranspiration separately, and the interception loss was 1.7 times larger than the transpiration. Although the atmospheric conditions are about the same for the two catchments, the net radiational heating, R_N, is about 10% larger with the forest-cover than with the grass-cover. This is not only because the forest is darker and absorbs more of the incident solar radiation, but also because, as a consequence of the larger evapotranspiration rate, the surface temperature of the forest is lower and emits less infrared radiation. It is clear, from numerous examples of this kind, that vegetation exerts a large control over the water and energy exchange between the land-surface and the atmosphere.

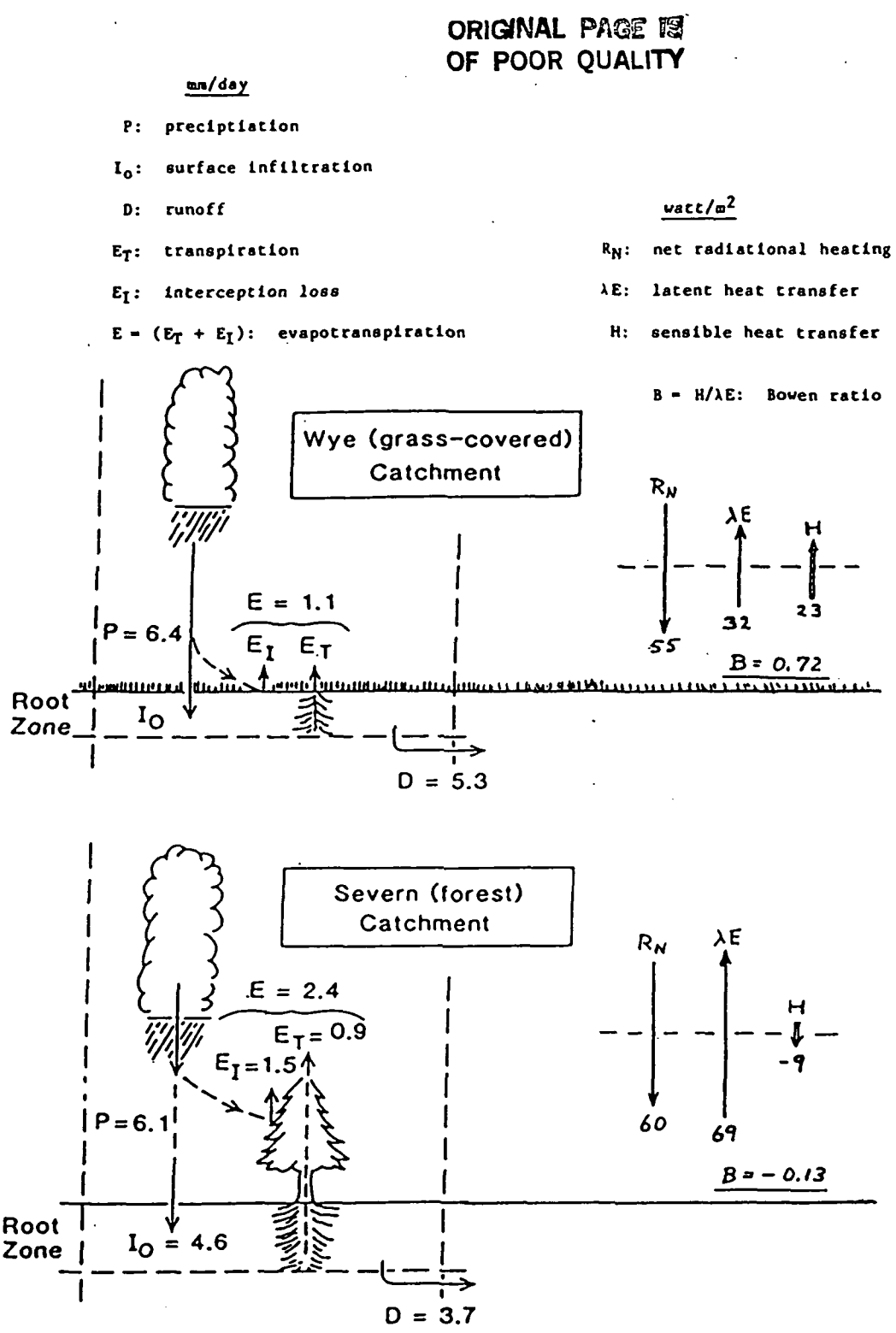

Fig. 2 Measured mean-annual water and energy balances of adjacent grass-covered and forest-covered catchments, in central Wales, U.K. (from Calder and Newson, 1979; Shuttleworth and Calder 1979).

A. Goals of the Proposed Research.

The objective of the proposed research is to construct a model biosphere which will produce realistic simulations of the water and energy transfers at the earth's surface. This will be done by constructing a numerical model of the earth's vegetation cover which embodies the principal morphological and physiological factors that control the water and energy transfers.

Morphology

The morphological factors (those which depend on the form and structure of the plants) will be the leaf area density (the total area of the leaf surfaces per unit volume of space) as a function of height, $L_D[Z]$; and the root length density (the total length of live roots per unit volume of space) as a function of depth, $RT_D(Z)$.

In the initial version of the model biosphere, $L_D[Z]$ and $RT_D[Z]$ will be prescribed for each grid area of the GCM as a function of the time of the year, as obtained from phenological observations.

In the second stage, $L_D[Z]$ and $RT_D[Z]$ will be made interactive with the model calculated atmospheric conditions (and soil moisture), so that aperiodic drought and extremes of heat and cold will also affect these two parameters on the phenological time scale.

In the final stage, the different vegetation formations themselves (i.e., rainforest, seasonal forest, woodland, desert; grassland) and not just their phenological changes will be made interactive with the atmospheric conditions (and soil moisture.)

Physiology

The principal physiological factor will be the stomatal resistance, r_{st} (the impedence to water vapor transfer from the saturated cavities within the leaves to the air outside.) r_{st} will depend not only upon the atmospheric variables, but also upon other internal resistances which affect the water flow from the soil to the leaves via the roots and stems.

B. Overview of the Proposed Biosphere.

As described in Section B.2, the vegetation of the model biosphere will have two or more discrete canopy layers and two root layers. The two important vertically continuous vegetation properties that will be discretized are $L_D[Z]$, the leaf area density as a function of height, and $RT_D[Z]$, the root length density as a function of depth.

B.1.i Governing equations for transpiration and water uptake by roots.

For the purpose of illustration, we show here the governing equations for the simple case where there is one canopy layer and one root layer.

For the definitions of the symbols, see Section C, Page 51.

Transpiration:

If the vegetation is represented as a single, continuous, transpiring surface of unit area per unit ground area, the governing equations for the energy transfers can be written:

$$\lambda E_T = \frac{(e_\ell - \underline{e_a})}{(r_{st} + r_a)} \frac{\rho C_p}{\gamma} \tag{1}$$

$$e_\ell = e^* [T_\ell] \tag{2}$$

$$\frac{(T_\ell - \underline{T_a})}{r_a} \rho C_p = H \tag{3}$$

$$H = (\underline{S_a} (1-\alpha) + \underline{R_{La}} - \sigma T_\ell^4) - \lambda E_T - \underline{G} \tag{4}$$

$$r_a = r_a[L_D[Z], \underline{u_a}, (T_\ell - \underline{T_a})] \tag{5}$$

$$r_{st} = r_{st}[r_{st,o}, \underline{S_{a,o}}, \psi_{\ell,min}, \underline{RH_a}, T_\ell, L_\sigma] \tag{6}$$

Given $\underline{e_a}$, $\underline{T_a}$, $\underline{u_a}$, $\underline{S_a}$ and $\underline{R_{La}}$ from the output of the atmospheric part of the general circulation model; $\underline{G}$ from the heat budget of the soil (see section iv); and ψ_ℓ from the solution for the water uptake from the soil, as described below, we can solve these six equations for the six unknowns: E_T, e_ℓ, T_ℓ, H, r_a, r_{st}.

(1) As shown schematically in Fig. 3, the main part of the transpiration loss is water which evaporates from the walls of the mesophyll cells that surround the sub-stomatal cavities in the leaves of the plant and then diffuses to the atmosphere through the stomatal openings. [The rate of water vapor transfer across the cuticle surface of the leaves, or across other parts of the plant surfaces, is usually one to two orders of magnitude smaller.] The rate of the water vapor transfer, from its origin in the sub-stomatal cavities to a given reference level in the atmosphere, is given by Eq. 1, where e_ℓ is the vapor pressure in the sub-stomatal cavity, and $\underline{e_a}$ is the vapor pressure at the reference level in the atmospheric boundary layer. r_{st} is the bulk resistance to the diffusion of water vapor through the stomatal opening, and r_a is the resistance to the diffusion of water vapor from the vegetation surface to the reference level. With $\underline{e_a}$ given, Eq. (1) has 4 unknowns: E_T, e_ℓ, r_{st}, r_a.

(2) e_ℓ can be taken as the saturation vapor pressure, e*, as given by the Clausius-Clapyron equation for the temperature of the leaf, T_ℓ. T_ℓ is assumed to be constant throughout the leaf (whose thickness is typically about 1 mm) and represents an additional unknown.

(3) T_ℓ is obtained from the diffusion equation for the sensible heat transfer from the surface of the leaf, at temperature T_ℓ, to the reference level in the atmosphere, at temperature, $\underline{T_a}$, where it is assumed that r_a is the same for the sensible heat diffusion as for the water vapor diffusion; which adds the unknown, H.

(4) H, the sensible heat transfer, is obtained from the total vertical energy transfer, where the sum of the three terms within the parentheses on the right, in Eq. 4, is the net radiation flux, R_N. $\underline{S_a}$ and $\underline{R_{La}}$

are the downward components of the solar and longwave radiation, as given by the atmospheric part of the GCM, α is the albedo of the vegetation surface, and σT_ℓ^4 is the upward longwave radiation, which depends on the temperature of that surface. $\underline{G}$ is the sensible heat transfer through the vegetation and into the soil, as given by the heat budget for the soil (section iv).

(5) The aerodynamic resistance, r_a, depends on the vertical distribution of the leaf area density, on the wind speed at the atmospheric reference level, and on the thermal stability of the air, $(T_\ell - T_a)$, (see, for example, Goudriaan, 1977). Typically, with wind speeds in the atmospheric boundary layer of a few meters per second and mid-day unstable lapse rates, r_a is of the order of $\underline{0.5}$ s cm^{-1} for herbacious vegetation (0.1 to 1 m high) and of the order of $\underline{0.05}$ s cm^{-1} for forests (10 to 20 m high).

(6) r_{st}, the bulk stomatal resistance reaches the minimum value for the plant species, $r_{st,o}$, when the stomates are fully open. Typically, when the leaf area index is about four, $r_{st,o}$ is of the order of $\underline{0.5}$ s cm^{-1} for herbacious plants, and somewhat larger, of the order of $\underline{1.0}$ s cm^{-1}, for trees.

The stomates close when the solar radiation, $\underline{S_a}$, drops below a critical value $\underline{S_{a,o}}$; they close when the relative humidity of the air, $RH_a = RH[\underline{e_a}, \underline{T_a}]$, falls below a critical value, $\underline{RH_{a,crit}}$; and they close under extremes in the leaf temperature, T_ℓ. In addition, the stomates close when the water potential in the guard cells (ψ_ℓ) that surround the stomates, falls to a limiting value, $\psi_{\ell,crit}$. (What controls the magnitude of ψ_ℓ is discussed below.) When the stomates are closed, the transpiration is only through the cuticle of the leaf,

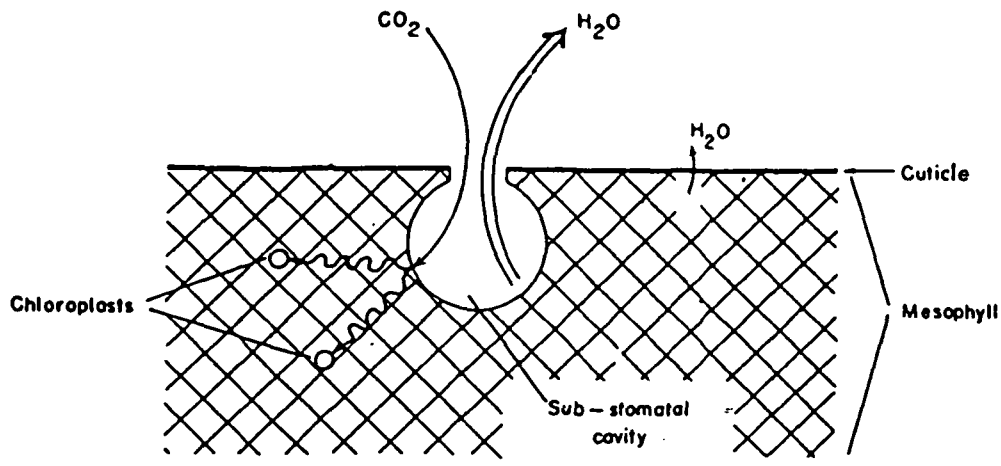

Fig. 3 Schematic representation of transpiration through the stomates and cuticle of a single leaf (after Hillel, 1971).

whose resistance to the water vapor transfer is typically about two orders of magnitude larger than r_{st}, or about 50 to 100 s cm^{-1} when L_σ equals four.

All these responses are interpreted as the evolutionary result of the plant's effort to maximize photosynthetic production (which requires the simultaneous presence of shortwave radiation, water, carbon dioxide, and solutes in the leaf chloroplast cells), to maintain a solute transport system, to avoid heat death, and to conserve water in the soil moisture store for future use. The first three demands are in direct conflict with the last, the conservation of water, which gives rise to the need for physiologically regulating the flow of water through the plant.

Water Uptake by the Roots:

The conservation of mass requires that the water vapor which moves away from the cell walls of the sub-stomatal cavities be replaced by a flow of liquid water toward the walls on the other side.

If, for the purpose of illustration, we neglect the small time rate of change of the water stored in the plant, we have

$$E_T = F_P = U_R \quad ,$$

where E_T is the rate of transpiration, F_P is the rate of liquid water flow through the plant, and U_R is the rate of water uptake by the roots.

When there is no divergence in the water flow through the plant (no change in the plant water storage), we can write the governing equations for the rate of water flow as

$$F_p = \frac{(\psi_s - \psi_\ell)}{g(r_s + r_c + r_x)} \tag{7}$$

$$\psi_s = \psi_s[\underline{\theta}] \tag{8}$$

$$r_s = r_s[\underline{\theta},\ RT_D[Z]] \tag{9}$$

$$r_c = r_c[r_{c,o},\ RT_D[Z]] \tag{10}$$

$$r_x = r_x[r_{x,o},\ F_{p,crit}] \quad . \tag{11}$$

Given the boundary condition, $F_p = E_T$, where E_T is obtained from the solution of equations (1, 2....6) above; and given $\underline{\theta}$ from the solution for

the soil water budget (section iv), we can solve these five equations for the five unknowns: ψ_ℓ, ψ_s, r_s, r_c and r_x.

There is an upper limit to F_p, which is believed to be the rate at which the water movement through the fine channels in the xylem (the water conducting elements of the stem) changes from laminar to turbulent flow. This limit, $F_{p,crit}$, is typically of the order of 1.5 mm/hr (when expressed as the area averaged flow). When $F_{p,crit}$ is reached, there is an abrupt and large increase in the xylem resistance, r_x; and, as Eq. (7) shows, for a given soil water potential, ψ_s, this will produce an abrupt and large fall in the leaf water potential, ψ_ℓ. ψ_ℓ itself has a critical value (of the order of -25 bars) which is when the water pressure in the stomatal guard cells can no longer maintain their turgor. When the cells collapse they constrict the stomatal opening, and $E_T = F_p$ is then limited to the value $F_{p,crit}$.

Fig. 4 is an electrical analog of the water transfer pathway through the soil-plant-atmosphere system (when $E_T = F_p = U_R$). The figure shows how the flow is controlled by the fixed resistance, r_c, and the four variable resistances, r_s, r_x, r_{st} and r_a.

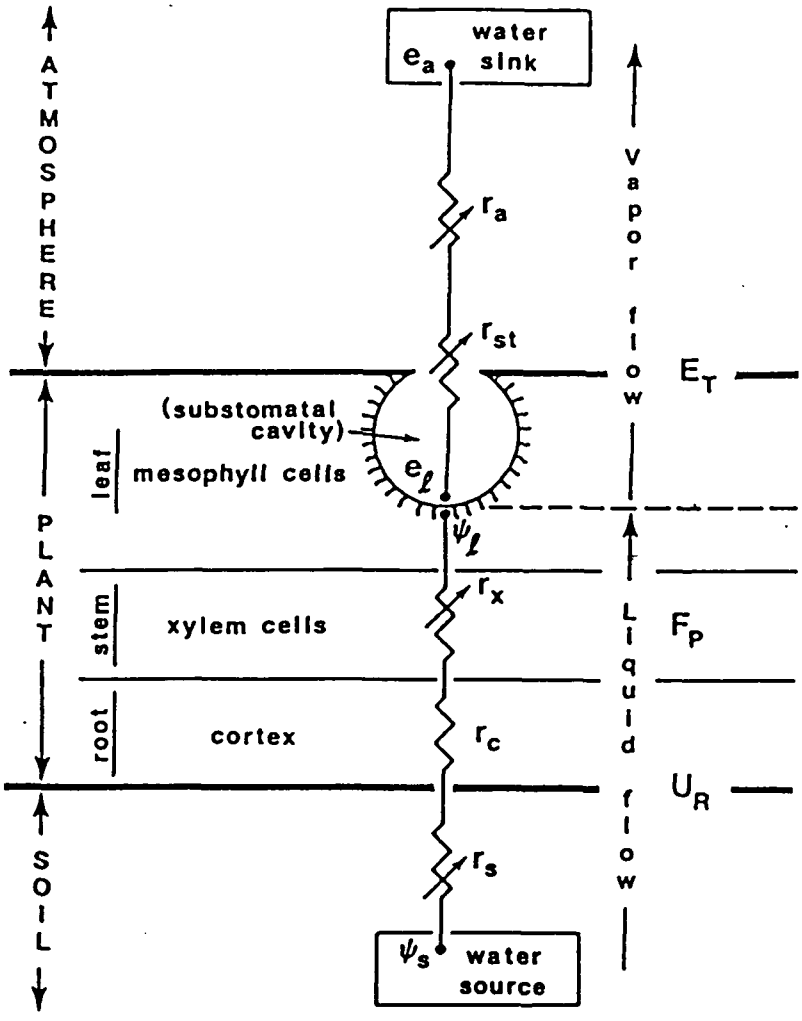

Fig. 4 Electrical analog representation of the potentials, and resistances to flow, of water vapor and liquid water in the soil-plant-atmosphere system.

ii. Rainfall Interception and Interception Loss.

For the single layer vegetation model, the governing equations for the interception loss and interception gain, when the canopy is completely wet, can be written:

$$\lambda E_I = \begin{cases} \dfrac{[e_s - e_a]}{r_a} \cdot \dfrac{\rho C_p}{\gamma} \cdot f(W_I), & \text{When } W_I > 0 \\ 0, \quad \text{when } W_I = 0 \\ \dfrac{[e_s - e_a]}{r_a} \cdot \dfrac{\rho C_p}{\gamma}, & \text{when } W_I \geq W_{I\,max} \end{cases} \qquad (12)$$

$W_{I\,max}$ is the maximum amount of water that can be held on all the upper leaf surfaces.

$$\frac{dW_I}{dt} = P\,(1 - p) - E_I - D\,[W_I] \quad . \qquad (13)$$

The interception loss and the interception gain are highly dependent on the vegetation morphology for two reasons:

i) The aerodynamic interaction between plant and atmosphere: As indicated in section B.1.i, tall, 'rough,' surfaces, like pine forests, maintain a relatively turbulent aerodynamic regime in and around their upper crowns. Within this well ventilated volume, the transfers of vapor and sensible heat are typically an order of magnitude faster than at an equivalent height above 'smoother' surfaces, like a grass cover, under the

same meteorological conditions. ($r_a \sim \underline{0.05}$ s cm^{-1} as against 0.5 s cm^{-1})

ii) The geometry and extent of intercepting surfaces: Vegetated regions commonly present 3 to 8 m^2 of surface area to the atmosphere for every square meter of ground area ($L_\sigma \approx 3\text{-}8$). Obviously, the larger the surface area the greater the amount of rainfall that may be held on the surface for later re-evaporation, and the smaller the amount that drains off to reach the soil moisture store. Typically, the interception capacity of vegetation is of the order of 1 to 3 mm depth of water. The geometrical arrangement of the canopy is important too - some coniferous trees maintain a large intercepting surface well above the level of the theoretical momentum sink.

The rate of interception loss depends very greatly on the rainfall regime. For a given time-averaged rainfall which is made up of high intensity, short duration episodes, there will be a comparatively low rate of interception loss. This is because the interception capacity is quickly reached after the onset of storms, allowing the remaining rainfall to be transmitted to the soil surface. Conversely, if the same time-averaged rainfall is made up of long-duration, low intensity storms, the interception loss will be larger, reaching its maximum if the interception capacity is not reached (i.e. if the water does not accumulate on the leaf surfaces to a level sufficient to initiate significant leaf drainage).

As indicated in section B.2, our intention is to model the water and heat transfer processes for the several observed vegetation formation types in a realistic fashion. This, however, will produce correct values of the interception loss only if the space-time variation of the rainfall is correctly represented. General circulation models produce half-hourly to

hourly amounts of rainfall as output; but as this is the average over a large grid area (of the order of $(300\ km)^2$), if used in an unadjusted form it will almost always produce an excessively high and unrealistic interception loss. It will be necessary, therefore, to relate the GCM produced grid area average rainfall to a realistic space variation of the rainfall on the sub-grid scale, using parameters extracted from the GCM simulation (which indicates, for example, whether the rainfall is of convective or large-scale upglide origin) and also climatology. Satellite based observations of regional surface temperature and soil moisture variations (Atlas and Thiele, 1981) may be able to provide information about typical time-area-intensity distributions in the different regions and seasons, from which we would construct the area-intensity functions for the GCM rainfall calculation. A possible solution lies in representing the spatial variation of the amount of water held on the vegetation surface by wave functions. A similar wave representation of the rainfall intensity would be superimposed to obtain the spatial variation of the rate of change of the water held on the surface. Another possibility would be to assume that the rainfall at a representative point within the grid area will be equal to the grid-area averaged rainfall when both are averaged over a time interval of the order of, say, 12 to 24 hours; and then to let the half-hourly values of the rainfall intensity at that point vary within the chosen time interval as a function of the GCM parameters and climatology.

iii. Snowfall Interception and Disposal.

The partition of snow into surface evaporation and melt water, which contributes towards soil moisture recharge and runoff, is of great importance for the surface energy balance and hydrology of a large part of the Northern Hemisphere continents. The energy balance at the snow surface can be modelled using derivations from the equation set outlined in section B.1.i. Major differences between the fluxes of latent and sensible heat with and without snow, under the same atmospheric conditions, arise from variations in the surface albedo and hence in the net radiation, and from the value of the aerodynamic resistance, r_a. [A review paper by Male and Granger, 1981, discusses these and other facets of snow surface processes in detail.] The energy available for evaporation and/or snowmelt in forested regions is characteristically much greater than that over bare or grass covered areas (Leonard and Eschner, 1968) due to the smaller albedo of the exposed parts of the forest canopy. This produces an appreciable transfer of heat, in radiative and sensible form, from the exposed parts of the tree canopy to the snow covered surfaces. This effect is enhanced in areas with evergreen vegetation. The use of a multilayer vegetation model coupled with a layered soil model is the most realistic way to simulate the energy exchange processes involving snow cover.

iv. Water and Heat Budget of the Soil.

For simulating the water and heat budgets of the soil, we shall follow one of the more physically realistic treatments (see, for example, the reports of Gurney and Camillo, 1982, Camillo and Schmugge, 1982). In these treatments, the fluxes of heat and moisture are coupled as both depend on the gradients of temperature and moisture. This requires the simultaneous solution of the equations:

$$q_\theta = D_\theta \left(\frac{d\theta}{dz}\right) - D_T\left(\frac{dT}{dz}\right) - K_\theta$$

$$q_h = K_T\left(\frac{dT}{dz}\right) - \lambda D_{\theta,vap}\left(\frac{d\theta}{dz}\right) \qquad (14)$$

where q_θ and q_h are, respectively, the fluxes of moisture and heat; $D_{T,\theta,vap}$ is the diffusivity of heat, water, or water vapor; and $K_{T,\theta}$ is the thermal or hydraulic conductivity of soil. It should be noted that D_θ and D_T have both liquid and vapor contributions:

$$D_\theta = D_{\theta,liq} + D_{\theta,vap}$$

$$D_T = D_{T,liq} + D_{T,vap} \qquad (15)$$

Equation (14) describes the dependence of the heat fluxes on the vertical gradients of θ and T. The time dependence of θ and T is given by the continuity equations:

$$\frac{d\theta}{dt} = -\left(\frac{dq_\theta}{dz}\right)$$

$$\frac{dT}{dt} = -\frac{1}{c_s}\left(\frac{dq_h}{dz}\right) \qquad (16)$$

where c_s is the specific heat of the soil.

Various numerical techniques may be applied to solve the equation set over finite time steps. It is usual practice to prescribe a deep soil temperature and moisture content as lower boundary conditions and an energy balance model at the soil surface to calculate q_θ, q_h, θ and T at the air-soil interface. The soil is then divided into a number of strata, which are taken as internally homogenous with uniform values of $D_{\theta,T}$ and $K_{\theta,T}$. The values of T and θ for each stratum are used to calculate the depth dependent derivatives at each time step.

The soil moisture store will be represented by three zones: a small near-surface store, from which not only root uptake but also direct evaporation can take place; an intermediate bulk soil moisture store, which is mainly drawn on by the root uptake; and a deep store, from which only capillary rise can bring water toward the surface. The last term can be significant on the seasonal time scale.

The hydraulic and thermal properties of the soil will be taken from the global data set prepared for the GLAS GCM by Lin and Alfano (Alfano, 1981).

It is impossible to model overland flow and soil interflow, in a direct way, without resort to an exceedingly fine grid size. Instead, we will use the 'lumped' catchment analytical model of Beven and Kirkby (1976). This makes use of functions which relate the total soil moisture storage to the size of the catchment contributing area, (which is the saturated area bordering stream channels), thus allowing a direct calculation of the different components of runoff: overland flow, interflow and base flow. It may be possible to use the geographical data relating to grid square soil type, topography and stream density to parameterize the necessary functions.

B.2 The Multilayer Vegetation Model.

1) Definition and Advantages of a Multilevel Model.

Definition:

In general, a multilayer model can be thought of as an elaborate extension of the short set of equations given in Section B.1.i. The vegetation canopy is represented by a vertical series of discrete plates, each of which exchanges sensible and latent heat with the immediately surrounding air and through which the fluxes must pass on the way to the free atmosphere (see Fig. 5). At the same time, the temperature of each plate depends on the net radiation it absorbs (which is a function of the temperatures of all the plates and the soil surface), and on the temperature and vapor pressure of the air in the surrounding (canopy) air space. It is apparent from Figure 5 that, given: (1) the air temperature (T_a) and vapor pressure (e_a) above the canopy, and their equivalents below the soil surface; (2) the values of the intermediate resistances and (3) a means of distributing the shortwave and downward longwave radiation among the plates, the equation set representing the energy budgets of all plates will reduce to n expressions with n unknowns, (where n is the number of leaf layer plates and the unknowns are the leaf temperatures.) A similar model will represent the layers of the soil. The combined system will represent the steady state energy balance of the vegetation and soil, and may be further extended to include non-steady state processes - such as the drying out of intercepted water which involve a dependence on the time variation of canopy and soil temperatures and water contents.

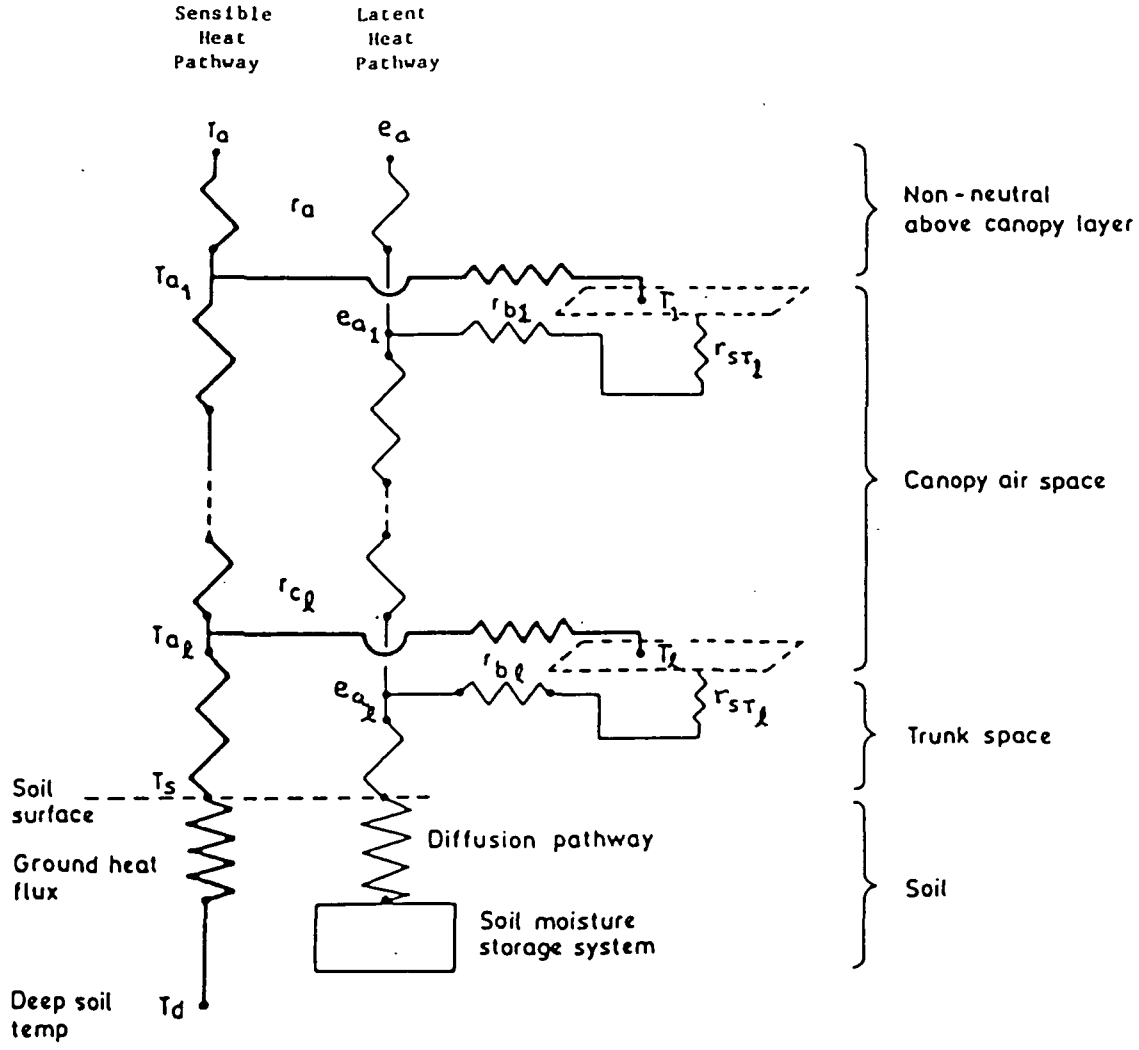

Fig. 5 Schematic representation of sensible and latent heat transfer using a multilayer model. The flow of water from soil to leaf layers has been omitted for clarity.

T_a	air temperature at reference height.
e_a	vapor pressure at reference height.
$T_{a\ell}$	air temperature of canopy air space of ℓ^{th} layer.
$e_{a\ell}$	vapor pressure of canopy air space of ℓ^{th} layer.
T_ℓ	leaf surface temperature of ℓ^{th} layer.
T_s	soil surface temperature.
T_d	deep soil temperature.
r_a	aerodynamic resistance from reference height to canopy top.
$r_{c\ell}$	aerodynamic resistance between canopy air space of the ℓ^{th} layer and the canopy air space of the ℓ-1^{th} layer.
$r_{b\ell}$	aerodynamic resistance between leaf surface and canopy air space of ℓ^{th} layer.
$r_{st\ell}$	stomatal resistance of ℓ^{th} layer.

Advantages:

The multilayer model is more realistic and is easier to validate than a unilayer model. The principal points to note are:

a) Vegetation morphology: A multilayer model can be constructed in such a way that the leaf area density, $L_D[Z]$, and the leaf area index, L_σ, are directly represented by the size and spacing of the leaf layer 'plates'.

b) Energy exchange processes: The exchanges of energy (in radiative, sensible and latent form) between the different layers of canopy, and between those layers and the soil, can be modelled. It need not be assumed that the multiple latent and sensible heat sources correspond to the momentum sink, as with a unilayer model.

c) Parameter correspondence with nature: The parameters of the model can be made to correspond directly to the physical and physiological properties of each vegetation type.

d) Interception loss and snowmelt: These processes cannot be modeled realistically using a unilayer treatment. Sellers (1981) demonstrated that a single-layer model consistently underestimates the rate of interception loss.

e) Validation: A multilayer model not only generates the latent and sensible heat fluxes, but also profiles of leaf temperature, air temperature, vapor pressure, soil temperature, and soil moisture potential. By comparison, the unilayer model outputs a single value of 'surface' temperature - a rather nebulous quantity when considering

that a tropical rainforest has been observed to have a mid-afternoon temperature difference of as much as 7° C between the top of the canopy and the soil surface (Pinker, 1980; and personal communication, 1982).

ii. Distribution of the Observed Vegetation Formations.

de Laubenfels (1975) has made the following classification of the earth's vegetation formations, whose distributions are shown in Fig. 6:

Region with tall trees whose crowns form a continuous canopy, and below which there is a continuous understory of shorter trees: designated Rainforest.

Region with trees whose crowns form a continuous canopy, but below which there is a discontinuous understory: designated Seasonal Forest.

Region with trees whose crowns do not form a continuous canopy, but where the total vegetation cover is continuous: designated Woodland.

Region where there is a discontinuous cover of plant growth, so that large areas of bare ground are exposed: designated Desert.

Region of continuous ground cover of herbacious plants (of which grass is the predominant form): designated Grassland.

Rainforest, Seasonal Forest, Woodland, and Desert are "undisturbed" vegetation formations. Grassland is the existing formation type where seasonal forest and woodland have been disturbed by fire and by grazing (which inhibits recovery after fire.)

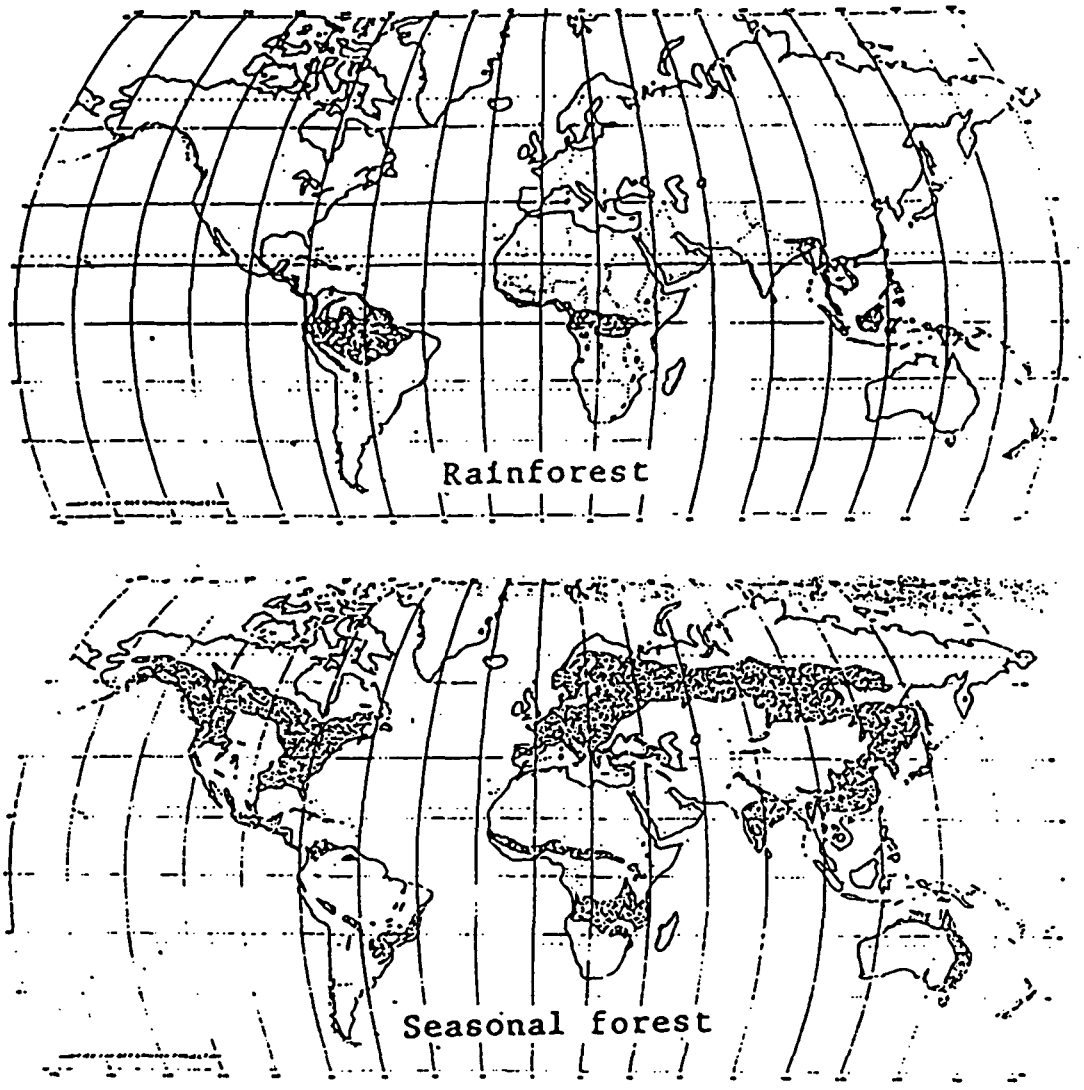

Fig. 6 Observed vegetation formations (from de Laubenfels, 1975).

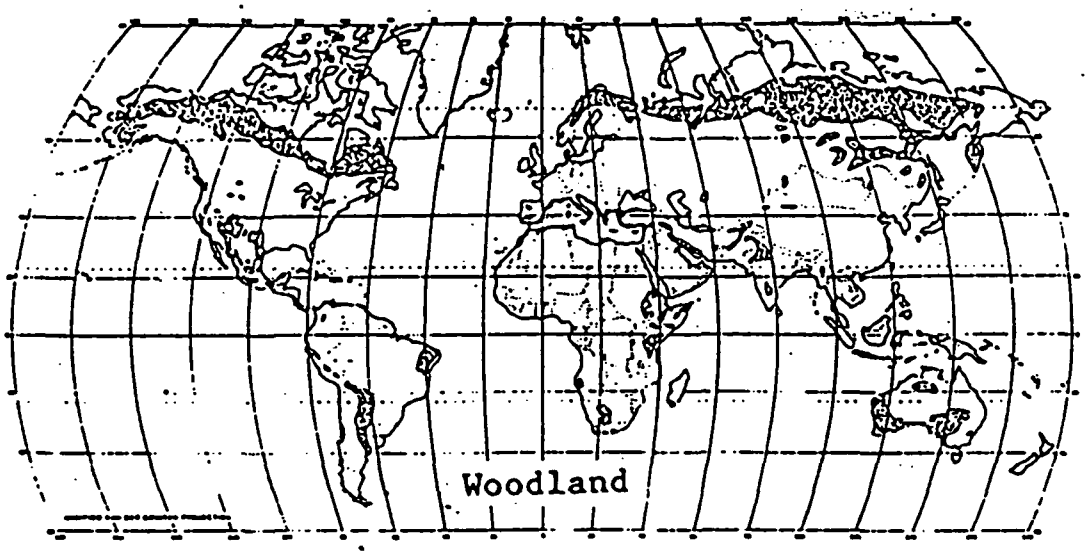

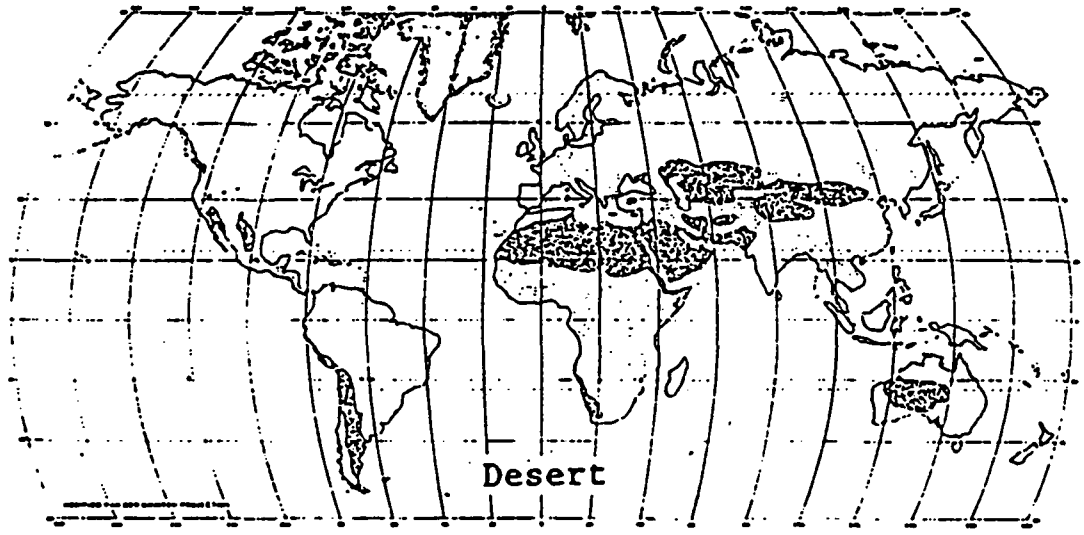

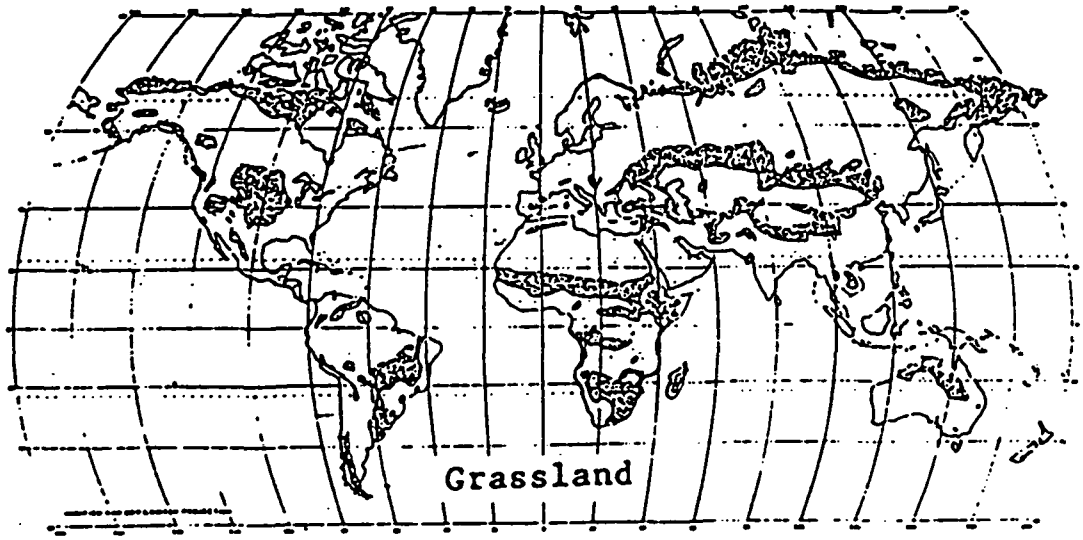

Fig. 6 - continued.

In the initial version of the proposed biosphere, the prescribed distribution of the vegetation formations will not change with time.

Eventually, we would like to have the vegetation formations change in response to forcing by the atmospheric part of the GCM. But inasmuch as the time scale of natural succession is of the order of 10^1 to 10^3 years (see, for example, Loucks, et. al., 1981) this will be an essential requirement for the biosphere only when a fully interactive ocean is made part of the general circulation model.

iii) Specification of the Multilayer Model.

There are two distinct requirements for the specification of the multilayer model. Firstly; the morphology of the vegetation community must be realistically represented by the size and spacing of the discretized leaf plates (see Fig. 5), and by the values of the boundary layer resistances, canopy air space resistances and root cortex resistances. The above canopy aerodynamic resistance, r_a, must also be properly related to the gross morphology of the vegetation community. Secondly; the physiology of the plant must be correctly reflected in the functional model of stomatal response and its interaction with the leaf water potential, xylem resistance, stem flow, and soil moisture potential.

Taking the morphology of the vegetation community first: Figs. 7A, B, C illustrate the process whereby measurable characteristics of the vegetation are transformed to model parameters. Fig. 7A shows the structure of a tropical rain forest in its natural state. Fig. 7B shows the corresponding leaf area density and root length density as functions of height. In the first version of the model, the seasonal variations in these vegetation parameters will be prescribed as functions of the time of the year. Later, the phenolgical changes in $L_D(Z)$ and $RT_D(Z)$ will be made dependent upon the model derived atmospheric variables and soil moisture.

To obtain the areas of the two plates that will represent the vegetation (see figure 7C), the leaf area density is integrated with height:

$$L_\sigma = \int_{Z_B}^{Z_T} L_D(Z) \cdot dZ \qquad (17)$$

where L_σ is the leaf area index (m^2/m^2), and Z_B and Z_T are the heights of the bottom and top of the storey.

The height of the plate is taken as the center of gravity of the plate, Z_m, where:

$$\int_{Z_B}^{Z_m} L_D(Z) \cdot dZ = \int_{Z_m}^{Z_T} L_D(Z) \cdot dZ \qquad (18)$$

Following the work of Goudriaan (1977), the bulk aerodynamic parameters of roughness length (Z_o) and zero plane displacement (d) may be determined from a numerical analysis of the reduction in shear stress with depth in the canopy; parameters which depend on the leaf area density and drag coefficient of leaf elements. The parameters z_o and d are used to determine the value of r_a, the above canopy resistance, by

$$r_{a\ h\ z_d} = \left[\frac{\ln\left[\frac{z-d}{z_o}\right]^2}{k^2 u} \right]_h^{z_d} \qquad (19)$$

where k is von Karman's constant, h is the height of the crop and z_d is the reference height (This equation holds for neutral conditions only; but Thom and Oliver (1977) describe a version which accounts for the effect of non-neutrality). A further analysis by Goudriaan (1977) provides the extinction of wind speed as a function of leaf area density.

The conductivity of mass, heat and momentum in the canopy air space is given as:

$$K_{m,v,h_{(z)}} = L_{m_{(z)}} \cdot I_{m_{(z)}} \cdot u_{(z)} \qquad (20)$$

where L_m is the local mixing length of the canopy air space (a function of the size and spacing of shoot elements) and I_m is the relative turbulence

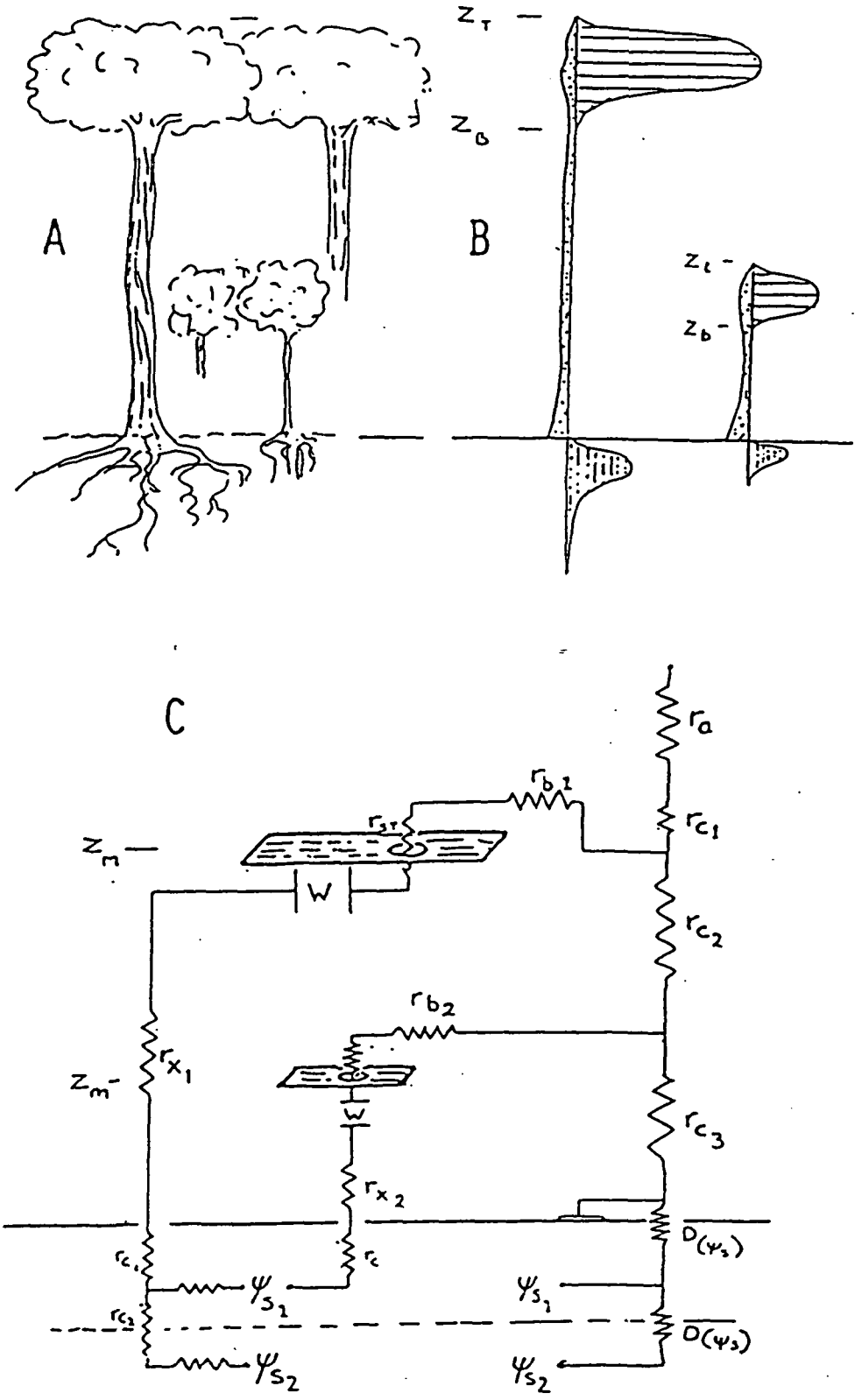

Fig. 7: A. Tropical rainforest vegetation; continuous canopy of tall trees above continuous under-storey.

B. Leaf area density ▤, stem area density ▦, and root length density ▥, as functions of height for the tropical rainforest shown in Figure A.

C. Electrical resistance analogue of the tropical rainforest represented in Figure B.

intensity - a factor that increases from 0.3 at the top of plant canopies to 0.8 at the base, and appears to be invariant with wind speed.

r_{c_ℓ}, the canopy air space resistance between one leaf layer and the next is given by:

$$r_{c_\ell} = \int_{Z_\ell}^{Z_{\ell-1}} \frac{1}{K_{m,v,h_{(z)}}} \cdot dZ \qquad (21)$$

The leaf laminar boundary layer resistance, r_{b_ℓ}, will be taken as a function of leaf area index, local wind speed, and a shape/shelter factor, χ_s:

$$r_{b_\ell} = f(L_{\sigma_{(z)}} \cdot u_{(z)} \cdot \chi_s) \qquad (22)$$

Several researchers, notably Goudriaan (1977) and Allen and Lemon (1976), have proposed different mathematical analyses to determine χ_s as a function of leaf size, shape and orientation.

The radiation absorption and transfer characteristics of the vegetation are determined by the canopy structure. A simple model of radiative transfer was proposed by Ross and Nilson (1971):

$$S_{a_{(L_\sigma)}} = S_{a_{[0]}}[f(w) + \exp(-f(\beta) \cdot L_\sigma)] \qquad (23)$$

where $S_{a_{(L_\sigma)}}$ is the shortwave radiation flux emerging from under a cumulative leaf area index L_σ, $S_{a_{[0]}}$ is the radiation intensity above the canopy, $f(w)$ is a scattering function, and $f(\beta)$ is an extinction coefficient that varies with the solar angle, β.

The root water uptake models of Cowan (1965), Hillel (1977) and others describe the movement of water from soil to root cortex as a radial flow towards individual root elements across a gradient of moisture potential - the difference between ψ_s, the soil water potential, and ψ_r, the root water potential. The plant parameter of importance is $RT_D[Z]$, the root length density ($m\ m^{-3}$), as a function of depth. Cowan (1965) originally proposed the expression:

$$\frac{\partial \psi_s}{\partial t} = \frac{D}{r} \frac{\partial}{\partial r} \left(r \frac{\partial \psi_s}{\partial r} \right) \qquad (24)$$

where D is the value of soil moisture diffusivity, and r is the distance from the root. Given that the roots have a typical radius of r_1 and that a root extracts water from a cylindrical volume of soil of radius r_2, where $r_2 = [1 / \pi.RT_D[Z]]^{1/2}$, equation (24) can be solved with the boundary conditions of

$$\frac{\delta \psi_s}{\delta r} = \begin{cases} \dfrac{d\theta}{dt} \dfrac{[r_2^2 - r_1^2]}{2r_1} & \text{at } r = r_1 \\ 0 & \text{at } r = r_2 \end{cases}$$

where dW_s/dt is the rate of reduction of soil water concentration.

The transfer of water from root cortex to leaf mesophyll involves aspects of plant morphology and physiology. The xylem elements, which conduct water up the stem are serially linked, elongated plant cells with narrow apertures at their end-to-end junctions. Poiseuille analyses of the flow in such elements (see, for example, Denmead, 1976) predicts a critical

flow velocity above which the flow regime changes from laminar to turbulent. This greatly increases the resistance imposed by the xylem and has the effect of lowering ψ_ℓ.

The end of the liquid transfer pathway is the leaf mesophyll cell. The leaf water content, W_ℓ, is determined by:

$$\frac{dW_\ell}{dt} = \frac{1}{g}\left[\frac{\psi_\ell - \psi_r}{r_c + r_x}\right] - E_T$$

Leaf water potential, ψ_ℓ, a critical variable in the calculation of stomatal resistance, is a function of W_ℓ,

$$\psi_\ell = f(W_\ell) \quad .$$

The particular form of stomatal response is dependent upon plant species, where each species can be thought of as being near perfectly adapted to survive in its natural environment. In the main, stomatal response is a function of shortwave radiation intensity, leaf water potential, vapor pressure, temperature and leaf age. Closure of the guard cells is brought about by a reduction in their turgor; this may be induced by a slow hydropassive process, whereby water is abstracted from the guard cells by strictly physical processes - such as evaporation or osmotic flow - or by a fast hydroactive process. It is believed that the latter, which can cause complete stomatal closure within seconds, is controlled by the transport and metabolism of ions into and out of the guard cells under the control of a plant hormone, Abscissic acid (ABA). The local concentration of ABA is determined by ψ_ℓ (see figure 8).

It is not proposed to model the biochemical and detailed biophysical responses of the leaf, although this has been done by some researchers

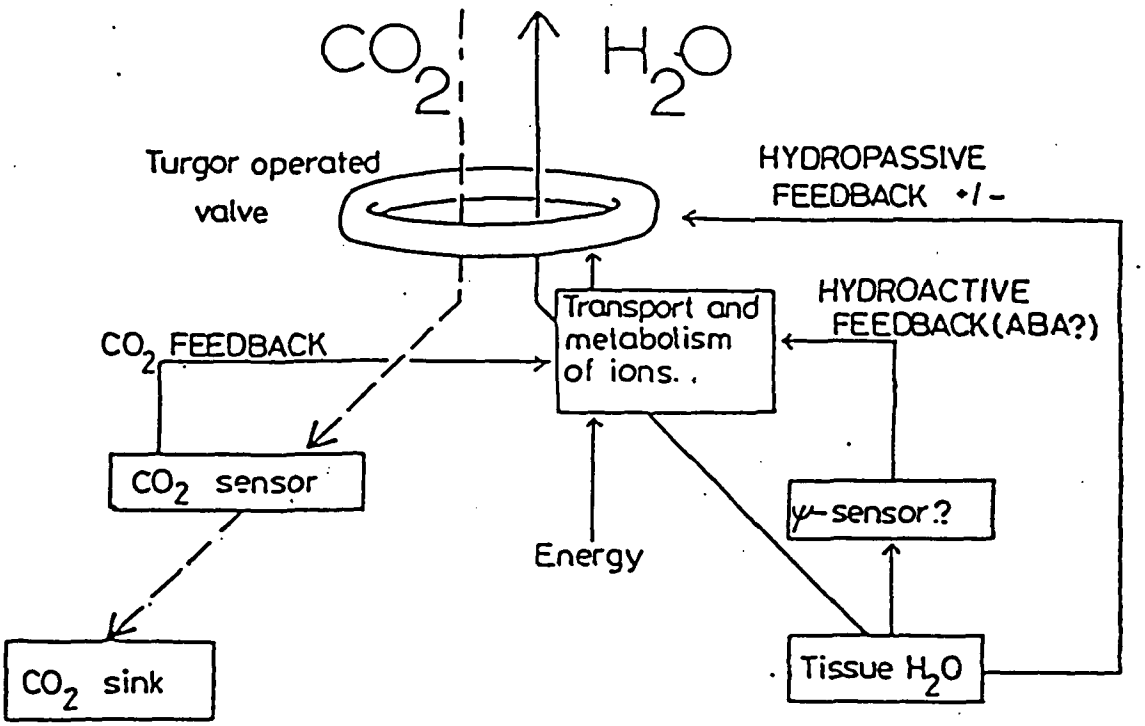

Fig. 8 Dependence of r_{st} on ψ_l and CO_2 concentration (From Raschke, 1975)

(see, for example the report of Penning de Vries; 1971); but rather to make the stomatal resistance a function of the leaf water potential and atmospheric forcing. Thus:

$$r_{st} = \frac{r_{st}(\underline{S_a})}{f(\psi_\ell) \cdot f(\underline{e_a}) \cdot f(\underline{T_a})} \tag{25}$$

Examples of the individual functions in equation (25) are given below.

Light

$$r_{st}(\underline{S_a}) = A_1/(A_2 - A_3 \cdot \underline{S_a}) \tag{26}$$

Denmead and Millar (1976)

where A_n is a species dependent constant.

Leaf water potential

$$f(\psi_\ell) = 1 - \exp(-A_4 \cdot \delta\psi_\ell)$$

$$\delta\psi_\ell = \psi_\ell - \psi_{\ell,crit} \tag{27}$$

$$0 < f_{(\psi_\ell)} < 1 \qquad \text{Turner (1974).}$$

where $\psi_{\ell,crit}$ is the value of ψ_ℓ below which the stomata close completely.

Vapor pressure

$$f_{(\underline{e_a})} = 1/[1 - A_5 (e^*[\underline{T_a}] - \underline{e_a})] \tag{28}$$

$$0 < f_{(\underline{e_a})} < 1$$

Jarvis (1976)

Temperature

$$f(\underline{T_a}) = A_6(\underline{T_a} - T_b)(T_u - \underline{T_a})^{A7}$$

$$A_6 = 1/(T_o - T_b)(T_u - T_o)^{A7}$$

$$A_7 = (T_u - T_o)/(T_o - T_b) \qquad (29)$$

$$0 < f(\underline{T_a}) < 1$$

Jarvis (1976)

where, T_b and T_u are the temperatures above which and below which the stomata open, and T_o is the temperature at which $f(\underline{T_a}) = 1$.

B.3 Comparisons of the Model Performance with Observations.

The checking of the model's performance will be done in three phases, each of which corresponds to a further level of horizontal integration. These are briefly stated below, starting at the lowest level of integration.

i) Field Measurements.

The complete vegetation-soil model for each vegetation type will be driven offline using local micrometeorological data. There are a number of case studies reported in the literature where a short time series of simultaneous observations were made of heat and vapor fluxes, temperature and humidity profiles, and micrometeorological conditions above the canopy. Use of these data sets should ensure that the characteristics of the various vegetation types are transformed to the model in a physically reasonable way.

ii) Water Balances in Catchments.

Here, the comparisons are made over a time period of a year or more for an area where long records of meteorological and streamflow observations exist. This will allow a checking of the simulated water balance components against the observations for the different vegetation types. It should be noted that in both (i) and (ii), no allowance is made for horizontal differences in meteorological conditions: the tests are essentially one-dimensional.

iii) FGGE Observations for the Globe.

Using a 4-dimensional dynamic assimilation of ground based and satellite based observations of the atmosphere during the FGGE year (1979), the GLAS GCM is producing a time series of the atmospheric state variables, T_a, e_a and u_a; and of the radiation transfers S_a and R_{La}, averaged for the model grid areas and at half-hourly time intervals. In addition, the GLAS model generates grid-area averaged rainfall, [P]; which will be converted into representative hourly local rainfall intensities, as indicated in section B.1.ii. The observed daily precipitation at 30,000 stations are available on tape for the FGGE year, and can also be used for input (10,000 of these are in the U.S. and have hourly records.)

This information will be used to force the model biosphere and, thereby, obtain a time series of the global fields of E_I, E_T, H, and σTs^4; W_I and W_S; and of the drainage, D_S; for the FGGE year.

The model derived σT_s^4, and its spatial and temporal variation as a function of W_I, snow cover, etc., (where T_s is the radiation temperture of the earth's surface) can be compared with satellite measurements of T_s. This will provide a quantitative evaluation.

E_T can be compared with the observed distribution of actively growing vegetation. C. J. Tucker has shown that growing and dying herbacious vegetation can be determined from Landsat observations. This, however, can only be a qualitative evaluation.

E_I, H and W_I will be difficult to evaluate. $W_{s,1}$, the moisture in the upper root zone, whose depth is of the order of 10 cm, may perhaps be compared with satellite microwave measurements of the moisture in the uppermost 5-15 cm of the soil in the desert and grassland regions (Schmugge, et.al., 1980).

D_S can be compared with the measured river flows during 1979, which are now being documented, on tape, as part of the FGGE Level 2-B data set.

•• It is the above (phenologically interactive) version of the biosphere that should be used when making weather predictions and predictions of monthly and seasonal climate anomalies with the general circulation model.

B.4 Numerical Simulation of the Vegetation Formations.

In the biosphere described above, the phenological changes of the vegetation formations will be interactive with the atmosphere and soil moisture, but the vegetation formations themselves will be prescribed (as in Figs. 6 A-E).

If the above goal of biosphere modeling is successfully accomplished by the beginning or early part of the third year, we shall undertake the next step: which is to model and simulate interactive vegetation formations. Here we will use empirical expressions which relate the climax vegetation type to the atmospheric and soil moisture conditions and thereby (starting from some initial state of the earth's vegetation cover) derive the distribution of the "undisturbed" vegetation formations: the forests, woodlands and deserts. Replacement by grassland would occur wherever atmospheric and soil moisture conditions make the forest and woodland vegetation tinder-dry: the assumption being that some mechanism for setting the dry vegetation on fire (lightning, dewdrops acting as burning lenses, or incendiary man) is always present.

A substantial extension of the above procedure would be to make use of the ecological processes which govern the growth, aging and succession of vegetation types. Starting from a given initial state, we would calculate the long term changes in the vegetation formation parameters.

Validation

Validation can be made, on the simplest non-trivial level, by forcing the biosphere with the non-interactive FGGE atmospheric data set. Here, we would assume that this one year data set represents the climate that produced the observed vegetation formations.

A higher level of validation would be to initalize the vegetation formations with the FGGE data set and then let the model atmosphere and biosphere operate in the interactive mode (with some large compression of the successional time scale.) In doing this, the presently observed ocean surface temperatures would be prescribed. Where the simulated and observed vegetation formations agreed, the model would be taken as being correct: where they disagree, we would conclude that either the model was not correctly formulated or that the presently observed vegetation formation is not in its natural equilibrium state.

Applications.

Atmosphere-biosphere fully interactive: ocean surface temperatures prescribed.

Besides the second level of validation indicated above, there will be relatively few uses for a fully interactive atmosphere-biosphere GCM when the ocean surface temperatures are prescribed (or when the ocean temperature is prognostic only in its thin boundary layer.) With given ocean temperatures, we are limited to the CLIMAP type of calculation. For example, we can prescribe the paleontologically derived global ocean surface temperatures of 18,000 years ago, and derive both the atmospheric state and the vegetation formations of 18,000 years ago.

Ocean-atmosphere-biosphere fully interactive.

Eventually we shall have a global ocean model which is fully interactive with the atmosphere and which correctly simulates the heat transport and heat storage in the deep ocean. (For a review of the near-current state of the art of ocean modelling, see Mintz, 1979.) When that is in hand, there will

be many interesting and important climate simulation and sensitivity experiments that can be made with the fully interactive ocean-atmosphere-biosphere GCM; some concerning natural variations in climate, others concerning anthropomorphic influences on climate.

An example, in the first category, would be the simulation of climate when the orbital parameters of the earth with respect to the sun are changed (i.e., a numerical test of the Milankovitch hypothesis on the ice ages.)

In the second category, which concerns man's influence on climate, perhaps the most important use of the fully interactive ocean-atmosphere-biosphere model would be to study the changes in the entire climate system (including the changes in the stores of carbon in the ocean, atmosphere and biosphere) as a result of the burning of fossil hydrocarbons, or of man's modification of the living biomass (through desertification and deforestation, or conservation and afforestation.)

C. Notation

A_n	species dependent constants
c_p	specific heat of air (J kg^{-1} $°C^{-1}$) (= 1.01 at s.t.p.)
c_s	specific heat of soil (J m^{-3} $°C^{-1}$)
d	zero plane displacement (m)
$D_{h,\theta,vap}$	diffusivity of heat, water or vapor in the soil (m s^{-2})
$D[W_I]$	drainage rate (Kg m^{-2} s^{-1})
e_a	vapor pressure (mb)
e*	saturation vapor pressure (mb)
e_ℓ	vapor pressure in the substomatal cavity (mb)
E_I	interception loss rate (Kg m^{-2} s^{-1})
E_T	transpiration rate (kg m^{-2} s^{-1})
$f(\underline{e_a})$	vapor pressure component of stomatal resistance
$f(\underline{T_a})$	air temperature component of stomatal resistance
f(w)	scattering coefficient of canopy
$f(\beta)$	radiation extinction coefficient as a function of solar angle
$f(\psi_\ell)$	leaf water potential component of stomatal resistance
F_p	flow of water through the plant stem (Kg m^{-2} s^{-1} or mm hr^{-1})
$F_{p,crit}$	limiting value of F_p (Kg m^{-2} s^{-1})
g	acceleration due to gravity (m s^{-2})
G	heat flux to ground (W m^{-2})
h	height of the crop (m)
H	sensible heat flux to atmosphere (W m^{-2})
I_m	relative turbulence intensity
k	von Karman's constant (= 0.41)

$K_{m,v,h_{(z)}}$ conductivity of momentum, vapor and heat in the air ($m\ s^{-2}$)

K_T thermal conductivity of soil ($W\ m^{-2}\ °C^{-1}$)

K_θ hydraulic conductivity of soil ($m\ s^{-1}$)

$L_D(Z)$ leaf area density ($m^2\ m^{-3}$)

L_M local mixing length (m)

L_σ leaf area index ($m^2\ m^{-2}$)

n number of leaf layers

p throughfall coefficient

P rainfall rate ($kg\ m^{-2}\ s^{-1}$)

r radius (m)

r_a aerodynamic resistance ($s\ m^{-1}$)

r_{b_ℓ} leaf laminar boundary layer resistance ($s\ m^{-1}$)

r_{c_ℓ} canopy air space resistance ($s\ m^{-1}$)

r_c root cortex resistance (s)

$r_{c,o}$ root cortex resistance per unit length of root ($s\ m^{-1}$)

r_s soil resistance (s)

r_{st} stomatal resistance ($s\ m^{-1}$)

$r_{st}(\underline{S_a})$ component of stomatal resistance dependent on shortwave radiative intensity only ($s\ m^{-1}$)

r_x xylem resistance (s)

$r_{x,o}$ xylem resistance per unit height ($s\ m^{-1}$)

$R_{\underline{La}}$ longwave radiation incident on the surface ($W\ m^{-2}$)

R_N net radiation ($W\ m^{-2}$)

$RT_D(Z)$ root length density ($m\ m^{-3}$)

$\underline{S_a}$ solar radiation incident on surface ($W\ m^{-2}$)

$\underline{S_{a(o)}}$ solar radiation incident above canopy ($W\ m^{-2}$)

$\underline{T_a}$ air temperature (°C)

T_b	temperature below which stomates close (°C)
T_d	deep soil temperature (°C)
T_ℓ	leaf temperature (°C)
T_o	temperature at which stomatal resistance factor, $f(\underline{T_a}) = 1$, (°C)
T_s	surface temperature (°C)
T_u	temperature above which stomates close (°C)
u	wind speed (m s^{-1})
U_R	flow of water through the plant root system (kg m^{-2} s^{-1} or mm hr^{-1})
W_ℓ	leaf water content (kg m^{-2} or mm)
W_I	water held on canopy surface (kg m^{-2} or mm)
z	height or depth (m)
z_b	height of bottom of canopy (m)
z_d	reference height (m)
z_ℓ	height of ℓth layer above ground (m)
z_m	height of leaf 'plate' (m)
z_o	roughness length (m)
z_T	height of top of canopy (m)
α	albedo
γ	psychrometric constant (mb $°C^{-1}$) = 0.646 at s.t.p.
λ	latent heat of vaporization (J kg^{-1}) = 2.501 at s.t.p.
ψ_ℓ	leaf water potential (bars)
ψ_r	root water potential (bars)
ψ_s	soil water potential (bars)
ρ	density of air (kg m^{-3}) (= 1.292 at s.t.p.)
θ	soil water content (kg m^{-3} or $m^3 m^{-3}$)
χ_s	leaf shape/shelter factor

D. References

Alfano, J. J., 1981: A Two-layer Ground Hydrology Model Interactive with an Atmospheric General Circulation Model. Ph.D. Thesis, University of Connecticut. 287 pp. and Appendices.

Allen, L. H. and Lemon, E. R., 1976: "Carbon Dioxide Exchange and Turbulence in a Costa Rica Tropical Rain Forest." In: Vegetation and the Atmosphere II; ed. by J. L. Monteith, pp. 265-308, Academic Press.

Atlas, D., and Thiele, O. T., 1981: "Precipitation Measurements from Space." Workshop Report, NASA, Goddard Space Flight Center, Greenbelt, Maryland 20771.

Beven, K. and Kirkby, M. J., 1976: "Towards a Simple, Physically-based, Variable Contributing Area Model of Catchment Hydrology." Leeds University, Department of Geography, Working Paper 154, 11 pp.

Calder, I. R. and Newson, M. D., 1979: "Land Use and Upland Water Resources in Britain - A Strategic Look." Water Resources Bulletin, American Water Resources Assoc., 15, pp. 1628-1639.

Camillo, P. J. and Schmugge, T. J., 1982: "A Computer Program for the Simulation of Heat and Moisture Flow in Soils." NASA Technical Memorandum 82121, Goddard Space Flight Center, Greenbelt, Maryland 20771.

Carson, D. J., 1981: "Current Parameterization of Land Surface Processes in Atmospheric General Circulation Models." In Proceedings of the JSC Study Conference on Land-Surface Processes in Atmosphere General Circulation Models, Greenbelt, USA, 5-10 January 1981.

Cowan, I. R., 1965: "Transport of Water in the Soil-Plant-Atmosphere System." J. Appl. Ecol., 2, pp. 221-239.

de Laubenfels, D. J., 1975: Mapping the World's Vegetation: Regionalization of Formations and Flora. Syracuse University Press. Syracuse, N.Y. 246 pp.

Denmead, O. T., 1976: "Temperate Cereals." In: Vegetation and the Atmosphere II. Ed. by J. L. Monteith, pp. 1-31, Academic Press.

Denmead, O. T. and Millar, B. D., 1976: "Water Transport in Plants (Wheat) in in the Field." Agron. J., 68, pp. 297-303.

Goudriaan, J., 1977: Crop Micrometeorology: A Simulation Study. Wageningen Center for Agricultural Publishing and Documentation. Wageningen, The Netherlands. pp.

Gurney, R. J. and Camillo, P. J., 1982: "Modelling Daily Evapotranspiration Using Remotely Sensed Data." NASA Technical Memorandum, (in press), Goddard Space Flight Center, Greenbelt, Maryland 20771.

Hillel, D., 1971: Soil and Water: Physical Principles and Processes. Academic Press, N.Y./San Francisco/London. 288 pp.

Hillel, D., 1977: "Computer Simulation of Soil-Water Dynamics: A Compendium of Recent Work." International Development Research Centre, Ottawa, Canada, pp. 214

Jarvis, P. G., 1976: "The Interpretation of the Variations in Leaf Water Potential and Stomatal Conductance found in Canopies in the Field." Phil. Trans. Roy. Soc. Lond. B. 273, pp. 593-610.

Leonard, R. E., and Eschner, A. R., 1968: "Albedo of Intercepted Snow." Water Resources Res., 4, pp. 931-935.

Loucks, O. L., Ek, A. R., Johnson, W. C. and Mouserud, R. A., 1981: "Growth, Aging and Succession." pp. 37-85 in Dynamic Properties of Forest Ecosystems, D. E. Reichle (ed.) Cambridge Univ. Press, Cambridge/London/N.Y. 683 pp. (International Biological Programme 23).

Male, D. H. and Granger, R. J., 1981: "Snow-Surface Energy Exchange. Water Resources Res., 17, pp 609-627.

Mintz, Y., 1979: "On the Simulation of the Oceanic General Circulation." In Report of the JOC Study Conference on Climate Models: Performance, Inter-Comparison and Sensitivity Studies, Washington, D.C., 3-7 April 1978. GARP Publication Series No. 22, Vol II, PP. 607-687. WMO, Geneva, 1979.

Mintz, Y., 1982: "The Sensitivity of Numerically Simulated Climates to Land-Surface Conditions." (Review paper presented at the JSC Study Conference on Land-Surface Processes in Atmospheric General Circulation Models, Greenbelt, USA, 5-10 January 1981. NASA Technical Memorandum 83985, Goddard Space Flight Center, 1982, 81 pp. [Will also appear in The Global Climate, J. Houghton, editor; Cambridge University Press, Cambridge/London/New York, 1983.]

Pinker, R.,1980: "The Microclimate of a Dry Tropical Forest." Agric. Meteor., 22, pp. 249-265.

Penning de Vries, F. W. T., 1971: "A Model for Simulating Transpiration of Leaves with Special Attention to Stomatal Functioning." J. Appl. Ecol., 9, pp. 57-77.

Raschke, K., 1975: "Stomatal action." Ann. Rev. Plant. Physiol., 26, pp. 309-340.

Ross, J. and Nilson, T. A., 1971: "A Mathematical Model of the Radiation Regime of Vegetation." In: V. K. Pyldmaa (Ed.) Actinometry and Atmospheric Optics, pp. 253-270.

Rutter, A. J., 1975: "The Hydrological Cycle in Vegetation." In Vegetation and the Atmosphere, Vol. 1, (ed. J. Monteith). Academic Press, London/New York/San Francisco. pp. 111-154.

Schmugge, T. J., Jackson, T. J. and McKim, H. L., 1980: "Survey of Methods for Soil Moisture Determination." Water Resources Research, 16, 6, pp 961-979.

Sellers, P. J., 1981: Vegetation Type and Catchment Water Balance: A Simulation Study. Ph.D. Thesis, Leeds University, Department of Geography, 836 pp.

Shukla, J. and Mintz, Y., 1982: "Influence of Land-Surface Evapotranspiration on the Earth's Climate." Science, 215, pp. 1498-1501.

Shuttleworth, W. J. and Calder, I. R., 1979: "Has the Priestley-Taylor Equation Any Relevance to Forest Evaporation?" J. Appl. Meteor., 18, pp. 639-646.

Thom, A. S., and Oliver, H. R., 1977: "On Penman's Equation for Estimating Regional Evaporation." Quart. J. Roy. Met. Soc., 101, pp. 93-105.

Turner, N. C., 1974: "Stomatal response to light and water under field conditions." Roy. Soc. N. Z. Bull. 12, pp. 423-432.

BIBLIOGRAPHIC DATA SHEET

1. Report No.	2. Government Accession No.	3. Recipient's Catalog No.
TM 84973		

4. Title and Subtitle	5. Report Date
ON THE DESIGN OF AN INTERACTIVE BIOSPHERE FOR THE GLAS GENERAL CIRCULATION MODEL	January 1983
	6. Performing Organization Code 911
7. Author(s)	8. Performing Organization Report No.
Y. Mintz, P. J. Sellers, and C. J. Willmott	
9. Performing Organization Name and Address	10. Work Unit No.
	11. Contract or Grant No.
	13. Type of Report and Period Covered
12. Sponsoring Agency Name and Address NASA Goddard Space Flight Center Greenbelt, MD 20771	NASA Technical Memorandum
	14. Sponsoring Agency Code

15. Supplementary Notes

16. Abstract Sensitivity experiments with general circulation models have shown that the large scale fields of rainfall, temperature and motion of the atmosphere are highly sensitive to the transfers of latent and sensible heat from land surface to atmosphere. It is proposed to improve the realism and accuracy of the GLAS general circulation model by adding an interactive biosphere that will simulate these transfers as functions of the atmospheric conditions and the morphology and physiology of the vegetation. In the model biosphere, the morphology will be represented by the areas and vertical distribution of discrete 'leaf-layer plates'. These will control the aerodynamic regime within and above the vegetation canopy, the amount of radiation absorbed by the foliage and ground, and the interception, evaporation and throughfall of precipitation. The vegetation physiology, principally through stomatal resistance, will control the flow of water from soil to atmosphere depending upon ambient conditions. Initially, the vegetation morphology and physiology will be prescribed as functions of location and season. Later, phenological and, ultimately, ecological changes in the vegetation community will be made dependent on the atmospheric variables calculated by the GCM. Surface and satellite observations will be used to evaluate the model.

17. Key Words (Selected by Author(s))	18. Distribution Statement
General Circulation Model Vegetation Evapotranspiration Biosphere	

19. Security Classif. (of this report)	20. Security Classif. (of this page)	21. No. of Pages	22. Price*
U	U		

*For sale by the National Technical Information Service, Springfield, Virginia 22151.